Exploring Single-Spin Asymmetries: A Next-to-Leading Order Study in the Twist-3 Collinear Factorization Framework

Dissertation
der Mathematisch-Naturwissenschaftlichen Fakultät
der Eberhard Karls Universität Tübingen
zur Erlangung des Grades eines
Doktors der Naturwissenschaften
(Dr. rer. nat.)

vorgelegt von
Patrick Tollkühn
aus Hechingen

Tübingen
2026

Gedruckt mit Genehmigung der Mathematisch-Naturwissenschaftlichen Fakultät der Eberhard Karls Universität Tübingen.

Tag der mündlichen Qualifikation:	16.06.2026
Dekan:	Prof. Dr. Thilo Stehle
1. Berichterstatter:	Prof. Dr. Werner Vogelsang
2. Berichterstatterin:	Prof. Dr. Barbara Jäger

Zusammenfassung

Die Quantenchromodynamik ist die Theorie der starken Wechselwirkung, einer der drei fundamentalen Kräfte im Standardmodell der Teilchenphysik. Zusammen mit der Faktorisierung ist sie von zentraler Bedeutung fr unser heutiges Verständnis der inneren Struktur von Materie auf Ebene ihrer elementaren Bausteine, den Quarks und Gluonen, sowie deren Wechselwirkungen. Als ein essenzielles Instrument in der Erforschung der starken Wechselwirkung und Validierung der Quantenchromodynamik haben sich Beschleunigerexperimente erwiesen, bei welchen subatomare Teilchen wie Protonen oder auch Elektronen bei hohen Energien kollidieren. Eine bemerkenswert faszinierende Observable stellt dabei die transversale Single-Spin Asymmetrie dar, nachdem Experimente in den 1970er-Jahren zeigten, dass diese entgegen der damaligen Erwartung nicht verschwindend klein ist. Seitdem wurden sowohl auf theoretischer als auch auf experimenteller Seite bedeutende Fortschritte erzielt und so sind heute zwei Mechanismen bekannt, die eine nicht-verschwindende transversale Single-Spin Asymmetrie erklären können.

Im Mittelpunkt der vorliegenden Dissertation steht einer dieser beiden Mechanismen. Es handelt sich dabei um sogenannte twist-3 Beiträge im Zusammenhang mit der kollinearen Faktorisierung. Im Rahmen dieses Formalismus werden nicht-verschwindende Asymmetrien über Beiträge mit Parton-Parton-Korrelationsfunktionen höherer Ordnung im Vergleich zu den gängigen Partondichtefunktionen und Fragmentationsfunktionen erklärt. Doch trotz des immensen Fortschrittes in den vergangenen Jahrzehnten ist nach wie vor wenig über die Observable in höheren Ordnungen der Störungstheorie bekannt. Das Ziel dieser Arbeit liegt daher darin begründet, einen Schritt zum tieferen Verständnis in höheren Ordnungen und insbesondere in nächstführender Ordnung zu leisten. Zu diesem Zweck wird die transversale Single-Spin Asymmetrie in der inklusiven Produktion eines Hadrons in Lepton-Nukleon-Streuung untersucht, wobei angenommen wird, dass das einlaufende Nukleon transversal spin-polarisiert ist. Ergebnisse für Korrekturen höherer Ordnung für derartige Prozesse werden vor allem im Hinblick auf den zukünftigen Electron-Ion Collider an Bedeutung gewinnen. Darüber hinaus eignet sich der Prozess hervorragend, um mehr über die notwendige Vorgehensweise für die erfolgreiche Berechnung der Observablen zu lernen, da bereits in diesem Beispiel neue Herausforderungen in Form komplexer mathematischer Strukturen im Vergleich zur herkömmlichen twist-2 Betrachtung auftreten, wie sie auch im Zusammenhang mit Nukleon-Nukleon-Streuprozessen zu erwarten sind. Dahingegen gestaltet sich die Struktur des Prozesses im Gegensatz zur zuletzt erwähnten Nukleon-Nukleon-Streuung noch geradezu übersichtlich und der Aufwand bleibt aufgrund der geringeren Anzahl an Beiträgen überschaubar.

Zu Beginn der Dissertation werden die notwendigen theoretischen Grundlagen, insbesondere die Quantenchromodynamik und die kollineare Faktorisierung, eingeführt. Daran anschließend werden im zweiten Kapitel Methoden vorgestellt, wie sie für gewöhnlich im Rahmen von Untersuchungen in nächst-führender Ordnung der Störungstheorie Anwendung finden. Zum einen sind Kenntnisse dieser Techniken für die Berechnung des Wirkungsquerschnittes der inklusiven Hadronenproduktion in unpolarisierter Nukleon-Lepton Streuung unumgänglich. Dieser wird neben dem spin-polarisierten äquivalent als zweiter zentraler Beitrag für die Bestimmung der Asymmetrie benötigt und wird aus diesem Grund ebenfalls in der vorliegenden Arbeit untersucht. Die Vorgehensweise bei der Berechnung als auch die zugehörigen Ergebnisse werden im dritten Teil der Arbeit vorgestellt. Es wird dabei festgestellt, dass die Resultate mit dem bereits aus der Literatur bekannten Wirkungsquerschnitt übereinstimmen. Darüber hinaus basiert die Analyse des spin-abhängigen Prozesses im Grundsatz auf denselben Methoden, weshalb Wissen über diese noch weiter an Bedeutung gewinnt.

Der vierte und letzte Abschnitt widmet sich schließlich der Untersuchung des spin-polarisierten Pendant des zuvor erwähnten Prozesses. Vor diesem Hintergrund werden zwei Kanäle auf Ebene der Partonen betrachtet. Im Verlauf der Betrachtungen werden verschiedene Schwierigkeiten und Besonderheiten, welche im twist-3 Formalismus anzutreffen sind, identifiziert sowie mögliche Lösungswege aufgezeigt. Abschließend werden, wie zuvor im unpolarisierten Fall, Resultate für den Wirkungsquerschnitt des Streuprozesses präsentiert und es wird insbesondere gezeigt, dass alle divergenten Terme, welche üblicherweise in Zwischenschritten von Berechnungen in höheren Ordnungen der Störungstheorie auftreten, der Erwartung entsprechend verschwinden und wir somit eine endliche physikalische Observable erhalten. Weiterhin werden sowohl im polarisierten als auch unpolarisierten Fall numerische Berechnungen präsentiert. Dabei ist sowohl für den polarisierten Wirkungsquerschnitt als auch die Asymmetrie zu beachten, dass die physikalische Aussagekraft dieser numerischen Resultate gering ist, da hierzu im Moment noch zu wenig über die notwendigen Parton-Parton-Korrelationsfunktionen bekannt ist. Dennoch sind sie ausreichend, um den Einfluss der Korrekturen nächst-führender Ordnung als auch deren Bedeutung zu veranschaulichen.

Summary

Quantum chromodynamics is the theory of the strong interaction, one of the three fundamental forces in the standard model of particle physics. Alongside factorization, it is crucial for our current understanding of the inner structure of matter at the level of its elementary building blocks, the quarks and gluons, and their interactions. Accelerator experiments, in which subatomic particles such as protons or electrons collide at high energies, have proven to be indispensable tools in researching the strong interaction and validating quantum chromodynamics. A remarkably intriguing observable is the transverse single-spin asymmetry, after experiments in the 1970s revealed that, contrary to expectations at the time, it is not vanishingly small. Since then, both theoretical and experimental advancements have significantly expanded our understanding, and two mechanisms explaining the large transverse single-spin asymmetries are nowadays known.

The thesis on hand delves into one of the two specific mechanisms, focusing on the so-called twist-3 contributions in the formalism of collinear factorization. Within this framework, non-vanishing asymmetries are attributed to higher-order parton-parton correlation functions, as opposed to the more commonly employed parton distribution and fragmentation functions. However, despite the immense advancements over the past decades, much remains unknown about the observable in higher orders of perturbation theory. Thus, the aim of this work is to take a step towards a deeper understanding of the higher order corrections, particularly at next-to-leading order. In order to achieve this, the transverse single-spin asymmetry in the inclusive production of a single hadron in lepton-nucleon scattering is investigated, assuming that the incoming nucleon is transversely spin-polarized. Higher order corrections for such processes will gain importance, especially with regards to the forthcoming electron-ion collider. Furthermore, the process serves as an excellent opportunity to learn more about the necessary procedures and techniques in order to successfully determine the observable as it introduces new challenges through complex mathematical structures, that surpass those found in more conventional twist-2 considerations. Similar challenges are also anticipated to emerge in nucleon-nucleon scattering processes as well. Conversely, unlike nucleon-nucleon scattering, the structure of this process remains relatively simple, and the effort required is manageable due to the smaller number of distinct contributions.

At the beginning of the thesis, the necessary theoretical foundations, in particular quantum chromodynamics and collinear factorization, are introduced. Subsequently, the second chapter presents methods that are usually applied in the context of considerations at next-to-leading order of perturbation theory.

On the one hand, knowledge of these techniques is crucial for the calculation of the cross section of inclusive hadron production in unpolarized nucleon-lepton scattering. Besides the spin-polarized equivalent, this is needed as a second central contribution for the determination of the asymmetry and is therefore also investigated in the present work. The calculation procedure and the associated results are presented in the third part of the paper. It is found that the results agree with the cross section already known from the literature. Moreover, the analysis of the spin-dependent process essentially relies on the same methods, further emphasizing the importance of this knowledge.

Finally, the fourth and last chapter is dedicated to the investigation of the spin-polarized pendant of the previously mentioned process. Against this background, two channels are considered at partonic level. In the course of the considerations, various challenges and peculiarities encountered in the twist-3 formalism are identified and possible solutions are shown. As before in the unpolarized case, results for the cross section of the process are presented and it is shown in particular that all divergent terms, which usually occur in intermediate steps of calculations at higher orders in the framework of perturbation theory, cancel out as expected and we thus obtain a finite physical observable. Furthermore, numerical computations are presented in both, the polarized and unpolarized case. However, it is important to note that the physical significance of these numerical results is limited for the polarized cross-section and the asymmetry, due to the current lack of knowledge about the necessary parton-parton correlation functions. Nevertheless, these results effectively illustrate the influence and importance of next-to-leading order corrections.

List of Publications

[1] Daniel Rein, Marc Schlegel, Patrick Tollkühn, Werner Vogelsang. Next-to-Leading-Order Corrections and Factorization for Transverse Single-Spin Asymmetries. *Phys. Rev. Lett., 135(25):251901*, 2025.

[2] Daniel Rein, Marc Schlegel, Patrick Tollkühn, Werner Vogelsang. Transverse nucleon single-spin asymmetry for single-inclusive hadron and jet production at NLO accuracy. *Phys. Rev. D, 112(11):114024*, 2025.

Contents

List of Figures

List of Tables

Chapter 1

Introduction

Chapter 1

Introduction

Since ancient times, people have sought to understand the world around them, what it is made of, and what fundamental forces glue it together. Already thousands of years ago in the ancient Greece, the idea of the átomos, the smallest, indivisible building blocks of matter, arose from purely philosophical considerations. However, a long time passed before the atomic hypothesis was taken up again by Dalton in 1808 and formulated on a scientific basis in order to explain the chemical elements and phenomena. Almost another century passed on the way from atomic physics to the first basic principles of particle physics in 1897, when J. J. Thomson succeeded in experimentally proving the existence of the electron as the first known elementary particle [205, 206]. But as our understanding grew, so did our questions, leading us to probe deeper into the nature of matter itself.

The 20^{th} marked a crucial era in humankind's quest to understand the world we live in, when the discovery of quantum mechanics and the theory of relativity revolutionized our view on the microscopic and macroscopic universe leading to the birth of modern physics. Around the same time, scattering proofed itself as a key tool in the endeavour to probe the inner structure of matter starting with the experiments carried out by Geiger, Marsden [100] and Rutherford [192]. The pattern observed in the scattering of α-particles on a thin gold foil contradicted the atomic models commonly used at the time and provided evidence for the existence of the atomic nucleus, forever changing our understanding of the atom. In the following decades, scattering became a window into the deep and complex quantum world with increasing technological advances. Especially the emergence of modern particle colliders, such as the Large Hadron Collider (LHC) at CERN or Relativistic Heavy Ion Collider (RHIC) at BNL, have notably contributed to this development. These marvels of engineering and physics smash particles at nearly the speed of light together creating conditions similar to those soon after the birth of the universe, producing exotic particles and providing invaluable insights into the inner structure of matter often leading to groundbreaking discoveries.

Both, the theoretical efforts and the experimental advances, culminated in the standard model of particle physics that encapsulates decades of scientific progress into a concise, yet comprehensive model. It summarizes our entire knowledge of the microscopic world, the particles that inhabit it, and the fundamental forces at work. The standard model categorizes all known elementary particles into three classes, namely fermions, gauge bosons and the Higgs boson. Bosons, like photons and gluons, are force-carrying particles with an integer spin that mediate interactions. The standard model identifies three fundamental forces governing the behaviour of elementary particles. The most commonly known is the electromagnetic interaction as it is responsible for phenomena such as electricity, magnetism and light and we hence encounter its effects in our everyday lives. It is conveyed by photons, the particles of light. The strong or nuclear force is the strongest of the three fundamental interactions, but its range is limited to distances in the order of the size of an atomic nucleus. It is mediated by gluons between colour-charged particles and functions as the glue that keeps the nucleus against the electromagnetic repulsion between protons intact. The weak force is transmitted by so-called $W^{\pm}$- and Z^0-bosons. It is associated with radioactive phenomena as well as nuclear fission, and it can change the flavour, the subatomic type of a particle, into another, which is a unique capability not known from the other forces. On the theoretical side, the successful formulation of quantum field theories, which combine principles of quantum mechanics and special relativity, represents a major milestone in physics, as every fundamental force is today well described by such a theory. Fermions, which involve quarks and leptons, are the building blocks of matter and carry half-integer spin. The different varieties, in which a fermion can appear, is called flavour. The standard model knows six flavours of quarks, namely up, down, strange, charm, top and bottom as well as six species of leptons, specifically electrons, muons, tauons, and the three types of lepton neutrinos. For each particle a corresponding antiparticle exists. The fermions are organized into three generations, or families. Each generation contains a pair of quarks and a pair of leptons. Particles differ between generations based on their flavour and mass. As the generation number and respectively the mass increases, particles become less stable, which is why only the first generation forms the stable matter observed in everyday life. Apart from that, quarks, which carry colour charge, are never observed in isolation; the strong interaction confines them within composite particles called hadrons, a group of particles that encompasses protons and neutrons as the most familiar examples among others.
Another particle, the Higgs boson, holds a peculiar position within the standard model. It was theorized for decades before its discovery in 2012 by the

ATLAS collaboration at CERN [64]. Its existence provides evidence for a field of the same name, that permeates the entire space and was proposed independently in 1964 by Peter Higgs [117, 118] as well as two research teams, one located at the Université Libre de Bruxelles [86] and another one at the Imperial College [108]. The underlying mechanism is associated with spontaneous symmetry breaking and crucial to explain the massive bosons of the weak force.

However, the journey doesn't end here and despite its successes and its accurate agreement with experimental data, the standard model is not the theory, able to describe the complete universe as it is lacking in various aspects. It does not incorporate gravity, the fourth fundamental force, described by the theory of general relativity, nor can it explain the nature of dark matter and dark energy or the asymmetry of matter and antimatter, to name just a few unanswered questions going beyond the standard model.

Nevertheless, there is still much to learn about the properties of hadrons within the framework provided by the standard model. A monumental leap in the quest to unravel the fundamental structure of nuclear matter in more detail and to improve our understanding of the strong interaction will be provided by the future Electron-Ion Collider (EIC) [3, 6, 217] at the BNL as one of the most advanced tools to explore the subatomic world. It is expected to bring forth unprecedented insights on, for example, the origin of the mass and spin carried by nucleons and the properties of dense systems of gluons. Moreover, it will make the 3D imaging of nucleons possible. However, in order to meet these purposes, technological challenges need to be overcome. The EIC will therefore feature a large center-of-mass energy range, a high luminosity and offer the opportunity to alter the alignment of the electrons' and protons' spin, while making use of innovative detectors and computational techniques.

Not only with regard to the future EIC, an observable of particular interest is the transverse single-spin asymmetry, whose study has been a challenging but also fascinating area of research in high-energy physics in recent decades. It arises when a single particle involved in the scattering is transversely spin-polarized and is in general defined by

$$A_N \equiv \frac{\Delta\sigma(s_T)}{\sigma} \equiv \frac{\sigma(s_T) - \sigma(-s_T)}{\sigma(s_T) + \sigma(-s_T)} \ . \tag{1.1}$$

in terms of a spin-dependent $\Delta\sigma$ and spin-averaged cross section σ, where s_T denotes the spin-vector. The interest in the transverse single-spin asymmetry is driven by its potential to shed new light on Quantum Chromodynamics, the theory of strong interaction, and the spin structure of the nucleon.

But despite the progress towards a better theoretical understanding of the underlying mechanisms as well as the nature of the asymmetry, the phenomenological insights are lagging behind and many existing studies are therefore limited to the lowest order of perturbation theory.

This thesis aims to delve into the complexities of the transverse single-spin asymmetry and to study this intriguing observable in the inclusive production of a hadron in nucleon-lepton scattering at next-to-leading order of perturbation theory. The specific scattering process is thereby chosen since similar structures are emerging as in the case of the more prominent nucleon-nucleon scattering in the required computations, while it is still easier to handle overall. To carry out our considerations, we will make use of the framework provided by the so-called collinear factorization at twist-3 level, one of the two well-established approaches known to successfully account for the large asymmetries.

The thesis is structured as follows. In the subsequent chapter, we will give an introduction on the theoretical background and basic concepts, which lay the foundation of our work. In this context, we will particularly discuss Quantum Chromodynamics as the theory forming the basis of our considerations, the framework provided by perturbation theory, which allows us to investigate scattering processes on the level of the fundamental particles and the factorization theorem, that provides a link between interactions on the level of hadrons and the elementary particles. Next, we complete the introduction by addressing the necessary computational techniques in chapter 3.

In chapter 4, we will present next-to-leading order calculations for the unpolarized process. In addition, we will use these considerations in order to further introduce methods commonly required in such calculations at higher orders of perturbation theory. We will conclude these discussions by presenting numerical results.

Finally, we will address the computation of the spin-dependent cross section and hence the transverse single-spin asymmetry at next-to-leading order in chapter 5. In the course of the considerations, we will face novel challenges unknown from ordinary leading-twist calculations for similar unpolarized processes and introduce methods to overcome these obstacles. Once again, we will conclude the chapter with the presentation of numerical studies.

Chapter 2

Theoretical Background

Chapter 2

Theoretical Background

2.1 Quantum Chromodynamics

The theoretical foundation of most of our knowledge about the subatomic world is laid by quantum field theories (QFTs). The principal assumptions behind these theories are based on two fundamental concepts: Firstly, particles are associated with quantum fields, and secondly, interactions are transmitted through the exchange of a distinct class of particles, known as gauge bosons. Among the major initial accomplishments was the formulation of Quantum electrodynamics (QED), which is the theory describing the electromagnetic interactions between charged particles, such as electrons, through the exchange of photons. However, the search for the right gauge theory describing the strong interaction that binds protons and neutrons in the atomic nucleus proved to be quite a challenge, taking around 20 years from the 1950s to the 1970s. The path to the discovery of the correct theory mostly followed two tracks. The first was a pure mathematical endeavour aimed at improving the comprehension of non-abelian gauge theories in general where a significant milestone was achieved by Chen-Ning Yang and Robert Mills in the 1950s, when they forged the foundations of such theories by extending the concept of local gauge invariance to non-abelian groups in [224]. The mathematical understanding was further improved by the work of Ludvig D. Faddeev and Victor N. Popov [87, 182], who introduced a path-integral method to consistently quantize non-abelian theories.

Parallel to the advancements in the understanding of non-abelian gauge theories, improving particle accelerators resulted in the discovery of a diverse range of new subatomic particles, categorized as hadrons, and the pursuit of an explanation for their existence prompted the emergence of a theory of strong interactions. But the first attempts to formulate a coherent theory, which were based on quantum fields corresponding to the observed hadrons, failed. On the other hand, many of the newly discovered particles were

found to be unstable leading to the hypothesis that, in contrast to electrons, hadrons are not elemental particles, but rather bound states of even smaller constituents. The idea was supported by experiments on electron-nucleon scattering conducted by Robert Hofstadter [122], who demonstrated that protons are not point-like. A few years later, in 1961, Murray Gell-Mann and Yuval Ne'eman proposed the eightfold way in [101, 172] as an organization scheme for hadrons to bring order into the chaotic particle zoo, which relies on a SU(3) symmetry group and ultimately led to the quark model. In the quark model, which was independently developed by Gell-Mann [102] and George Zweig [233], all hadrons consist of point-like constituents, called quarks. The quarks are spin-1/2 fermions which, in addition to properties such as mass or electric charge, also possess a distinct flavour, which can be understood as a kind of subatomic type. The original model suggested three flavours, up (u), down (d) and strange (s), but nowadays the standard model counts six different flavours and the corresponding anti-flavours. Besides the first three flavours, there are charm (c), top (t) and bottom (b). The model's remarkable feat included not only to explain the plethora of the discovered particles, but also to naturally organize them into two classes. Hadrons are classified as either bound states of three quarks with a half-integer spin, called baryons, or mesons which are composed of a quark-antiquark pair, possessing an integer spin. It further proofed its worth by successfully predicting the existence of the Ω^- baryon which was experimentally found at the Brookhaven National Laboratory in 1964 [41]. Nevertheless, following years of futile searches for these point-like constituents (see e.g. [164]), physicists posited quarks as purely mathematical constructs, which, despite their utility, are not closely related to any tangible physical entity. But the confidence in the model began to further grow only after deep inelastic scattering (DIS) experiments at the Stanford Linear Accelerator revealed signs for the existence of quarks and an inner structure of the proton for the first time in 1968 [47, 56]. Over the next few decades, evidence was found for all six quark flavours, with the top quark being experimentally discovered as the last one at the Fermi National Accelerator Laboratory in 1995 [2, 4].
But despite the considerable success of the quark model, new challenges emerged when a conflict between the model and the Pauli exclusion principle arose. The matter at hand pertains to the wave function of the Δ^{++} baryon, which, at the time, was thought to be a convolution of a space, flavour and spin function and appeared to be symmetric, although it must be antisymmetric given that baryons are fermions. In order to solve the contradiction, another hidden internal degree of freedom was taken into account, the three-valued colour charge, which was first introduced by Oscar W. Greenberg in 1964 [104]. The charge of colour was later linked to the $SU(N_c)$ colour group, where $N_c = 3$ is the number of colour charges, and identified as the source of the strong interaction between quarks in a model proposed by Yoichiro Nambu and Moo Young Han [110, 171].

Ultimately, these developments led to the foundation of Quantum Chromodynamics in 1973 when Gell-Mann, Harald Fritzsch and Heinrich Leutwyler presented a theory for the strong interaction between colour charged particles in [96] based on the lagrangian by Yang and Mills.

The gauge theory of strong interaction, Quantum Chromodynamics (QCD), is hence a standard Yang-Mills theory based on the $SU(N_c)$ colour group. The matter particles of the theory, the fermions, are the quarks already known from the quark model. The strong interaction is then mediated by the exchange of the theory's gauge bosons, known as gluons. However, unlike the electric neutral photons in QED, the gluons themselves carry a colour charge allowing them to not only mediate the force but to participate in the strong interaction as well.
A central quantity in QFTs is the lagrangian density, commonly referred to as just the lagrangian, as it encompasses the dynamics and interactions of the theory's particles. In the context of QCD, the derivation of the lagrangian density is a subject that is extensively covered in many textbooks and may be found in e.g. [85, 109, 162, 179]. Therefore, only a brief summary of its construction will be given in the remainder of this chapter. To commence, the complete lagrangian of QCD can be formulated as

$$\mathscr{L}_{\text{QCD}} = \mathscr{L}_{\text{quark}} + \mathscr{L}_{\text{gluon}} + \mathscr{L}_{\text{gauge-fixing}} + \mathscr{L}_{\text{ghost}} \tag{2.1}$$

wherein the first two terms describe the quark, respectively gluon content of the theory, whereas the last two are necessary to fix the gauge and eliminate unphysical degrees of freedom of the gluons. As in QED, the lagrangian for a free fermion

$$\mathscr{L}_0 = \bar{\psi}_f \big(i\not{\partial} - m_f\big)\psi_f \tag{2.2}$$

is employed as an ansatz for the quark content where ψ_f denotes a quark field with flavour f and mass m_f. Here, we introduced the Feynman slash notation

$$\not{v} \equiv \gamma_\mu v^\mu \tag{2.3}$$

for an arbitrary four-vector v. Since experiments showed no dependence on the colour degree of freedom, it can be concluded that physical observables are independent of the colour configuration and one therefore demands a local $SU(N_c)$ symmetry in QCD. This implies that the quarkonic lagrangian must be invariant under $SU(N_c)$ transformations like

$$U(x) = e^{ig_s\theta_a(x)T^a} \tag{2.4}$$

where T^a stands for the standard representation of the $SU(N_c)$ generators, $a \in \{1, ..., N_c^2 - 1\}$ denotes a colour index and $\vartheta_a(x)$ is a real differentiable function. As a result of the unitarity of these transformations, the $\mathrm{SU}(N_c)$ generators T^a satisfy the commutator relation

$$\big[T^a, T^b\big] = if^{abc}T^c \tag{2.5}$$

with f^{abc} being the antisymmetric structure constant. The quark fields then transform as

$$\psi_f \to \psi'_f = U(x)\psi_f \ , \tag{2.6}$$
$$\bar{\psi}_f \to \bar{\psi}'_f = \bar{\psi}_f U^\dagger(x) \ . \tag{2.7}$$

It is straightforward to demonstrate that the mass term in equation 2.2 remains invariant under the transformations. Nonetheless, owing to the derivative, the kinematic term, as presented in the free lagrangian, is not invariant, necessitating the inclusion of a covariant derivative

$$D_\mu \equiv \partial_\mu - ig_s A^a_\mu T_a \ , \tag{2.8}$$

to also render this term invariant. In the second term of the covariant derivative, the coupling strength g_s of QCD is emerging besides the gluon field A^a_μ, and it hence may be understood as a term describing the interaction between quarks and gluons. Replacing the derivative in equation 2.2 finally yields

$$\mathscr{L}_{\text{quark}} = \bar{\psi}_f \big(i\not{D} - m_f\big)\psi_f \tag{2.9}$$

as the correct contribution for the quark content of QCD. However, we still need a kinematic term for the gluons. In analogy to QED, a field strength tensor $G^a_{\mu\nu}$ can be introduced via the commutator of the covariant derivative

$$\big[D_\mu, D_\nu\big]\psi_f \equiv ig_s T_a G^a_{\mu\nu}\psi_f \ , \tag{2.10}$$

which then becomes

$$G^a_{\mu\nu} = \partial_\mu A^a_\nu - \partial_\nu A^a_\mu - g_s f^{abc} A^b_\mu A^c_\nu \ , \tag{2.11}$$

where the first two terms remind of the photonic equivalent in QED. The last term is novel and arises due to the non-abelian nature of QCD, which permits self-interactions between the gauge bosons of the theory, namely the gluons. Having introduced the field strength tensor, the same approach as in QED can be employed for the kinematic term and the gluonic contribution hence reads

$$\mathscr{L}_{\text{gluon}} = -\frac{1}{4} G^a_{\mu\nu} G^{\mu\nu}_a \ . \tag{2.12}$$

The combination of the lagrangians for the quark and the gluon content results in the classical lagrangian

$$\mathscr{L}_{\text{class}} = \bar{\psi}_f \big(i\not{D} - m_f\big)\psi_f - \frac{1}{4} G^a_{\mu\nu} G^{\mu\nu}_a \ , \tag{2.13}$$

which contains cubic and quadric terms in the gluon fields, thereby causing the three- and four-gluon vertices observed in QCD, in addition to the quark-gluon vertex.

The classical lagrangian, however, is not sufficient to formulate a valid gluon propagator in QCD which is why another term needs to be added to fix the gauge. To set a covariant gauge satisfying the condition $\partial_\mu A_a^\mu = 0$, a term of the form

$$\mathscr{L}_{\text{gauge-fixing}} = -\frac{1}{2\xi}\left(\partial_\mu A_a^\mu\right)^2 \tag{2.14}$$

must be added, where the parameter ξ specifies the gauge. Common choices are the Feynman gauge $\xi = 1$ or the Landau gauge $\xi = 0$. But the Faddeev-Popov method then suggests that adding such a term to fix the gauge requires to include another one involving unphysical scalar fermion fields η_a and $\bar{\eta}_a$, called ghosts. These terms are necessary to remove the unphysical degrees of freedom of the gluon fields and thus to receive meaningful results for physical observables in QCD. They are given by

$$\mathscr{L}_{\text{ghost}} = \partial_\mu \bar{\eta}_a \partial^\mu \eta_a + g_s \partial^\mu \bar{\eta}_c f^{abc} A_\mu^b \eta_a \ . \tag{2.15}$$

Finally, all four contributions can be added leading to the complete lagrangian of QCD which becomes

$$\begin{aligned}\mathscr{L}_{\text{QCD}} &= \mathscr{L}_{\text{quark}} + \mathscr{L}_{\text{gluon}} + \mathscr{L}_{\text{gauge-fixing}} + \mathscr{L}_{\text{ghost}} \\ &= \bar{\psi}_f\left(i\not{D} - m_f\right)\psi_f - \frac{1}{4}G_{\mu\nu}^a G_a^{\mu\nu} - \frac{1}{2\xi}\left(\partial_\mu A_a^\mu\right)^2 \\ &\quad + \partial_\mu \bar{\eta}_a \partial^\mu \eta_a + g_s \partial^\mu \bar{\eta}_c f^{abc} A_\mu^b \eta_a \ . \end{aligned} \tag{2.16}$$

Note that the sum over flavour, colour and Dirac indices need to be understood implicitly here. In principle, the lagrangian above describes the full dynamics of quarks and gluons. However, as the theory is not exactly solvable, one needs approximative methods to study the strong interaction and learn more about the structure of matter. The two most commonly employed and well-established approaches to QCD are based on lattice methods and perturbation theory. The first relies on the idea to solve QCD on a discrete grid of points in space and time and is usually applied at low energies where perturbative methods fail. The latter considers the interaction as a small perturbation of the free theory. As it will be later seen, the framework provided by perturbation theory can be applied in QCD at high energies and is therefore particularly suitable for studying scattering experiments.

2.1.1 Regularization & Renormalization

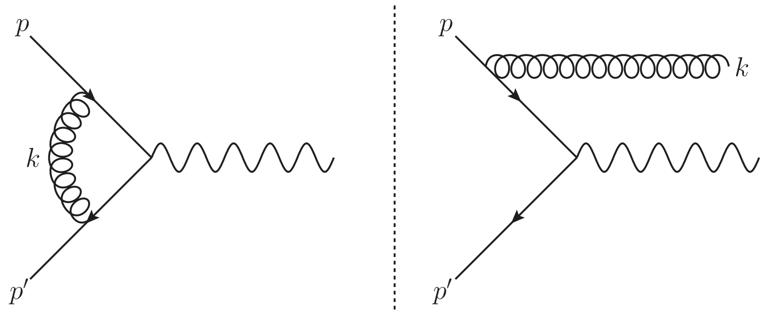

Figure 2.1: Examples for diagrams causing divergences. The left-hand diagram depicts a loop contribution, which is a source of ultraviolet and infrared divergences. The diagram on the right-hand side shows the emission of a real gluon and produces infrared and collinear singularities.

Divergences that arise during the intermediate stages of calculations within the framework of perturbation theory constitute a recurring concern in QFTs and, undoubtedly, in QCD as well. They were apparently first found by Werner Heisenberg and Wolfgang Pauli in 1929 [113, 114], long before QCD was even discovered, and later confirmed in calculations by Julius R. Oppenheimer [174]. Today, they are well understood and it is known that the infinities observed at that time belong to a class of singularities referred to as *ultraviolet* (UV) divergences, and that the sources are loop integrals with an unconstrained loop momentum, which are linked to diagrams like the one shown on the left hand side of figure 2.1. The diagram depicted above, for instance, prompts one to contemplate a loop integral, which reads

$$\sim \int \frac{d^4k}{(2\pi)^4} \frac{f(k)}{k^2(p-k)^2(p'-k)^2} \; . \tag{2.17}$$

It is noteworthy that the integral will consequently diverge in the event that the numerator $f(k)$ contains contributions of a sufficiently high order in k, if the loop momentum becomes large, i.e. $k \to \infty$.

Apart from UV singularities, two more classes of infinities are nowadays known. One of them are *infrared* (IR) divergences which are encountered in theories with massless particles and occur when one of the particles involved in the scattering process becomes soft, which means that its momentum becomes small. They can originate from both, virtual loop corrections and real corrections, where an additional particle is emitted, in higher orders of perturbation theory. The two diagrams in figure 2.1, for example, will both lead to a propagator given as

$$\frac{1}{(p-k)^2} = \frac{1}{2E_k E_p\big(1+\cos(\vartheta)\big)} \tag{2.18}$$

where E_p and E_k are the energies of the particles with momentum p, respectively k, and ϑ denotes the angle between them. The expression evidently diverges, in kinematic regions of the phase space, where the energy of the outgoing particle with momentum k becomes small, i.e. $E_k \to 0$. Fundamental research on IR singularities is attributed to Felix Bloch and Arnold Nordsieck, who demonstrated that the divergences between loop diagrams and contributions, where additional photons are radiated, cancel each other in QED, when all diagrams of a given order of perturbation theory are taken into account [46]. Their observation was later generalized independently by Toichiro Kinoshita [143] as well as Tsung-Dao Lee and Michael Nauenberg [155] in the Kinoshita-Lee-Nauenberg theorem (KLN theorem). In the particular situation, when all IR divergences cancel each other out, a physical observable is referred to as infrared safe.

The third category of singularities is associated with diagrams as shown on the right-handed side in figure 2.1 and also emerges from propagators like the one given in equation 2.18. As it can be seen from the equation, the expression diverges when $\big(1+\cos(\vartheta)\big) \to 0$ and consequently $\vartheta \to \pi$. In this scenario, the two particles become collinear and the corresponding singularity is therefore called *collinear divergence*.

In the 1940s, Bethe, Feynman, Schwinger, Tomonaga and Dyson proposed a program of *renormalization* to handle the UV singularities by absorbing them into redefined physical quantities, marking a significant initial step towards understanding the divergences (see eg. [76, 91, 92, 193, 194, 207]). However, throughout the subsequent decades, the technique was deemed an impromptu method solely justified by the concordances between theoretical findings and experimental data with high accuracy, until the 1970s, when Kenneth G. Wilson laid the foundations for our contemporary comprehension of renormalization [219–221, 223]. So today, the singularities arising in QFTs, and more particularly in QCD, are well understood and procedures to deal with them are known.

To begin with, methods are needed to identify the divergences and make them manifest. In the course of these procedures, known as *regularization*, a parameter, the regulator, is introduced. Today, multiple schemes to introduce such a regulator consistently, like the cut-off method or the Pauli-Villars regularization [178], are known. Nevertheless, a particular technique, known as *dimensional regularization*, has prevailed and is now widely applied. The scheme, which was independently developed by Juan

J. Giambiagi, along with Carlos G. Bollini [51] as well as Gerard 't Hooft and Martinus J. G. Veltman [203] in 1972, relies on the idea to continue the four dimensional space-time to

$$d = 4 - 2\varepsilon \tag{2.19}$$

dimensions. Dimensional regularization is relatively simple to implement in calculations and is able to regulate all three types of divergences, ultraviolet, infrared and collinear ones, making it quite practical in contrast to other schemes where the implementation can become strenuous. Beyond that, it provides another advantage by preserving lorentz and gauge invariance. However, as a consequence of continuing the space-time dimensions, it is imperative to make adjustments to the coupling constant and spin averaging for bosons, which must be replaced by

$$g_s \to g_s \mu^{\varepsilon} \ , \tag{2.20}$$

$$\frac{1}{2} \to \frac{1}{2\,(1-\varepsilon)} \ , \tag{2.21}$$

where μ is an arbitrary mass scale. It is introduced to guarantee that the coupling constant remains dimensionless for any choice of ε in dimensional regularization. Now, that all infinities have been identified and made manifest in terms of the regulator, the UV divergences can be addressed by renormalizing the theory. In the case of QCD, the process of renormalization requires the introduction of renormalized counterparts of the bare fields ψ_0, A_0^{μ}, η_0, the coupling constant g_0 and the quark masses m_0. Both quantities, bare and renormalized, are interconnected through the so-called renormalization constants, as follows

$$\psi_0 = \sqrt{Z_2}\psi_R \ , \tag{2.22}$$

$$A_0 = \sqrt{Z_3}A_R \ , \tag{2.23}$$

$$m_0 = Z_m m_R \ , \tag{2.24}$$

$$g_0 = Z_g g_R \ . \tag{2.25}$$

A common programme to execute the renormalization of a theory is provided by the BPHZ approach, named after Bogoliubov and Parasiuk [50], Hepp [115] and Zimmermann [232]. It utilizes the relations given in the equations 2.22 to 2.25 to rewrite the lagrangian of the bare theory as

$$\mathscr{L}_0 = \mathscr{L}_R + \mathscr{L}_{c.t.} \ , \tag{2.26}$$

in terms of two new lagrangians, where $\mathscr{L}_R$ corresponds to the renormalized theory and $\mathscr{L}_{c.t.}$ is associated with so-called counterterms. The counterterms are linked to the singular part of the theory and thus allow to study the UV divergent loop corrections. Next, the renormalization constants must be determined in such a way that the UV divergences cancel out.

At one-loop in QCD for instance, it is therefore inevitable to examine diagrams describing the quark self-energy and vertex corrections. However, the precise selection of the constants is not exclusive, and distinct schemes are in existence. An intuitively reasonable renormalization scheme is offered by the *minimal subtraction* (MS), which was independently proposed by 't Hooft [202] and Weinberg [215] in 1973. It uses constants that are chosen in such a manner that only the ε-poles are removed. But commonly, they are accompanied by supplementary contributions and often occur in the combination

$$\frac{1}{\varepsilon} - \gamma_{\mathrm{E}} + \ln\left(4\pi\right) \,, \tag{2.27}$$

which makes another scheme, the *modified minimal subtraction* ($\overline{\mathrm{MS}}$) [40] more practical. In this prescription, the renormalization constants are selected appropriately to not only remove the ε-poles but also the additional terms.

Finally, the question remains as to when a theory can be renormalized. A common approach to determine whether a theory is renormalizable is to establish a superficial degree of divergence D. In the course of the method, referred to as *power counting*, the superficial degree of divergence is defined as

$$D = 4L - 2I \tag{2.28}$$

with L being the number of loop integrals and I the number of internal lines. The procedure reveals that a diagram might diverge when $D \geq 0$ and the theory exhibits renormalizability if only a limited number of divergent diagrams exist.

2.1.2 Running Coupling

In the preceding section, renormalization was presented as a technique to address UV divergences by redefining the fields, the coupling constant g_s and the quark masses m_q. But in the course of the procedure, an arbitrary mass scale, the renormalization scale μ, was introduced and consequently, the coupling constant and the quark masses will show a dependence on said scale. The section at hand is specifically devoted to the scale dependence of the coupling constant and is intended to provide a deeper insight into this topic.

But before dealing with the scale dependence, we want to introduce another quantity

$$\alpha_s \equiv \frac{g_s^2}{4\pi} \ . \tag{2.29}$$

which is defined in complete analogy to the fine structure known from QED. The new constant α_s is conveniently used instead of g_s as results for physical observables calculated in the framework of perturbative QCD can be usually written as series in even powers of g_s. Hence, the dependence of α_s instead of g_s on the mass scale will be discussed in the remainder of this chapter

Generally speaking, the scale dependence is a prevalent feature of perturbation theory and a remnant of not knowing the full theory and only being able to determine observables to a fixed order. This implies that there would be no such dependence if it were feasible to calculate physical quantities analytically and precisely, which seems reasonable as a meaningful observable must not be subject to an arbitrary scale.

In order to mathematically formulate the demand for a physical observable to be independent of the renormalization scale, we commence by considering an arbitrary observable

$$\mathcal{O} \equiv \mathcal{O}\left(\alpha_s(\mu^2), m_q(\mu^2), \mu^2\right) \tag{2.30}$$

and apply the operator $\mu^2 \frac{d}{d\mu^2}$, which yields the *renormalization group equation* (RGE)

$$0 = \mu^2 \frac{d}{d\mu^2} \mathcal{O}\left(\alpha_s(\mu^2), m_q(\mu^2), \mu^2\right) \tag{2.31}$$

$$= \left\{ \mu^2 \frac{\partial}{\partial \mu^2} + \beta(\alpha_s) \frac{\partial}{\partial \alpha_s} - \gamma_m(\alpha_s) m_q \frac{\partial}{\partial m_q} \right\} \mathcal{O}\left(\alpha_s(\mu^2), m_q(\mu^2), \mu^2\right) \tag{2.32}$$

after making use of the chain rule for the derivative in the second line. The functions arising in the equation are the anomalous dimension γ_m and the beta function β, which is sometimes also called the Callan-Symanzik beta function, referring to Curtis Callan [61] and Kurt Symanzik [201], who each introduced the function independently in 1970. It follows from the aforementioned RG equation that they can be defined through [215]

$$\beta\left(\alpha_s\right) \equiv \mu^2 \frac{\partial}{\partial\mu^2} \alpha_s\left(\mu^2\right) \ , \tag{2.33}$$

$$\gamma_m\left(\alpha_s, m\right) \equiv -\frac{\mu^2}{m} \frac{\partial}{\partial\mu^2} m \ . \tag{2.34}$$

Moreover, they can be expressed as a power series in the running coupling α_s, where the expansion for the beta function reads

$$\beta\left(\alpha_s\right) = -\alpha_s \sum_{n=0}^{\infty} \beta_n \left(\frac{\alpha_s}{4\pi}\right)^{n+1} \tag{2.35}$$

with some coefficients β_n. The coefficients can be found via equation 2.33. As discussed in the previous section, the renormalized coupling may be written in terms of the bare counterpart as well as some renormalization constant. The dependence on the renormalization scale μ is through this completely shifted into the renormalization constants, which can be determined by studying loop corrections order-by-order. It is then possible to insert the running coupling as a function of the bare equivalent and the renormalization constants into equation 2.33 at a fixed order, allowing to carry out the derivative, and afterwards to read off the coefficients β_n. For about two decades, the coefficients have been known up to the four loop level [71, 79, 154, 209], but they were determined also at the five loop level [37, 116, 159, 160] in recent years. In the two lowest orders, they are given by

$$\beta_0 = \frac{11}{3} C_A - \frac{4}{3} T_R n_f \ , \tag{2.36}$$

$$\beta_1 = \frac{34}{3} C_A^2 - 4 C_F T_R n_f - \frac{20}{3} C_A T_R n_f \ , \tag{2.37}$$

where n_f is the number of active flavours, $C_A = N_c$ as well as $C_F = \frac{N_c^2-1}{2N_c}$ are the $SU(N_c)$ Casimir operators and $T_R = \frac{1}{2}$ denotes the Dynkin index.

With the coefficients of the beta function now known, the scale dependence of the running coupling can be investigated in more detail. At lowest order, equation 2.33 results in a differential equation

$$\mu^2 \frac{\partial\alpha_s}{\partial\mu^2} = -\frac{\beta_0}{4\pi} \alpha_s^2 \tag{2.38}$$

for $\alpha_s\left(\mu^2\right)$ which can be solved by separating the variables, yielding

$$\int_{\alpha_s(\mu_0^2)}^{\alpha_s(\mu^2)} \frac{d\alpha_s}{\alpha_s^2} = -\frac{\beta_0}{4\pi} \int_{\mu_0^2}^{\mu^2} \frac{d\mu^2}{\mu^2} \tag{2.39}$$

with a reference scale μ_0. Evaluating the integrals and solving the equation for the running coupling finally gives

$$\alpha_s\left(\mu^2\right) = \frac{\alpha_s\left(\mu_0^2\right)}{1 + \frac{\beta_0}{4\pi}\alpha_s\left(\mu_0^2\right)\ln\left(\frac{\mu^2}{\mu_0^2}\right)} \tag{2.40}$$

where the coupling constant evaluated at the reference scale need to determined experimentally. However, this procedure unfortunately only works at the lowest order, which is why approximation methods are necessary to compute $\alpha_s\left(\mu^2\right)$ at higher orders.

The strong coupling exhibits a remarkable behaviour as implied by its progression as function shown in figure 2.2, which allows to distinguish between two regimes in QCD. At low energies, the strong coupling is increasing significantly. In this particular regime, the interactions between quarks and gluons become sufficiently strong, leading to the occurrence of an effect known as *colour confinement*, which implies that colour-charged states cannot exist in isolation resulting in the absence of free quarks and gluons in nature. On the other hand, QCD shows a property known as *asymptotic freedom*, which was first discovered by David Gross, Frank Wilczek [107] and independently by David Politzer [180] in 1973, at high energies. In this region, the coupling constant becomes small, and the colour charged particles behave quasi-free.

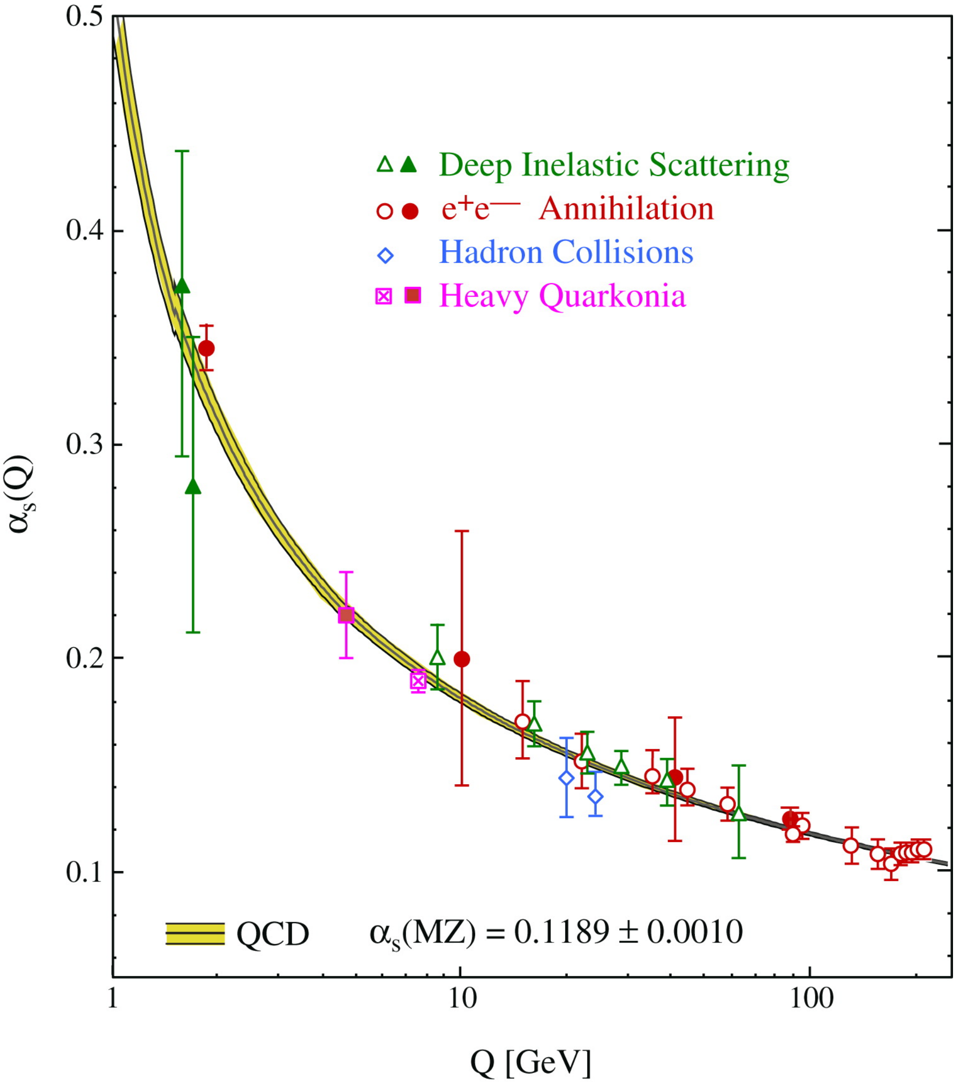

Figure 2.2: Scale dependence of the strong coupling constant α_s. The diagram shows a comparison between experimental data and theoretical predictions. Figure taken from [43].

2.1.3 Basics of Perturbation Theory

As previously stated, the utilization of approximation techniques is inevitable to study QCD and to learn more about the inner structure of hadrons as well as the strong interaction between colour charged particles. One such approach, which has demonstrated its efficacy as a powerful instrument and has been successfully applied numerous times, is provided by the framework of *perturbation theory*, which focuses on the notion of treating the interaction as a minor perturbation of the free theory. In this particular approach, the complete lagrangian L of the theory is subdivided into two distinct components, namely

$$L = L_0 + L_{int} \ , \tag{2.41}$$

where the first contribution L_0 pertains to the lagrangian function of the free theory, while the latter L_{int} describes the interaction. In the same manner, the Hamiltonian H of a system may be written as

$$H = H_0 + H_{int} \ . \tag{2.42}$$

The interaction Hamiltonian H_{int}, that appears in this decomposition, satisfies the Schrödinger-like equation

$$i\frac{d}{dt}\left|\psi(t)\right\rangle_D = H_{int,D}\left|\psi(t)\right\rangle_D \tag{2.43}$$

in the Dirac picture, where $\left|\psi(t)\right\rangle_D$ denotes the system's state vector. The differential equation was first solved by Freeman Dyson in 1949, who therefore introduced the *Dyson series* [76]

$$U_D\big(t, t_0\big) = \mathcal{T}\exp\left\{ -i\int_{t_0}^{t} dt' H_{int,D}\big(t'\big)\right\} \tag{2.44}$$

under the premise that the time evolution of the state is governed by a time-evolution operator $U(t, t_0)$ in such a way that

$$\left|\psi(t)\right\rangle_D = U_D(t, t_0)\left|\psi(t_0)\right\rangle_D \ . \tag{2.45}$$

Here, the time ordering operator $\mathcal{T}$ was introduced.

These fundamental prerequisites establish the foundation to study scattering processes within the framework of perturbation theory. Scattering can now be viewed as the time evolution of a system, starting from an initial state $|i\rangle = |\psi(-\infty)\rangle$ long before the hard process and ending in a final state $|f\rangle = |\psi(+\infty)\rangle$ long after the process. It must be further assumed that these states are unaffected by any interactions and, consequently, can be regarded as free states. In this representation, the cross section of a scattering process is then linked to the probability $\mathscr{P}_{i\to f}$ of a transition from the initial state $|i\rangle$ into the final state $|f\rangle$. By making use of an operator, the S-matrix, which was first introduced by John A. Wheeler [216] in 1937 and later independently developed by Werner Heisenberg [112] in 1943, the transition probability becomes

$$\mathscr{P}_{i\to f} \propto |\, \langle f|\, S - \mathbb{1}\, |i\rangle\, |^2 \ , \tag{2.46}$$

where the S-matrix itself can be introduced through the time evolution operator and may be written as

$$S \equiv U(\infty, -\infty) = \mathcal{T} \exp\left\{ i \int_{-\infty}^{\infty} \mathscr{L}_{int} \right\} \tag{2.47}$$

with $\mathscr{L}_{int}$ representing the lagrangian density of the interaction part. Nonetheless, a more usually employed operator, known as the matrix element $\mathcal{M}_{if}$, has been established for practical purposes. The S-matrix and the matrix element are thereby related via

$$\langle f|\, S - \mathbb{1}\, |i\rangle = (2\pi)^4 i \delta^4 \big(\sum_i p_i - \sum_f p_f \big) \mathcal{M}_{if} \tag{2.48}$$

where the p_i's and p_f's denote the momenta of the particles in the initial, respectively the final state. The cross section then reads

$$\sigma = \frac{1}{F} \int dPS_n |\mathcal{M}_{if}|^2 \tag{2.49}$$

with F being a flux factor and dPS_n denoting the n-body phase space. A common task in perturbation theory is therefore to determine the matrix element and its absolute value squared, which can be determined order by order and then be expressed as a power series in the theory's coupling constant. A suitable method for performing such calculations will be introduced later.

Lastly, the question remains as to when perturbation theory can be applied. As already mentioned previously in the course of the section, the technique relies on the assumption that interactions can be regarded as a minor disturbance. In quantum field theories, the respective coupling constant provides a measure for the strength of the interaction and as discussed in the last section, the strong coupling constant α_s becomes small at high energies. In QCD, perturbation theory can thus be applied at large energy scales where the theory becomes asymptotically free.

2.2 Parton Model and Collinear Factorization

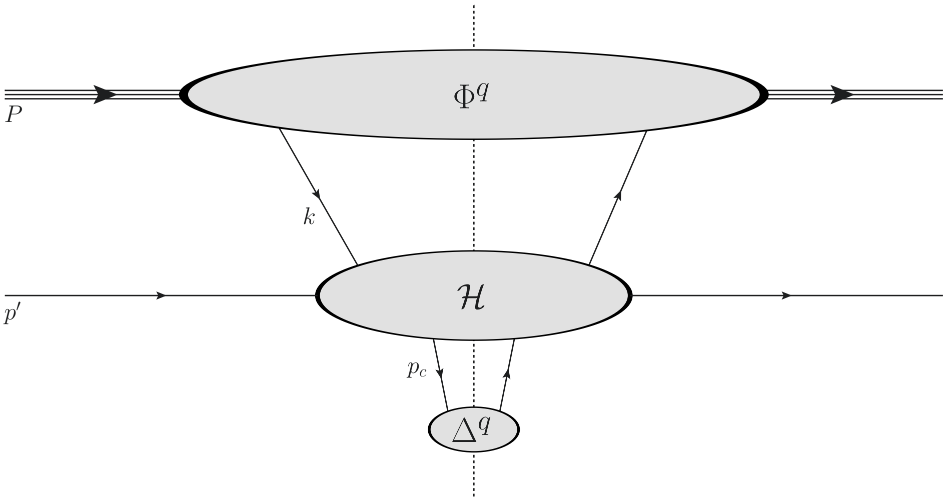

Figure 2.3: Illustration of a generic contribution to single hadron production in lepton-nucleon scattering. The topmost blob represents the incoming nucleon's state. The blob in the middle is representative for the hard scattering process and the bottom blob shows the fragmentation into the hadron.

Towards the end of the 1960s, James Bjorken, who was attempting to explain the Adler sum rule [15] and the Bjorken inequality [44], suggested that the nucleons' structure function shows a scaling behaviour, which is today known as Bjorken scaling in reference to him. More specifically, he suggested that the structure functions behave like [45]

$$\lim_{Q^2\to\infty} \nu W_2(Q^2,\nu) = MF_2(x) \tag{2.50}$$

$$\lim_{Q^2\to\infty} W_1(Q^2,\nu) = F_1(x) \tag{2.51}$$

for a large transferred momentum Q^2, where the fraction ν/Q^2 is assumed to be fixed, and they therefore become functions of only one variable

$$x = \frac{Q^2}{2M\nu} \ , \tag{2.52}$$

the Bjorken scaling variable as implied by the experimental data and theoretical predictions shown in figure 2.4. The behaviour proposed by Bjorken could actually be proven experimentally in the following decades by modern collider experiments, as implied by the data and theoretical predictions from HERA shown in figure 2.4. Nonetheless, the overview of data given in the aforementioned figure also shows a violation of the scaling for both large and small x, which can be attributed to higher order effects in QCD.

It was Richard P. Feynman, who then recognized that the scaling behaviour could be interpreted in such a manner that nucleons are composed of point-like constituents, which he referred to as partons, when he developed the *parton model* [93] to describe high energy scattering. Initially, the identity of these partons remained a mystery, but it is today clear that they are the quarks and gluons of the quark model, which was developed around the same time.
According to the parton model, the components of a hadron can be assigned to one of three classes: valence quarks, sea quarks and gluons. The valence quarks correspond to those from the quark model, which identify a hadron as either a baryon or meson. The sea quarks, on the other hand, are temporary quark-antiquark pairs, which together with the gluons contribute to the hadrons' properties like spin or mass.

The mathematical and quantum field theoretical realization of the parton model is provided by the *collinear factorization theorem.* In the framework of collinear factorization, a cross section of a process including hadrons may be written as a convolution of non-perturbative objects, the parton distribution functions and fragmentation functions, and the appropriate cross section formulated on the level of the partons, which can be calculated perturbatively. It thus reads, for instance,

$$\sigma^{N+N\to h+X} = PDF_1 \otimes PDF_2 \otimes \sigma^{a+b\to c+X} \otimes FF \ , \tag{2.53}$$

$$\sigma^{N+\ell\to h+X} = PDF_1 \otimes \sigma^{a+l\to c+X} \otimes FF \ , \tag{2.54}$$

where the first line delineates the production of a hadron in nucleon-nucleon scattering while the second line provides the cross section for such a production in nucleon-lepton scattering. In order to provide a more comprehensive explanation of the factorization theorem and its associated quantities, i.e. the PDFs and FFs, a formula for the factorized cross section in the case of single hadron production in unpolarized nucleon-lepton scattering will be derived in the following.

For this purpose, it is advisable to work in light cone coordinates, as they simplify the problem. With this in mind, two light-like vectors n and $\bar{n}$ can be introduced which satisfy the relations

$$n^2 = 0,\ n \cdot P_h = 1 \ , \tag{2.55}$$

$$\bar{n}^2 = 0,\ \bar{n} \cdot P = 1 \ , \tag{2.56}$$

where P denotes the incoming nucleon's momentum and P_h is the momentum of the produced hadron. The cross section of the process is generated by contributions such as the one depicted in figure 2.3 and subsequently reads

$$\begin{aligned} d\sigma^{N\ell\to hX} &= \frac{1}{2S}\sum_{a,c}\int\frac{d^4k}{(2\pi)^4}\int\frac{d^4p_c}{(2\pi)^4}\mathcal{H}^{a\ell\to c\ell}_{ij;kl}(k,pc) \\ &\times\left\{\int d^4\xi e^{-ip_c\cdot\xi}\langle 0|\,\psi_{c,l}(0)\bar{\psi}_{c,i}(\xi)\,|0\rangle\right\} \\ &\times\left\{\int d^4\lambda e^{ik\cdot\lambda}\langle P|\,\bar{\psi}_{f,k}(0)\psi_{f,j}(\lambda)\,|P\rangle\right\} \\ &\equiv\frac{1}{2S}\sum_{a,c}\int d^4k\int d^4p_c\Phi^a_{jk}(k)\mathcal{H}_{ij;kl}(k,p_c)\Delta^c_{li}(p_c) \end{aligned} \tag{2.57}$$

in the chosen gauge, where the quark-quark- (qq-)correlator Φ^f and the fragmentation correlator Δ^f have been introduced in the last line. If a covariant gauge is selected in lieu of the light cone gauge, it is inevitable to incorporate Wilson lines [222], which become unity in light cone gauge, into the formal definition of these correlators. They are defined by path ordered exponentiated gluon fields

$$\mathcal{W}[x,y]=\mathscr{P}\exp\left\{ig_s\int_x^y dz_\mu A^\mu(z)\right\}\ , \tag{2.58}$$

with $\mathscr{P}$ being the path ordering operator, and are necessary to guarantee gauge invariance. Next, it is imperative to perform the collinear expansion of the hard scattering function. Against this background, it is assumed that the momenta of the partons are collinear to that of the associated hadrons and can therefore be written as

$$k\approx xP \tag{2.59}$$

$$p_c\approx\frac{1}{z}P_h\ , \tag{2.60}$$

where the variables x and z represent the fractions of the respective hadrons' momenta. The function can now be expanded, whereby only the lowest order contributes to the cross section in the unpolarized process and we are thus led to consider

$$\mathcal{H}^{a\ell\to c\ell}(k,p_c)\approx\mathcal{H}^{a\ell\to c\ell}\left(xP,\frac{1}{z}p_c\right) \tag{2.61}$$

in the factorization formula. With this, the integrals over non-longitudinal components can now be evaluated by writing them as

$$\int d^4k\to\int dx\int d(k\cdot P)d^2k_\perp \tag{2.62}$$

$$\int d^4p_c\to\int\frac{dz}{z^2}\int d(p_c\cdot P_h)d^2p_{c,\perp} \tag{2.63}$$

and making use of the relations

$$\Delta^c_{li}(z) = \int d\big(p_c \cdot P_h\big) \int d^2 p_{c,\perp} \Delta^c_{li}\big(p_c\big) \tag{2.64}$$

$$\Phi^a_{jk}(x) = \int d\big(k \cdot P\big) \int d^2 k_\perp \Phi^a_j k\big(k\big) \tag{2.65}$$

for the qq- and fragmentation-correlators. Finally, it is required that the correlators may be parametrized as [48, 103, 135, 169]

$$\begin{aligned}\Phi^q(x) = \frac{1}{2}\Big\{ & \not{P} f^q_1(x) + M e^q(x) \\ & - M\big(S \cdot \bar{n}\big)\not{P}\gamma_5 g^q_1(x) + \frac{1}{2}M^2\big(S \cdot \bar{n}\big)\big[\not{P}, \not{\bar{n}}\big]\gamma_5 h^q_L(x) \\ & - \frac{1}{2}\big[\not{P}, \not{S}\big]\gamma_5 h^q_1(x) - M\big(\not{S} - \big(S \cdot \bar{n}\big)\not{P}\big)\gamma_5 g^q_T(x)\Big\}\end{aligned} \tag{2.66}$$

and

$$\begin{aligned}\Delta^q(z) = \frac{1}{z}\Big\{ & \not{P}_h D^q_1(z) + M_h E^q(z) + \frac{i}{2} M_h \big[\not{P}_h, \not{n}\big] H^q(z) \\ & - M_h\big(S_h \cdot n\big)\not{P}_h\gamma_5 G^q_1(z) \\ & + \frac{1}{2}M_h^2\big(S_h \cdot n\big)\big[\not{P}_h, \not{n}\big]\gamma_5 H^q_L(z) - M_h^2\big(S_h \cdot n\big) i\gamma_5 E^q_L(z) \\ & - \frac{1}{2}\big[\not{P}_h, \not{S}_h\big]\gamma_5 H^q_1(z) - M_h \varepsilon^{P_h n \alpha S_h}\gamma_\alpha D^q_T(z) \\ & - M_h\big(\not{S}_h - \big(S_h \cdot n\big)\not{P}_h\big)\gamma_5 G^q_T(z)\Big\}\end{aligned} \tag{2.67}$$

where $f^q_1(x)$ and $D^q_1(x)$ represent the usual unpolarized parton density and fragmentation function, respectively. In the remainder of this thesis, the subscripts are omitted and the PDFs and FFs will be denoted by $f^{q/N}(x)$ and $D^{q/h}(z)$. The other functions encountered in these parametrizations will either contribute in spin-polarized processes, like the helicity parton density h_1, or at higher twist. What all these functions have in common is that they cannot be determined by perturbation theory and must instead be extracted from experimental data (see e.g. [38, 39, 123]) or need to be calculated by employing lattice methods (see e.g. [26, 129, 142]). By making use of these parametrizations, the factorized cross section ultimately becomes

$$d\sigma^{N\ell \to hX} = \frac{1}{S}\sum_{a,c}\int \frac{dz}{z^2}\int \frac{dx}{x} f^{a/N}(x) d\sigma^{a\ell \to c\ell} D^{c/h}(z) \tag{2.68}$$

after shifting $\big(\frac{1}{z}\not{P}_h\big)_{li}$ and $\big(\not{P}\big)_{jk}$ into the hard scattering function, which then can be identified as the differential cross section on parton level. In the case that a gluon participates in the hard process, a similar formula is obtained, where only the PDF or the FF must be suitably adjusted depending on the process and replaced by equivalent quantities for gluons.

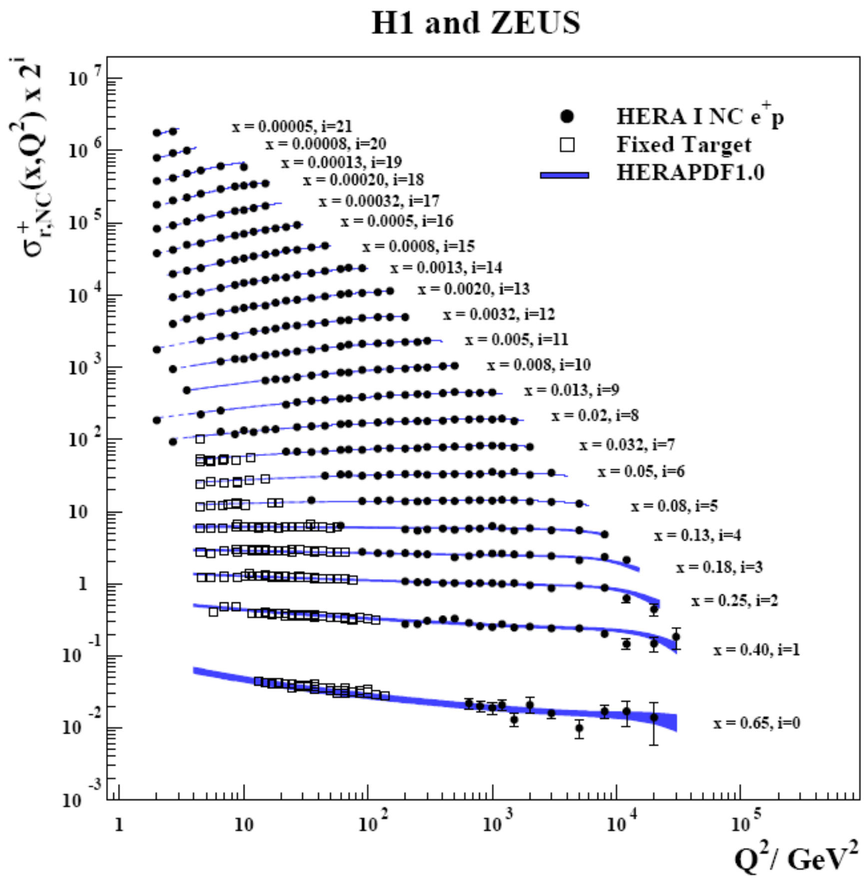

Figure 2.4: Modern DIS data compared to QCD predictions. The diagram shows data from HERA compared to a HERAPDF 1.0 fit. Figure taken from [1].

2.2.1 Evolution of Parton Distribution Functions

Previously, PDFs and FFs were introduced which have a significant impact on numerous applications of pQCD as they serve as a link between long distance and short distance physics and describe the non-perturbative components in factorization theorems. These, as stated before, can only be calculated in the framework of lattice QCD or extracted from experimental data. However, once they have been determined, the attribute of being universal in the sense of being process-independent can be exploited. The remainder of this section will now serve the purpose of presenting the PDFs in greater detail as representatives of both, PDFs as well as FFs, and, most importantly, to examine their scale dependence. The argumentation can be applied to FFs in a similar way. More detailed discussions can be found in [57, 68, 69, 85].

In the Breit frame, also known as infinite momentum frame, the parton distributions become number densities to find a parton carrying a momentum fraction ξ. In general, they are given by

$$f^{j/N}\big(\xi\big) = \int \frac{d\lambda}{2\pi} e^{i\lambda x} \left\langle P\right| \bar{\psi}_j(0) \not{n} \mathcal{W}\big[0, \lambda n\big] \psi_j(\lambda n) \left|P\right\rangle \tag{2.69}$$

for a quark with flavour j and

$$f^{g/N}\big(\xi\big) = \int \frac{d\lambda}{2\pi} e^{i\lambda x} \left\langle P\right| n_\mu F_a^{\mu\nu}(0) \mathcal{W}\big[0, \lambda n\big] n_\rho F^{\rho}_{b\;\nu}(\lambda n) \left|P\right\rangle \tag{2.70}$$

in the case of a gluon where a and b denote colour indices and $\mathcal{W}$ are the Wilson lines needed to ensure gauge invariance. However, since the parton densities depend on UV divergent operator products, they require renormalization. The reason for this is that these distributions were integrated over transverse momentum components $k_\perp$, as it can be guessed from the equations 2.65 and 2.66, and the integrand diverges for large $k_\perp$. Once again, the renormalization procedure introduces an arbitrary scale, the factorization scale μ_f, and makes the PDFs dependent on it. Today, the behaviour of the PDFs with a varying energy scale is well understood and is governed by the Dokshitzer-Gribov-Lipatov-Altarelli-Parisi (DGLAP) evolution equations [28, 75, 105], which will be discussed in the following.

As seen before for other quantities, the renormalized parton distribution $f^{j/N}\big(\xi, \mu_f^2\big)$ can be introduced in a multiplicative way.

It may be expressed as [65, 66]

$$\begin{aligned} f^{j/N}(\xi, \mu_f^2) &= \frac{\alpha_s(\mu_f^2)}{2\pi} \Big\{ \sum_k Z_{jk} \otimes f^{k/N} \Big\}(\xi) \\ &= \frac{\alpha_s(\mu_f^2)}{2\pi} \sum_k \int_\xi^1 \frac{d\zeta}{\zeta} Z_{jk}(\zeta, \alpha_s(\mu^2)) f^{k/N}\left(\frac{\xi}{\zeta}\right) \end{aligned} \tag{2.71}$$

where the multiplication thus has to be understood as a convolution of the bare function and an appropriate renormalization constant Z_{jk}. The determination of the scale dependence of the PDFs now essentially follows the same line of reasoning that was already used in the case of the coupling constant. Likewise, RG invariance is demanded and one obtains

$$\frac{d}{d\ln(\mu_f^2)} f^{j/N}(\xi, \mu_f) = \frac{\alpha_s(\mu_f^2)}{2\pi} \sum_k \int_\xi^1 \frac{d\zeta}{\zeta} P_{jk}(\zeta, \alpha_s(\mu_f^2)) f^{k/N}\left(\frac{\xi}{\zeta}\right) \tag{2.72}$$

after employing the operator $d/d\ln(\mu_f^2)$ with the splitting-kernel

$$P_{jk}(\zeta, \alpha_s(\mu_f^2)) \equiv \frac{d}{d\ln(\mu_f^2)} Z_{jk}(\zeta, \alpha_s(\mu_f^2)) \; . \tag{2.73}$$

The splitting function describes the probability for a parton to split into another one with a momentum fraction ζ and can be expressed as a perturbative expansion in α_s as

$$P_{jk}(\zeta, \alpha_s(\mu_f^2)) = P_{jk}^{(0)}(\zeta) + \frac{\alpha_s(\mu_f^2)}{2\pi} P_{jk}^{(1)}(\zeta) + \ldots \tag{2.74}$$

Nevertheless, the evolution equation given in 2.72 strictly applies only to the non-singlet quark distributions q^{ns}. In general, the DGLAP evolution equation is a $(2n_f + 1)$-dimensional matrix equation and reads

$$\frac{\partial}{\partial \ln(\mu_f^2)} \begin{pmatrix} q_i \\ g \end{pmatrix} = \frac{\alpha_s(\mu_f^2)}{2\pi} \sum_{j=1}^{2n_f} \begin{pmatrix} P_{q_i q_j} & P_{q_i g} \\ P_{g q_j} & P_{gg} \end{pmatrix} \otimes \begin{pmatrix} q_j \\ g \end{pmatrix} \tag{2.75}$$

where q_i and g denote the quark respectively gluon distribution and the convolution has to be understood similar as previously in equation 2.71. Furthermore, it must be noted that the sum arising in this equation runs over all quark flavours $j = u, \bar{u}, d, \bar{d}, ...$ In addition, it is common to represent the evolution equation in a different basis, which utilizes the singlet quark distribution

$$\Sigma(\xi, \mu_f^2) \equiv \sum_i \Big[q_i(x, \mu_f^2) + \bar{q}_i(x, \mu_f^2) \Big] \; . \tag{2.76}$$

The evolution equation then becomes

$$\frac{\partial}{\partial \ln\left(\mu_f^2\right)} \begin{pmatrix} \Sigma \\ g \end{pmatrix} = \frac{\alpha_s(\mu_f^2)}{2\pi} \begin{pmatrix} P_{qq} & P_{qg} \\ P_{gq} & P_{gg} \end{pmatrix} \otimes \begin{pmatrix} \Sigma \\ g \end{pmatrix} . \tag{2.77}$$

Finally, the splitting function can be calculated by making use of perturbative techniques. Today, they are known up to three loop level [168, 212, 213] and progress has been recently made in computing them at four loop level [88, 89, 166, 167]. Hence, they are evidently known in leading order, where they are given by

$$P_{qq}^{(0)}(\xi) = C_F\left(\frac{1+\xi^2}{(1-\xi)_+} + \frac{3}{2}\delta(1-\xi)\right) \tag{2.78}$$

$$P_{qg}^{(0)}(\xi) = T_R\big(\xi^2 + (1-\xi)^2\big) \tag{2.79}$$

$$P_{gq}^{(0)}(\xi) = C_F\left(\frac{1+(1-\xi)^2}{\xi}\right) \tag{2.80}$$

$$\begin{aligned} P_{gg}^{(0)}(\xi) = 2C_A&\left(\frac{1-\xi}{\xi} + \xi(1-\xi) + \frac{\xi}{(1-\xi)_+}\right) \\ &+ \left(\frac{11}{6}C_A - \frac{1}{3}n_f\right)\delta(1-\xi) \end{aligned} \tag{2.81}$$

where $(1-\xi)_+$ denotes the plus distribution. A more detailed introduction to the distribution can be found in appendix D. Thanks to the now known splitting functions and evolution equations, it is sufficient to determine the parton distributions at a reference value for the scale, which allows to evolve the PDFs to any other scale.

2.2.2 Higher twist

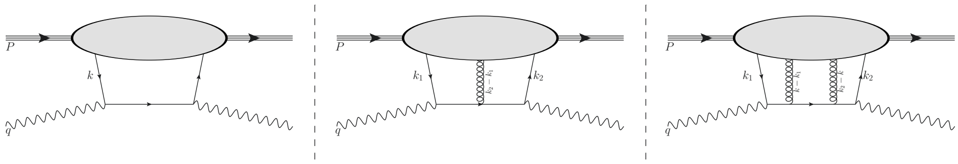

Figure 2.5: Generic contributions to deep inelastic scattering (DIS). The diagrams show generic twist-2, twist-3 and twist-4 contributions to DIS from left to right.

The factorization as presented up to this point actually only represents the leading-power contribution and so far it has been concealed that there are further contributions in QCD. These contributions are usually suppressed by powers of the hard scale $1/Q$ and for most applications the leading power is sufficient. Today, the term *twist* is commonly used to refer to the different contributions to factorization. The notion of twist was first introduced by Gross and Treiman in 1971 [106] as the difference between an operator's dimension and spin, i.e.

$$\tau = d - s \ , \tag{2.82}$$

where τ denotes the twist, d the dimension and s the spin. In our modern understanding, the term is used to designate the various contributions to factorization. Here, the leading contribution, which is usually studied in the case of many physical processes and provides the factorization theorem as presented earlier, is called twist-2. The contribution that is suppressed by $1/Q$ is referred to as twist-3, the contribution that is suppressed by $1/Q^2$ is referred to as twist-4, and so on. Figure 2.5 shows some generic twist-2, twist-3 and twist-4 contributions to the cross section for deep inelastic scattering (DIS). They may be written as

$$\sigma_{\mathrm{twist-2}} \sim \Phi^{(2)}(k) \otimes \sigma \tag{2.83}$$

$$\sigma_{\mathrm{twist-3}} \sim \Phi^{(3)}(k_1, k_2) \otimes \sigma \tag{2.84}$$

$$\sigma_{\mathrm{twist-4}} \sim \Phi^{(4)}(k) \otimes \sigma \tag{2.85}$$

in a symbolic way as a convolution of a hard scattering function and a twist-2, twist-3 respectively twist-4 correlator. In case of the leading power contribution, the hard scattering function is the usual differential cross section.

Early studies on higher twist contributions focused on the twist-4 contribution to unpolarized DIS (see e.g. [83, 84, 126, 184]) as the first non-leading twist in this case. Twist-3 on the other hand plays a significant role in certain spin polarized processes.

As Plitzer pointed out already in 1980 [181], studying higher twist contributions can provide new insights into the inner structure of hadrons as they

are associated with correlations between partons and quantum interference effect. Factorization at higher twist requires the extension of the ordinary PDFs to multi-parton correlation functions and the introduction of appropriate non-perturbative matrix elements. At twist-3 level, one therefore encounters qqq- and qgq-correlators and at twist-4 qqqq- and qggq-correlators. The evolution equations for all twist-3 and twist-4 functions are nowadays known [54, 58, 59, 197, 198].
In this context, twist-3 collinear factorization is of particular interest, as it is directly accessible through a physical observable. These are transverse single spin asymmetries. However, as multiparton-correlations depend on more than one fractional momentum, studying the suitable processes is much more complicated and can become tedious.

Chapter 3

Methods

Chapter 3

Methods

In the preceding chapter, the theoretical framework that forms the foundation of the thesis at hand was presented. However, the main focus of the work is on the application of these concepts, particularly perturbation theory and collinear factorization, to study scattering processes and to compute predictions for cross section as well as spin asymmetries. For this reason, the present chapter serves the purpose of providing a brief overview of the methods and techniques which are crucial for such considerations and commonly employed in the domain of high-energy physics.

As demonstrated in section 2.1.3 of the last chapter, the matrix element as well as its squared absolute value hold paramount significance in determining cross sections and can be calculated order by order within the framework of perturbation theory. The first section of this chapter therefore presents a method that permits such computations to be carried out conveniently at a fixed order.
Once the squared absolute value of the matrix element has been found, it must be integrated over the phase space of the particles in the final state. In our case, the two- and three-body phase space will be needed and hence being discussed in the second section.
As it will turn out, considerations in the leading order of perturbation theory are usually quite straightforward. In higher orders, however, as already stated previously, divergent contributions occur. After the UV divergences are treated by renormalizing the theory, namely QCD, and the IR singularities cancel each other out by summing up all virtual and real corrections, collinear divergent contributions remain. They are then subtracted as part of the factorization and shifted into the PDFs and FFs. The procedures required for this purpose are the primary focus of the third and concluding section of this chapter.

3.1 Feynman Diagrams

As demonstrated in chapter 2.1.3, the calculation of the squared absolute value of the matrix element holds a central significance in the context of perturbation theory, and consequently, for practical applications of QCD and most other quantum field theories. A large portion of applications of pQCD hence entail the calculation of such matrix elements, resulting in a great demand for appropriate techniques. The remainder of this chapter therefore serves the purpose of presenting such a method in more detail, which stands out due to its exceptional practicality and traces its roots back to Feynman.

Feynman introduced the so-called Feynman diagrams as pictorial representations for scattering processes and proposed a prescription for calculating the amplitude for any given diagram. Furthermore, the diagrams provide additional insights into the physical process, thereby facilitating their interpretation. Particles interact in every possible way through the interchange of virtual particles, where each possible interaction is linked to a distinct diagram. Each component of such an illustration can be assigned to one of three classes: external lines, internal lines and vertices, respectively. External lines represent real incoming or outgoing particles. On the other hand, internal lines are associated with the virtual particles that are exchanged in the course of the interactions. Lastly, the points of interaction, where several lines meet, are called vertices. In particular, the momentum is conserved at these intersections.
Each topological feature is associated with a mathematical term in the matrix element and the necessary prescription are called Feynman rules. In general, the Feynman rules can be derived from the generating functional of the theory, and the procedure required for this is described in great detail in [179]. At this point, they are instead merely motivated, following the line of argumentation as presented in [98, 111], by making use of the action

$$S = i \int d^4x \mathscr{L}_{\text{QCD}} \ , \tag{3.1}$$

whereby two examples are considered. As a first example, the quark propagator will be considered, for which the term $\sim \big(\bar{\psi}_f \big(i\partial\!\!\!/ - m_f\big)\psi_f\big)$ from the lagrangian as given in equation 2.16 must be examined. Inserting the Fourier transforms

$$\psi_f(x) = \int \frac{d^4p}{(2\pi)^4} e^{-ip\cdot x}\Phi_f(p) \tag{3.2}$$

of the quark fields allows to first carry out the spatial integration, which yields a delta function $\delta(p - p')$. With its help, one of the momentum integrals, stemming from the Fourier transforms, can then be evaluated, and an expression of the form

$$\int \frac{d^4p}{(2\pi)^4} \bar{\Phi}_f(p) \{ \not{p} - m \} \Phi_f(p) \tag{3.3}$$

finally remains from the contribution in the action. In essence, this enables the extraction of the inverse quark propagator in momentum space, which corresponds to the expression enclosed in curly brackets. The quark propagator thus reads

$$S_0(p) = \frac{i(\not{p} + m)}{p^2 - m^2 + i\varepsilon} \, , \tag{3.4}$$

where the $i\varepsilon$ prescription is a convenient way to take the pole at $p^2 = m^2$ into account by slightly shifting it off the real axis into the complex plane.

In complete analogy, the gluon propagator $\Delta_{\mu\nu}$ can be constructed from the contribution bilinear in the gluon fields $A_\mu A_\nu$, which is encountered in the term $\sim \frac{1}{4} G^a_{\mu\nu} G^{\mu\nu}_a$ of the lagrangian. Following the procedure as outlined for the quark propagator, we are led to consider the condition

$$i\Delta_{\mu\nu}(p) \{ p^2 g^{\nu\rho} - p^\nu p^\rho \} = g^\rho_\mu \tag{3.5}$$

in momentum space. However, since the term in curly brackets is not invertible, the expression is by no means sufficient to define a proper gluon propagator. As outlined previously in chapter 2.1, a gauge-fixing term has to be added to remove unphysical degrees of freedom. In a covariant gauge, such a term may be written as

$$\mathscr{L}_{\text{gauge-fixing}} = -\frac{1}{2\xi} \left(\partial_\mu A^\mu_a \right)^2 \tag{3.6}$$

and the gluon propagator thus becomes

$$\Delta_{\mu\nu}(p) = \frac{-i}{p^2 + i\varepsilon} \left\{ g_{\mu\nu} - \left(1 - \xi\right) \frac{p_\mu p_\nu}{p^2} \right\} \, . \tag{3.7}$$

Another common choice of gauge is an axial gauge which can be introduced by a gauge-fixing langrangian of the form

$$\mathscr{L}_{\text{gauge-fixing}} = -\frac{1}{2\xi} \left(n_\mu A^\mu_a \right)^2 \tag{3.8}$$

where n denotes an arbitrary four-vector with $p \cdot n \neq 0$. In this case the gluon propagator reads

$$\Delta_{\mu\nu}(p) = \frac{-i}{p^2 + i\varepsilon} \left\{ g_{\mu\nu} - \frac{n_\mu p_\nu + n_\nu p_\mu}{n \cdot p} + n^2 \frac{p_\mu p_\nu}{(p \cdot n)^2} \right\} \, . \tag{3.9}$$

A particularly advantageous choice for an axial gauge, which is also utilized in this thesis, is the light-cone gauge, where the vector n becomes light-like and thus needs to satisfy the condition $n^2 = 0$. A summary of the Feynman rules of QCD is given in appendix A. They are taken from [94]. The rules of QED are similar but above all simpler, since no colour structure can occur. Moreover, there are no equivalents to the three- and four-gluon vertices, as there can be no photon-photon interaction.

These rules now basically allow the computation of the matrix element as well as its absolute squared value for any given process. Nonetheless, it should not go unmentioned that products of spinors and gamma matrices occur in the context of such calculations and that methods for dealing with them are therefore required. One such technique is known as Casimir's trick, named after Hendrik Casimir. It makes use of the completeness relations

$$\sum_s u^{(s)}(p)\bar{u}^{(s)}(p) = \not{p} + m \tag{3.10}$$

$$\sum_s v^{(s)}(p)\bar{v}^{(s)}(p) = \not{p} - m \tag{3.11}$$

for the spinors of particles, respectively antiparticles, to rewrite the arising products in terms of traces of gamma matrices. Applying the trick to, for example, a product as it might occur in the leading order of perturbation theory gives

$$\sum_{s_1,s_2} \left(\bar{u}^{(s_1)}(p)\gamma^\mu u^{(s_2)}(k)\right)\left(\bar{u}^{(s_2)}(k)\gamma^\nu u^{(s_1)}(p)\right) = \mathrm{Tr}\left[\not{p}\gamma^\mu \not{k}\gamma^\nu\right] \tag{3.12}$$

for two massless particles with momenta p and k. It can therefore be surmised that a central as well as time-consuming task in perturbative considerations is the calculation of such traces. Fortunately, this task no longer have to be done by hand nowadays and can instead be accomplished through the utilization of computer algebra systems. For this purpose, the software system Wolfram Mathematica is used together with the packages Tracer [128], FeynCalc [165, 195, 196] and Package-X [177] in this work.

3.2 Phase Space

Once the spin and colour averaged matrix element, as well as its absolute value squared, are determined, the subsequent step is to integrate it over the phase space of the final-state particles, since the cross section and the matrix element are intertwined in this manner, as shown in equation 2.49. The phase space represents the mathematical space of all possible momenta of the particles in the final state. It therefore takes into account the limited knowledge about the final state and the resulting need to sum over all permitted configurations when computing a physical observable. For an arbitrary scattering process with n_i particles in the initial state and n_f massless particles in the final state, it is given by

$$dPS_{n_f} = \left(\prod_{f=1}^{n_f} \frac{d^d p_{n_f}}{(2\pi)^{d-1}} \delta\big(p_f^2\big) \right) (2\pi)^d \delta^{(d)} \big(\sum_{i=1}^{n_i} p_i - \sum_{f=1}^{n_f} p_f \big) \tag{3.13}$$

in d dimensions, where the p_i's denote the momenta of the incoming particles and the p_f's represent those of the outgoing particles. The focus of this thesis is on the study of lepton nucleon scattering in leading and next-to-leading order for the unpolarized process but also in the case where the nucleon is transversely spin-polarized. As it will be seen, this requires the two-body phase space for the tree-level amplitude and the virtual corrections on the one hand but also the three-body phase space for the real corrections on the other hand, which for this reason are examined in more detail in this section and the following two subsections. Our considerations will commence with the examination of the two-body phase space in the first subsection, which proves to be exceptionally simple and straightforward to handle. This is particularly true in comparison to the three-body phase space, which is the focus of the second subsection. The primary object of the second section and thus the treatment of the three-body phase space will be the reduction of the momentum integrals to two angular integrals and the derivation of a standard expression. The approach provides the advantage that the occurring matrix elements can always be rearranged in such a way that the integrand takes on a form for which the solutions of the angular integrals are well known. However, during the process of reorganizing the matrix elements, it is imperative to apply partial fraction decomposition extensively before parameterizations for the various particle momenta can be inserted and the integrals can finally be solved.

3.2.1 Two-Body Phase Space

When computing the Born cross section or the virtual next-to-leading order corrections, the two-body phase space integral is required, which reads

$$\int dPS_2 = \int \frac{d^d k_1}{(2\pi)^{d-1}} \int \frac{d^d k_2}{(2\pi)^{d-1}} \delta\big(k_1^2\big)\delta\big(k_2^2\big)\big(2\pi\big)^d \delta^{(d)}\big(p + p' - k_1 - k_2\big) \tag{3.14}$$

as it follows from equation 3.13 for an arbitrary $2 \to 2$ process of the form

$$a(p) + b(p') \to c(k_1) + d(k_2)$$

where a, b, c and d represent some unspecified massless particles with momenta p, p', k_1 and k_2. The d-dimensional δ-function arising in this expression is needed to take the momentum conservation into account as it applies in the process. But the function can also be employed to carry out the integral over the momentum k_2 and we are thus left with the k_1-integration. To evaluate the remaining integral two steps are needed. First, it turns out as convenient and beneficial for the problem to choose the center-of-mass frame of the two incoming particles a and b. In this frame, the momenta p and p' of the initial state particles may be written as

$$p = \frac{\sqrt{s}}{2}\big(1, 0, 0, 1, 0, ...\big) \tag{3.15}$$

$$p' = \frac{\sqrt{s}}{2}\big(1, 0, 0, -1, 0, ...\big) \tag{3.16}$$

where the Mandelstam variable

$$s \equiv \big(p + p'\big)^2 \approx 2p \cdot p' \tag{3.17}$$

was introduced which in this specific frame can be related to the center-of-mass energy of the incoming particles. Next, the d-dimensional momentum and the associated integral can be decomposed into an energy component k_1^0 and its $d-1$ spatial components $\vec{k}_1$. This approach allows to use the δ-function $\delta\big(k_2^2\big) = \delta\big(s - 2\sqrt{s}k_1^0\big)$, which originally guaranteed the on-shell condition for particle d, to evaluate the integral over the energy component as its argument now solely depends on s and k_1^0 after the latter steps. The remaining spatial integration can be carried out in $d-1$-dimensional spherical coordinates and one finally obtains

$$\frac{dPS_2}{dtdu} = \frac{1}{2s}\frac{1}{\Gamma\big[1-\varepsilon\big]}\left(\frac{1}{4\pi}\right)^{1-\varepsilon}\left\{\frac{tu}{s}\right\}^{-\varepsilon}\delta\big(s + t + u\big) \tag{3.18}$$

by introducing the additional Mandelstam variables

$$t \equiv \big(p - k_1\big)^2 = -\frac{s}{2}\big(1 - \cos(\vartheta)\big) \tag{3.19}$$

$$u \equiv \big(p' - k_1\big)^2 = -\frac{s}{2}\big(1 + \cos(\vartheta)\big) \tag{3.20}$$

where ϑ denotes the scattering angle of particle c.

3.2.2 Three-Body Phase Space

When addressing the real next-to-leading order corrections, we will be faced with handling $2 \to 3$ scattering, i.e. processes of the type

$$a(p) + b(p') \to c(k_1) + d(k_2) + e(k_3) \ ,$$

where all particles involved in the hard scattering are assumed to be massless. Consequently, the lorentz invariant three-body phase space integral will arise in the computation of the cross section, which may be written as

$$\int dPS_3 = \int \frac{d^d k_1}{(2\pi)^{d-1}} \int \frac{d^d k_2}{(2\pi)^{d-1}} \int \frac{d^d k_3}{(2\pi)^{d-1}} \delta\big(k_1^2\big)\delta\big(k_2^2\big)\delta\big(k_3^2\big) \\ \times \big(2\pi\big)^d \delta^{(d)}\big(p + p' - k_1 - k_2 - k_3\big) \tag{3.21}$$

as it can be derived from equation 3.13. Here, the d-dimensional δ-function again ensures momentum conservation, and the three δ-functions over squared momenta are linked to the on-shell conditions of the particles in the final-state. The aim of this subsection is now to acquire a better understanding of the three-body phase space and to derive a formula which can be employed in practical applications to integrate the squared matrix element. In light of this, we closely follow the procedure outlined in [34, 35]. Against this background, two quantities are defined by

$$k_{23} \equiv k_2 + k_3 \tag{3.22}$$

$$s_{23} \equiv k_{23}^2 = \big(k_2 + k_3\big)^2 \tag{3.23}$$

where the first one is a d-momentum. It is evident from their definitions that they satisfy

$$1 = \int d^d k_{23} \delta^{(d)}\big(k_{23} - k_2 - k_3\big) \tag{3.24}$$

$$1 = \int ds_{23} \delta\big(s_{23} - k_{23}^2\big) \tag{3.25}$$

and the phase space integral can thus be written as

$$\int dPS_3 = \int ds_{23} \int d^d k_{23} \int \frac{d^d k_1}{(2\pi)^{d-1}} \delta\big(k_1^2\big)\delta\big(s_{23} - k_{23}^2\big) \\ \times \delta\big(p + p' - k_1 - k_{23}\big) \Bigg\{ \int \frac{d^d k_2}{(2\pi)^{d-1}} \int \frac{d^d k_3}{(2\pi)^{d-1}} \delta\big(k_2^2\big) \\ \times \delta\big(k_3^2\big) \big(2\pi\big)^d \delta^{(d)}\big(k_{23} - k_2 - k_3\big) \Bigg\} \tag{3.26}$$

after inserting the relations for k_{23} and s_{23}. In this approach, the phase space is thus decomposed into two parts, and therefore the $2 \to 3$ process is treated as a $2 \to 2$ scattering process immediately followed by a $1 \to 2$ decay of the particle with momentum k_{23}.

For the further treatment, the expression $\mathscr{I}_{1\to2}$ in curly brackets, which is related to the $1 \to 2$ decay, will be investigated in more detail. The procedure needed to deal with this contribution is almost identical to the one which was used for the two-body phase space and presented in the preceding chapter. To begin with, the δ-function is employed to evaluate the integral over the momentum k_3 before the center-of-mass frame of the two outgoing particles d and e is used in order to simplify the remaining integrand. In the center-of-mass frame of the two particles, one obtains

$$\mathscr{I}_{1\to2} = \big(2\pi\big)^{2-d} \int dE_d \int d^{d-1}\vec{k}_2\, \delta\big(E_d^2 - \vec{k}_2^2\big)\delta\big(s_{23} - 2\sqrt{s_{23}}E_d\big) \tag{3.27}$$

with E_d being the energy of particle d. Again, the integral over the energy E_d is straightforward to evaluate. The remaining integration over spatial components can be carried out by making use of spherical coordinates, resulting in the final outcome of

$$\begin{aligned}\mathscr{I}_{1\to2} &= \frac{4^{2-d}\pi^{(1-d)/2}}{\Gamma\big(\frac{d}{2}-\frac{3}{2}\big)}\big(k_{23}^2\big)^{\frac{d}{2}-2}\int_0^\pi d\vartheta_1 \int_0^\pi d\vartheta_2 \sin^{d-3}\big(\vartheta_1\big)\sin^{d-4}\big(\vartheta_2\big)\\ &\equiv \frac{4^{2-d}\pi^{(1-d)/2}}{\Gamma\big(\frac{d}{2}-\frac{3}{2}\big)}\big(k_{23}^2\big)^{\frac{d}{2}-2}\mathscr{I}_{\vartheta_1,\vartheta_2}\end{aligned} \tag{3.28}$$

for this part of the three-body phase space. With this interim result, we return to examining the complete phase space where it is left to handle the integral over the momentum k_1 since the other two integrals over k_{23} and s_{23} can be calculated by utilizing the δ-functions. The full phase space thus becomes

$$\int dPS_3 = \frac{4^{2-d}\pi^{(1-d)/2}}{(2\pi)^{d-1}\Gamma\big(\frac{d}{2}-\frac{3}{2}\big)}\int d^dk_1\delta\big(k_1^2\big)\big\{s+t+u\big\}^{\frac{d}{2}-2}\mathscr{I}_{\vartheta_1,\vartheta_2} \tag{3.29}$$

where the three Mandelstam variables

$$s \equiv \big(p+p'\big)^2 \tag{3.30}$$

$$t \equiv \big(p-k_1\big)^2 \tag{3.31}$$

$$u \equiv \big(p'-k_1\big)^2 \tag{3.32}$$

have been introduced. To solve the k_1 integral, it is beneficial to work in the center-of-mass frame of the two particles in the initial state and to write the momentum k_1 as

$$k_1 = E_c\big(1, 0, \sin(\varphi_1)\cos(\varphi_2), \cos(\varphi_1), ...\big)\ , \tag{3.33}$$

which makes it possible to reduce the integration to two integrals, one over the energy E_c and the other over the angle φ_1. Finally, two new variables v, w are usually introduced via

$$v = 1 + \frac{t}{s} \text{ and } w = -\frac{u}{s+t} \tag{3.34}$$

and the phase space is reformulated in terms of these variables as well as the angles ϑ_1 and ϑ_2. It thus becomes

$$\begin{aligned}\frac{dPS_3}{dvdw} =& \frac{s}{(4\pi)^4\Gamma(1-2\varepsilon)}\left(\frac{4\pi}{s}\right)^{2\varepsilon} v^{1-2\varepsilon}(1-v)^{-\varepsilon}w^{-\varepsilon}(1-w)^{-\varepsilon} \\ &\times \int_0^\pi d\vartheta_1 \int_0^\pi d\vartheta_2 \sin^{1-2\varepsilon}(\vartheta_1)\sin^{-2\varepsilon}(\vartheta_2)\end{aligned} \tag{3.35}$$

in $d = 4 - 2\varepsilon$ dimensions.

When doing calculations in higher orders of perturbation theory, solving the angular integrals can purport to be another time-consuming task. Among other things, this is due to the fact that the matrix elements after the calculation via the Feynman rules exhibit a form that is usually unsuitable for the direct evaluation of the angular integrals. Instead, the excessive use of partial fraction decomposition is necessary to rearrange the matrix element. Through this procedure, the resulting expressions can be reorganized such that most of the arising angular integrals reduce to the basic integral

$$\begin{aligned}\Omega_{j,k} \equiv& \int_0^\pi d\vartheta_1 \int_0^\pi d\vartheta_2 \sin^{1-2\varepsilon}(\vartheta_1)\sin^{-2\varepsilon}(\vartheta_2) \\ & \frac{1}{\big(1-\cos(\vartheta_1)\big)^j\big(1-\cos(\vartheta_1)\cos(\chi)-\sin(\vartheta_1)\cos(\vartheta_2)\sin(\chi)\big)^k},\end{aligned} \tag{3.36}$$

where j and k are some integers and χ denote an additional angle. The solution of this integral is well-known and given by

$$\begin{aligned}\Omega_{j,k} =& 2\pi\frac{\Gamma(1-2\varepsilon)}{\Gamma(1-\varepsilon)^2}2^{-j-k}B\big(1-\varepsilon-j, 1-\varepsilon-k\big) \\ &\times {}_2F_1\left(j,k,1-\varepsilon,\cos^2(\tfrac{\chi}{2})\right)\end{aligned} \tag{3.37}$$

with B being the Beta function and ${}_2F_1$ the hypergeometric function. Other than the partial fraction decomposition, parametrizations for the momenta are also required in this context. More details on the techniques needed to solve the angular integrals especially on the momentum parametrizations are given in the appendices B and C.
Besides the standard integral given in equation 3.36, a slightly more general variant is needed for certain contributions, which occur in particular in the case of the spin-dependent cross section for the process where the incoming nucleon is transversally spin-polarized. The required formulation of the angular integrals is known from [42] and reads

$$\begin{aligned}I_n^{(k,l)} =& \int_0^\pi d\vartheta_1 \int_0^\pi d\vartheta_2 \sin^{n-3}(\vartheta_1)\sin^{n-4}(\vartheta_2)\big(a+b\cos(\vartheta_1)\big)^{-k} \\ &\times \big(A+B\cos(\vartheta_1)+C\sin(\vartheta_1)\cos(\vartheta_2)\big)^{-l}\end{aligned} \tag{3.38}$$

where the coefficients are functions of the external kinematic variables.

The solutions of said integrals are basically known and listed in the appendix of the last-mentioned paper. As it can be seen from the aforementioned list, they can be divided into three distinct categories, depending on whether and how the coefficients are related to each other. Unfortunately, not all integrals that we need can be found in this list. But it turns out that relations to known integrals via derivatives exist, making it straightforward to calculate them. Following the notation proposed in [42], we would need the integral $\tilde{I}^{(3,1)}_{4-2\varepsilon}$ which belongs to group 3 in the previously mentioned classification scheme. But since the coefficients a and b are not related to each other for integrals in this group, the derivative with respect to a can be taken without difficulty, yielding

$$\begin{aligned}
&\frac{\partial^2}{\partial a^2}\tilde{I}^{(1,1)}_{4-2\varepsilon}\\
&= 2\int_0^\pi d\vartheta_1 \int_0^\pi d\vartheta_2 \frac{\sin^{1-2\varepsilon}\left(\vartheta_1\right)\sin^{-2\varepsilon}\left(\vartheta_2\right)\big(a+b\cos(\vartheta_1)\big)^{-3}}{\big(A+B\cos(\vartheta_1)+C\sin(\vartheta_1)\cos(\vartheta_2)\big)}\\
&= 2\tilde{I}^{(3,1)}_{4-2\varepsilon}\ ,
\end{aligned} \tag{3.39}$$

where the solution of $\tilde{I}^{(1,1)}_{4-2\varepsilon}$ is already known. We thus obtain the relation

$$\tilde{I}^{(3,1)}_{4-2\varepsilon} = \frac{1}{2}\frac{\partial^2}{\partial a^2}\tilde{I}^{(1,1)}_{4-2\varepsilon} \tag{3.40}$$

or more generally

$$\tilde{I}^{(n+1,1)}_{4-2\varepsilon} = \frac{1}{n!}\frac{\partial^n}{\partial a^n}\tilde{I}^{(1,1)}_{4-2\varepsilon} \tag{3.41}$$

for a positive integer n. As similar relations can be found for the other unknown integrals, we now possess the necessary components to solve all encountered angular integrals.

3.3 Subtraction of Collinear Divergences

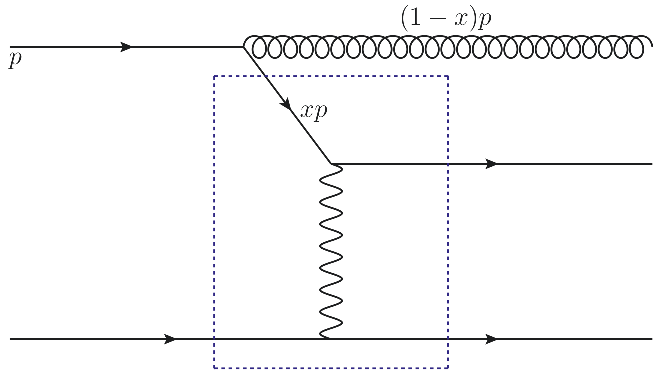

Figure 3.1: Generic collinear configuration. The diagram shows a configuration as it could arise in lepton-nucleon scattering, which is associated with a singularity due to the collinear emission of a gluon by the incoming quark. The blue dotted box indicates the Born cross section that will be convoluted with an appropriate splitting function to subtract the collinear divergence.

In the study of QCD and the application of perturbation theory, another significant obstacle lies in the handling of collinear divergences, which persist after the UV singularities have been addressed during the renormalization of the theory, and the soft divergences have been cancelled between virtual and real corrections to the same order of perturbation theory. They appear as $1/\varepsilon$-poles and arise due to configuration where two external legs become collinear, i.e. when a particle is emitted collinearly to another one. However, collinear divergences do not affect predictive power of QCD for physical observables since techniques have been developed to handle these singularities, ensuring that the limit $\varepsilon \to 0$ can be safely taken and the observables calculated in the framework of pQCD remain finite as well as physically meaningful. A powerful tool to address them is provided by the collinear factorization theorem, which allows to separate long- and short-distance effects and was already introduced in chapter 2.2. The remainder of this section serves the purpose to delve deeper into the nature of collinear divergences and explore how the collinear factorization theorem can be effectively employed to manage them as this understanding is crucial to successfully apply pQCD and ultimately, to gain accurate predictions.
Figure 3.1 shows a generic contribution and illustrates the basic structure responsible for collinear divergences. In the depicted example the singularity is caused by the collinear emission of a gluon by the incoming quark. Of course, equivalent configurations can occur on the other external legs giving rise of further collinear divergences and thus need to be taken into account, too. Nonetheless, the example from the figure will be used in the following to introduce the necessary techniques in more detail.

The procedure relies on the fact that pQCD enables to determine the cross section of partonic reactions although cross sections of hadronic processes are actually of interest since they represent the physical meaningful quantity and can be observed experimentally. It must therefore be demanded that hadronic cross sections, as physical observables, are free of singularities and thus finite. In the framework of factorization, they are written as convolutions of non-perturbative objects, the parton distributions and fragmentation functions, and partonic cross sections, allowing to factorize the collinear divergences into the bare PDFs and FFs. In the course of said procedure, the factorization scale μ_F, which was already mentioned against the background of the evolution of PDFs in section 2.2.1, has to be introduced.

In practical applications, the collinear subtraction is performed by adding suitable counterterms which are given by convolutions of the structure

$$-\frac{\alpha_s}{2\pi}\int_0^1 dx\, H_{ij}\big(x,\mu_F\big)d\sigma\big(s',t',u'\big)\delta\big(s'+t'+u'\big) \tag{3.42}$$

where $d\sigma$ denotes a d-dimensional cross section at tree-level and s', t', u' represent Mandelstam variables for adjusted kinematics. Here, the encountered function H_{ij} is defined via the LO splitting kernels P_{ij} and reads

$$H_{ij}\big(x,\mu_F\big)=\bigg(-\frac{1}{\varepsilon}+\gamma_E-\ln\big(4\pi\big)\bigg)P_{ij}(x)\bigg(\frac{\mu^2}{\mu_F^2}\bigg)^{\varepsilon}+h_{ij}(x) \tag{3.43}$$

where $h_{ij}(x)=0$ in the $\overline{\mathrm{MS}}$ scheme.

In the example shown in figure 3.1, the relevant splitting function is the qq-splitting kernel and the needed Born cross section is the one for the process $q\ell\to q\ell$ as indicated by the blue box. Above that, the incoming quark in the Born process carries the momentum xp and the Mandelstam variables thus need to be adjusted and become

$$s'=xs,\qquad t'=xt,\qquad u'=u. \tag{3.44}$$

The appropriate contribution to subtract the associated collinear divergences therefore reads

$$-\frac{\alpha_s}{2\pi}\int_0^1 dx\, H_{qq}\big(x,\mu_F\big)d\sigma^{q\ell\to q\ell}\big(xs,xt,u\big)\delta\big(x(s+t)+u\big). \tag{3.45}$$

As noted earlier, other configurations beyond the one illustrated in the example may likewise induce divergences. In a practical application, it is therefore essential to examine all Feynman diagrams that contribute to the process for such configurations and to formulate suitable subtraction terms following the outlined procedure. After adding all of them to the cross section, a finite result is obtained and the limit $\varepsilon\to 0$ can finally be taken.

3.4 Weizsäcker-Williams contribution

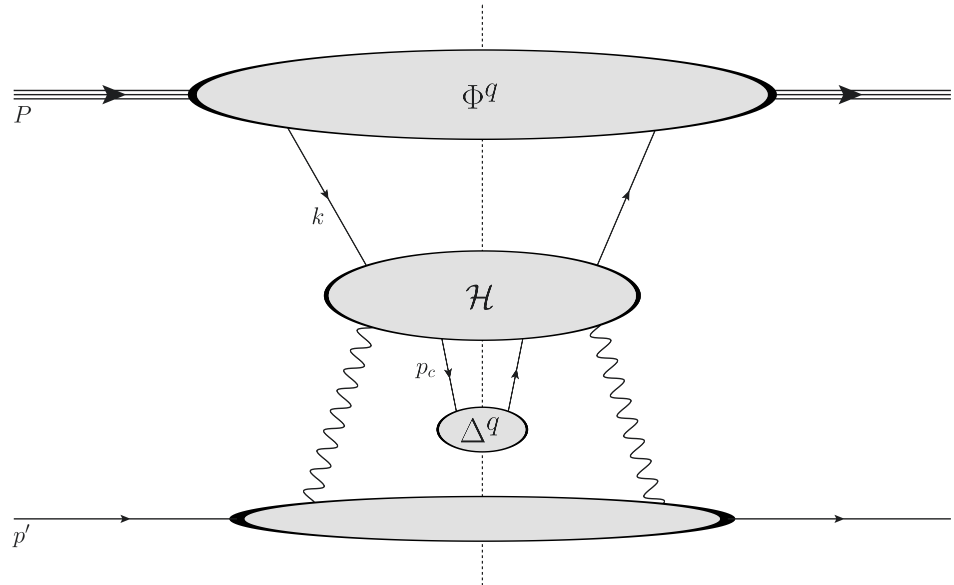

Figure 3.2: Schematic illustration of the Weizsäcker-Williams contribution. The diagram represents the single-inclusive production of a hadron in nucleon-lepton scattering, where the photon is now viewed as a parton from the lepton.

As it will become apparent in the further course of this thesis, an additional challenge in our considerations, which address nucleon-lepton scattering, will be posed by the occurrence of singularities originating from momentum configurations where a photon is emitted collinear to the external lepton. To handle this specific class of divergences, we'll employ a method that relies on using so-called Weizsäcker-Williams contributions to subtract the divergences in the framework of factorization. This section therefore serves the purpose of introducing the fundamental background of the procedure.
The origin of the name is traced to C. F. von Weizsäcker [214] and E. J. Williams [218], who independently developed an approximation to simplify calculations pertaining to processes involving relativistic charged particles in the early 1930's, in response to studies on the behaviour of atoms in the vicinity of electric fields generated by passing charged particles, which have been carried out by Fermi in 1924 [90]. Among their most significant discoveries was that the electric field of a passing relativistic charge predominantly comprises transverse components. They argued that the observed effects can therefore be described in a picture, which uses photons of the same energy spectrum as the particle's original field. Over the subsequent decades, the model has been successfully applied (see e.g. [70, 72, 204]) and improved [97].

In the context of our considerations, we shall closely adhere to the procedure outlined in [120] and we will thereby provide a comprehensive summary of the methodology described in the aforementioned work. The approach relies on the idea to introduce QED parton distribution functions likewise as those known for nucleons. One of the partons is the lepton itself and the appropriate distribution is hence given by

$$f^{\ell/\ell}(\xi) = \delta\big(1-\xi\big) \tag{3.46}$$

at the lowest order which corresponds to the usual scattering process like it will be considered in the next chapter at tree level. Another possibility, however, is indicated in figure 3.2. As illustrated in the diagram, the photon, which was previously assumed to be a virtual particle exchanged in the course of the hard process, now acts as a parton of the lepton. As a result, it takes on the role of a quasi-real external particle entering the hard process and consequently, photon-parton subprocesses need to be taken into account. The new distributions can be defined following the same line of reasoning as in the case of the nuclear PDFs. They thus also require renormalization and the relation between the bare and renormalized distribution may be expressed as

$$f^{\gamma/\ell}_{\text{bare}}(\xi) = f^{\gamma/\ell}_{\text{ren}}(\xi,\mu) + \frac{\alpha_{\text{em}}}{2\pi}\frac{(4\pi)^{\varepsilon}}{\varepsilon}\frac{1}{\Gamma\big(1-\varepsilon\big)}\left(P_{\gamma\ell}\otimes f^{\ell/\ell}_{\text{ren}}\right)(\xi,\mu) \tag{3.47}$$

in complete analogy to the nuclear counterpart for the gluon distributions, where we can set $f^{\ell/\ell}_{\text{ren}}(\xi) = \delta\big(1-\xi\big)$ and where the splitting function arising in this expression is given by

$$P_{\gamma\ell}(\xi) = \frac{1}{C_F}P_{gq}(\xi) = \frac{1+\big(1-\xi\big)^2}{\xi}. \tag{3.48}$$

In the next step, it is necessary to determine the bare photon-in-lepton distribution. The appropriate definition of the distribution in question follows immediately from that of the gluon and it thus becomes [138]

$$\begin{aligned}\Omega^{\mu\nu}(\xi) &\equiv \int\frac{d\lambda}{2\pi\xi}e^{i\lambda y}\left\langle\ell\right| F^{n\nu}_{\text{em}}(0)\mathcal{W}\big[0;\lambda n\big]F^{n\mu}_{\text{em}}(\lambda n)\left|\ell\right\rangle \\ &= -\frac{g^{\mu\nu}_{\perp}}{2(1-\varepsilon)}f^{\gamma/\ell}_{\text{bare}}\big(\xi,\mu\big)\end{aligned} \tag{3.49}$$

after removing the colour structure, where n is again a light-cone vector satisfying $n^2 = 0$ and $p'\cdot n = 1$. Furthermore, $\mathcal{W}$ denotes the Wilson line, which is needed to ensure gauge invariance, $F^{\mu\nu}_{\text{em}} = \partial^{\mu}A^{\nu} - \partial^{\nu}A^{\mu}$ represents the electromagnetic field strength tensor and the tensor

$$g^{\mu\nu}_{\perp} = g^{\mu\nu} - \big(p'^{\mu}n^{\nu} + n^{\mu}p'^{\nu}\big) \tag{3.50}$$

is the transverse projector.

The bare photon-in-lepton distribution as previously introduced can be calculated perturbatively in QED as long as the strong interaction is neglected. To the lowest order, it is given by

$$f_{\text{bare}}^{\gamma/\ell}(\xi,\mu) = \frac{\alpha_{\text{em}}}{2\pi} P_{\gamma\ell}(\xi) \frac{(4\pi)^{\varepsilon}}{\Gamma(1-\varepsilon)} \left\{ \frac{1}{\varepsilon} + \ln\left(\frac{\mu^2}{\xi^2 m_\ell^2}\right) - 1 \right\} + \mathcal{O}(\alpha_{\text{em}}^2). \quad (3.51)$$

With this result together with the relation given in equation 3.47, the distribution can be renormalized following the same procedure as known for the nuclear PDFs. In this manner, the renormalized photon-in-lepton distribution becomes

$$f_{\text{ren}}^{\gamma/\ell}(\xi,\mu) = \frac{\alpha_{\text{em}}}{2\pi} P_{\gamma\ell}(\xi) \left\{ \ln\left(\frac{\mu^2}{\xi^2 m_\ell^2}\right) - 1 \right\} + \mathcal{O}(\alpha_{\text{em}}^2) \quad (3.52)$$

in the $\overline{\text{MS}}$-scheme. The outcome for the renormalized distribution allows us to formulate contributions to subtract the collinear divergences from the real corrections by following the procedure as outlined in chapter 3.3. It turns out that these contributions may be written in the form of a generic cross section as

$$\begin{aligned} E_h \frac{d^3\sigma_{WW}^{N\ell\to hX}}{dP_h^3} =& \frac{1}{S} \sum_{a,c} \int_0^1 \frac{dz}{z^2} \int_0^1 \frac{dx}{x} \int_0^1 dy \delta\left(y + \frac{t}{s+u}\right) \\ & \times f^{a/N}(x,\mu) D^{c/h}(z,\mu) f_{\text{ren}}^{\gamma/\ell}(y,\mu) \sigma^{\gamma a\to c}(v,w), \quad (3.53) \end{aligned}$$

where $\sigma^{\gamma a\to c}$ represents cross sections for processes with a real incoming photon, which need to be calculated within the framework of perturbation theory. Finally, two more remarks on the Weizsäcker-Williams contribution should be mentioned: First, as argued in [120], it can be shown that the distribution introduced here are in fact related to the original Weizsäcker-Williams approximation. Second, the divergences are an artifact of neglecting the lepton's mass and would not be encountered when the mass is kept finite. It can be shown that both approaches yield consistent results.

Chapter 4

Inclusive Hadron Production in Lepton-Nucleon Scattering

Chapter 4

Inclusive Hadron Production in Lepton-Nucleon Scattering

The primary objective of the present thesis is to study the transverse single-spin asymmetry at next-to-leading order. Along the way to attain the stated goal, two obstacles must be overcome as the spin asymmetry is defined via the fraction of the spin-dependent and the spin-averaged cross section. On the one hand, it is thus essential to determine the spin-dependent cross section which will turn out to be the more challenging aspect due to the substantial larger number of contributing Feynman diagrams and some novel technical issues. But on the other hand, it is equally important to know the spin-averaged cross section. This chapter is therefore devoted to analyzing the single-inclusive hadron production in unpolarized nucleon-lepton scattering, with the ultimate goal of determining the spin-averaged cross section for this process at next-to-leading order. We therefore study the process

$$N + \ell \to h + X, \tag{4.1}$$

which distinguishes from the more prominent deep-inelastic (DIS) and semi-inclusive deep-inelastic scattering (SIDIS), i.e. the processes

$$\text{DIS: } \ell + N \to \ell + X, \quad \text{SIDIS: } \ell + N \to \ell + h + X$$

by the fact that only a single hadron from the final-state is observed while the lepton remains unobserved. DIS and SIDIS have proven themselves to be immensely powerful tools for deepening our understanding of the internal structure of matter and for testing the validity of our theoretical frameworks. On top of that, SIDIS offers the additional advantage of providing direct insight into the hadronization process. The study of the inclusive production of a single hadron, in contrast to the formerly mentioned two processes, offers other advantages, particularly in regard to the transverse single-spin asymmetry, since the structure of the contributions is more similar to those observed, when nucleon-nucleon scattering is examined, while it overall remains less complex and the necessary computations are hence less time-consuming. The scattering process is thus well suited to learn how to handle the technical challenges, which might occur in higher-order calculations of the single-spin asymmetry.

In the past years, the process has been the subject of different experiments, with the majority of them being focused on spin-dependent observables. The transverse single-spin, for instance, has been measured in the scattering of leptons and protons by the HERMES collaboration [22, 190, 208], where they observed the production of charged pions and kaons. Among their key findings in the course of these experiments was the observation that the data is dominated by the kinematic regime of quasi-real photoproduction.

Other measurements were carried out by the Jefferson Lab Hall A collaboration [27, 229, 230], where the scattering of an electron beam on a fixed 3He-target was studied. In these experiments non-zero transverse single-spin asymmetries for charged pions and kaons were observed at relatively low transverse momentum $P_{h\perp}$ of the produced hadron. But besides the single-spin asymmetry, the double spin asymmetry was also investigated for the process. At SLAC, similar experiments were performed with longitudinally polarized protons and deuterons by the E155 collaboration [32, 52]. Lastly, a similar but different process was studied by the COMPASS collaboration. In these measurements, a muon beam was used as a source for quasi-real photons which were then used for photon-nucleon scattering experiments [16, 158]. But besides the interest from the experimental site, there also have been theoretical considerations on the scattering process. Many of them concern the transverse single spin asymmetry (see e.g. [30, 31, 99, 134, 145]). In [121] the double-longitudinal spin-asymmetry was studied at NLO. On top of that, results for the unpolarized cross section at NLO are given in [120]. Another spin observable was examined in [133]. Here, the longitudinal transverse double-spin asymmetries was studied, where the incoming lepton was assumed to be longitudinally polarized and the nucleon was considered to be transversally polarized.

In this chapter, we will present results for the spin-averaged cross section. They are in accordance with those presented in the latter mentioned work. The computation of the spin-averaged cross section provides our first step towards the transverse single-spin asymmetry at NLO and will be used here as an example to further introduce the methods which are commonly employed in perturbative calculations at higher orders. The chapter is structured as follows: First, we will introduce the general framework and present the leading-order results. Subsequently, we will give further insights into our NLO considerations, where we will distinguish between virtual and real contributions. After dealing with the collinear singularities in the framework of collinear factorization, we obtain a finite outcome, which will be used in the last part of this chapter for numerical studies.

4.1 Framework and Leading Order Results

Before proceeding with the actual calculation of the cross section in the context of perturbation theory, it is inevitable to establish the framework that forms the foundation of our considerations. Among other things, the present section precisely serves this purpose for the stated reason as well as the presentation of the computations in the Born approximation. Since we are interested in the single-inclusive production of hadrons in lepton-nucleon scattering, we have to investigate the process

$$N\big(P\big) + \ell\big(p'\big) \to h\big(P_h\big) + X$$

and, of course, need to study the corresponding subprocesses on partonic level. The foundation is laid by the collinear factorization theorem, which was introduced in chapter 2.2, and we therefore assume that the momenta of the incoming parton p and the fragmenting parton p_c may be written as

$$p \approx xP, \qquad p_c \approx \frac{1}{z} P_h \tag{4.2}$$

in the course of the collinear expansion, where x and z denote momentum fractions of the associated parent hadrons. On the one hand, these preliminary steps permit the introduction of the Mandelstam variables as

$$s = \big(p + p'\big)^2 = xS, \tag{4.3}$$

$$t = \big(p - p_c\big)^2 = \frac{x}{z} T, \tag{4.4}$$

$$u = \big(p' - p_c\big)^2 = \frac{1}{z} U, \tag{4.5}$$

with the variables denoted by capital letters being the hadronic counterparts, which are defined in complete analogy by substituting the partonic momenta with their hadronic equivalents. On the other hand, the approach allows to make use of the formula for the factorized cross section given in equation 2.68, which reads

$$\begin{aligned} E_h \frac{d^3\sigma^{N\ell\to hX}}{dP_h^3} = \frac{1}{S} \sum_{a,c} \int_0^1 \frac{dz}{z^2} \int_0^1 \frac{dx}{x} f^{a/N}(x, \mu_F) \\ \times \sigma^{a\ell\to cX}\big(s, t, u, \mu, \mu_F, \mu_D\big) D^{c/h}(z, \mu_D), \end{aligned} \tag{4.6}$$

where μ, μ_F and μ_D represent the renormalization, factorization and fragmentation scale in this order. The next step is to calculate the partonic cross section, for which the possible subprocesses and the associated Feynman diagrams must first be identified. Subsequently, the techniques outlined in chapter 3 can be employed to determine the corresponding matrix elements and their absolute value squared by utilizing the Feynman rules and then to perform the phase space integration.

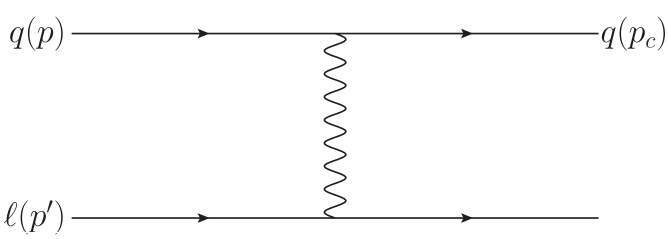

Figure 4.1: Feynman diagram representing quark-lepton scattering in LO. Momentum is transferred in the electromagnetic interaction between the quark and the lepton via the exchange of a virtual photon.

The Born contribution and the virtual corrections will require us to deal with the particularly straightforward case of the two-body phase space, whereas we will confront the three-body phase space when dealing with the real corrections and we hence encounter angular integrals as discussed in chapter 3.2.2. On the top of that, another tedious task awaits us specifically in the treatment of virtual corrections where loop integrals over the momenta of virtual particles need to be solved.

Nonetheless, the treatment of the process in leading order proves to be peculiarly simple, as only a single subprocess at partonic level is involved in this instance, which turns out to be the scattering of a quark and a lepton, i.e. the process

$$q(p) + \ell(p') \to q(p_c) + \ell(p_d).$$

Furthermore, the structure of the associated Feynman diagram, which is shown in figure 4.1, is also by no means excessively intricate and the calculation of the matrix element is therefore rather straightforward. Following the procedure as outlined previously, the matrix element as well as its absolute squared value related to the diagram can be computed and we are led to consider two traces, containing four γ-matrices, of the form

$$\mathrm{Tr}\big[\gamma^\mu\gamma^\nu\gamma^\rho\gamma^\sigma\big] = 4\big(g^{\mu\nu}g^{\rho\sigma} - g^{\mu\rho}g^{\nu\sigma} + g^{\mu\sigma}g^{\nu\rho}\big). \tag{4.7}$$

Once these traces have been evaluated and all indices have been suitably contracted, the cross section at tree level is finally found, which then becomes

$$\sigma_{LO}^{q\ell\to q\ell}\big(s,t,u\big) = 2\alpha_{em}^2 e_q^2 \frac{s^2+u^2}{t^2}\delta\big(s+t+u\big) \tag{4.8}$$

as a function of the Mandelstam variables s, t, u, where α_{em} is the fine structure constant and e_q denotes the charge fraction of a quark with flavour q. In principle, the expression could now be inserted in the factorization formula given in equation 4.6. However, often it is convenient to choose two other variables, namely v and w, to express partonic cross sections as well as the factorization formula, specifically the integrals over momentum fractions.

The variables can be introduced via the Mandelstam variables and read

$$v \equiv 1 + \frac{t}{s}, \qquad w \equiv -\frac{u}{s+t}. \tag{4.9}$$

As it was previously the case with the Mandelstam variables, hadronic counterparts can be defined in a similar manner and are then denoted by capital letters. But in order to rewrite the integrals in equation 4.6 in terms of the new variables, the aforementioned relations are not sufficient, and instead equations are needed to forge links between the variables and the momentum fractions. It can be found that

$$x = \frac{1-v}{vw}\frac{U}{T}, \qquad z = -\frac{1}{1-v}\frac{T}{S} \tag{4.10}$$

applies and we thus obtain

$$\frac{1}{S}\frac{dz}{z^2}\frac{dx}{x} = \frac{1}{S}\frac{dw}{w}\frac{dv}{(1-v)z} = \left(-\frac{U}{S^2}\right)\frac{dv}{v(1-v)}\frac{dw}{w^2}\frac{1}{xz^2} \tag{4.11}$$

by employing the usual procedure utilizing the jacobian to perform the variable transformation of the integrals. In summary, we find that the factorized cross section for single-inclusive production of a hadron in lepton-nucleon scattering may be written as

$$\begin{aligned} E_h \frac{d^3\sigma^{N\ell\to hX}}{dP_h^3} = \left(-\frac{U}{S^2}\right)^2 \sum_{a,c} \int_{v_{\min}}^{v_{\max}} \frac{dv}{v(1-v)} \int_{w_{\min}}^{1} \frac{dw}{w^2} \frac{f^{a/N}(x,\mu_F)}{x} \\ \times \frac{D^{c/h}(z,\mu_D)}{z^2} \sigma^{a\ell\to cX}\big(v,w,\mu,\mu_F,\mu_D\big) \end{aligned} \tag{4.12}$$

where the integral boundaries are

$$v_{\min} = \frac{U}{T+U}, \quad v_{\max} = 1 + \frac{T}{S}, \quad w_{\min} = \frac{1-v}{v}\frac{U}{T}. \tag{4.13}$$

Above that, it turns out that the Born cross section becomes

$$\sigma_{LO}^{q\ell\to q\ell}\big(v,w\big) = \frac{2\alpha_{em}^2 e_q^2}{(-sv)}\frac{1+v^2}{(1-v)^2}\delta\big(1-w\big) \tag{4.14}$$

as a function of v and w and we are thus ascertained that our LO result is in agreement with [120].

4.2 Next-to-Leading Order Contributions

The leading order term, we have presented in the preceding section, is the simplest contribution to calculate as it involves the fewest number of particles. But despite the fact that it already yields a qualitatively satisfactory approximation, it is frequently not sufficient to make predictions in order to gain new physical insights from contemporary collider experiments due to the increasing precision of the measurements. This leads to the necessity of including higher-order corrections to achieve greater accuracy as well as to increase the predictive power of the theory and to match the experimental precision. Especially in the case of the next-to-leading order corrections, which constitute the first set of higher-order terms, it has been demonstrated in calculations of various physical observables that the numerical effects can attain significant magnitude, and they thus play a pivotal role in refining the predictions of perturbative quantum field theories in general and pQCD in particular. Furthermore, they are crucial for a better understanding of the inner structure of protons, as they allow for the extraction of parton distribution functions from experimental data more accurately. Above that, another reason contributing to the significance of higher-order corrections concerns the dependence on the arbitrary renormalization scale. As noted previously, the dependence on the choice of scale is an artifact from the renormalization of the theory and would be eliminated if we were able to compute observables analytically. In this particular context, the implementation of higher-order corrections leads to a reduction of the scale dependence, thereby enhancing the reliability of the predictions achieved. Lastly, it is noteworthy to mention that NLO correction can lead to novel physical effect, like new production mechanisms, to come into play in some cases, and thus provide access to study these phenomena. They are therefore not merely quantitative refinements, but can also bring new physical insights.

In conclusion, NLO corrections in QCD are an indispensable tool for understanding the strong interaction that governs the behaviour of quarks and gluons. They allow us to test QCD in a variety of high-energy processes and explore the frontier of our knowledge in particle physics. In this chapter we now want to present our considerations at next-to-leading order. To be more precise, we'll study the QCD corrections to the single-inclusive hadron production on nucleon-lepton scattering, which means, we'll consider contributions of the order

$$\mathcal{O}\big(\alpha_{em}^2 \alpha_s\big). \tag{4.15}$$

Of course, there actually also exist pure QED corrections, i.e. contributions of the order $\mathcal{O}\big(\alpha_{em}^3\big)$; however, their impact play a far less significant role, as their magnitude is expected to be considerably lower in comparison to the QCD corrections.

One of the reasons for this is that the strong coupling exceeds the fine structure constant, and it is thus justified to solely focus on the QCD corrections. Initially, our attention is primarily focused on two distinct tracks that can be handled in a more or less independent manner, namely the examination of Feynman diagrams for both virtual and real corrections. As a starting point, we again make use of the factorized cross section given in equation 4.12 and continue by studying the virtual corrections where the major challenge will be the evaluation of the soft and UV divergent loop integrals.
We then proceed by addressing the real corrections, where an additional real parton is emitted. In this particular context, we observe the possibility of gluon fragmentation as a new phenomenon in contrast to the leading order process among other things and as a result, the treatment of the real corrections will turn out to be more time-consuming due to the increased number of Feynman diagrams. Furthermore, another tenacious task will be provided by carrying out the angular integration as a part of the three-body phase space.
When the phase space integrated absolute value squared of the matrix elements from both classes of corrections have been finally determined, the resulting expression will be free of UV and soft divergences, and it remains to handle the collinear singularities in the framework of collinear factorization. Against this background, we will observe that the usual parton distributions and fragmentation functions are not sufficient to cancel all collinear singularities and instead another novel phenomenon arises, which are the Weizsäcker-Williams contributions introduced in the last chapter. They are an artifact of neglecting the lepton's mass and need to be taken into account in order to cancel collinear divergences from momentum configurations where the virtual photon, which is exchanged in the course of the hard scattering process between the incoming quark and lepton, is collinear to the lepton.
Lastly, it has to be noted, that we will employ dimensional regularization as the procedure to identify the singularities and to make them manifest. We therefore set

$$d = 4 - 2\varepsilon \tag{4.16}$$

and the divergences will thus occur as poles in ε as outlined previously.

4.2.1 Virtual Corrections to the Order $\mathcal{O}\big(\alpha_{\mathbf{em}}^2\alpha_s\big)$

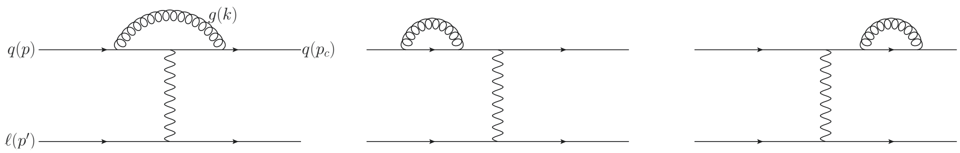

Figure 4.2: Feynman diagrams representing the virtual NLO corrections to quark-lepton scattering. The diagram on the left-hand side illustrates the QCD one-loop vertex corrections to the process. The remaining two diagrams are quark self-energy corrections.

As already announced, we commence our considerations in next-to-leading order by studying the virtual corrections within the framework of pQCD, which implies that we essentially need to revisit the $2 \to 2$ process

$$q\big(p\big) + \ell\big(p'\big) \to q\big(p_c\big) + \ell\big(p_d\big)$$

at partonic level. But in contrast to the tree-level contribution, we now examine one-loop diagrams, wherein an additional virtual gluon occurs, and we are thereby able to identify three potential Feynman diagrams, which may yield a contribution in this particular case. The respective diagrams are those shown in figure 4.2, which in turn can be further subdivided into two distinct classes: Diagrams, whose structure bears resemblance to that depicted on the left-hand side of the figure, belong to a category of loop diagrams referred to as vertex corrections. The diagrams depicted in the middle and on the right-hand side of the illustration can be taken as examples for self-energy corrections, which are characterized by the phenomenon that the virtual particle is emitted and absorbed by the same external leg. Another class of loop diagrams is provided by so-called box diagrams. However, we refrain from engaging in a more comprehensive discussion regarding such corrections, as no box diagram is present in the order $\mathcal{O}\big(\alpha_{em}^2\alpha_s\big)$, which is the primary focus of our considerations. Nonetheless, box diagrams might arise in higher orders beyond NLO in perturbation theory.
But in our case, only the aforementioned diagrams need to be taken into account and consequently, we are faced with handling loop integrals like

$$\int_{-\infty}^{\infty} \frac{d^dk}{\big(2\pi\big)^d} \frac{k^{\mu_1}...k^{\mu_n}}{k^2\big(p-k\big)^2\big(p_c-k\big)^2} \tag{4.17}$$

$$\int_{-\infty}^{\infty} \frac{d^dk}{\big(2\pi\big)^d} \frac{k^{\mu_1}...k^{\mu_n}}{k^2\big(p_i-k\big)^2} \tag{4.18}$$

where integrals of the type as given in the first line are associated with the vertex correction and integrals like the one stated in the second line are related to the self-energy diagrams with p_i being either p or p_c, depending on whether the loop is located in the initial or the final state.

In the subsequent stage, we therefore require strategies to handle such tensor integral. One potential approach for addressing such integrals is to employ the technique of tensor decomposition, which enables the reduction of tensor integrals to sums of scalar integrals that are much simpler to compute. To further elucidate the methodology, we shall assume the integral given in equation 4.17 but with only a single power of the loop momentum k^μ in the numerator as an example. The technique relies on the idea that the solution of an arbitrary tensor integral can be formulated as a superposition of all feasible independent tensors of the same rank, which, in the context of loop integrals in quantum field theories, are typically products of external momenta p^μ and p_c^μ and the metric tensor. In our example, this implies, that the solution of the integral must be proportional to the two external momenta as they are the only independent four-vectors in the problem. It is therefore reasonable to make the ansatz

$$\int_{-\infty}^{\infty} \frac{d^d k}{(2\pi)^d} \frac{k^\mu}{k^2 (p-k)^2 (p_c - k)^2} = \int_{-\infty}^{\infty} \frac{d^d k}{(2\pi)^d} \frac{A p^\mu + B p_c^\mu}{k^2 (p-k)^2 (p_c - k)^2} \tag{4.19}$$

where A and B are appropriate coefficients which need to be determined in the following. In order to find the coefficient, the equation above can be contracted with p^μ or p_c^μ respectively. However, this approach means that the coefficients initially depend on scalar products $p_i \cdot k$ $(p_i = p, p_c)$ of the loop momentum as well as the external momenta and we hence need to rearrange these expressions by completing the square and by making use of the relation

$$p_i \cdot k = \frac{1}{2}\left[k^2 - (p_i - k)^2\right]. \tag{4.20}$$

Obviously, the contributions given on the right-hand side of the latter equation cancel against the propagators in the denominator of the loop integral and we thus obtain

$$\begin{aligned} &\int_{-\infty}^{\infty} \frac{d^d k}{(2\pi)^d} \frac{k^\mu}{k^2 (p-k)^2 (p_c - k)^2} \\ &= \int_{-\infty}^{\infty} \frac{d^d k}{(2\pi)^d} \left\{ \frac{p^\mu}{k^2 (p-k)^2} + \frac{p_c^\mu}{k^2 (p_c - k)^2} - \frac{p^\mu + p_c^\mu}{(p-k)^2 (p_c - k)^2} \right\} \end{aligned} \tag{4.21}$$

for the reduction of the tensor integrals into a sum of scalar integrals. It is important to note, however, that this example is a particularly simple case and that, in general, the reduction can be much more complex and time-consuming. A more systematic approach to reduce tensor integrals of higher rank was introduced by Passarino and Veltman in 1978 [176], which is also utilized by one of the earlier mentioned packages for Mathematica, namely Package-X, that is mostly used by us to solve loop integrals. Therefore, we have finally developed all the methods needed to solve every loop integral, which we encounter in our calculations.

Once all integrals have been evaluated, it turns out that the contributions from the self-energy diagrams vanish in the approximation of massless quarks, resulting in the vertex correction being the sole contributor to the partonic cross section. As only the interference between the virtual corrections and the Born diagram contributes, it now remains to construct the absolute square from the matrix elements of the vertex correction, as well as the diagram at tree level, which was previously presented in section 4.1, to ultimately calculate the contribution of the virtual corrections to the partonic cross-section in the order $\mathcal{O}\big(\alpha_{em}^2\alpha_s\big)$. Since we are, in principle, dealing with a $2 \to 2$ process, the outcome must be integrated over the two-body phase space and the kinematics of the cross section, which we obtain, thus resembles the leading order case. This especially implies, that we are able to set $w \to 1$, as the result is again proportional to the delta function $\delta\big(1-w\big)$. All-in-all. we find that the virtual corrections may be written as a product of the d-dimensional LO cross section and a suitable divergent term as it is already known from [173]. More precisely, the cross section becomes

$$\begin{aligned}\sigma^{q\ell\to q\ell}_{\text{virt.},d=4-2\varepsilon}\big(v,w,\mu^2\big) =& C_F\frac{\alpha_s\big(\mu^2\big)}{2\pi}\frac{\Gamma^2(1-\varepsilon)\Gamma(1+\varepsilon)}{\Gamma(1-2\varepsilon)}\left(\frac{4\pi\mu^2}{s(1-v)}\right)^{\varepsilon}\\ &\times\sigma^{q\ell\to q\ell}_{LO,d=4-2\varepsilon}\big(v,w\big)\times\left(-\frac{2}{\varepsilon^2}-\frac{3}{\varepsilon}-8\right)\end{aligned}\tag{4.22}$$

where the LO cross section in $d = 4 - 2\varepsilon$ dimensions is given by

$$\sigma^{q\ell\to q\ell}_{LO,d=4-2\varepsilon}\big(v,w\big) = 2\alpha_{em}^2 e_q^2\frac{1}{sv}\left(\frac{1+v^2}{(1-v)^2}-\varepsilon\right)\delta\big(1-w\big).\tag{4.23}$$

4.2.2 Real Corrections to the Order $\mathcal{O}(\alpha_{em}^2 \alpha_s)$

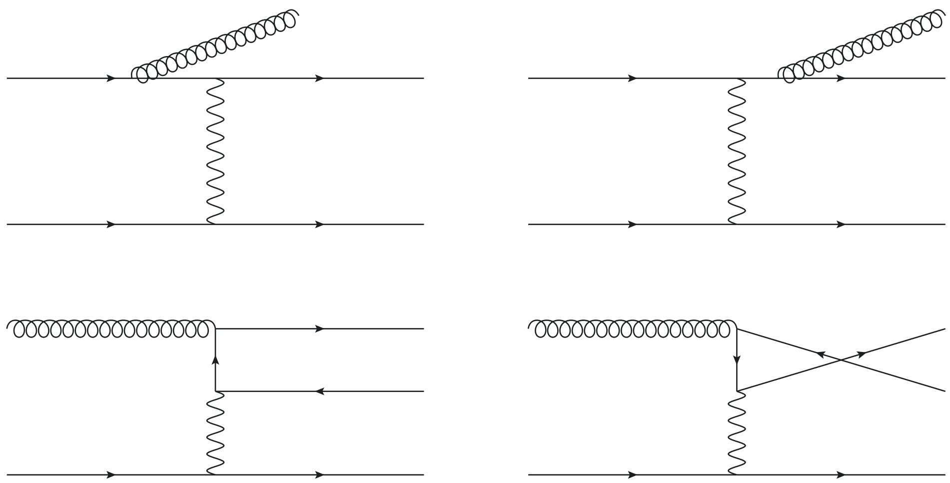

Figure 4.3: Feynman diagrams associated with the real NLO corrections. The diagrams in the upper line are linked to the corrections to quark-lepton scattering, where an extra gluon is emitted and either the quark or the gluon in the final state is assumed to be observed. The diagrams in the lower line illustrate another partonic subprocess where a gluon is located in the initial state and a quark-antiquark pair is produced.

The second component of our NLO analysis pertains to the treatment of real corrections at the order $\mathcal{O}(\alpha_{em}^2 \alpha_s)$, which essentially consist of $2 \to 3$ processes, where an additional parton is emitted and consequently located in the final state. It is intuitive, that we need to revisit quark-lepton scattering as a potential partonic subprocess that may contribute to the real corrections, where the final-state quark undergoes fragmentation and thus is presumed to be observed. But in the context of the real corrections, we need to take an extra gluon into account that is emitted by one of the external quark legs. However, it can be discerned that there are two more possible channels beyond the latter mentioned one. The first one of these two scattering processes is rather obvious since it is essentially the same process as before, but where now the emitted gluon is assumed to be observed instead of the quark. The third partonic subprocess is somewhat more difficult to identify. In this case a gluon is located in the initial state and a quark-antiquark pair is produced in the course of the hard scattering. All-in-all, we thus have to investigate the three partonic subprocesses

$$
\begin{aligned}
q(p) + \ell(p') &\to q(p_c) + g(r) + \ell(p_d) \\
q(p) + \ell(p') &\to g(p_c) + q(r) + \ell(p_d) \\
g(p) + \ell(p') &\to q(p_c) + \bar{q}(r) + \ell(p_d)
\end{aligned}
$$

where in each case the parton with momentum p_c is assumed to be observed.

On the other hand, the lepton and the remaining parton are unobserved. It is noteworthy, that in the case of the third process it is in principle also possible to observe the antiquark instead of the quark. Nevertheless, it is not necessary to examine this configuration separately. The Feynman diagrams associated with these processes are shown in figure 4.3. They enable us to employ the Feynman rules again to compute the matrix elements and their absolute value squared following the procedure as outlined previously. In comparison to the Born approximation and the virtual corrections, where the matrix elements were written in terms of three Mandelstam variables, we can now make use of a set of ten Mandelstam variables, which are defined by

$$s \equiv \left(p + p'\right)^2, \tag{4.24}$$
$$t_1 \equiv \left(p - p_c\right)^2, \tag{4.25}$$
$$t_2 \equiv \left(p - p_d\right)^2, \tag{4.26}$$
$$t_3 \equiv \left(p - r\right)^2, \tag{4.27}$$
$$u_1 \equiv \left(p' - p_c\right)^2, \tag{4.28}$$
$$u_2 \equiv \left(p' - p_d\right)^2, \tag{4.29}$$
$$u_3 \equiv \left(p' - r\right)^2, \tag{4.30}$$
$$s_{12} \equiv \left(p_c + p_d\right)^2, \tag{4.31}$$
$$s_{13} \equiv \left(p_c - r\right)^2, \tag{4.32}$$
$$s_{23} \equiv \left(p_d + r\right)^2 \tag{4.33}$$

to express our results since we now have to deal with another unintegrated momentum in contrast to the previous two cases. Nonetheless, it can be observed that these ten variables are not completely independent of each other and instead relations among them may be found via momentum conservation. The relations are given by

$$t_3 = -s - -t_1 - t_2 \tag{4.34}$$
$$u_3 = -s - u_1 - u_2 \tag{4.35}$$
$$s_{13} = s + t_2 + u_2 \tag{4.36}$$
$$s_{12} = -s - t_1 - t_2 - u_1 - u_2 \tag{4.37}$$
$$s_{23} = s + t_1 + u_1 \tag{4.38}$$

and allow us to reorganize the matrix elements as functions of only five of the ten variables. However, the outcome is still not suited to carry out the angular integration of the three-body phase space and we thus have to rearrange it by making extensive use of partial fraction decomposition as well as the relations among the Mandelstam variables.

Our aim is to reorganize the matrix elements in such a way that every single term depends on no more than two variables with an angular dependency. For this purpose, we utilize the observation that we can write

$$\frac{1}{XY} = \frac{1}{X+Y}\left[\frac{1}{X} + \frac{1}{Y}\right] \tag{4.39}$$

where in our case X and Y are always proportional to two distinct, angular dependent Mandelstam variables. It turns out that the sum $X + Y$ can be reorganized by using the aforementioned relations in a manner that it either cancels out or which allows to represent it in terms of angle-independent quantities. However, the terms we encounter in our analysis often exhibit a more intricate structure, making it necessary to repeat the procedure multiple times before one receives an integrable result, which may be expressed in the form of the standard integral given in equation 3.36 by employing the parametrizations presented in appendix B. As an example, we can consider the expression

$$\begin{aligned}\frac{t_3}{s_{13}u_2} &= -\frac{t_1}{s_{13}u_2} - \frac{s+t_2}{s_{13}u_2} \\ &= -\frac{t_1}{s_{13}u_2} - \frac{s+t_2}{s_{13}-u_2}\left[-\frac{1}{s_{13}} + \frac{1}{u_2}\right] \\ &= -\frac{t_1}{s_{13}u_2} + \frac{1}{s_{13}} - \frac{1}{u_2},\end{aligned} \tag{4.40}$$

which we actually encounter in the computations concerning the scattering process $q\ell \to qX$. Here, we have first used the relations among the Mandelstam variables to replace t_3 before applying the partial fraction decomposition. In the last step, we utilized that $s + t_2 = s_{13} - u_2$ which again follows from the previously introduced relations. This procedure must now be repeated for all contributions in the matrix elements, which can be a time-consuming task, but which can be significantly accelerated thanks to modern computer algebra systems. We then finally arrive at an outcome where all terms may be expressed in the form of the standard integral enabling us to ultimately carry out the angular integration. It should be noted that contributions $\sim \big(1-w\big)^{-1-\varepsilon}$ arise after evaluating the phase space integrals, which obviously diverge for $w \to 1$. They can be handled by using the identity

$$\big(1-w\big)^{-1-\varepsilon} \approx \frac{1}{\varepsilon} + \left(\frac{1}{1-w}\right)_+ - \varepsilon\left(\frac{\ln\big(1-w\big)}{1-w}\right)_+ + \mathcal{O}\big(\varepsilon^2\big) \tag{4.41}$$

to expand the terms for small ε, where we have introduced the so-called plus distribution which is denoted by the $+$ in the subscript.

The plus distribution can be defined via an integral relation for an arbitrary function by

$$\int_0^1 dx f(x)\big[g(x)\big]_+ \equiv \int_0^1 dx\big\{f(x)-f(1)\big\}g(x). \tag{4.42}$$

A more detailed discussion on said distribution is given in appendix D. We thus finally obtain a result for the soft as well as collinear divergent contributions to the real NLO corrections. We find that they may be written as

$$\begin{aligned}\sigma =& C_F\frac{e_q^2\alpha_{em}^2\alpha_s}{2\pi\Gamma\big(1-2\varepsilon\big)}\frac{1}{sv}\left(\frac{4\pi\mu^2}{s(1-v)v}\right)^{\varepsilon}\times\left\{\frac{4}{\varepsilon^2}\frac{1+v^2}{(1-v)^2}\delta\big(1-w\big)\right.\\ &+\frac{1}{\varepsilon}\left[A_1\delta\big(1-w\big)+A_2\left(\frac{1}{1-w}\right)_+ + A_3\right]\\ &\left.+B_1\delta\big(1-w\big)+B_2\left(\frac{1}{1-w}\right)_+ + B_3\left(\frac{\ln\big(1-w\big)}{1-w}\right)_+ + B_4\right\}\end{aligned} \tag{4.43}$$

in the case of the subprocess $q\ell\to qX$, where the coefficients are functions of v and w. It immediately catches the eye, that the divergent contribution $\sim\frac{1}{\varepsilon^2}$ cancels against the corresponding contribution from the virtual corrections given in equation 4.22. In fact, it turns out that all soft singularities vanish by adding the real and virtual corrections and consequently, only collinear divergences remain as expected. Similar expressions can be found for the remaining two subprocesses, where, however, no quadratic poles in ε occur.

It now remains to handle the collinear singularities in the framework of collinear factorization as outlined in section 3.3. We thus need to formulate appropriate subtraction terms as previously explained. They are given as convolutions of functions H_{ij}, which are defined via the splitting kernels, and suitable LO cross section as stated in equation 3.42. To subtract all collinear divergences arising in the NLO corrections to the single-inclusive production of a hadron in nucleon-lepton scattering, we will need the splitting functions

$$P_{qq}^{(0)}\big(\xi\big) = C_F\left(\frac{1+\xi^2}{\big(1-\xi\big)_+}+\frac{3}{2}\delta\big(1-\xi\big)\right) \tag{4.44}$$

$$P_{qg}^{(0)}\big(\xi\big) = T_R\big(\xi^2+(1-\xi)^2\big) \tag{4.45}$$

$$P_{gq}^{(0)}\big(\xi\big) = C_F\frac{1+(1-\xi)^2}{\xi} \tag{4.46}$$

$$P_{\gamma\ell}^{(0)}\big(\xi\big) = \frac{1+(1-\xi)^2}{\xi} \tag{4.47}$$

where the last one is associated with the Weizsäcker-Williams contributions. Beyond the splitting functions, we will need LO cross sections in $d=4-2\varepsilon$

dimensions. One of them is already known as it is the cross section for $q\ell \to q\ell$ scattering. Above that, we will need the cross sections for the photon-parton processes $q\gamma \to qX$, $q\gamma \to gX$ and $g\gamma \to qX$, which include a real photon in the initial state and are thus linked to the Weizsäcker-Williams contributions. The corresponding Feynman diagrams for the three processes are shown in figure 4.4 where the diagrams in the top line apply to the two processes $q\gamma \to qX$ as well as $q\gamma \to gX$. All-in-all, we obtain

$$\sigma^{q\gamma\to q}_{\mathrm{LO},d=4-2\varepsilon}\big(s,v\big) = C_F \frac{2\pi\alpha_s\alpha_{em}e_q^2}{\Gamma\big(1-\varepsilon\big)}\left(\frac{4\pi\mu^2}{s(1-v)v}\right)^{\varepsilon}\frac{1+v^2-\varepsilon\big(1-v\big)^2}{sv} \tag{4.48}$$

$$\sigma^{q\gamma\to g}_{\mathrm{LO},d=4-2\varepsilon}\big(s,v\big) = C_F \frac{2\pi\alpha_s\alpha_{em}e_q^2}{\Gamma\big(1-\varepsilon\big)}\left(\frac{4\pi\mu^2}{s(1-v)v}\right)^{\varepsilon}\frac{2-2v+v^2-\varepsilon v^2}{s(1-v)} \tag{4.49}$$

$$\sigma^{g\gamma\to q}_{\mathrm{LO},d=4-2\varepsilon}\big(s,v\big) = T_R \frac{2\pi\alpha_s\alpha_{em}e_q^2}{\Gamma\big(1-\varepsilon\big)}\left(\frac{4\pi\mu^2}{s(1-v)v}\right)^{\varepsilon}\frac{1-2v+2v^2-\varepsilon}{sv(1-v)} \tag{4.50}$$

for the necessary cross sections at tree-level and we are finally able to formulate the contributions needed to subtract the collinear divergences. As an example, we find that we need to consider

$$\begin{aligned}
&-\frac{\alpha_s}{2\pi}\left\{\frac{1}{sv}H_{qq}\big(x=w,\mu_F^2\big)\,\sigma^{q\ell\to q\ell}_{LO,d=4-2\varepsilon}\Big|_{s=sw}\right.\\
&\left.+\frac{1}{s(1-v+vw)}H_{qq}\big(x=1-v+vw,\mu_D^2\big)\,\sigma^{q\ell\to q\ell}_{LO,d=4-2\varepsilon}\Big|_{v=\frac{vw}{1-v+vw}}\right\}\\
&-\frac{\alpha_{\mathrm{em}}}{2\pi}H_{\gamma\ell}\left(x=\frac{1-v}{1-vw},m_\ell^2\right)\sigma^{q\gamma\to qg}_{LO,d=4-2\varepsilon}\Big|_{s=s\frac{1-v}{1-vw},v=vw}
\end{aligned} \tag{4.51}$$

to subtract the collinear singularities in the case of the partonic $2\to 3$ subprocess $q\ell \to q$, where we followed the procedure as outlined in chapter 3.3 and then made use of the δ functions to evaluate the integrals. By repeating the procedure for the other two subprocesses. we ultimately receive a finite result.

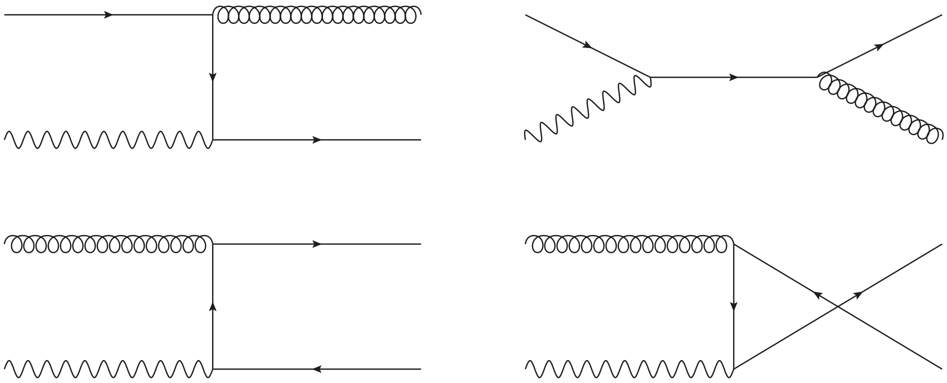

Figure 4.4: Feynman diagrams for the processes contributing to the Weizsäcker-Williams contributions. The upper line shows the diagrams contributing to the $q\gamma \to q$- and $q\gamma \to g$-channel, while the bottom line represents the $g\gamma \to q$ scattering.

4.2.3 Summary and finite Results: Next-to-Leading Order Corrections

Now that we have determined both, the virtual and the real corrections, in the previous sections, we are finally able to formulate an analytical expression for the cross section at the partonic level. The outcome is free of any divergences, since the UV singularities have been treated by renormalizing the theory, the soft divergences cancel out in the sum of virtual and real corrections, and ultimately the infinities by collinear momentum configurations have been addressed in the framework of factorization. All-in-all, we find that our result is in accordance with the one presented in [120] and we are consequently able to write the factorized cross section for the single-inclusive production of hadrons in nucleon-lepton scattering in the same manner as

$$\begin{aligned}E_h \frac{d^3\sigma^{N\ell\to hX}}{dP_h^3} =& \left(-\frac{U}{S^2}\right)^2 \sum_{a,c} \int_{v_{\min}}^{v_{\max}} \frac{dv}{v(1-v)} \int_{w_{\min}}^{1} \frac{dw}{w^2} \frac{f^{a/N}(x,\mu)}{x} \\ &\times \frac{D^{c/h}(z,\mu)}{z^2} \Bigg\{ \sigma_{\mathrm{LO}}^{a\ell\to c}(v,w) + \frac{\alpha_s(\mu^2)}{\pi} \sigma_{\mathrm{NLO}}^{a\ell\to c\ell}(v,w,\mu^2) \\ &+ \frac{\alpha_s(\mu^2)}{\pi} f^{\gamma/\ell}\left(\frac{1-v}{1-vw},\mu^2\right) \sigma_{\mathrm{LO}}^{a\gamma\to c}(v,w) \Bigg\}. \end{aligned} \tag{4.52}$$

The hadronic cross section as given in equation 4.52 thus comprises three parts: the LO cross section, the NLO corrections and the Weizsäcker-Williams contributions. The partonic cross section in the Born approximation have already been noted in one of the preceding sections. It hence remain to present results for the NLO corrections and the Weizsäcker-Williams contributions in the following.

As presented in [120], the next-to-leading cross sections for the contributing partonic subprocesses may be written as

$$\begin{aligned}\sigma_{\text{NLO}}^{q\ell\to q}\big(v,w,\mu^2\big) =& C_F\frac{\alpha_{\text{em}}^2 e_q^2}{svw}\Bigg\{A_0^{q\to q}\delta\big(1-w\big)+A_1^{q\to q}\left(\frac{\ln\big(1-w\big)}{1-w}\right)_+\\ &+\left(\frac{1}{1-w}\right)_+\Bigg[B_1^{q\to q}\ln\left(\frac{1-v}{v(1-v+vw)}\right)\\ &+B_2^{q\to q}\ln\big(1-v+vw\big)+B_3^{q\to q}\ln\left(\frac{sv^2}{\mu^2}\right)\Bigg]\\ &+C_1^{q\to q}\ln\big(v(1-w)\big)+C_2^{q\to q}\ln\left(\frac{w(1-v)}{1-vw}\right)\\ &+C_3^{q\to q}\ln\left(\frac{1-v}{(1-vw)(1-v+vw)}\right)\\ &+C_4^{q\to q}\ln\left(\frac{s}{\mu^2}\right)+C_5^{q\to q}\Bigg\}\end{aligned} \tag{4.53}$$

for the subprocess $q\ell \to qX$ and

$$\begin{aligned}\sigma_{\text{NLO}}^{q\ell\to g}\big(v,w,\mu^2\big) =& C_F\frac{\alpha_{\text{em}}^2 e_q^2}{svw}\Bigg\{C_1^{q\to g}\ln\big(1-v+vw\big)\\ &+C_2^{q\to g}\ln\left(\frac{1-v}{(1-vw)(1-v+vw)}\right)\\ &+C_3^{q\to g}\ln\left(\frac{sv(1-w)}{\mu^2}\right)+C_4^{q\to g}\end{aligned} \tag{4.54}$$

in the case of the $q\ell \to gX$ channel, respectively

$$\begin{aligned}\sigma_{\text{NLO}}^{g\ell\to q}\big(v,w,\mu^2\big) =& T_R\frac{\alpha_{\text{em}}^2 e_q^2}{svw}\Bigg\{C_1^{g\to q}\ln\left(\frac{(1-v)w}{1-vw}\right)\\ &C_2^{g\to q}\ln\left(\frac{sv(1-w)}{\mu^2}\right)+C_3^{g\to q}\Bigg\}\end{aligned} \tag{4.55}$$

for $g\ell \to qX$ scattering. The coefficients arising in these expressions are listed in the appendix of the latter mentioned study. The photon-parton cross sections encountered in equation 4.52 are truly functions of v and w which is a consequence of adjusted kinematics following the integration over the δ-function when dealing with the collinear configurations. They read

$$\sigma^{q\gamma\to q}\big(v,w\big) = 2\pi C_F\frac{\alpha_{\text{em}}^2 e_q^2}{s(1-v)}\frac{1+v^2w^2}{vw} \tag{4.56}$$

$$\sigma^{q\gamma\to g}\big(v,w\big) = 2\pi C_F\frac{\alpha_{\text{em}}^2 e_q^2}{s(1-v)}\frac{1+(1-vw)^2}{1-vw} \tag{4.57}$$

$$\sigma^{g\gamma\to q}\big(v,w\big) = 2\pi T_R\frac{\alpha_{\text{em}}^2 e_q^2}{s(1-v)}\frac{v^2w^2+(1-vw)^2}{vw(1-vw)} \tag{4.58}$$

in $d = 4$ dimensions.

4.3 Phenomenological Studies

In the foregoing sections of the present chapter, the single-inclusive production of hadrons in unpolarized nucleon-lepton scattering was investigated analytically. In the course of our discussion, we introduced the general framework and derived a formula for the factorized cross section as a preliminary step. We then computed the cross sections for the partonic subprocesses at leading and next-to-leading order by employing techniques from perturbation theory. Ultimately, we found that the hadronic cross section may be written as

$$\begin{aligned} E_h \frac{d^3\sigma^{N\ell\to hX}}{dP_h^3} =& \left(-\frac{U}{S^2}\right)^2 \sum_{a,c} \int_{v_{\min}}^{v_{\max}} \frac{dv}{v(1-v)} \int_{w_{\min}}^{1} \frac{dw}{w^2} \frac{f^{a/N}(x,\mu)}{x} \\ & \times \frac{D^{c/h}(z,\mu)}{z^2} \Bigg\{ \sigma_{\mathrm{LO}}^{a\ell\to c}(v,w) + \frac{\alpha_s(\mu^2)}{\pi} \sigma_{\mathrm{NLO}}^{a\ell\to c\ell}(v,w,\mu^2) \\ & + \frac{\alpha_s(\mu^2)}{\pi} f^{\gamma/\ell}\left(\frac{1-v}{1-vw},\mu^2\right) \sigma_{\mathrm{LO}}^{a\gamma\to c}(v,w) \Bigg\} \end{aligned} \tag{4.59}$$

in terms of two contributions. Here, the first part contains exclusively the commonly known parton distributions and fragmentation functions and the relevant subprocesses are those with a lepton as well as a parton originating from the nucleon in the initial state. The second contribution, on the other hand, is not limited to the formerly mentioned parton distributions and fragmentation functions, but also includes photon-in-lepton distributions. Consequently, photon-parton processes need to be considered this time. The second part of the hadronic cross section is hence related to the previously introduced Weizsäcker-Williams contribution involving processes where the lepton acts as a source for quasi-real photons entering the hard scattering.

The formula for the factorized cross section, which was presented in the equations 4.52 and 4.59, enables us to conduct phenomenological studies for real-world experiments by applying numerical procedures. Against this background, our task consists in particular of evaluating the v- and w-integrals numerically. In more detail, we make use of a VEGAS algorithm written in the programming language Fortran. The VEGAS algorithm was originally developed by Gerard P. Lepage [156, 157] for multidimensional integration with the purpose to reduce numerical errors. It relies on the principle of importance sampling and uses a probability distribution to narrow down the search to regions of the integrand that yield substantial contributions to the integral.
But beyond the numerical integration method, some input for the parton densities and fragmentation functions will be needed. In the case of the studies, which will be presented in the following subsections, we resort to

the CTEQ6.6 [170] set of parton distribution functions. Above that, we use the DSS [73, 74] set of fragmentation functions. Among other advantages, the choice of these sets is expected to provide a better comparability with the numerical results presented in [120].

In light of these preliminaries, we will carry out numerical studies on the single-inclusive production of hadrons in unpolarized nucleon-lepton scattering for three different experiments in the remainder of the section at hand. First, we will investigate the production of charged pions and kaons at HERMES. Second, we will present results on the scattering of muons and nucleons for kinematic conditions as they are common for COMPASS. In this case, we will study the production of neutral pions. Lastly, we will again consider the production of charged pions but this time for the kinematics of a future EIC. Finally, it should be noted, that we assume all encountered scales, like the factorization or fragmentation scale, to be equal to a hard scale of the scattering. In the course of our numerical considerations, we select the transverse momentum of the produced hadron as a choice for said scales. Besides the relevant cross sections, we will also present the so-called K-factor

$$K \equiv \frac{\sigma_i}{\sigma_{\rm LO}}, \tag{4.60}$$

where σ_i in the numerator is either given by the full NLO cross section or the sum of the LO cross section and the Weizsäcker-Williams contributions.

4.3.1 Hermes

The first numerical calculations, which we want to present, concern the production of charged pions and kaons at HERMES, where the center-of-mass energy is given by $\sqrt{S} = 7.25\,\mathrm{GeV}$. As it can be seen in e.g. [22], the observables are portrayed in terms of the variables $P_{h\perp}$ and x_F by the HERMES Collaboration, where the first denotes the transverse momentum of the produced hadron and the second represents a Feynman variable, which is a measure for the momentum fraction of the produced hadron along the beam axis. Before we can carry out the numerical computations, we need to reformulate the factorized cross section given in equation 4.59 in terms of the aforementioned variables. For this purpose, we exploit the fact that the Feynman variables x_T and x_F may be written as

$$x_F = \frac{2P_{h,z}}{\sqrt{S}} = \frac{T-U}{S} \quad \text{and} \quad x_T = \frac{2P_{h\perp}}{\sqrt{S}} \tag{4.61}$$

in the center-of-mass frame of the incoming nucleon and lepton. We then find the relation

$$\frac{d^2\sigma^{N\ell\to hX}}{dx_F dP_{h\perp}} = \frac{2\pi P_{h\perp}}{\sqrt{x_F^2 + x_T^2}} E_h \frac{d^3\sigma^{N\ell\to hX}}{dP_h^3} \tag{4.62}$$

for the factorized cross section, which allows us to finally carry out the numerical computations. In the figures 4.5, 4.7, 4.9 and 4.11, the cross sections for the production of charged pions and kaons as functions of x_F are shown. They were therefore integrated over $1.0\,\text{GeV} \leq P_{h\perp} \leq 2.2\,\text{GeV}$. In contrast, the figures 4.6, 4.8, 4.10 and 4.12 show the cross sections as a function of the transverse momentum $P_{h\perp}$, which means that they have been integrated over $0.30 \leq x_F \leq 0.55$. In all cases, we observe a similar outcome. First, it can be noted that the NLO corrections yield a large contribution. Second, the Weizsäcker-Williams contributions make up a significant proportion of the NLO corrections. Especially in the case of the production of the K^- hadron, the NLO corrections dominate the cross section as it can be seen in the figures 4.11 and 4.12. Furthermore, it is remarkable that the Weizsäcker-Williams contributions determine the NLO corrections almost completely in these two instances.

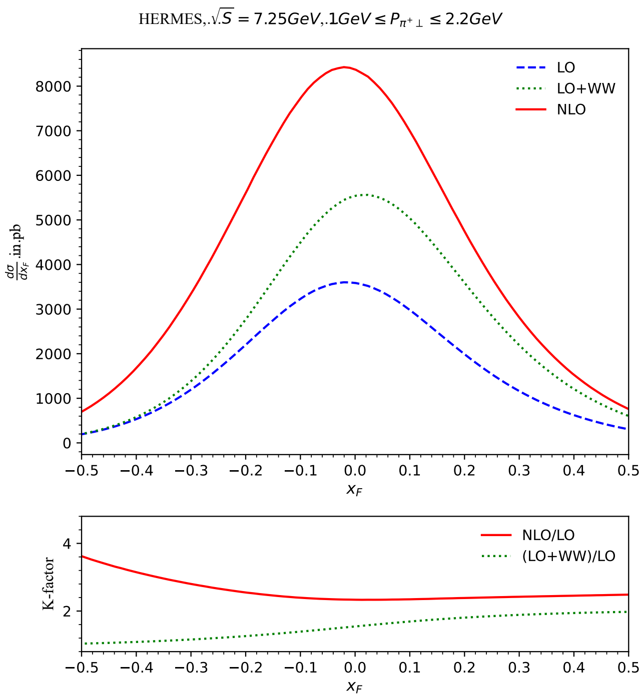

Figure 4.5: Cross section for $p\ell \to \pi^+ X$ at HERMES as a function of x_F. The upper picture shows the cross section, which was integrated over $1.0\,\text{GeV} \leq P_{\pi^+\perp} \leq 2.2\,\text{GeV}$. The lower diagram illustrates the K-Factor.

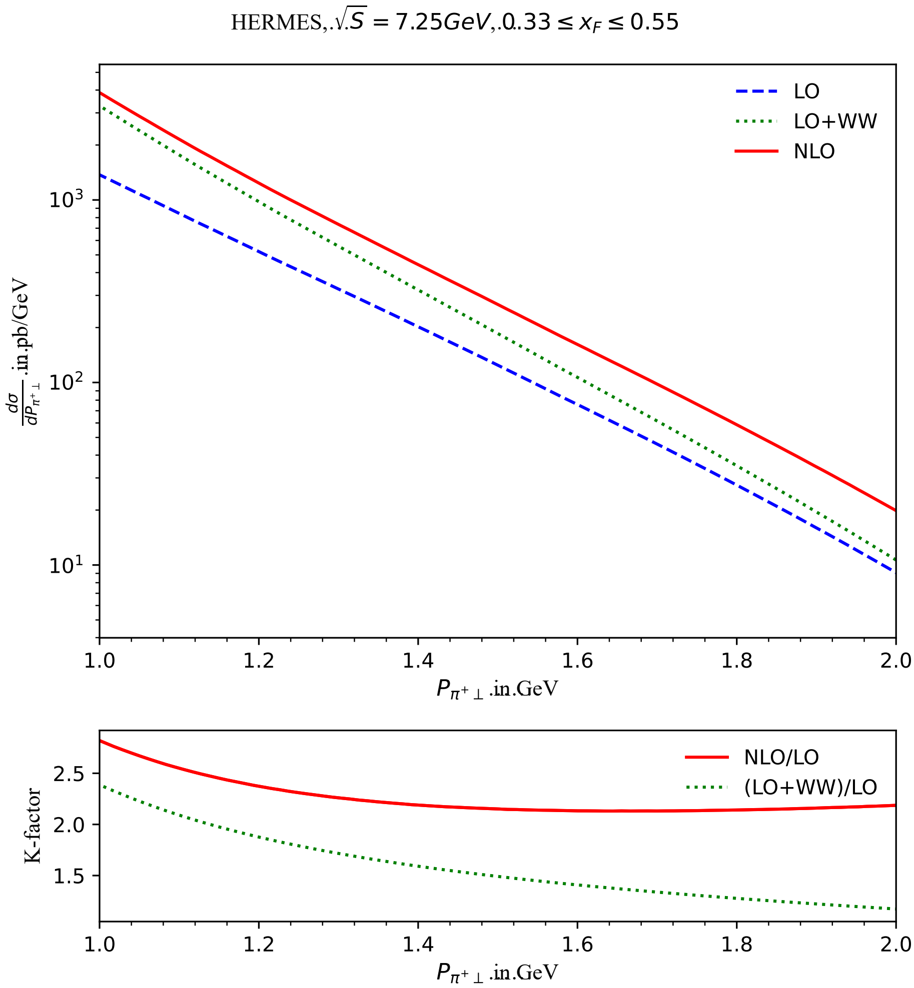

Figure 4.6: Cross section for $p\ell \to \pi^+ X$ at HERMES as a function of $P_{\pi^+\perp}$. The cross section was integrated over $0.30 \le x_F \le 0.55$.

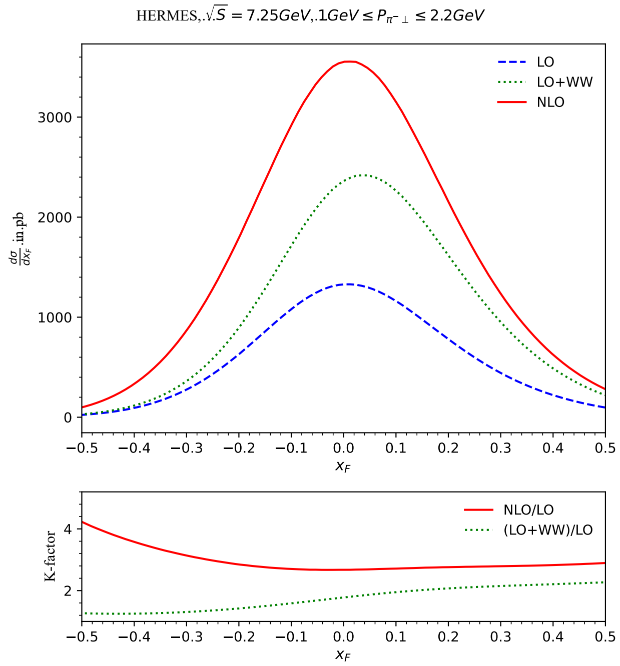

Figure 4.7: Cross section for $p\ell \to \pi^- X$ at HERMES as a function of x_F. The cross section was integrated over $1.0\,\mathrm{GeV} \leq P_{\pi^-\perp} \leq 2.2\,\mathrm{GeV}$.

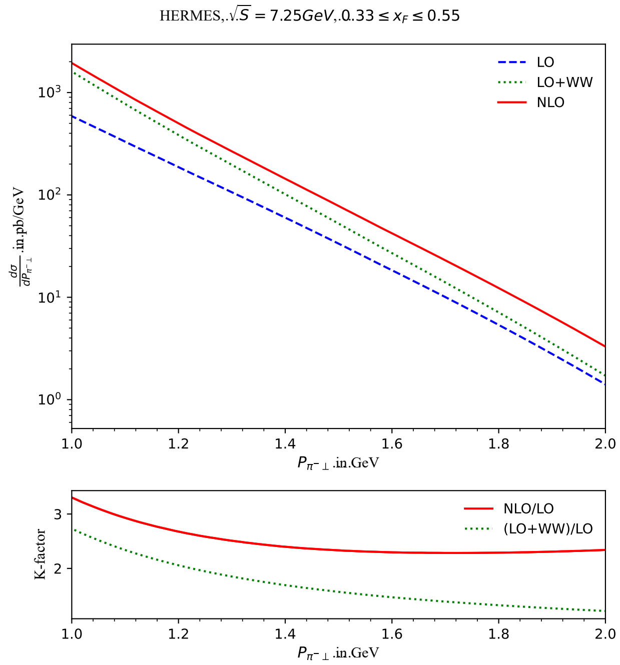

Figure 4.8: Cross section for $p\ell \to \pi^- X$ at HERMES as a function of $P_{\pi^-\perp}$. The cross section was integrated over $0.30 \leq x_F \leq 0.55$.

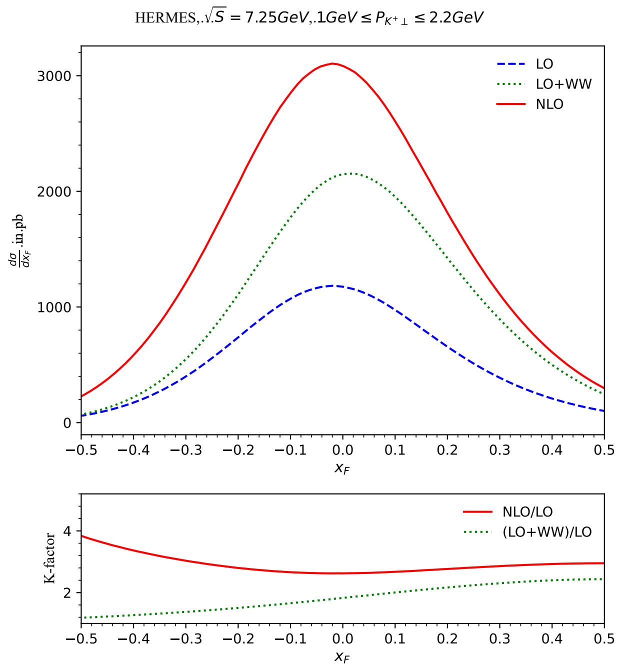

Figure 4.9: Cross section for $p\ell \to K^+X$ at HERMES as a function of x_F. The cross section was integrated over $1.0\,\mathrm{GeV} \leq P_{K^+\perp} \leq 2.2\,\mathrm{GeV}$.

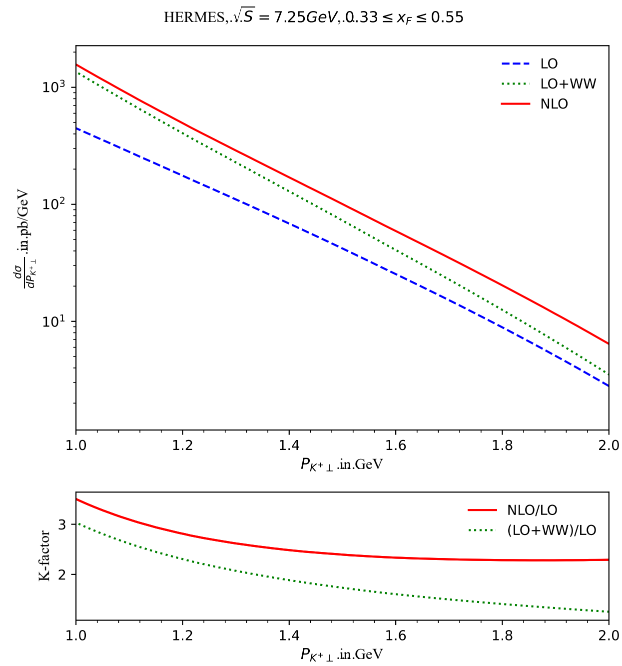

Figure 4.10: Cross section for $p\ell \to K^+X$ at HERMES as a function of $P_{K^+\perp}$. The cross section was integrated over $0.30 \leq x_F \leq 0.55$.

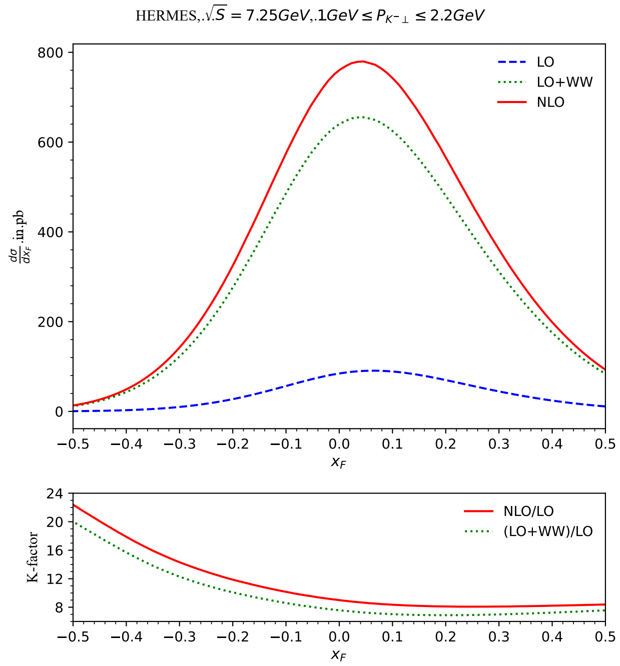

Figure 4.11: Cross section for $p\ell \to K^- X$ at HERMES as a function of x_F. The cross section was integrated over $1.0\,\mathrm{GeV} \leq P_{K^-\perp} \leq 2.2\,\mathrm{GeV}$.

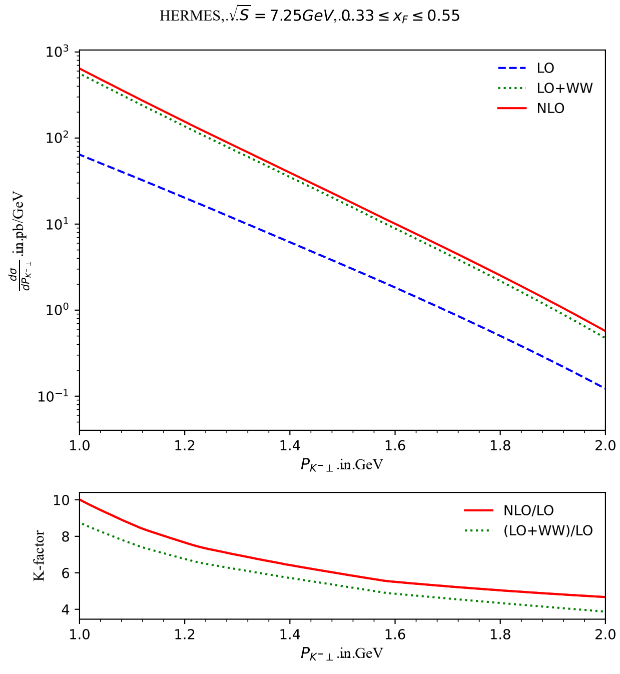

Figure 4.12: Cross section for $p\ell \to K^- X$ at HERMES as a function of $P_{K^-\perp}$. The cross section was integrated over $0.30 \leq x_F \leq 0.55$.

4.3.2 Preliminaries for COMPASS and EIC

In the previous subsection, we presented numerical results for HERMES, where the computed cross sections have been expressed as functions in the transverse momentum $P_{h\perp}$ of the produced hadron and the Feynman variable x_F. In the subsequent sections, similar considerations will be presented for COMPASS and the future EIC. However, in these instances, we will choose another set of variables to represent the appropriate differential cross section. The first variable will be again the transverse momentum $P_{h\perp}$, which was already made use of in the context of HERMES. The second one will be the pseudorapidity η, that is commonly introduced as

$$\eta \equiv -\ln\left[\tan\left(\frac{\vartheta}{2}\right)\right] \tag{4.63}$$

in terms of the scattering angle ϑ between the particle direction and the beam axis. The Mandelstam variables T and U can now be written as functions of these two variables, i.e. the transverse momentum and the pseudorapidity. They then read

$$T = -P_{h\perp}\sqrt{S}e^{\eta} \ , \tag{4.64}$$

$$U = -P_{h\perp}\sqrt{S}e^{-\eta} \ , \tag{4.65}$$

which allows to rewrite the differential cross section and finally leads to the relation

$$\frac{d^2\sigma^{N\ell\to hX}}{d\eta dP_{h\perp}} = 2\pi P_{h\perp}E_h\frac{d^3\sigma^{N\ell\to hX}}{dP_h^3} \tag{4.66}$$

that will be employed in our numerical considerations. Beyond that, the relation

$$x_F = 2\frac{P_{h\perp}}{\sqrt{S}}\sinh\left(\eta\right) \tag{4.67}$$

between x_F, $P_{h\perp}$ and η can be found.

In the next two subsections, we will make use of the equations and relations presented here, to compute the cross section for kinematics as they are common for experimentes by the COMPASS collaboration, respectively at the future EIC and study the cross section's dependence on the transverse momentum of the produced hadron as well as on the pseudorapidity. As before, we will distinguish between the LO contribution, the full NLO corrections and the Weizsäcker-Williams contributions. On top of that, we will also again determine the corresponding K-factors.
In the following, we will only present numerical results for the production of a π^0 at COMPASS, respectively π^+ at the EIC, since the outcome for the different particle types qualitatively differ only sightly as it was already seen in the case of HERMES.

4.3.3 Compass

As noted at the beginning in the introduction to the chapter, the single hadron quasi-real photoproduction was studied by the COMPASS collaboration, where a μ-beam has been used as a source for the photons. We take these experiments as a motivation to examine the inclusive production of a hadron in unpolarized muon-nucleon scattering, i.e. the process

$$p + \mu \to hX,$$

where we assume kinematic conditions as they are usual for COMPASS. Both processes are similar and overall we could already observe in our numerical considerations for HERMES that the Weizsäcker-Williams contributions associated with quasi-real photons make a significant contribution to the cross section. In the following, we will therefore present a numerical study of the production of neutral pions. Of course, the numerical investigations can also be carried out for charged pions or kaons, whereby the results do not differ greatly in terms of quality as it has already been observed in the context of our considerations on HERMES. We will therefore leave it at presenting results for the aforementioned process, which we can compare with those given in [120].

More precisely, we study the production of neutral pions at a center-of-mass energy $\sqrt{S} = 17.4\,\mathrm{GeV}$. We start our considerations by investigating the behaviour of the unintegrated cross section

$$\frac{d^2\sigma^{N\ell\to hX}}{d\eta dP_{h\perp}} \tag{4.68}$$

as function of η at a fixed value of the produced hadron's transverse momentum, which is chosen to be $P_{\pi^0\perp} = 2\,\mathrm{GeV}$. The corresponding result is shown in figure 4.13. In the next step, the cross section is integrated over $-0.10 \leq \eta \leq 2.38$ and its behaviour as a function of $P_{\pi^0\perp}$ is examined, which is illustrated in figure 4.14. In addition to the cross section, both figures show a second diagram that involves the appropriate K-factors in each case.

The figures show that although the Weizsäcker-Williams contributions still provide a sizeable correction to the leading-order cross section, it is overall less significant in view of the full next-to-leading order result, which is particularly noticeable in comparison to the previously presented HERMES results.

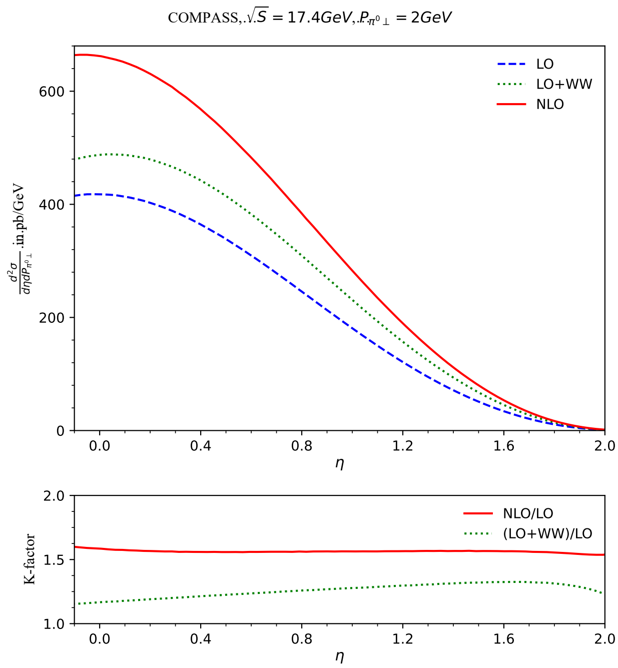

Figure 4.13: Cross section for $p\mu \to \pi^0 X$ at COMPASS as a function of η. The transverse momentum of the produced π^0 is fixed at $P_{\pi^0\perp} = 2\,\text{GeV}$.

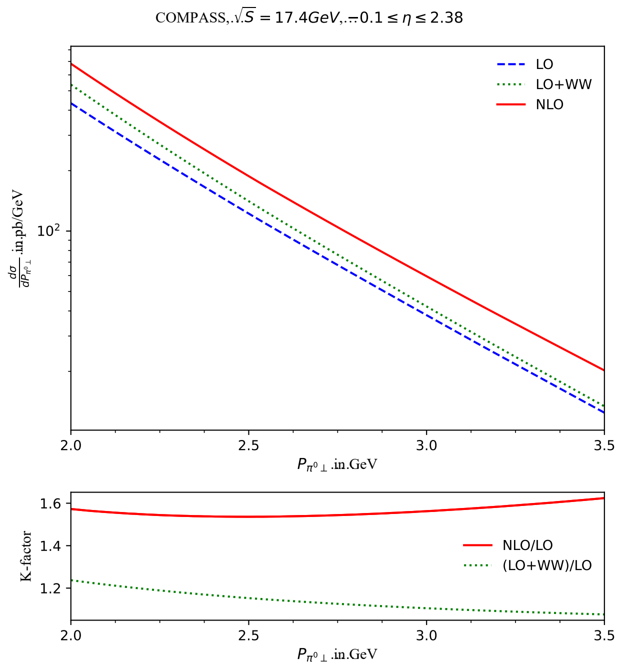

Figure 4.14: Cross section for $p\mu \to \pi^0 X$ at COMPASS as a function of $P_{\pi^0\perp}$. The cross section was integrated over $-0.10 \leq \eta \leq 2.38$.

4.3.4 Electron-Ion-Collider

Finally, we consider the cross section in a kinematic regime as it will be common for the EIC. The EIC is a future particle accelerator colliding electrons with protons or nuclei whose design will be particularly suitable for studies relating to the strong interaction. Beyond a better understanding of the strong force in general, it offers a possibility to improve our knowledge on the spin effects due to its technological capabilities to polarize the particle beams.

In the following, we present results on the production of the π^+ in electron-proton scattering at a center-of-mass energy $\sqrt{S} = 100\,\text{GeV}$. In the course of these investigations, we will proceed as previously for the COMPASS experiment. In the first step, we therefore examine the dependence of the differential cross section on the pseudorapidity η, where we assume the transverse momentum of the produced hadron to be fixed at $P_{\pi^+\perp} = 10\,\text{GeV}$. The corresponding results are shown in figure 4.15. Next, we continue our considerations by studying the behaviour of the cross section integrated over $-2 \leq \eta \leq 2$ as a function of the produced hadron's transverse momentum. The results can be found in figure 4.16. In this case, the results are again more similar to those we have already found for HERMES and so the Weizsäcker-Williams contributions make a significant contribution to the corrections at next-to-leading order.

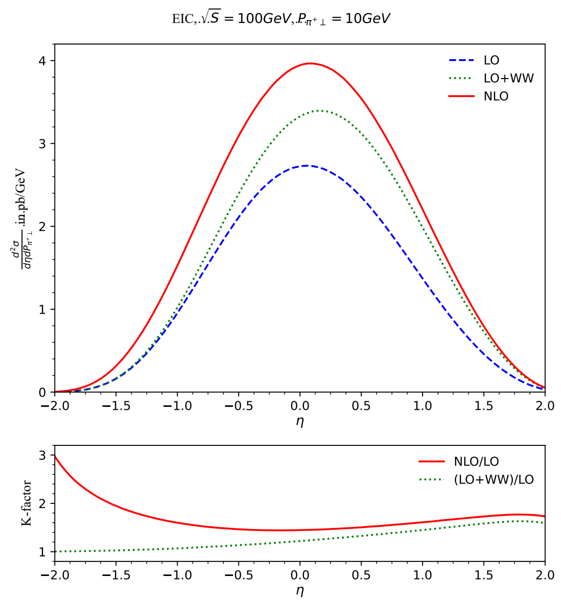

Figure 4.15: Cross section for $pe^- \to \pi^+ X$ at EIC as a function of η. The transverse momentum of the produced π^+ is fixed at $P_{\pi^+\perp} = 10\,\text{GeV}$.

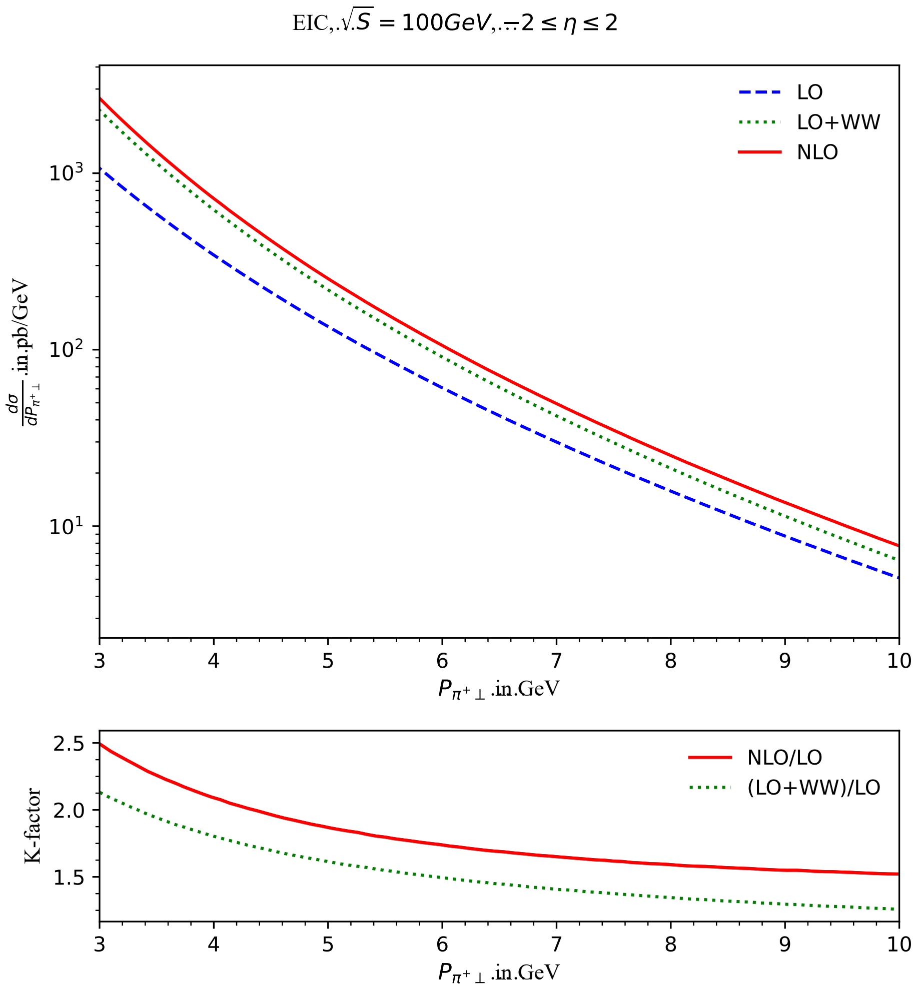

Figure 4.16: Cross section for $pe^- \to \pi^+ X$ at EIC as a function of $P_{\pi^+\perp}$. The cross section was integrated over $-2 \leq \eta \leq 2$.

4.4 Conclusion

In the present chapter, we have dealt intensively with the inclusive production of a hadron in unpolarized lepton-nucleon scattering in preparation for the spin-polarized process. The unpolarized process has the advantage that the structures involved are less complicated than in the polarized case and the number of contributions is more manageable, which makes it very suitable for introducing the basic techniques and procedures required in calcuation at higher orders of perturbation theory. In more detail, we have computed the next-to-leading order QCD corrections to the partonic cross section, where we needed to take Weizsäcker-Williams contributions into account in addition to the commonly known methods. Overall, we found that our result for the cross section is in agreement with those that were presented in [120].

In the second part, we presented numerical studies for experimental setups that are common for HERMES, COMPASS and at the future EIC. Among our key observations is that the next-to-leading order corrections make a large contribution to the cross section and are essential for an accurate and reliable analysis of experimental data. This could be an indicator that a similar situation might occur when the same process is studied but with a transversely polarized nucleon.

Furthermore, we have explicitly studied the influence of the Weizsäcker-Williams contributions. We found that they can provide significant contributions to the cross section. In some cases, it seems that they even dominate the NLO correction to the cross section as it has been observed for the production of the K^- at HERMES. The latter process could therefore also provide an opportunity to test these special contributions. On the other hand, however, it is not guaranteed that the NLO corrections are dominated by the domain of quasi-real photons as it can be seen from the results on the π^0 production at COMPASS, for example, where the contributions turned out to be sizeable but not dominant.

In summary, it can be thus said, that the Weizsäcker-Williams contributions can be large and usually play a non-negligible role but they are not governing the NLO corrections in general. Instead, higher order QCD effects like gluon loops or the emission of real gluons have to be taken into account for a complete analysis.

Chapter 5

Transverse Single-Spin Asymmetry in Nucleon-Lepton Scattering

Chapter 5

Transverse Single-Spin Asymmetry in Nucleon-Lepton Scattering

The transverse single-spin asymmetry has garnered significant theoretical and experimental attention since the 1970's, when strikingly large asymmetries were observed in the production of polarized hyperons $\mathrm{p}+\mathrm{Be} \to \Lambda^{0\uparrow}+\mathrm{X}$ at FermiLab [60] and in the production of pions $\mathrm{p}^{\uparrow}(s_T)+p \to \pi^{\pm}+\mathrm{X}$ at the Argonne National Laboratory [144] in forward direction. The asymmetry is defined for scattering processes involving a single transversely spin-polarized particle by the difference in cross sections where the polarized particle's transverse spin is flipped divided by the spin-averaged counterpart as

$$A_{\mathrm{N}} \equiv \frac{\Delta\sigma(s_T)}{\sigma} \equiv \frac{\sigma(s_T)-\sigma(-s_T)}{\sigma(s_T)+\sigma(-s_T)} \ . \tag{5.1}$$

Following their initial observations, the existence of large asymmetries was confirmed through further measurements in proton-proton collisions at FermiLab [8–11, 153] and RHIC [7, 12–14, 33, 210], as well as experimental studies pertaining to semi-inclusive scattering of nucleons and leptons by HERMES [18–22, 175, 190] at DESY, COMPASS [17, 24, 25, 163] and SMC [55] at CERN and at JLAB [27, 183, 228].

On the contrary, the theoretical understanding of the asymmetries ranging around ten percent and more as measured in the aforementioned experiments, has proven to be a daunting task. Despite the success of perturbative Quantum Chromodynamics in describing unpolarized processes, it fails to explain the transverse single-spin asymmetry at leading power in the framework of collinear factorization and predicts vanishing contributions. It therefore requires an extension of the factorization theorem beyond leading twist where one uses the commonly known twist-2 parton densities and fragmentation functions. Another factor that renders the theoretical analysis particularly intricate is the requirement for an additional phase to obtain a non-zero asymmetry. Nowadays, two mechanisms to generate large asymmetries are known and have been established for phenomenological applications.

The first one relies on a generalized factorization scheme that utilizes parton distribution and fragmentation functions with a dependence on an intrinsic partonic transverse momentum and is applied in kinematic regions where the produced hadron in the final state carries small transverse momentum. In the framework of so-called transverse momentum dependent distributions (TMD) [36, 49, 67, 199, 200], two effects, the Sivers- and Collins-effect, contributing to non-zeros TSSAs have been identified. The Sivers-effect is associated with an initial state hadron whereas the Collins-effect concerns the fragmentation process.

The second approach describes the transverse single-spin asymmetry as a twist-3 observable in the framework of collinear factorization and applies when the transverse momentum of the produced hadron is large. As it was first pointed out by Efremov and Teryaev in [77, 78], a non-zero asymmetry might be generated by going beyond the leading power in collinear factorization where the spin-dependent cross section is related to a convolution of twist-3 multi-parton correlations, like quark-gluon-quark correlations, and the usual twist-2 distribution functions. A first systematic procedure to carry out such twist-3 calculations in pQCD was developed by Qiu and Sterman in [185–187]. In this framework, the necessary phase between interfering amplitudes is provided by imaginary parts which can be extracted from pole contributions arising due to internal lines going on-shell. In general, the encountered pole contributions can be arranged in three categories: soft-gluon (SGP), soft-fermion (SFP) and hard poles (HP) where each type of pole is associated with a certain structure of the propagator. Another feature contributing to the complexity of perturbative calculations in the framework of twist-3 factorization is the occurrence of a derivative with respect to a transverse momentum. Due to this, all results may be written in terms of a derivative part proportional to the first derivative of a twist-3 matrix element and a non-derivative part proportional to the twist-3 matrix element itself but where a derivative of the hard scattering function need to be taken.

In the past, it has been shown in [130–132, 149, 227] that both approaches, TMD and twist-3 collinear factorization, lead to consistent results in kinematic regions where both apply which increased the confidence in their validity among theorists. However, most phenomenological studies are still limited to the leading order in pQCD (see e.g. [23, 99, 136, 137, 148, 152]) and only a few works concerning TSSAs at NLO for Drell-Yan [62, 211] and SIDIS [63] exist. Recently, a new study [95] was published with the intention of gaining new insights into the transverse single-spin asymmetry at next-to-leading order. Instead of performing the full NLO calculation, they used an estimation that relies on the NLO corrections for the unpolarized part for the inclusive production of a single hadron in nucleon-lepton scattering. However, we are still lacking a full NLO calculation and especially not much is known of the derivative-piece at higher orders in neither lepton-nucleon scattering nor proton-proton collisions. One the other hand, it has been frequently demonstrated in regular pQCD calculations that corrections in next-to-leading order are typically significantly large. Therefore, expecting next-to-leading order correction to TSSAs to be of similar importance seems reasonable. In particular, with regard to the Electron-Ion Collider (EIC) which will provide measurements with higher accuracy in comparison to the already existing experiments, next-to-leading order results might play a crucial role for a sufficient analysis of the data which will be gathered at this facility in the future. Alongside the stated developments arguing for an emerging need for NLO corrections to SSAs, understanding these observables at higher orders could also provide a test for QCD factorization beyond leading power.

In the chapter at hand, we will explore the spin-dependent part of the transverse single-spin asymmetry, arising in the numerator of equation 5.1, at next-to-leading order. To this end, we essentially follow the procedure that was already employed in [119], but also extend the approach to include further contributions enabling us to finally determine the next-to-leading order corrections. Furthermore, we would like to emphasize that, within the scope of the present thesis, we pursue a different approach to the analytical calculations than the one, we employed in [188, 189]. Both approaches yield identical divergent contributions. In contrast, differences arises in the finite parts of so-called hard pole contributions from the real corrections. While [188, 189] provides the complete contributions, the alternative approach allows only for the extraction of the divergent parts. However, the alternative approach offers the advantage of being methodologically simpler and less time-consuming, and it may be used to cross-check the full calculation. Moreorver, it is already sufficient to obtain significantly improved and quantitatively more reliable results compared to a pure leading order consideration, and can therefore serve as a valuable alternative to the full next-to-leading order calculation for complex processes when a first estimate is required within a short time.

5.1 Introduction of the General Framework

Mirroring our previous discussion, when we examined unpolarized scattering, we commence our considerations by establishing the general framework which serves as the foundation of our calculations. The primary focus of our considerations is once again on the investigation of the inclusive production of a single hadron in nucleon-lepton scattering, albeit with the assumption that the incoming nucleon is transversely spin-polarized. This means that we consider the process

$$N^{\uparrow}\big(P, s_T\big) + \ell\big(p'\big) \to h\big(P_h\big) + X,$$

where the nucleon's spin vector s_T is perpendicular to the direction of motion, and we want to determine the spin-dependent cross section.
As already mentioned in the introduction of the present chapter, two distinct approaches can be employed to describe such processes, where one of them relies on the application of so-called transverse momentum weighted distributions. However, in what follows we shall rely on the second approach based on collinear factorization, the framework that we have already employed in our analysis of the spin-averaged cross section. The transverse single-spin asymmetry, respectively the spin-dependent part arsing in the numerator, is regarded as a higher twist effect in this specific framework. In more detail, it is a twist-3 observable and the associated factorized cross section can therefore be written as a convolution of a twist-3 function, further twist-2 parton densities as well as fragmentation functions and a perturbatively computable cross section on the level of the partons. In the course of this section, we will see that contributions to such a spin-dependent cross section could in principle be generated by two classes of diagrams. The first category includes the diagrams that we previously encountered in our analysis concerning the unpolarized process. This is attributed to the fact, that the diagrams are linked to the quark-quark-correlator, which can be parameterized through the use of twist-2 but also twist-3 functions, as known from equation 2.66 and we thus need to examine possible non-vanishing contributions by the arising twist-3 functions. The second class of diagrams involves multi-parton correlators which only appear at higher twist. In our particular scenario, contributions proportional to the quark-gluon-quark or the gluon-gluon-gluon correlator could in general occur, however, we shall solely focus on those related to the quark-gluon-quark correlator as they are expected to yield the major contribution to the single-spin asymmetry.

In the remainder of the present section, we want to study both classes of diagrams and ascertain whether they can lead to a non-vanishing contribution. In the course of this endeavor, we aim to derive a factorization formula for the spin-dependent cross section. Note that we will closely follow the procedure outlined in [81].

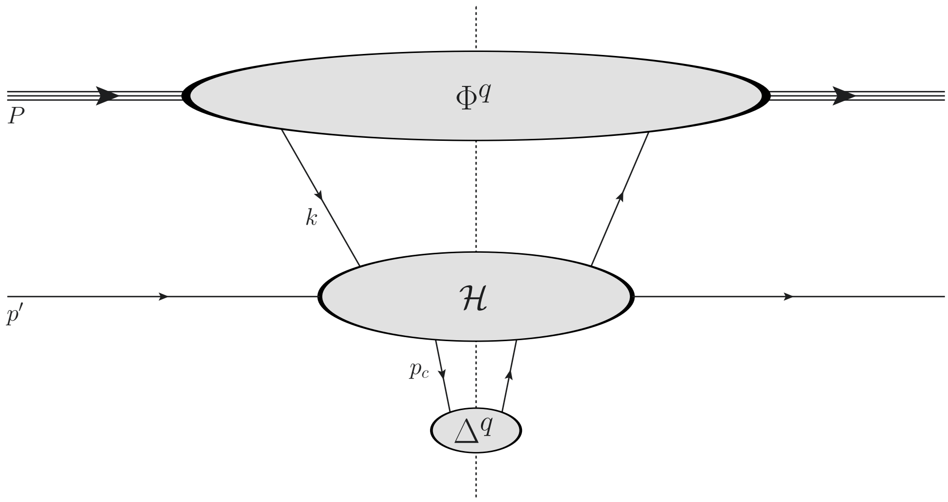

Figure 5.1: First type of contribution to spin-dependent cross section in the single inclusive production of a hadron in nucleon-lepton scattering. The upper blob represents the nucleon, which is now assumed to be transversely polarized. Otherwise, it is the same diagram as shown in figure 4.1.

To derive the formula, we will work in light-cone gauge since the encountered matrix elements become particularly simple as the gauge links are given by identity matrices in this specific gauge. Likewise as in section 2.2 of the introduction of the theoretical background, we will need to introduce a light-like four-vector n at some point, which fulfills $n^2 = 0$ and $n \cdot P = 1$. Furthermore, the spin vector satisfies the properties $s_T^2 = -1$ and $s_T \cdot P = s_T \cdot n = 0$ in this particular framework.
We start our analysis with the diagram shown in figure 5.1 that we already know from the unpolarized considerations presented in the last chapter. In this instance, a parton from the polarized nucleon and the incoming lepton enter the hard scattering process and the cross section thus contains the quark-quark correlator $\Phi^a_{jk}(k, s_T)$. It is noteworthy that the fragmentation process can be handled in complete analogy as outlined previously. We therefore refrain from a detailed introduction and instead adopt the already known result. The diagram shown in the figure is linked to a contribution to the factorized spin-dependent cross section, which may be written as

$$\begin{aligned} d\Delta\sigma(s_T) &= \frac{1}{2S} \sum_{a,c} \int \frac{dz}{z^2} D^{c/h}(z) \int \frac{d^4k}{(2\pi)^4} \mathcal{H}_{kj}(k) \\ &\quad \times \int d^4\lambda e^{ik\cdot\lambda} \langle P, s_T | \bar{\psi}_{a,k}(0) \psi_{a,j}(\lambda) | P, s_T \rangle \qquad (5.2) \\ &= \frac{1}{2S} \sum_{a,c} \int \frac{dz}{z^2} D^{c/h}(z) \int d^4k\, \mathcal{H}_{kj}(k) \Phi^a_{jk}(k, s_T), \qquad (5.3) \end{aligned}$$

where $\mathcal{H}$ denotes an appropriate hard scattering function.

Just like before, we need to expand the hard scattering function around the quark's momentum in the collinear limit. In the view of the foregoing discussions, we assume that the quark's momentum is collinear to the parent nucleon's momentum and write it as

$$k \approx xP + k_\perp \tag{5.4}$$

with $k_\perp$ being a small transverse component of the parton's momentum k. We can now expand the hard scattering function in the light of these circumstances and hence obtain

$$\mathcal{H}_{kj}(k) \approx \mathcal{H}_{kj}(xP) + \frac{\partial \mathcal{H}_{kj}(k)}{\partial k^\alpha}\bigg|_{k\approx xP} \omega^\alpha{}_\beta k^\beta + \mathcal{O}\big(k_\perp^2\big), \tag{5.5}$$

where the tensor $\omega^{\alpha\beta}$ is given by

$$\omega^{\alpha\beta} \equiv g^{\alpha\beta} - P^\alpha n^\beta \tag{5.6}$$

with n being the aforementioned four-vector satisfying $n^2 = 0$ and $n \cdot P = 1$. According to the definition, the tensor allows to extract the transverse components of a four-vector and we can thus find the relation $k_\perp^\alpha = \omega^{\alpha\beta} k_\beta$.

As a reminder, the parameterization of the quark-correlator, which is already known from the introduction of the theoretical background and especially equation 2.66, will be explicitly presented again at this point. As stated back then, it may be written as

$$\begin{aligned}
\Phi^q(x) = \frac{1}{2}\bigg\{ & \not{P} f_1^q(x) + M e^q(x) \\
& - M\big(S\cdot\bar{n}\big)\not{P}\gamma_5 g_1^q(x) + \frac{1}{2}M^2\big(S\cdot\bar{n}\big)\big[\not{P},\not{\bar{n}}\big]\gamma_5 h_L^q(x) \\
& - \frac{1}{2}\big[\not{P},\not{S}\big]\gamma_5 h_1^q(x) - M\big(\not{S} - \big(S\cdot\bar{n}\big)\not{P}\big)\gamma_5 g_T^q(x)\bigg\}
\end{aligned} \tag{5.7}$$

in terms of scalar leading twist and twist-3 functions. Based on the parameterization, it can be discerned that the relevant contribution to the transverse single-spin asymmetry stems from the term $\sim g_T^a(x)$ and it can be therefore concluded that the quark-correlator encountered in the factorization formula, as presented in equation 5.3, can be substituted by $\Phi_{jk}^a(x) \to -\frac{M}{2}\big(\not{s}_T\gamma_5\big)_{jk} g_T^a(x)$. After finally inserting the expansion of the hard scattering function into the factorized cross section, we obtain two possible contributions, where the first contains the function itself at $k = xP$, whereas its derivative occurs in the second term.

The lowest order of the hard scattering function's expansion leads to a possible term in the spin-dependent cross section, which reads

$$\sim \int dx\, \mathcal{H}_{kj}(xP)\bigg(- \frac{M}{2}\bigg)\big(\not{s}_T\gamma_5\big)_{jk} g_T^a(x). \tag{5.8}$$

However, such an expression can be neglected in the final result for the cross section as it will be purely imaginary instead of real. This property originates from the fact, that the traces arising in this contribution contain the γ_5 matrix and will hence lead to an imaginary outcome. But since all other arising quantities are real the total contribution from this part to the cross section is imaginary too and it is thus justified to neglect it.
The second contribution, which contains the derivative of the hard scattering function becomes

$$\begin{aligned} &\sim \int d^4k\, \Phi^a_{jk}(k) \frac{\partial \mathcal{H}^{a\ell\to cX}_{kj}(k)}{\partial k^\alpha}\bigg|_{k\approx xP} \omega^\alpha{}_\beta k^\beta \\ &= i \int dx\, \Phi^{a,\beta}_{jk,\partial}(x) \omega^\alpha{}_\beta \frac{\partial \mathcal{H}^{a\ell\to cX}_{kj}(k)}{\partial k^\alpha}\bigg|_{k\approx xP} \end{aligned} \tag{5.9}$$

after evaluating all integrals over non-longitudinal components.
Here, we have used that a product of the quark-correlator and a component of the momentum k^β may be written as

$$\begin{aligned} k^\beta \Phi^a_{jk}(k) &= \int \frac{d^4\lambda}{(2\pi)^4} k^\beta e^{ik\cdot\lambda} \langle P, s_T | \,\bar{\psi}_{a,k}(0)\psi_{a,j}(\lambda)\, | P, s_T\rangle \\ &= \int \frac{d^4\lambda}{(2\pi)^4} \Big(-i\partial^\beta e^{ik\cdot\lambda}\Big) \langle P, s_T | \,\bar{\psi}_{a,k}(0)\psi_{a,j}(\lambda)\, | P, s_T\rangle \\ &= i \int \frac{d^4\lambda}{(2\pi)^4} e^{ik\cdot\lambda} \langle P, s_T | \,\bar{\psi}_{a,k}(0)\partial^\beta\psi_{a,j}(\lambda)\, | P, s_T\rangle \end{aligned} \tag{5.10}$$

where we have applied integration by parts in the last line. It should be noted that the boundary terms, which usually occur with this integration method, disappear in this case. Moreover we introduced the matrix element $\Phi^{a,\beta}_{jk,\partial}$ via the relation

$$\Phi^{a,\beta}_{jk,\partial}(x) = \int d^2k_\perp k^\beta_\perp \Phi^a_{jk}(k) \tag{5.11}$$

for the quark-correlator.

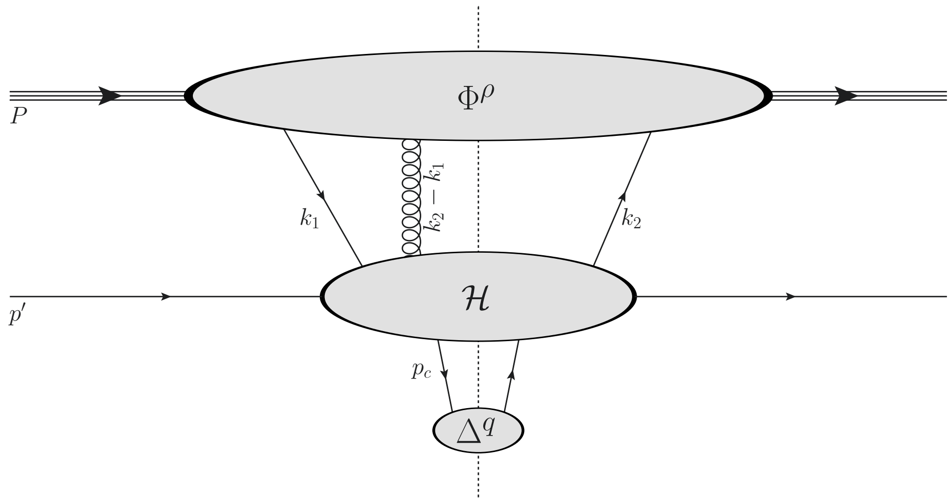

Figure 5.2: Second type of contribution to spin-dependent cross section in the single inclusive production of a hadron in nucleon-lepton scattering. The upper blob represents the nucleon, which is now assumed to be transversely polarized. Otherwise, it is the same diagram as shown in figure 4.1.

The second type of diagram, that could potentially contribute to the transverse single-spin asymmetry, involves multi-parton correlations like the example shown in figure 5.2. In the illustrated example, an additional gluon from the polarized proton enters the hard scattering besides the quark and the factorized cross section hence involves the quark-gluon-quark correlator. Other but similar diagrams linked to the gluon-gluon-gluon correlator exist. However, we will restrict our analysis to diagrams linked to the quark-gluon-quark correlator since they are expected to be responsible for the major contribution to the single-spin asymmetry. Following the same procedure as outlined previously, the spin-dependent cross section associated with the diagram shown in figure 5.2 can be written as

$$\begin{aligned} d\Delta\sigma\big(s_T\big) &= \frac{1}{2S}\sum_{a,c}\int \frac{dz}{z^2} D^{c/h}(z) \int \frac{d^4k_1}{(2\pi)^4}\int \frac{d^4k_2}{(2\pi)^4}\mathcal{H}^{a\ell\to cX}_{jk,\rho}\big(k_1,k_2\big) \\ &\quad\times \int d^4\lambda \int d^4\mu\, e^{ik_1\cdot\lambda} e^{i(k_2-k_1)\cdot\mu} \\ &\quad\times \langle P, s_T|\, \bar\psi_{a,k}(0) g_{\mathrm{s}} A^\rho(\mu)\psi_{a,j}(\lambda)\,|P, s_T\rangle \qquad (5.12) \\ &\equiv \frac{1}{2S}\sum_{a,c}\int \frac{dz}{z^2} D^{c/h}(z) \int \frac{d^4k_1}{(2\pi)^4}\int \frac{d^4k_2}{(2\pi)^4}\mathcal{H}^{a\ell\to cX}_{jk,\rho}\big(k_1,k_2\big) \\ &\quad\times \Phi^\rho_{kj}\big(k_1,k_2\big) \qquad (5.13) \end{aligned}$$

where Φ^ρ denotes a twist-3 matrix element, namely the quark-gluon-quark correlator. As indicated in the diagram, the gluon is assumed to carry the momentum $k_2 - k_1$.

In the next step, we again have to carry out the collinear expansion. However, in contrast to the previous case, where only a single parton momentum occurred, namely k, we now need to expand the hard scattering function around the momenta k_1 and k_2 of the two quarks. We again assume the momenta to be collinear to the parent nucleon's momentum P and approximately write them as

$$k_1 \approx x_1 P + k_{1,\perp} \quad \text{and} \quad k_2 \approx x_2 P + k_{2,\perp} \tag{5.14}$$

with suitable momentum fractions x_1 and x_2 and small transverse components $k_{1,\perp}$ as well as $k_{2,\perp}$. The expansion of the hard scattering function then becomes

$$\begin{aligned}\mathcal{H}_{jk,\rho}\big(k_1,k_2\big) =& \mathcal{H}_{jk,\rho}\big(x_1 P, x_2 P\big) + \frac{\partial \mathcal{H}_{jk,\rho}\big(k_1,k_2\big)}{\partial k_1^\alpha}\bigg|_{k_i \approx x_i P} \omega^\alpha{}_\beta k_1^\beta \\ &+ \frac{\partial \mathcal{H}_{jk,\rho}\big(k_1,k_2\big)}{\partial k_2^\alpha}\bigg|_{k_i \approx x_i P} \omega^\alpha{}_\beta k_2^\beta + \mathcal{O}\big(k_{i,\perp}^2\big)\end{aligned} \tag{5.15}$$

where the tensor $\omega^{\alpha\beta}$ is defined in the exact same way as before. It can be concluded from the definition of the tensor that we are allowed to write

$$\begin{aligned}&\Phi_{kj}^\rho\big(k_1,k_2\big)\mathcal{H}_{jk,\rho}\big(k_1,k_2\big) \\ &= \Phi_{kj}^\rho\big(k_1,k_2\big)\omega^\alpha{}_\rho \mathcal{H}_{jk,\alpha}\big(k_1,k_2\big) + \Phi_{kj}^\rho\big(k_1,k_2\big) n_\rho P^\alpha \mathcal{H}_{jk,\alpha}\big(k_1,k_2\big)\end{aligned} \tag{5.16}$$

and we thus find two contributions when we insert the lowest order of the hard scattering function's expansion into the factorization formula. In fact, we are led to consider the expression

$$\begin{aligned}\sim \int dx_1 \int dx_2 \Big\{ &\Phi_{kj}^\rho\big(x_1,x_2\big) n_\rho \mathcal{H}_{jk}\big(x_1,x_2\big) \\ &+ \Phi_{kj}^\rho\big(x_1,x_2\big)\omega^\alpha{}_\rho \mathcal{H}_{jk,\alpha}\big(x_1,x_2\big)\Big\}\end{aligned} \tag{5.17}$$

in the factorized cross section by following the procedure outlined previously, where the matrix element $\Phi_{kj}^\rho\big(x_1,x_2\big)$ is given by

$$\begin{aligned}\Phi_{kj}^\rho\big(x_1,x_2\big) = &\int \frac{d\lambda}{2\pi} \int \frac{d\mu}{2\pi} e^{i\lambda x_1} e^{i\mu(x_2-x_1)} \\ &\times \langle P, s_T |\, \bar\psi_k(0) g_s A^\rho\big(n\mu\big)\psi_j(n\lambda)\, | P, s_T\rangle \,.\end{aligned} \tag{5.18}$$

As stated in [81], the first term arising in equation 5.17 doesn't contribute to the cross section, due to the same line of reasoning, which was before used to argue that the contribution presented in equation 5.8 is imaginary and can be neglected. Consequently, only the second line of the contribution remains.

Next, we continue our consideration with the contributions that emerges by inserting the terms of first order from the expansion of the hard scattering function into the factorization formula. The resulting contributions therefore contain derivatives of the hard scattering function. But prior to proceeding with a thorough examination of the aforementioned contributions, we want to take a closer look at the behaviour of the correlation function $\Phi^{\rho}_{kj}(k_1, k_2)$. On the one hand we find that

$$\begin{aligned}
&\int dk_1^- d^2k_{1,\perp} \int dk_2^- d^2k_{2,\perp} k_1^{\beta} \Phi^{\rho}_{kj}(k_1, k_2) \\
&= i \int \frac{d\lambda}{2\pi} \int \frac{d\mu}{2\pi} e^{ix_1\lambda} e^{i(x_2-x_1)\mu} \langle P, s_T| \bar{\psi}_k(0) g_s A^{\rho} n_{\rho}(n\mu) \partial^{\beta} \psi_j(n\lambda) |P, s_T\rangle \Big] \\
&\equiv i\Phi^{\beta}_{kj,\partial_1}(x_1, x_2). \qquad (5.19)
\end{aligned}$$

Here, we have first substituted the component of the momentum k_1 by an appropriate derivative acting on the exponential function before we made use of integration by parts to shift the derivative to the matrix element. Likewise, we obtain

$$\begin{aligned}
&\int dk_1^- d^2k_{1,\perp} \int dk_2^- d^2k_{2,\perp} k_2^{\beta} \Phi^{\rho}_{kj}(k_1, k_2) \\
&= i \int \frac{d\lambda}{2\pi} \int \frac{d\mu}{2\pi} e^{ix_1\lambda} e^{i(x_2-x_1)\mu} \Big[\langle P, s_T| \bar{\psi}_k(0) g_s \Big(\partial^{\beta} A^{\rho}(n\mu) n_{\rho} \Big) \psi_j(n\lambda) |P, s_T\rangle \\
&\quad + \langle P, s_T| \bar{\psi}_k(0) g_s A^{\rho}(n\mu) n_{\rho} \partial^{\beta} \psi_j(n\lambda) |P, s_T\rangle \\
&\equiv i\Phi^{\beta}_{kj,\partial_2}(x_1, x_2). \qquad (5.20)
\end{aligned}$$

The relations for the correlation functions presented above can be employed to evaluate the integrals over the k_i^-- and $k_{i,\perp}$-components and to simplify the contributions from the first order of the hard function's expansion to the factorized cross section. Combining the outcome together with the second term from equation 5.17 yields

$$\begin{aligned}
d\Delta\sigma(s_T) =& \frac{1}{2S} \int \frac{dz}{z^2} D^{c/h}(z) \int dx_1 \int dx_2\, \omega^{\alpha}{}_{\beta} \Big[\Phi^{\beta}_{kj}(x_1, x_2) \mathcal{H}_{jk,\alpha}(x_1, x_2) \\
&+ i \Big(\Phi^{\beta}_{kj,\partial_2}(x_1, x_2) - \Phi^{\beta}_{kj,\partial_1}(x_1, x_2) \Big) \frac{\partial \mathcal{H}_{jk}(k_1, k_2)}{\partial k_2^{\alpha}} \Big|_{k_i \approx x_i P} \\
&+ i\Phi^{\beta}_{kj,\partial_1}(x_1, x_2) \Big\{ \frac{\partial \mathcal{H}_{jk}(k_1, k_2)}{\partial k_1^{\alpha}} + \frac{\partial \mathcal{H}_{jk}(k_1, k_2)}{\partial k_2^{\alpha}} \Big\}_{k_i \approx x_i P} \Big]
\end{aligned} \qquad (5.21)$$

where we have introduced two new twist-3 matrix elements. The first one is the so-called F-type matrix element and is given by

$$\begin{aligned}
\Phi^{\beta}_{F}(x_1, x_2) \equiv& \int \frac{d\lambda}{2\pi} \int \frac{d\mu}{2\pi} e^{i\lambda x_1} e^{i\mu(x_2-x_1)} \\
&\times \langle P, s_T| \bar{\psi}(0) g_s F^{\beta\rho}(\mu n) n_{\rho} \psi(\lambda n) |P, s_T\rangle \qquad (5.22)
\end{aligned}$$

while the second one reads

$$\tilde{\Phi}^{\beta}(x_1, x_2) \equiv \int \frac{d\lambda}{2\pi} \int \frac{d\mu}{2\pi} e^{i\lambda x_1} e^{i\mu(x_2-x_1)} \\ \times \langle P, s_T | \, \bar{\psi}(0) g_s n_\rho \big(\partial^\rho A^\beta(\mu n)\big) \psi(\lambda n) \, |P, s_T\rangle \, . \tag{5.23}$$

It can be shown that the correlation functions satisfy the relations

$$\tilde{\Phi}^{\beta}(x_1, x_2) = -i(x_2 - x_1)\Phi^{\beta}(x_1, x_2) \\ \Phi^{\beta}_{\partial_2}(x_1, x_2) - \Phi^{\beta}_{\partial_1}(x_1, x_2) = \Phi^{\beta}_{F}(x_1, x_2) + \tilde{\Phi}^{\beta}(x_1, x_2), \tag{5.24}$$

where integration by parts is needed in order to proof the upper equation. Making use of these relations further simplifies the contribution from the diagram in figure 5.2 to the factorization formula for the spin-dependent cross section and allows to rewrite it as

$$d\Delta\sigma(s_T) = \frac{1}{2S} \int \frac{dz}{z^2} D^{c/h}(z) \int dx_1 \int dx_2 \, \omega^{\alpha}{}_{\beta} \\ \times \Bigg[i\Phi^{\beta}_{F,kj}(x_1, x_2) \frac{\partial \mathcal{H}_{jk}(k_1, k_2)}{\partial k_2^\alpha}\bigg|_{k_i \approx x_i P} + \Phi^{\beta}_{kj}(x_1, x_2) \\ \times \bigg\{ \mathcal{H}_{jk,\beta}(x_1, x_2) + (x_2 - x_1) \frac{\partial \mathcal{H}_{jk}(k_1, k_2)}{\partial k_2^\alpha}\bigg|_{k_i \approx x_i P} \bigg\} \\ + \Phi^{\beta}_{kj,\partial_1}(x_1, x_2) \bigg\{ \frac{\partial \mathcal{H}_{jk}(k_1, k_2)}{\partial k_1^\alpha} + \frac{\partial \mathcal{H}_{jk}(k_1, k_2)}{\partial k_1^\alpha} \bigg\}_{k_i \approx x_i P} \Bigg] . \tag{5.25}$$

However, the expression is still unsuitable for calculating the transverse single-spin asymmetry and requires additional attention instead. To continue the treatment of the formula, we need to employ that the hard scattering function fulfils the relations

$$\left[\frac{\partial \mathcal{H}_{\alpha}(k_1, k_2)}{\partial k_1^\beta} + \frac{\partial \mathcal{H}_{\alpha}(k_1, k_2)}{\partial k_2^\beta} \right]_{k_i \approx x_i P} = 0 \\ \mathcal{H}_{\alpha}(x_1 P, x_2 P) + (x_2 - x_1) P^\alpha \frac{\partial \mathcal{H}_{\alpha}(k_1, k_2)}{\partial k_2^\beta}\bigg|_{k_i \approx x_i P} = 0 \tag{5.26}$$

which can both be concluded from the fact that the hard scattering function satisfies the Ward identity

$$(k_2 - k_1)^\alpha \mathcal{H}_\alpha(k_1, k_2) = 0. \tag{5.27}$$

for the gluon from the polarized nucleon. Thanks to these equations, the factorization formula can be simplified immensely and rearranged in such a way that only the F-type correlation function remains.

More precisely, the outcome for the cross section can be written as

$$\Delta\sigma(s_T) = \frac{1}{S}\int \frac{dz}{z^2} D^{c/h}(z) \int dx_1 \int dx_2\, i\omega^{\alpha}{}_{\beta}\Phi^{\beta}_{F,kj} \frac{\partial \mathcal{H}_{jk}(k_1,k_2)}{\partial k_2^{\alpha}}\Big|_{k_i\approx x_i P} . \tag{5.28}$$

As previously seen in the case of the quark-correlator, the F-type matrix element can be parameterized too. Such a parameterization can be found in [80, 81, 127] and reads

$$\begin{aligned}\Phi^{\beta}_{F,kj}(x_1,x_2) =& \frac{M}{4}(\not{P})_{kj}\varepsilon^{\beta P n s_T} G_F(x_1,x_2) \\ &+ i\frac{M}{4}(\gamma_5\not{P})_{kj} s_T^{\beta}\tilde{G}_F(x_1,x_2) + ...\end{aligned} \tag{5.29}$$

where we dropped twist-4 contributions. The function G_F is often referred to as Qiu-Sterman function and of particular interest for our considerations since we will express all results in terms of it.

Finally, we arrive at an expression for the factorization formula, which will serve as the starting point for all our further computations, by substituting the F-type correlation function $\Phi^{\beta}_{F,kj}(x_1,x_2) \to \frac{M}{4}(\not{P})_{kj}\varepsilon^{\beta P n s_T} G_F(x_1,x_2)$. We then obtain

$$\begin{aligned}d\Delta\sigma =& i\frac{M}{4S}\varepsilon^{\beta P n s_T}\int \frac{dz}{z^2} D^{c/h}(z) \\ &\times \int dx_1 \int dx_2\, G_F(x_1,x_2)\omega^{\alpha}{}_{\beta}\frac{\partial \mathcal{H}(k_1,k_2)}{\partial k_2^{\alpha}}\Big|_{k_i\approx x_i P}\end{aligned} \tag{5.30}$$

where $(\not{P})_{kj}$ has been shifted into and contracted with the hard scattering function.

5.2 F- and D-Type function

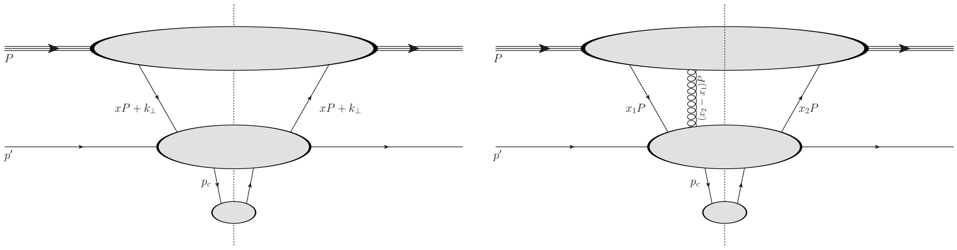

Figure 5.3: Generic contributions involving the D-type correlator functions. Here, the upper blob describes the proton's state, the middle blob represents the hard scattering and the blob in the bottom illustrates the fragmentation. Furthermore, the diagram on the left-hand side is associated with the kinematic twist-3 part whereas the diagram on the right contributes to the dynamic twist-3 piece.

In the last section, we introduced the F-type function, when we elucidated the framework, forming the foundation of our considerations, and derived the factorization formula for the spin-dependent cross section. However, the approach that we presented in the aforementioned section, is not the only possibility enabling us to compute the transverse single-spin asymmetry. Another procedure to determine the spin-dependent part of the asymmetry is, for example, employed in [135], where a distinction is made between a kinematic and a dynamic twist-3 contribution. Within the scope of this approach, Feynman diagrams of the type as shown in figure 5.3 must be taken into account. From an application-oriented perspective, the new diagrams differ from those presented in the previous chapter primarily in the way how the $k_\perp$-dependency is considered. By carrying out the necessary calculations, it can be ascertained that the kinematic and dynamic twist-3 contributions are linked to a further twist-3 correlator, the D-type function.

The F-type correlator and its parametrization was already noted in the previous section, but it will be given again at this point as a reminder. It reads

$$
\begin{aligned}
&\Phi^{\alpha}_{F,ji}(x_1, x_2) \\
&= \int \frac{d\lambda}{2\pi} \int \frac{d\mu}{2\pi} e^{i\lambda x_1} e^{i\mu(x_2 - x_1)} \langle P, s_T | \bar{\psi}_j(0) g_s F^{\alpha\beta}(\mu n) n_\beta \psi_i(\lambda n) | P, s_T \rangle \\
&= \frac{M}{4} (\not{P})_{ij} \varepsilon^{\alpha P n s_T} G_F(x_1, x_2) + i \frac{M}{4} (\gamma_5 \not{P})_{ij} s_T^\alpha \tilde{G}_F(x_1, x_2) + \ldots \qquad (5.31)
\end{aligned}
$$

where we are particularly interested in the part associated with the Qiu-Sterman function. A similar expression as well as a parametrization can be given in the case of the D-type correlator.

As stated in e.g. [80, 81, 127, 231], the second type of twist-3 matrix element may be written as

$$\begin{aligned}
&\Phi^{\alpha}_{D,ji}(x_1,x_2)\\
&=\int\frac{d\lambda}{2\pi}\int\frac{d\mu}{2\pi}e^{i\lambda x_1}e^{i\mu(x_2-x_1)}\left\langle P,s_T\right|\bar{\psi}_j(0)D^{\alpha}_{\perp}(\mu n)\psi_i(\lambda n)\left|P,s_T\right\rangle\\
&=\frac{M}{4}(\not{P})_{ij}\varepsilon^{\alpha P n s_T}G_D(x_1,x_2)+i\frac{M}{4}(\gamma_5\not{P})_{ij}s^{\alpha}_T\tilde{G}_D(x_1,x_2)+... \qquad (5.32)
\end{aligned}$$

where $iD^{\alpha}_{\perp}=i\partial^{\alpha}+g_{\mathrm{s}}A^{\alpha}_{\perp}$ denotes the covariant derivative. It is important to note that the F- and D-type functions are not independent of each other. Instead, they are related via the equations

$$G_D(x_1,x_2)=\mathrm{PV}\frac{1}{x_1-x_2}G_F(x_1,x_2) \qquad (5.33)$$

$$\tilde{G}_D(x_1,x_2)=\mathrm{PV}\frac{1}{x_1-x_2}\tilde{G}_F(x_1,x_2)+\delta(x_1-x_2)\tilde{g}(x) \qquad (5.34)$$

with PV being the principal value and where the function $\tilde{g}(x)$ is explicitly given in [80, 231]. According to [80], it can be expressed in terms of the F-type distributions $G_F(x_1,x_2)$ and $\tilde{G}_F(x_1,x_2)$ as well as the twist-2 quark helicity distribution. Due to these relations, the F- and D-type correlators form an overdetermined set of functions. This allows to reformulate results, which were originally written in terms of the D-type function, as expressions including the F-type functions, especially the Qiu-Sterman function.

Nonetheless, besides the relation between the F- and D-type correlators, other properties of the emerging function can be of interest. It can be found, that the symmetry and antisymmetry relations

$$G_F(x_1,x_2)=G_F(x_2,x_1) \qquad (5.35)$$

$$\tilde{G}_F(x_1,x_2)=-\tilde{G}_F(x_2,x_1) \qquad (5.36)$$

$$G_D(x_1,x_2)=-G_D(x_2,x_1) \qquad (5.37)$$

$$\tilde{G}_D(x_1,x_2)=\tilde{G}_D(x_2,x_1) \qquad (5.38)$$

are satisfied by the functions.

5.3 Evolution Equation for the Qiu-Sterman Function

In the introduction of the theoretical background, the scale dependence of the twist-2 parton distributions and fragmentation functions was discussed and the DGLAP equation was introduced as a differential equation that governs this dependence. In a later chapter, which was dedicated to the required computational methods, a significant application of the framework was presented, when it was explained, how appropriate subtraction terms can be formulated with the help of the splitting kernels, to handle the collinear divergences and to finally obtain a physically meaningful result for cross sections. However, as the transverse single-spin asymmetry, which we want to address in the present chapter, is a twist-3 observable, gaining knowledge of a respective evolution equation for the quark-gluon-quark correlator and, more specifically, the Qiu-Sterman function is inevitable. As a final step of preparation before we turn to our actual calculations, we would therefore like to take a closer look at this topic.

Knowing the evolution equation for the Qiu-Sterman function alongside the equivalent formulas for the twist-2 functions and the Weizsäcker-Williams contributions is necessary to handle the collinear divergences in the course of a twist-3 discussion. The evolution of the Qiu-Sterman function has been addressed multiple times in the past (see e.g. [53, 139–141, 161, 226]). Our following considerations rely on the equation given in [53], which reads

$$\begin{aligned}
&\frac{\partial}{\partial \ln\left(\mu^2\right)} G_F(w_0, w_0, \mu^2) \\
&= \frac{\alpha_s}{2\pi} \int_{w_0}^{1} \frac{dx}{x} \left\{ \left[P_{qq}\left(\frac{w_0}{x}\right) - C_A \delta\left(1 - \frac{w_0}{x}\right) \right] G_F(x, x) \right. \\
&\quad + \frac{1}{2C_A}\left(1 - 2\frac{w_0}{x}\right) G_F(w_0, w_0 - x) \\
&\quad \left. + \frac{C_A}{2}\left[\frac{1 + \frac{w_0}{x}}{1 - \frac{w_0}{x}} \left(G_F(w_0, x) - G_F(x, x)\right) + \frac{w_0}{x} G_F(x, x) \right] \right\}
\end{aligned} \tag{5.39}$$

where $w_0 = xw$ and with

$$P_{qq}(\xi) = C_F \left(\frac{1 + \xi^2}{(1 - \xi)_+} + \frac{3}{2}\delta(1 - \xi) \right) \tag{5.40}$$

denoting the usual leading-order splitting kernel. However, as it will be seen at a later point of the chapter, the leading order cross section is proportional to the combination $G_F(x, x) - x\frac{dG_F(x,x)}{dx}$, and we will therefore require the evolution for this combination. In the next step, we must hence focus on the determination of the evolution equation for the aforementioned combination.

Against this background, we will proceed as follows. First, we take the derivative of the Qiu-Sterman function's evolution given in equation 5.39 with respect to w_0. In the course of forming the derivative, some care has to be taken as not only the integrands but also the lower boundaries of the integrals depend on the variable w_0. In such cases, the derivative can be calculated by employing the Leibniz integral rule, which, among other things, produces a boundary term $\sim G_F(1,1)$ that vanishes since $G_F(1,1) = 0$. After successfully calculating the derivative, we can immediately write down the evolution equation for the combination $G_F(x,x) - x\frac{dG_F(x,x)}{dx}$. It becomes

$$\begin{aligned}
&\frac{\partial}{\partial \ln\left(\mu^2\right)}\left(G_F(w_0,w_0,\mu^2) - w_0 G'_F(w_0,w_0,\mu^2)\right) \\
&= \frac{\alpha_s}{2\pi}\Bigg\{\int_{w_0}^1 \frac{dx}{x}\Bigg\{\left[P_{qq}\left(\frac{w_0}{x}\right) - C_A\delta\left(1-\frac{w_0}{x}\right)\right]\left(G_F(x,x) - xG'_F(x,x)\right) \\
&+ \frac{C_A}{2}\int_{w_0}^1 \frac{dx}{x}\Bigg[\frac{G_F(x,w_0) - G_F(x,x)}{1-w_0/x} \\
&- \left(1+\frac{w_0}{x}\right) w_0 \frac{d}{dw_0}\left(\frac{G_F(x,w_0) - G_F(x,x)}{1-w_0/x}\right)\Bigg] \\
&+ \frac{C_A}{2}\left(G_F(w_0,w_0) - w_0 G'_F(w_0,w_0)\right) - \frac{1}{2C_A}G_F(w_0,0) \\
&+ \frac{1}{2C_A}\int_{w_0}^1 \frac{dx}{x}\left[G_F(w_0,w_0-x) - \left(1-2\frac{w_0}{x}\right)w_0\frac{d}{dw_0}G_F(w_0,w_0-x)\right]\Bigg\}.
\end{aligned} \tag{5.41}$$

A key feature arising in twist-3 considerations can be already recognized from the equation above. The various pieces of a twist-3 observable can be categorized on the basis of the pole contributions provided and assigned to one of three classes. Contributions, where the Qiu-Sterman function is evaluated at equal arguments are associated with soft-gluon poles. When one of the arguments vanishes, they are linked to soft-fermion poles. Otherwise, the contributions are related to hard poles. The meaning of the pole contributions as well as their origin will be discussed in more detail when we present our calculations. They are linked to the imaginary part required from the hard scattering function.

With the derivation of the evolution equation, we have completed all the preparations necessary to compute the transverse single-spin asymmetry. It will make handling the collinear divergences arising at next-to-leading order feasible.

5.4 Leading order

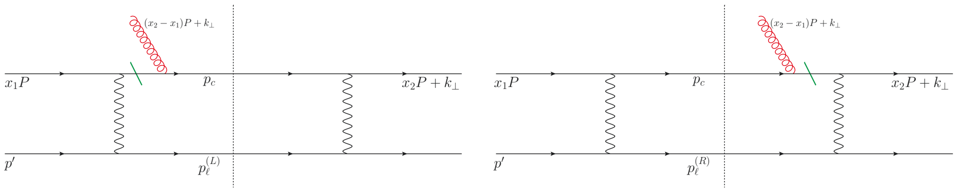

Figure 5.4: Feynman diagrams contributing to the transverse single-spin asymmetry at LO. A characteristic feature of the diagrams is the occurrence of an additional gluon from the polarized nucleon, which can couple to another parton on either the left- or right-hand side of the cut (vertical dashed line). The imaginary part is provided by the internal line marked by a green bar.

As previously shown, the factorized spin-dependent cross section may be written as

$$\begin{aligned} d\Delta\sigma =& i\frac{M}{4S}\varepsilon^{\beta P n s_T}\int \frac{dz}{z^2}D^{c/h}(z) \\ &\times \int dx_1 \int dx_2\, G_F(x_1,x_2)\omega^{\alpha}{}_{\beta}\frac{\partial\mathcal{H}(k_1,k_2)}{\partial k_2^{\alpha}}\Big|_{k_i\approx x_iP} \end{aligned} \tag{5.42}$$

where the Qiu-Sterman function G_F and a hard scattering function $\mathcal{H}$ arise. Like in the unpolarized case, the next step in our analysis is the perturbatice calculation of the hard scattering part. However, in contrast to our previous considerations, a new difficulty emerges as we now require an imaginary part from the function in order to obtain a real result for the cross section overall. Said imaginary part can be generated by internal propagators when they reach their on-shell limit. In this section, we will give further insights on how propagators provide the necessary imaginary part and introduce the computational methods needed to extract it. In this context, we will use the leading-order consideration as an example to review the methods required to determine the cross section in the framework of twist-3 collinear factorization.

Our analysis of the transverse single-spin asymmetry will be based on so-called pole contributions which, as mentioned before, are obtained by propagators in their on-shell limit. Under these circumstances, the imaginary part can be extracted by making use of the relation

$$\frac{1}{x \pm i\varepsilon} = PV\frac{1}{x} \mp i\delta(x) \tag{5.43}$$

with PV denoting the principal value. Extracting the imaginary part thus introduces a delta function according to the formula above, which will turn out to yield constraints on the momentum fractions x_1 as well as x_2 and hence on the involved partons' momenta.

The propagators associated with the pole contributions can be always rearranged in such a way that they exhibit one of the three structures

$$\frac{1}{x_1 - x_2 \pm i\varepsilon} \to \mp i\pi\,\delta\big(x_1 - x_2\big), \tag{5.44}$$

$$\frac{1}{x_j \pm i\varepsilon} \to \mp i\pi\,\delta\big(x_j\big) \qquad (x_j = x_1, x_2), \tag{5.45}$$

$$\frac{1}{x_j + a \pm i\varepsilon} \to \mp i\pi\,\delta\big(x_j - a\big) \qquad (x_j = x_1, x_2, x_1 - x_2)\ , \tag{5.46}$$

allowing to cast them into three categories. A contribution as shown in equation 5.44 is related to a so-called soft-gluon pole (SGP) as it fixes the kinematics in a manner that the Qiu-Sterman function is evaluated at equal arguments and the momentum of the incoming gluon is set to zero. Likewise, the second structure presented in equation5.45 gives rise of a soft-fermion pole (SFP) since one of the momentum fractions and consequently the appropriate quark momentum become zero. The last structure encountered in equation 5.46 is linked to hard pole contributions (HP), which set neither a quark's nor the gluon's momentum to zero.

In the remainder of this section, we will now present our calculation on the leading-order contribution to the spin-dependent cross section. This means that we study the process $q\ell \to qX$ but with an additional gluon from the incoming polarized nucleon. In the future, we will often refer to the gluon as twist-3 gluon to indicate its special role as it is not handled in the same way as real gluon in an ordinary twist-2 process. Moreover, we would like to note at this point, that we will parameterize the emerging momenta in such a way that the dependence on transverse momentum components is completely shifted into k_2. We will thus write

$$k_1 = x_1 P \quad \text{and} \quad k_2 = x_2 P + k_\perp, \tag{5.47}$$

which is a convention that we will also keep using in our considerations at next-to-leading order. Under these preliminaries, the product $\omega^\alpha{}_\beta \frac{\partial}{\partial k_2^\alpha}$ may be written as a derivative with respect to a component of the transverse momentum $k_\perp$ and the collinar limit can be taken by $k_\perp \to 0$.

At leading-order of perturbation theory, two Feynman diagrams can contribute to the absolute value squared of the matrix element and therefore need to be taken into account as illustrated in figure 5.4. The diagrams are characterized by an additional interaction of the incoming twist-3 gluon with the final-state quark. Of course, the Feynman rules would in principle permit configurations where such an interaction happens between the gluon and the quark in the initial-state. However, it is easy to confirm, that the associated diagrams yield vanishing contributions to the spin-dependent cross section at least at leading order. This might change in higher orders of perturbation theory when another momentum is involved.

In the next step, the imaginary part of the hard scattering functions linked to the shown diagrams needs to be extracted. The internal lines yielding the pole contributions are marked by a green bar and as indicated in figure 5.4, two classes can be distinguished depending on whether the pole is taken on the left- or the right-hand side of the cut. When the additional interaction takes place and the pole is taken on the left-hand side of the cut, the appropriate propagator reads

$$\frac{1}{\big(p_c - \big(x_2 - x_1\big)P - k_\perp\big) + i\varepsilon} \rightarrow \frac{i\pi}{T}\delta\big(x_1 - x_2 + v_1 \cdot k_\perp\big) \tag{5.48}$$

and yields a soft-gluon pole contribution in its on-shell limit. Here, the arising four vector v_1 is defined by

$$v_1 \equiv \frac{2p_c}{T}. \tag{5.49}$$

When, on the other hand, the pole is taken on the right-hand side of the cut, we receive the same expression for the imaginary part but with opposite sign. So consequently, we in fact need to take the difference between the two diagrams, where the pole is either taken on the left or the right-hand side of the cut, instead of the sum.

Substituting the appropriate propagator by its imaginary part causes contributions where the $k_\perp$-derivative from equation 5.42 acts on the delta function. Such terms can be handled by making use of integration by parts, which will, among other things, shift the derivative to the Qiu-Sterman function leading to terms $\sim \frac{dG_F}{dx}$. Another source for these contributions may be provided by the delta function from the phase space, which puts the unobserved lepton in the final-state on its mass shell. In this case, too, the contributions of the two diagrams differ and must therefore be treated separately. For an attachment on the left, we obtain

$$p_\ell^{(L)} = x_2 P + k_\perp + p' - p_c \tag{5.50}$$

for the unobserved lepton's momentum $p_\ell^{(L)}$ by employing momentum conservation. We therefore find

$$\delta\bigg(\big(p_\ell^{(L)}\big)^2\bigg) = \frac{1}{S+T}\delta\big(x_2 - \xi - v_2 \cdot k_\perp\big) \tag{5.51}$$

with

$$v_2 \equiv \frac{2p_c}{S+T} \quad \text{and} \quad \xi \equiv -\frac{u}{S+T}, \tag{5.52}$$

where the variable ξ introduced above coincides with the commonly known momentum fraction x in the limit $k_\perp \rightarrow 0$.

Likewise, it can be shown that

$$p_\ell^{(R)} = x_1 P + p' - p_c \tag{5.53}$$

$$\delta\Big(\big(p_\ell^{(R)}\big)^2\Big) = \frac{1}{S+T}\delta\big(x_1 - \xi\big) \tag{5.54}$$

when the pole is taken on the right-hand side of the cut. After incorporating the results for the propagators, that yield the soft-gluon pole contributions, and for the unobserved lepton's momentum, we can evaluate the x_1- and x_2-integrals emerging in equation 5.42 by making use of the delta functions. Upon adherence to this approach, we are led to consider a contribution of the form

$$\begin{aligned}\sim&\frac{i\pi}{T\big(S+T\big)}\int dPS_2' \lim_{k_\perp\to 0}\frac{\partial}{\partial k_\perp^\rho}\Big[G_F\big(\xi + (v_2 - v_1)\cdot k_\perp, \xi + v_2\cdot k_\perp\big)\\ &\times H_L\big(\xi + (v_2 - v_1)\cdot k_\perp, \xi + v_2\cdot k_\perp, k_\perp\big) - G_F\big(\xi, \xi + v_1\cdot k_\perp\big)\\ &\times H_R\big(\xi, \xi + v_1\cdot k_\perp, k_\perp\big)\Big],\end{aligned} \tag{5.55}$$

where H_L and H_R denote the hard scattering function for an attachment on the left, respectively on the right, and with dPS_2' representing the remaining portion of the conventional two-body phase space following the separation of the delta function, which ensures the on-shell condition for the final-state lepton's momentum. Nonetheless, the expression can be further simplified by carrying out the $k_\perp$-derivative and taking the limit $k_\perp \to 0$ as much as possible and we hence obtain

$$\begin{aligned}\sim&\frac{i\pi}{T\big(S+T\big)}\int dPS_2'\Big[\big(v_2 - v_1\big)_\rho H_L\big(\xi,\xi,0\big)\frac{dG_F\big(\xi,\xi\big)}{d\xi}\\ &+ G_F\big(\xi,\xi\big)\lim_{k_\perp\to 0}\frac{\partial}{\partial k_\perp^\rho}\Big\{H_L\big(\xi + (v_2 - v_1)\cdot k_\perp, \xi + v_2\cdot k_\perp, k_\perp\big)\\ &- H_R\big(\xi, \xi + v_1\cdot k_\perp, k_\perp\big)\Big\}\Big]\end{aligned} \tag{5.56}$$

where we have used that $H_L\big(\xi,\xi,0\big) = H_R\big(\xi,\xi,0\big)$ in the limit $k_\perp \to 0$. At this point, it is helpful to re-introduce a momentum fraction x as it appears in any ordinary twist-2 calculation. In view of this, the momentum fraction in question is defined via the relation $p = xP$ in complete analogy to a consideration concerning a twist-2 observable. Here, one could think of the unpolarized scattering process, for instance, where p denotes the incoming quarks momentum and P represents the parent nucleon's momentum. In this context, one can easily convince themself, that

$$\xi = -\frac{u}{S+T} = x \tag{5.57}$$

really applies in the limit $k_\perp \to 0$.

By making use of the newly defined momentum fraction, we can introduce an integral over x in the structure given in equation 5.56, which then becomes

$$\sim \frac{i\pi}{T(S+T)} \int dPS_2' \int dx\, \delta\Big(x + \frac{u}{S+T}\Big) \Big[\big(v_2 - v_1\big)_\rho H_L\big(x,x,0\big) \frac{dG_F\big(x,x\big)}{dx} + G_F\big(x,x\big) \lim_{k_\perp \to 0} \frac{\partial}{\partial k_\perp^\rho} \Big\{ H_L\big(x + (v_2 - v_1)\cdot k_\perp, x + v_2 \cdot k_\perp, k_\perp\big) - H_R\big(x, x + v_1 \cdot k_\perp, k_\perp\big) \Big\} \Big] \tag{5.58}$$

through implementing an appropriate delta function. In the same manner as we introduced the momentum fraction, we can orient ourselves to a twist-2 calculation and define a new momentum for the unobserved lepton as

$$p_\ell \equiv xP + p' - p_c, \tag{5.59}$$

which allows to reconstruct the full two-body phase space. Against this background, we need that

$$\int dPS_2' \int dx \, \frac{\delta\big(x + \frac{u}{S+T}\big)}{S+T} = \int dPS_2' \int dx\, \delta\big(p_\ell^2\big) = \int dPS_2, \tag{5.60}$$

which is simple to proof. By making use of the equation noted above, the structure, that is encountered in the factorized cross section, simplifies and becomes

$$\sim \frac{i\pi}{T} \int dPS_2 \Big[\big(v_2 - v_1\big)_\rho H_L\big(x,x,0\big) \frac{dG_F\big(x,x\big)}{dx} + G_F\big(x,x\big) \lim_{k_\perp \to 0} \frac{\partial}{\partial k_\perp^\rho} \Big\{ H_L\big(x + (v_2 - v_1)\cdot k_\perp, x + v_2 \cdot k_\perp, k_\perp\big) - H_R\big(x, x + v_1 \cdot k_\perp, k_\perp\big) \Big\} \Big] \tag{5.61}$$

and we are finally left with computing the hard scattering functions before carrying out the remaining derivative and taking the limit. However, when calculating the hard scattering function, some care needs to be taken. This is primarily attributable to two changes in comparison to an equivalent twist-2 consideration, whose origin can be traced back to the F-type twist-3 correlation function. First, the colour averaging factor for the incoming parton together with the extra twist-3 gluon needs to be adjusted. In the case of an incoming quark, the hard scattering function has to be contracted with

$$\Big(\frac{2}{N_c^2 - 1}\Big) T_{ij}^b, \tag{5.62}$$

whereas we need the factor $\big(-\frac{2i}{N_c^2-1}\big)T_{ij}^b$ for processes where the incoming quark from the polaized hadron is replaced by a gluon.

The second complication occurs in regards to the traces over Dirac matrices. Here, we need to keep in mind that the hard scattering function is contracted with an additional $\not{P}$. Consequently, the arguments of the traces contain a larger number of dirac matrices compared to an equivalent twist-2 calculation and we find for example

$$H_L \sim \mathrm{Tr}\big[\not{p}_c \not{P}\big(\not{p}_c - \big(x_2 - x_1\big)\not{P} - \not{k}_\perp\big)\gamma^\mu \not{P} \gamma^\nu\big], \tag{5.63}$$

which further increases the total workload and the required computational time. Note that all the calculations can be done by utilizing the tracer1.1-package for the computer algebra system Mathematica. It turns out that the outcome greatly simplifies and becomes

$$\begin{aligned} d\Delta\sigma\big(s_T\big) =& \frac{1}{2}\frac{\pi M}{T}\varepsilon^{P_h P p' s_T} \int_{v_{\min}}^{v_{\max}} dv \int_{w_{\min}}^{1} \frac{dw}{w}\frac{x}{z} D^{c/h}(z) \\ & \times \left[G_F\big(x,x\big) - x\frac{dG_F\big(x,x\big)}{dx}\right] \frac{\alpha_{\mathrm{em}}^2 e_a^2}{s^3 v^2} \frac{1+v^2}{\big(1-v\big)^3}\delta(1-w) \end{aligned} \tag{5.64}$$

in terms of the formerly introduced variables v and w. Here, the integration boundaries are the same as in the case of the unpolarized process. The factorization formula can be rearranged in such a way that it becomes

$$\begin{aligned} d\Delta\sigma\big(s_T\big) =& \frac{1}{2}\frac{\pi M}{S^2 U^2}\varepsilon^{P_h P p' s_T} \int_{v_{\min}}^{v_{\max}} dv \int_{w_{\min}}^{1} \frac{dw}{w} D^{c/h}(z) \\ & \times \left[G_F\big(x,x\big) - x\frac{dG_F\big(x,x\big)}{dx}\right] \sigma_{\mathrm{tw-3}}^{(\mathrm{LO})}(v)\delta(1-w) \end{aligned} \tag{5.65}$$

where the partonic twist-3 cross section reads

$$\sigma_{\mathrm{tw-3}}^{(\mathrm{LO})}(v) = \alpha_{\mathrm{em}}^2 e_a^2 \frac{1+v^2}{\big(1-v\big)^4} \tag{5.66}$$

5.5 Next-to-Leading Order: $q\ell \to gX$-channel

As it was likewise observed in our previous considerations regarding the unpolarized lepton-nucleon scattering, multiple channels can contribute to the cross section in the case of the spin-dependent process at next-to-leading order. However, the required calculations for the individual subprocesses turn out to be much more extensive in comparison to the unpolarized counterpart, and therefore it makes sense to study them separately as well as to dedicate each of the channels a separate chapter.
In the single-inclusive production of a hadron in unpolarized lepton-nucleon scattering, the three subprocesses $q\ell \to qX$, $q\ell \to gX$ and $g\ell \to qX$ have been identified as the sources for non-vanishing contributions to the cross section at NLO. Likewise, the same processes but with an additional incoming parton from the transversely polarized nucleon may contribute to the spin-dependent cross section in a similar manner. Nonetheless, we will focus solely on the first two cases, i.e. $q\ell \to qX$ and $q\ell \to gX$, as they are associated with the Qiu-Sterman function and expected to yield the dominating contribution. Accordingly, the third channel shall remain as a potential subject matter for future research.

In the section at hand, we would like to commence our next-to-leading order analysis with a detailed examination of the second channel, i.e. the correction to the Born process, where an additional real gluon is emitted by one of the involved quarks, which is finally assumed to fragment, respectively to be observed. More precisely, we consider the $2 \to 3$ process

$$q + \ell \to g + q + \ell \tag{5.67}$$

where we haven't included the twist-3 gluon in the reaction equation. The subprocess is particularly suitable to serve as an introduction to the required computational methods, as some of the difficulties and challenges that we may encounter at NLO in general are already present, while the effort involved is still manageable. This is partially attributable to the fact that no virtual corrections can yet occur in this channel, and we can therefore concentrate fully on handling the real corrections. Furthermore, only diagrams that are similar to those known from the unpolarized case, except for the additional incoming gluon, contribute to the relevant cross section, whereas new diagrams, that can occur exclusively in twist-3, do not yet emerge. However, it is noteworthy that despite these simplifying circumstances, it is evident that not only soft-gluon pole contributions, like in leading order, but also soft-fermion and hard pole contributions will arise. In particular, the hard poles will require special attention, as they cannot be directly integrated over the phase space after calculating the appropriate matrix element and we will therefore need additional methods for handling them.

In the further course of the chapter, we will present our calculations for the $q\ell \to gX$-channel, where we have to deal with soft-gluon, soft-fermion and hard poles as stated previously. We will thereby start by discussing the soft-gluon pole contributions where we in principle follow exactly the same procedure as at tree level but with some adjustments to take the additional momentum in the final-state into account.

Subsequently, we will turn our attention towards a special kind of hard poles in the next part of the chapter. It will be easy to see that they yield additional soft-gluon pole contributions in certain kinematic regions of the three-body phase space. However, due to new difficulties arising against the background of these special poles, the associated matrix elements cannot be directly integrated over the phase space and we will therefore need to develop new methods for the further treatment and to extract the ε-poles. As we shall demonstrate, the treatment of hard pole contributions not only generates additional soft-gluon poles but also gives rise to soft-fermion poles.

This leads us to the next aspect of our considerations concerning the $q\ell \to gX$-subprocess, where we have to deal with the pure soft-fermion poles. In the context of these pole contributions, we will obtain kinematical constraints, which fix one of the momentum fractions, either x_1 or x_2, to be zero. However, it will turn out that the treatment of the soft-fermion poles is rather straightforward and follows mostly the same procedure that was already applied in regard of the soft-gluon poles.

Finally, we have to deal with collinear divergences after the computation of all relevant phase-space integrated matrix element for soft-gluon, soft-fermion and hard poles. For this purpose, we again need to take appropriate subtraction terms in the framework of collinear factorization into account. We especially again encounter the Weizsäcker-Williams contribution, which we have already got to know in the view of the unpolarized process. Following the outlined procedure, we will ultimately obtain a finite result for the $q\ell \to gX$-channel.

5.5.1 Soft-Gluon Pole contributions in $q\ell \to gX$-scattering

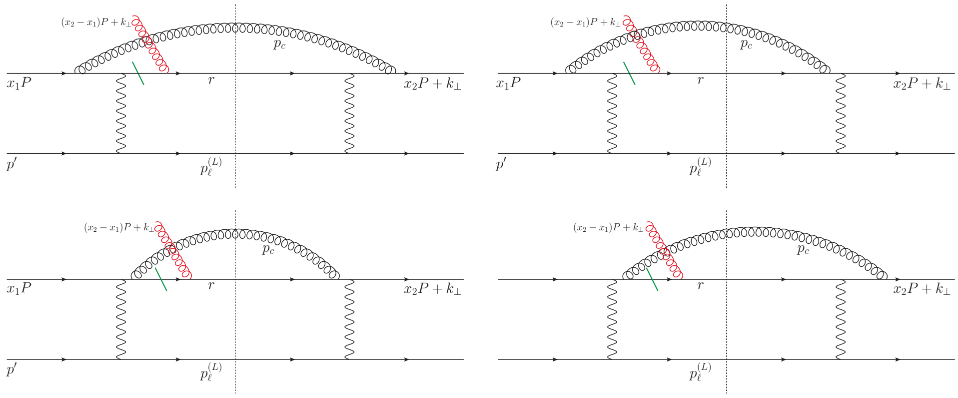

Figure 5.5: Feynman diagrams yielding soft-gluon pole contributions in the $q\ell \to gX$-channel. The figure shows the diagrams in the case when the pole is taken on the left-hand side of the cut. Again, the internal line associated with pole contribution is marked by a green bar.

In the following, we want to present the first part of our calculations concerning the $q\ell \to gX$-channel. Just as we did previously in our leading order considerations, we return to the factorization formula

$$d\Delta\sigma = i\frac{M}{4S}\varepsilon^{\beta P n s_T} \int \frac{dz}{z^2} D^{c/h}(z) \times \int dx_1 \int dx_2 \, G_F(x_1, x_2) \omega^\alpha{}_\beta \frac{\partial \mathcal{H}(k_1, k_2)}{\partial k_2^\alpha}\bigg|_{k_i \approx x_i P} \tag{5.68}$$

for the spin-dependent cross section known from equation 5.42 as a starting point for our considerations. In the course of our computations regarding this particular channel, we will encounter soft-fermion as well as hard poles besides the soft-gluon pole contributions, which already emerged at leading order. However, the first part of our considerations, which will be presented in the remainder of the present section, focuses solely on the pure soft-gluon pole contributions and it will be seen that they can be treated by following more or less the same procedure as previously except for a few small adjustments to take the third momentum r in the final-state into account. In this context, we can make use of the same set of ten Mandelstam variables, that we introduced in chapter 4.2.2. Furthermore, it should be obvious that we will again be confronted with the three-body phase space instead of its two-body counterpart. Fortunately, it turns out that we can mostly apply the same calculational methods as known from the unpolarized process.

It is noteworthy that we can make use of the colour factor carried by the Feynman diagrams to further classify the contributions to the cross section and in order to further structure the problem, beyond using the type of the encountered pole contribution. With this in mind, we want to commence our analysis by studying a class of Feynman diagrams carrying the colour factor

$$\sim C_F - \frac{C_A}{2}. \tag{5.69}$$

Again, we can distinguish between contributions where the pole is taken on the left- or the right-hand side of the cut. The appropriate diagrams for the first case, when the pole is taken on the left, are shown in figure 5.5.

Our further procedure now essentially consists of two steps. First, we need to separate the delta function from the three-body phase space, which ensures the on-shell condition for the unobserved lepton and rewrite it as a function of the momentum fractions x_1 and x_2. Note that the remainder of the phase space will be again labeled by a prime as dPS_3'. On the other hand, it is inevitable to extract the imaginary part from the hard scattering function. For this purpose, we will closely follow the procedure as outlined previously and examine appropriate propagators in their on-shell limit.

By analyzing the momentum flow in the diagrams shown in figure 5.5 and applying momentum conservation, we find that the unobserved lepton's momentum may be written as

$$p_\ell^{(L)} = x_2 P + k_\perp + p' - p_c - r. \tag{5.70}$$

If this expression is squared, scalar products of external momenta will arise that can be replaced by suitable Mandelstam variables. We therefore obtain

$$\delta\Big(\big(p_\ell^{(L)}\big)^2\Big) = \frac{1}{S + T_1 + T_3}\delta\big(x_2 - \xi - v_2 \cdot k_\perp\big) \tag{5.71}$$

for the delta function from the phase space when the twist-3 gluon attaches on the left. Here, we have defined the variable

$$\xi \equiv -\frac{u_1 + u_3 + s_{13}}{S + T_1 + T_3} \tag{5.72}$$

as well as the four-vector

$$v_2 \equiv \frac{2\big(p_c + r\big)}{S + T_1 + T_3}. \tag{5.73}$$

Just as before, it can be observed, that the variable ξ coincides with the commonly known momentum fraction x in the limit $k_\perp \to 0$, which can be used later in our considerations to reconstruct the full three-body phase space by introducing an appropriate x-integral and a suitable delta function.

Next, we turn our attention towards the internal lines and the associated propagators that yield the pole contribution in their on-shell limit to extract the required imaginary part from the hard scattering function. In general, several internal lines are possible candidates to provide the imaginary part. But since we are interested in the pure soft-gluon pole contributions, we are led to consider the lines marked by a green bar in figure 5.5. The related propagators read

$$\frac{1}{\big(r - (x_2 - x_1)P - k_\perp\big)^2 + i\varepsilon} \to \frac{i\pi}{T_3}\delta\big(x_1 - x_2 + v_1 \cdot k_\perp\big), \tag{5.74}$$

where the four-vector v_1 is given by

$$v_1 \equiv \frac{2r}{T_3} \tag{5.75}$$

and where the imaginary part has already been extracted on the right side. It goes without saying that the contribution actually is a soft-gluon pole as the delta function becomes $\delta\big(x_1 - x_2\big)$ in the limit $k_\perp \to 0$ and the Qiu-Sterman function is hence evaluated at equal arguments.

We now have all the necessary ingredients for the case when the pole is located on the left-hand side of the cut and it remains to repeat the same analysis for Feynman diagrams where the twist-3 gluon attaches on the right. As the exemplary Feynman diagram shown in figure 5.6 illustrates, the diagrams required in the second case can be easily constructed from those for an attachment on the left by shifting the green bar and the twist-3 gluon, which is drawn in red, to the right-hand side of the cut, that is indicated as a dashed line. We therefore refrain from presenting all four diagrams explicitly.

Essentially, nothing more needs to be done than following the exact same procedure as in the last instance, where we studied the attachment on the left. Starting with the unobserved lepton's momentum, we obtain

$$\delta\Big(\big(p_\ell^{(R)}\big)^2\Big) = \frac{1}{S + T_1 + T_3}\delta\big(x_1 - \xi\big) \tag{5.76}$$

in complete analogy by applying momentum conservation. Moreover, the propagator providing the soft-gluon pole contribution reads

$$\frac{1}{\big(r + (x_2 - x_1)P + k_\perp\big)^2 - i\varepsilon} \to -\frac{i\pi}{T_3}\delta\big(x_1 - x_2 + v_1 \cdot k_\perp\big), \tag{5.77}$$

which again differs only by a sign from the case when the pole is taken on the left-hand side. We hence conclude that effectively, we need to take the difference between the diagrams contributing in the two cases.

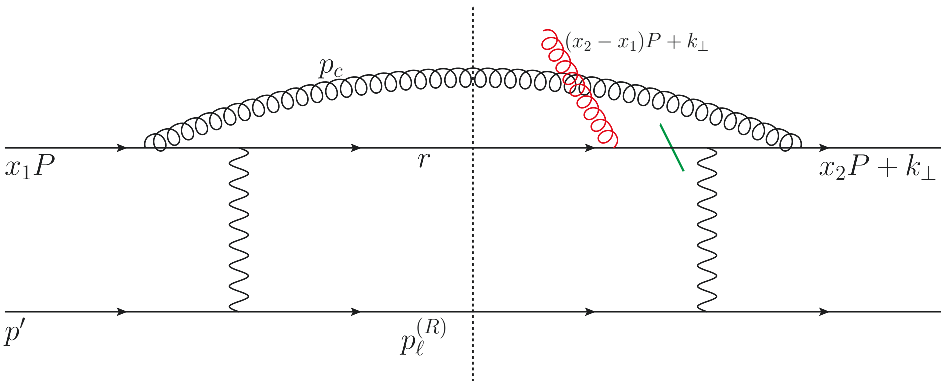

Figure 5.6: Example for the Feynman diagrams, when the soft-gluon pole is located on the right-hand side of the cut. The counterpart for the case when the twist-3 gluon attaches on the left is shown in the top left corner of figure 5.5. The example illustrates that the diagrams for an attachment on the right can be easily constructed from the previously presented diagrams by a suitable shift of the green bar and the twist-3 gluon.

Likewise as in the Born approximation, we are led to consider the structure

$$\begin{aligned}\sim & \frac{i\pi}{T_3(S+T_1+T_3)} \int dPS_3' \Big[(v_2 - v_1)_\rho H_L(\xi,\xi,0) \frac{dG_F(\xi,\xi)}{d\xi} \\ & + G_F(\xi,\xi) \lim_{k_\perp \to 0} \frac{\partial}{\partial k_\perp^\rho} \Big\{ H_L(\xi + (v_2 - v_1)\cdot k_\perp, \xi + v_2 \cdot k_\perp, k_\perp) \\ & \qquad - H_R(\xi, \xi + v_1 \cdot k_\perp, k_\perp) \Big\} \Big] \end{aligned} \tag{5.78}$$

in the factorized cross section after making use of the delta functions to evaluate the x_1- and x_2-integrals, where we have already carried out the $k_\perp$-derivative and taken the limit $k_\perp \to 0$ as much as possible. It again turns out that $H_L(\xi,\xi,0) = H_R(\xi,\xi,0)$. In the next step, we define a new momentum p_ℓ for the unobserved lepton by

$$p_\ell \equiv xP + p' - p_c - r \tag{5.79}$$

as it would arise in an ordinary twist-2 calculation with the usual momentum fraction that is introduced via the relation $p = xP$ between the initial-state quark's and the parent nucleon's momenta. It is easy to proof, that the momentum fraction x and the variable ξ really coincide in the limit $k_\perp \to 0$, i.e. that $\xi = x$, and we can hence use that

$$\frac{1}{S+T_1+T_3} \int dx\, \delta\Big(x + \frac{u_1 + u_3 + s_{13}}{S+T_1+T_3}\Big) = \int dx\, \delta(p_\ell^2) \tag{5.80}$$

to reconstruct the full three-body phase space.

The previously presented structure encountered in the factorization formula thus becomes

$$\sim \frac{i\pi}{T_3} \int dPS_3 \Big[\big(v_2 - v_1\big)_\rho H_L\big(x,x,0\big) \frac{dG_F\big(x,x\big)}{dx} + G_F\big(x,x\big) \lim_{k_\perp \to 0} \frac{\partial}{\partial k_\perp^\rho} \Big\{ H_L\big(x + (v_2 - v_1)\cdot k_\perp, x + v_2 \cdot k_\perp, k_\perp\big) - H_R\big(x, x + v_1 \cdot k_\perp, k_\perp\big) \Big\} \Big] \tag{5.81}$$

and it in principle remains to compute the hard scattering functions H_L and H_R, which can be done supported by computer algebra systems like Mathematica using the same techniques as introduced earlier.

We would like to note that we temporarily interrupt our considerations concerning the first part at this point after computing the relevant matrix element. Consequently, we postpone the integration over the phase space to a later point. Instead, we want to focus on the next set of diagrams providing pure soft-gluon pole contributions. These diagrams, which are shown in figure 5.7 for an attachment on the left, carry the colour factor

$$\sim \frac{C_A}{2} \tag{5.82}$$

and are characterized by the appearance of a three-gluon vertex. As before, the equivalent Feynman diagrams for the case, when the pole is taken on the right-hand side of the cut, can be easily constructed by shifting the green bar and the twist-3 gluon.

Basically, we have to follow exactly the same procedure as before in connection with these new diagrams, and we will therefore limit ourselves to a brief summary of the most important interim results instead of an extensive discussion of the necessary calculations. First, we find that the momentum of the final-state lepton remains unchanged and we thus obtain

$$\delta\Big(\big(p_\ell^{(L)}\big)^2\Big) = \frac{1}{S + T_1 + T_3} \delta\big(x_2 - \xi - v_2 \cdot k_\perp\big) \tag{5.83}$$

$$\delta\Big(\big(p_\ell^{(R)}\big)^2\Big) = \frac{1}{S + T_1 + T_3} \delta\big(x_1 - \xi\big) \tag{5.84}$$

for the delta function separated from the three-body phase space. Next, we need to examine the propagators providing the soft-gluon pole contributions. The responsible propagators read

$$\frac{1}{\big(p_c \mp \big(x_2 - x_1\big)P \mp k_\perp\big)^2 \pm i\varepsilon} \to \pm \frac{i\pi}{T_1} \delta\big(x_1 - x_2 + v_1 \cdot k_\perp\big) \tag{5.85}$$

where the upper signs hold for an attachment on the left while the lower signs apply when the pole is taken on the right-hand side of the cut.

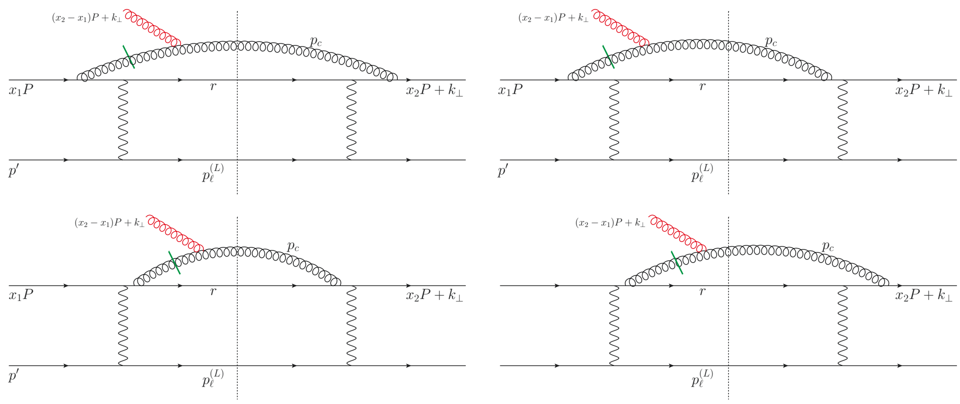

Figure 5.7: Feynman diagrams providing soft gluon poles in the $q\ell \to gX$-channel, which are carrying the colour factor $\frac{C_A}{2}$. The figure shows only the diagrams where the additional interaction with the twist-3 gluon is located on the left-hand side of the cut. A special feature is the appearance of the three-gluon vertex.

Of course, it is immediately apparent that the expression is essentially identical to the one we found earlier, with the only difference being the substitution of the momentum r by p_c. It thus follows that the four-vector v_1 now reads

$$v_1 \equiv \frac{2p_c}{T_1}, \tag{5.86}$$

whereas the second vector v_2 remains unchanged. Beyond that, we again find a relative sign between the diagrams with an attachment on the left respectively on the right and we hence need to take the difference between the related matrix elements in the same manner as previously.

All-in-all, we are led to consider the structure

$$\begin{aligned}\sim\frac{i\pi}{T_1}\int dPS_3\Big[&\big(v_2 - v_1\big)_\rho H_L\big(x,x,0\big)\frac{dG_F\big(x,x\big)}{dx}\\ &+ G_F\big(x,x\big)\lim_{k_\perp\to 0}\frac{\partial}{\partial k_\perp^\rho}\Big\{H_L\big(x+(v_2-v_1)\cdot k_\perp, x+v_2\cdot k_\perp, k_\perp\big)\\ &\qquad - H_R\big(x, x+v_1\cdot k_\perp, k_\perp\big)\Big\}\Big]\end{aligned} \tag{5.87}$$

in the factorized cross section after reconstructing the full three-body phase space by following the procedure as outlined previously. The outcome reminds of the result, which was obtained for the first set of diagrams carrying the colour factor $C_F - \frac{C_A}{2}$, but where T_3 has been replaced by T_1.

It now remains to compute the hard scattering functions for both sets of diagrams after we have found the results presented in the equations 5.81 and 5.87.

In addition, we need to continue taking the $k_\perp$-derivative as well as the limit $k_\perp \to 0$ for the second parts of the given expressions. In the course of this, we will receive contributions, that are proportional to a component of the unobserved parton's momentum r^ρ, which will require further treatment. Those terms can be handled by making use of a tensor decomposition to rewrite them in terms of the fixed external momenta p, p' and p_c. This can be attributed to the fact that the expression has to be integrated over the momentum r as part of the three-body phase space and that the outcome after carrying out said integration can only depend on the remaining momenta, namely p, p' and p_c. This means for us, that we can employ the ansatz

$$\int d^d r \, r^\rho f\big(s, t_1, u_1, ...\big) = Ap^\rho + Bp'^\rho + Cp_c^\rho \tag{5.88}$$

with suitable coefficients A, B, C and where f denotes an arbitary scalar function of the Mandelstam variables. The approach is reminiscent of the tensor decomposition, which was previously used to reduce loop integrals when we dealt with the virtual corrections to the unpolarized scattering process. In fact, the further treatment is quite similar and relies on contracting the equation with the momenta p_ρ, p'_ρ, respectively $p_{c,\rho}$ yielding a system of linear equations. By solving the system of equations, it turns out that we are allowed to use the substitution

$$r^\rho \to \frac{t_1 u_3 + t_3 u_1 - s s_{13}}{2 t_1 u_1} p_c^\rho, \tag{5.89}$$

where we already took into account that the contributions $\sim p^\rho$ and p'^ρ will vanish due to the ε-tensor encountered in the factorization formula.

To conclude our considerations regarding the pure soft-gluon pole contributions, we reorganize the calculated, but still unintegrated, matrix elements according to two criteria. First, we split them into a C_F and a C_A part according to their colour factors. Second we combine the derivative and non-derivative part in a suitable way to obtain a contribution

$$\sim \left(G_F\big(x, x\big) - x \frac{dG_F\big(x, x\big)}{dx} \right). \tag{5.90}$$

Note that this is the same combination of the Qiu-Sterman function and its first derivative that we already encountered at leading-order. The remainder then yields a term $\sim G_F\big(x, x\big)$. Both rearrangements offer the advantage to simplify the respective outcome making the necessary phase space integration easier. With this, we will conclude the discussion of the soft-gluon poles at this point and turn to the hard pole contributions before we continue with carrying out the phase space integration.

5.5.2 Hard Pole contributions in $q\ell \to gX$-scattering

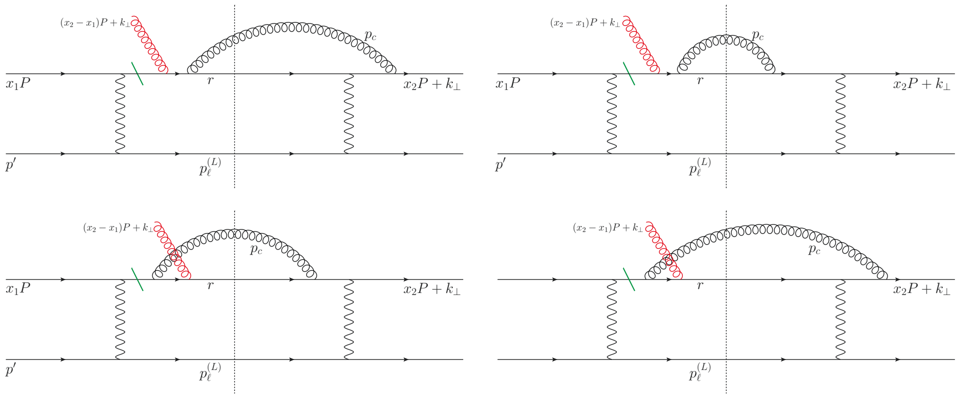

Figure 5.8: Feynman diagrams carrying the colour factor $C_F - \frac{C_A}{2}$ that yield hard pole contributions. The internal lines, which are associated with the pole contributions, are again marked by a green bar. Note that that the two diagrams in the bottom line have already been encountered in figure 5.5.

After addressing the pure soft-gluon poles in the last section, we will now proceed with our discussion by examining the hard pole contributions arising in the $q\ell \to gX$-channel. Generally speaking, hard poles emerge as a result of internal lines, where neither the twist-3 gluon nor the incoming quark become soft, but which still fix the kinematics for x_1 and x_2.

Our considerations regarding the hard poles will closely follow the same line of reasoning and the methodology that were already applied in the case of the soft-gluon poles, particularly in the first steps. In more detail, this means that we again first categorize the required Feynman diagrams according to their associated colour factor. In the next step, we will need to analyse the unobserved lepton's momentum and separate the appropriate delta function from the three-body phase space that ensures the on-shell condition. Finally, we will examine the propagators yielding the hard pole and extract the imaginary part needed to receive a real-valued cross section. In this manner, we will again obtain two delta functions which can be employed to evaluate the x_1- and x_2- integrals and it will finally remain to compute the hard scattering function.
However, it will turn out that new problems and challenges will arise with regard to the phase space integration. Therefore, the result, that we will obtain, cannot be integrated immediately over the three-body phase space, in contrast to the previous discussed soft-gluon pole contributions where this would in principle have been feasible without further ado. After these preliminary remarks, we would now like to take a closer look at our calculations of the hard pole contributions.

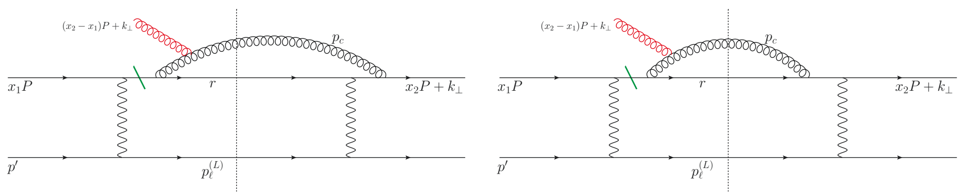

Figure 5.9: Feynman diagrams carrying the colour factor $\frac{C_A}{2}$ that yield hard pole contributions. The diagrams are already known from figure 5.7, but as indicated by the green bar, the pole is provided by a different internal line.

We commence our analysis by identifying all contributing Feynman diagrams, which can be split into two sets as before. The first set of diagrams carry the colour factor

$$C_F - \frac{C_A}{2} \tag{5.91}$$

and is shown in figure 5.8. It is noteworthy that only the two diagrams in the upper line are new, whereas those two in the bottom line have already provided soft-gluon pole contributions previously. As it can be noted by comparing the figures 5.8 and 5.5, the illustrated diagrams can be distinguished by the internal lines, which are each highlighted by a green bar and provide the pole contributions.
In the same sense, we find the Feynman diagrams shown in figure 5.9 carrying the colour factor

$$\frac{C_A}{2}, \tag{5.92}$$

that provide further hard pole contributions. However, unlike before in the case of the first set, no new diagrams emerge in the second set and all diagrams have thus been seen previously in figure 5.7. Again, the only difference is the internal line, which is linked to the pole.
Note that the corresponding Feynman diagrams, when the pole is taken on the right-hand side of the cut, can be easily constructed by suitably shifting the twist-3 gluon and the green bar to the right. Moreover, the further treatment turns out to be quite similar for both sets of diagrams and the intermediate results coincide. We will therefore refrain from discussing them separately and instead succinctly present the essential calculations for both together.
The considerations, that we will present in the following, again pursue the goal of transforming and processing the factorization formula for the spin-dependent cross section given in equation 5.30 in such a way that we obtain an expression that allows us to determine the hard pole contributions by calculating the necessary hard scattering functions. Against this background, we have to follow two tracks as it has been seen before. On the one hand, we need to examine the final-state leptons momentum. On the other hand, we need to investigate the propagator yielding the pole and extract its imaginary part in its on-shell limit.

First, we start by considering the momentum of the unobserved lepton in the final-state. By employing momentum conservation and analyzing the momentum flow along the respective Feynman diagrams, it turns out that the momentum takes the same form as previously, when we discussed the pure soft-gluon poles. It therefore immediately follows, that we obtain the exact same expression for the delta function, which are separated from the three-body phase space and ensure the on-shell conditions. More precisely, they read

$$\delta\Big(\big(p_\ell^{(L)}\big)^2\Big) = \frac{1}{S+T_1+T_3}\delta\big(x_2-\xi-v_2\cdot k_\perp\big) \tag{5.93}$$

$$\delta\Big(\big(p_\ell^{(R)}\big)^2\Big) = \frac{1}{S+T_1+T_3}\delta\big(x_1-\xi\big) \tag{5.94}$$

where we are using the same notation as before. As a reminder, this means that $p_\ell^{(L)}$ applies for an attachment on the left whereas $p_\ell^{(R)}$ holds when the pole is taken on the right-hand side of the cut.

Next, we need to turn our attention towards the internal line and the corresponding propagator yielding the pole contribution. When the pole is taken on the left-hand side of the cut, we need to consider the internal line marked by a green bar as illustrated in figure 5.8 for each contributing Feynman diagram and the associated propagator then reads

$$\frac{1}{\big(p_c+r-\big(x_2-x_1\big)P-k_\perp\big)^2+i\varepsilon} \to \frac{i\pi}{T_1+T_3}\delta\big(x_1-x_2+x\tilde{x}+v_1\cdot k_\perp\big), \tag{5.95}$$

where we already extracted the imaginary part in the on-shell limit. Likewise, we obtain a similar outcome for an attachment of the twist-3 gluon on the right after constructing the diagrams, namely

$$\frac{1}{\big(p_c+r+\big(x_2-x_1\big)P+k_\perp\big)^2-i\varepsilon} \to -\frac{i\pi}{T_1+T_3}\delta\big(x_1-x_2+x\tilde{x}+v_1\cdot k_\perp\big), \tag{5.96}$$

and we thus again observe a relative sign between the two results and we hence effectively need to take the difference between the hard scattering functions.

The four-vectors emerging in the arguments of the delta functions are defined in a comparable way as previously and are given by

$$v_1 \equiv \frac{2\big(p_c+r\big)}{T_1+T_3} \tag{5.97}$$

$$v_2 \equiv \frac{2\big(p_c+r\big)}{S+T_1+T_3}. \tag{5.98}$$

Here, it is especially noteworthy that v_2 remains unchanged.

Besides the two four-vectors v_1 and v_2, the new variable $\tilde{x}$ is introduced in the arguments of the delta functions given in the equations 5.95 and 5.96. It is defined by

$$\tilde{x} \equiv -\frac{s_{13}}{t_1 + t_3} \tag{5.99}$$

as a function of the Mandelstam variables. Of course, it is immediately apparent that $\tilde{x}$ will introduce an angular dependence in the argument of the Qiu-Sterman function with regard to the phase space integration since the Mandelstam variables s_{13} and t_3 already exhibit such a dependency. However, since no known analytic expression for the aforementioned function exist, the evaluation of the angular integrals arising in the three-body phase space will be complicated, leading to an emerging need for the discovery of a suitable workaround. But this should not be our concern just yet, and we will further discuss this in more detail later instead.

At this point, we have again extracted the required imaginary part and found the $k_\perp$-dependent delta functions, which can be employed to fix the kinematics for x_1 and x_2. In the next step, we insert the results into the factorization formula and evaluate the x_1- and x_2-integrals by making use of the aforementioned delta functions. Following the outlined procedure, we are led to consider the structure

$$\begin{aligned} \sim & \frac{i\pi}{T_1 + T_3} \int dPS_3\, G_F\big(x, x(1-\tilde{x})\big) \\ & \times \lim_{k_\perp \to 0} \frac{\partial}{\partial k_\perp^\rho} \Big\{ H_L\big(x(1-\tilde{x}) + (v_2 - v_1)\cdot k_\perp, x + v_2 \cdot k_\perp, k_\perp\big) \\ & \qquad - H_R\big(x, x(1-\tilde{x}) + v_1 \cdot k_\perp, k_\perp\big) \Big\} \Big] \end{aligned} \tag{5.100}$$

for both sets of diagrams as it arises in the factorized cross section after carrying out the $k_\perp$-derivative as well as taking the limit $k_\perp \to 0$ as far as possible and reconstructing the full three-body phase space. Here, we have already used that the derivative part vanishes and only the non-derivative contributions $\sim G_F\big(x, x(1-\tilde{x})\big)$ remains, when the corresponding hard scattering functions are finally computed. It is now clear that the variable $\tilde{x}$ actually emerges in the argument of the Qiu-Sterman function, which therefore exhibits an angular dependency leading to the previously mentioned challenges.

The next step is once again to calculate the hard scattering functions encountered in the structure given above in equation 5.100. Afterwards we can compute the remaining $k_\perp$-derivative and take the limit $k_\perp \to 0$. The results, obtained in this way, are again divided into two parts according to their respective colour factor, namely a C_F and a C_A contribution, which makes the matrix elements simpler overall.

After the hard scattering functions have been successfully calculated, it turns out that the outcome for the hard pole contributions can be schematically written as

$$\mathcal{HP} = G_F\big(x, x(1-\tilde{x})\big)\mathcal{M}_{\mathrm{HP}}\big(s_{13}, t_3, u_2\big) \tag{5.101}$$

for both, the C_F and the C_A part, where $\mathcal{M}_{\mathrm{HP}}$ denotes the final matrix element after all $k_\perp$-derivatives have been evaluated and the limit $k_\perp \to 0$ has been taken.

Two features of said schematically written result are particularly striking. The first one is the previously mentioned angular dependency in the argument of the Qiu-Sterman function G_F, which is introduced via the variable $\tilde{x}$ as a function of s_{13} and t_3 and makes the phase space integration complicated. Secondly, it can be observed that the Qiu-Sterman function is again evaluated at equal arguments, when $\tilde{x}$ becomes particularly small, leading to further soft-gluon pole contributions. This is possible when $s_{13} \to 0$ and therefore $p_c \cdot r \to 0$. The hard poles thus provide further soft-gluon poles in kinematic regions of the phase space, where these conditions are matched. In fact, it seems to be a reccuring feature of the single-spin asymmetry that the three types of poles are not completely independent at higher orders of perturbation theory. Instead, we will find that the hard poles not only yield more soft-gluon but also soft-fermion poles. On the other hand, it hence follows that three classes of poles cannot be treated separately to, for example, focus on some dominant contribution and instead always need to be considered together, contributing to the complexity of the transverse single-spin asymmetry and increasing the workload.

To further treat the hard pole contributions, we want to focus on a workaround to at least extract all ε-poles. As previously mentioned, the hard poles yield additional soft-gluon poles in certain kinematic regions of the phase space, where the variable $\tilde{x}$ becomes small motivating us to expand the Qiu-Sterman function around small $\tilde{x}$. The appropriate Taylor expansion around $\tilde{x} = 0$ reads

$$\begin{aligned}\mathcal{HP} = &\Bigg\{ G_F\big(x,x\big) - \frac{1}{2}\tilde{x}\left(x\frac{dG_F\big(x,x\big)}{dx}\right) \\ &\quad + \sum_{k=2}^{\infty} \frac{(-1)^k \tilde{x}^k}{k!}\left(x^k \frac{d^k G_F\big(x,y\big)}{dy^k}\right)_{y=x}\Bigg\}\mathcal{M}_{\mathrm{HP}}\big(s_{13}, t_3, u_2\big)\end{aligned} \tag{5.102}$$

and it immediately catches the eye that the first two terms of the expansions really yield soft-gluon poles as the Qiu-Sterman function and its first derivative are here evaluated at equal arguments. For the further treatment, it now seems reasonable to divide the hard pole contributions into three parts according to the expansion.

The lowest order contribution

$$G_F(x,x)\mathcal{M}_{\rm HP}(s_{13},t_3,u_2) \tag{5.103}$$

can be combined with the remaining non-derivative pieces from the pure soft-gluon poles. It turns out that following said procedure will helps to make the resulting matrix elements even simpler overall with regard to the phase space integration. The next term

$$-\frac{1}{2}\tilde{x}\left(x\frac{dG_F(x,x)}{dx}\right), \tag{5.104}$$

which contains the first derivative of the Qiu-Sterman function, can be treated individually and integrated directly over the three-body phase space. It will contribute another derivative piece.

However, the remainder of the Taylor expansion

$$\sum_{k=2}^{\infty}\frac{(-1)^k\tilde{x}^k}{k!}\left(x^k\frac{d^kG_F(x,y)}{dy^k}\right)_{y=x}\mathcal{M}_{\rm HP}(s_{13},t_3,u_2) \tag{5.105}$$

cannot be handled without further ado and requires special attention. In particular, there seems to be no way to carry out the phase space integration by employing the usual and commonly known methods. We will therefore devote the remainder of the subsection to these contributions, in which we want to develop a procedure to at least extract the ε-poles. Nevertheless, we would like to anticipate at this point, that we will ignore some of the finite pieces stemming from this part and leave their determination as a subject for future research.

In order to extract the ε-poles, we commence our considerations by including the phase space integral in the remainder of the Taylor expansion, which then may be written as

$$\begin{aligned}&\sum_{k=2}^{\infty}\frac{(-1)^k}{k!}\left(x^k\frac{d^kG_F(x,y)}{dy^k}\right)_{y=x}\int dPS_3\,\tilde{x}^k\mathcal{M}_{\rm HP}(s_{13},t_3,u_2)\\ &=\sum_{k=0}^{\infty}\frac{(-1)^k}{(k+2)!}\left(x^{k+2}\frac{d^{k+2}G_F(x,y)}{dy^{k+2}}\right)_{y=x}\int dPS_3\,\tilde{x}^{k+2}\mathcal{M}_{\rm HP}(s_{13},t_3,u_2)\end{aligned} \tag{5.106}$$

after suitably shifting the index of summation k. The shift in the index of summation proves to be useful in the sense that we can now extract the product $\tilde{x}^2\mathcal{M}_{\rm HP}$ and examine it separately. In general, the matrix element can in principle contain divergent contributions that are proportional to $1/s_{13}$, $1/t_3$ and $1/u_2$ as well as their squared values in both cases, the $q\ell \to gX$-subprocess, which we discuss in the present chapter, and the $q\ell \to qX$-channel, that will be presented later. But since, on the other hand, $\tilde{x} \sim s_{13}$ applies, the product $\tilde{x}^2\mathcal{M}_{\rm HP}$ is free of any terms that are singular for $s_{13} \to 0$. However, it is worth mentioning that this approach is not actually necessary in the case of the $q\ell \to gX$-channel, as the matrix element is free of such singularities from the outset. Nonetheless, with regard to the $q\ell \to qX$-channel, which is to be considered later, it makes sense to use this approach here too in order to proceed consistently in both cases. Based on these observations on the singular behaviour of the product $\tilde{x}^2\mathcal{M}_{\rm HP}$, the approach of dividing the expression into three parts and writing it as

$$\tilde{x}^2\mathcal{M}_{\rm HP} = \mathcal{M}_1 + \mathcal{M}_2 + \mathcal{M}_3 \tag{5.107}$$

can be justified. Here, we have introduced three new matrix elements, which need to be understood as follows. The first quantity $\mathcal{M}_1$ contains all terms that are singular for $u_2 \to 0$. In principle, it could hence contain contributions $\sim 1/u_2$ as well as $\sim 1/u_2^2$. The second piece $\mathcal{M}_2$ is defined in the same manner but for the contributions from the original product, which are divergent for $t_3 \to 0$. Finally, the third part is completely finite. However, in order to be able to separate the product in this manner, it is necessary to make extensive use of partial fraction decomposition, where some care has to be taken. The decomposition now enables us to extract the ε-poles by forming the collinear limit for each of the contributions $\mathcal{M}_1$ and $\mathcal{M}_2$. In more detail, this means that will substitute the Mandelstam variables by making use of the momentum parametrizations given in appendix B and examine a limit for the angle ϑ_1 that is suitable in the sense that either $u_2 \to 0$ or $t_3 \to 0$ follows.

In this context, we start by considering $\tilde{x}^k\mathcal{M}_2$, which arises on the right-hand side of equation 5.106 after inserting the aforementioned decomposition given in equation 5.107 and is singular for $t_3 \to 0$ as noted previously. For the further treatment, we choose the set of parametrizations for the momenta, where $t_3 \sim \big(1+\cos(\vartheta_1)\big)$ applies and as it turns out, that $\mathcal{M}_2$ contains no terms $\sim 1/t_3^2$ in the case of the gluon-channel, the product $\tilde{x}^k\mathcal{M}_2$ may be written as

$$\tilde{x}^k\mathcal{M}_2 = \frac{\mathcal{F}\big(\vartheta_1,\vartheta_2\big)}{1+\cos(\vartheta_1)} \tag{5.108}$$

after inserting the parametrization with a function $\mathcal{F}$ in the numerator that may be defined by $\mathcal{F} \equiv \tilde{x}^k\mathcal{M}_2\, t_3$. It then follows that the collinear limit, where $t_3 \to 0$, can be taken by forming the limit $\vartheta_1 \to \pi$. Under these preconditions, we formulate the Taylor series expansion of the numerator $\mathcal{F}$ around $\vartheta_1 = \pi$, where we only take the zeroth order into account as it will provide the required ε-pole. However, it turns out that the zeroth order of the numerator's expansion vanishes, i.e. $\mathcal{F}\big(\vartheta_1,\vartheta_2\big) = 0 + \mathcal{O}\big(\vartheta_1\big)$, for both, the C_F and the C_A part. Consequently, we obviously find that

$$\int dPS_3\, \tilde{x}^k \mathcal{M}_2 = 0 \tag{5.109}$$

in the collinear limit and the remainder of the Taylor expansion given in equation 5.106 at least provides no further ε-poles for the contribution by $\mathcal{M}_2$.

Next, we continue our considerations by investigating $\tilde{x}^k \mathcal{M}_1$, which is singular for $u_2 \to 0$ as noted previously. In the light of this contribution, we basically follow the same procedure as outlined previously for $\mathcal{M}_2$ but with some minor adjustments. Among other things, we choose a different set of parametrization, namely the one for which u_2 assumes a particularly simple structure and $u_2 \sim \big(1-\cos(\vartheta_1)\big)$ applies. Moreover, $\mathcal{M}_1$ contains terms $\sim 1/u_2$ and $\sim 1/u_2^2$, unlike $\mathcal{M}_2$, and we hence decompose the product $\tilde{x}^k \mathcal{M}_1$ into two pieces and write it as

$$\tilde{x}^k \mathcal{M}_1 = \frac{\mathcal{F}_1\big(\vartheta_1, \vartheta_2\big)}{1-\cos(\vartheta_1)} + \frac{\mathcal{F}_2\big(\vartheta_1, \vartheta_2\big)}{\big(1-\cos(\vartheta_1)\big)^2} \tag{5.110}$$

where we now need to introduce two functions in the numerators, that are defined in a similar manner as previously. At this point, we continue our analysis by taking the collinear limit, which in the present case can be done by considering the limit $\vartheta_1 \to 0$. We therefore have to determine the Taylor series expansions of $\mathcal{F}_1$ as well as $\mathcal{F}_2$. Since we are again only interested in extracting the ε-poles, taking the zeroth order of the expansion into account is sufficient for $\mathcal{F}_1$, whereas $\mathcal{F}_2$ has to be expanded up to the quadratic order. However, it turns out that in the case of $\mathcal{F}_2$, only the second order contributes as the zeroth and first order both vanish. Following the outlined procedure, we observe that the structure of the outcome greatly simplifies and only a few rather undemanding angular integrals remain. The required integrals read

$$\int_0^\pi d\vartheta_1 \int_0^\pi d\vartheta_2\, \frac{\sin^{1-2\varepsilon}(\vartheta_1)\sin^{-2\varepsilon}(\vartheta_2)}{1-\cos(\vartheta_1)} = -\frac{\pi}{\varepsilon} + \text{finite} \tag{5.111}$$

$$\int_0^\pi d\vartheta_1 \int_0^\pi d\vartheta_2\, \frac{\sin^{1-2\varepsilon}(\vartheta_1)\sin^{-2\varepsilon}(\vartheta_2)\cos^2(\vartheta_2)}{1-\cos(\vartheta_1)} = -\frac{\pi}{2\varepsilon} + \text{finite} \tag{5.112}$$

and enable us to evaluate the phase space integrals in the collinear limit. We find that the integrated product $\tilde{x}^k \mathcal{M}_1$ may be written as

$$\int dPS_3\, \tilde{x}^k \mathcal{M}_1 = \frac{1}{\varepsilon} f(v,w) + \text{finite} \tag{5.113}$$

for both, the C_F as well as the C_A part, with f being a rational function of the kinematic variables v and w.

A particularly intriguing aspect of this outcome is the complete abolition of the dependence on the index of summation. By inserting the result into equation 5.106 we are able to reverse the Taylor expansion and convert it into a combination of Qiu-Sterman functions with different arguments. In more detail, we find that

$$
\begin{aligned}
&\sim \frac{1}{\varepsilon}\sum_{k=0}^{\infty}\frac{(-1)^k}{(k+2)!}\left(x^{k+2}\frac{d^{k+2}G_F(x,y)}{dy^{k+2}}\right)_{y=x} f(v,w) \\
&= \frac{1}{\varepsilon}\left\{\sum_{k=2}^{\infty}\frac{(-1)^k}{k!}\left(x^{k}\frac{d^{k}G_F(x,y)}{dy^{k}}\right)_{y=x}\right\} f(v,w) \\
&= \frac{1}{\varepsilon}\left\{-G_F(x,x)+\frac{1}{2}xG'_F(x,x)+\sum_{k=0}^{\infty}\frac{(-1)^k}{k!}\left(x^{k}\frac{d^{k}G_F(x,y)}{dy^{k}}\right)_{y=x}\right\} f(v,w) \\
&= \frac{1}{\varepsilon}f(v,w)\left\{G_F(x,0)-G_F(x,x)+\frac{1}{2}x\frac{dG_F(x,x)}{dx}\right\}, \qquad (5.114)
\end{aligned}
$$

where we first added a zero in a suitable way in the third line to supplement the series with the missing lowest order contributions. Afterwards, we identified the series to be the expansion of the Qiu-Sterman function when one of the arguments is zero, i.e. $G_F(x,0)$. So, as we mentioned at an earlier point in our discussion, it now really appears that the hard pole contributions are actually providing further soft-fermion poles alongside the expected additional soft-gluon poles.

At this point, it still remains to explicitly state the result for the function $f(v,w)$. By making use of the earlier noted angular integrals, we obtain

$$
\frac{1}{\varepsilon}f_{C_F}(v,w) = -\frac{2vw\big(2v^2w^2-2v^2w+v^2-2vw+1\big)}{\varepsilon(1-v)^4(1-vw)} + \mathcal{O}\big(\varepsilon^0\big) \qquad (5.115)
$$

for the C_F part and

$$
\frac{1}{\varepsilon}f_{C_A}(v,w) = \frac{vw\big(2v^2w^2-2v^2w+v^2-2vw+1\big)}{\varepsilon(1-v)^4(1-vw)^2} + \mathcal{O}\big(\varepsilon^0\big) \qquad (5.116)
$$

in the case of the C_A part where we have factored out the coupling constants alongside other constant prefactors. They will be included in the full factorization formula. It will be later necessary to accordingly add these ε-poles to the soft-gluon and soft-fermion pole contributions to finally obtain a finite result for the $q\ell \to gX$ subprocess.

5.5.3 Soft-Fermion Pole Contributions in $q\ell \to gX$-scattering

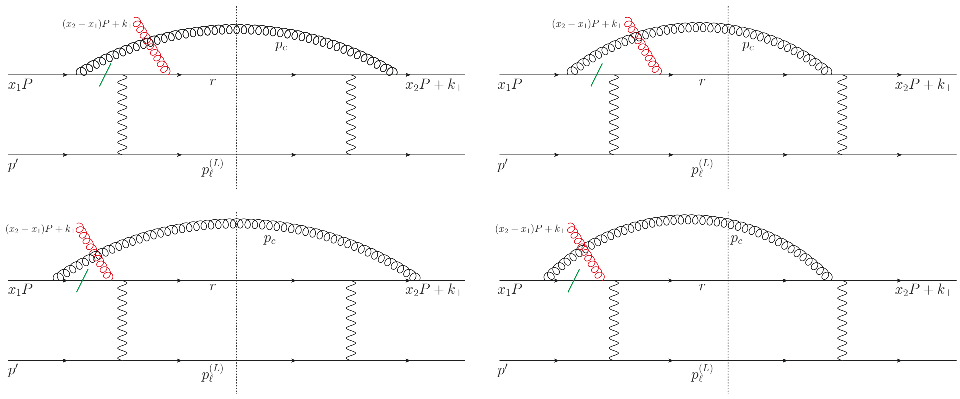

Figure 5.10: Feynman diagrams providing soft-fermion pole contributions. The diagrams in the upper line are already known from our previous considerations for the soft-gluon pole contributions. The remaining two diagrams in the bottom line, were an attachment of the twist-3 gluon happens in the initial-state are new.

Lastly, we want to discuss the pure soft-fermion pole contributions as the last type of the possible pole contributions. In view of the following discussion, we will mainly follow the same procedure as outlined previously and we will thus limit the presentation of our considerations to a brief summary of the key results. But before we continue with the presentation of these results, we would like to recall the necessary procedure. Starting from the factorization formula as given in equation 5.30, we proceed by following to tracks in parallel. On the one hand, we separate the delta function from the three-body phase space that ensures the unobserved lepton's on-shell condition. On the other hand, we study suitable propagators in their on-shell limit, which provide the soft-fermion pole. With these preliminaries, we will be able to compute the required hard scattering function.

The relevant Feynman diagrams are shown in figure 5.10. It is immediately apparent that the diagrams in the upper line have been encountered previously and therefore, that only the two diagrams in the bottom line are new. As before, the internal lines providing the poles are marked by a green bar. Alongside the two new diagrams, another novel feature is noticeable. While the additional attachment and the internal line providing the pole contribution always occured in the final-state in the course of our previous discussion, both can now also be encountered in the initial-state. Note that the respective diagrams for an attachment on the right can again be easily constructed by shifting the green bar and the twist-3 gluon highlighted in red appropriately.

Again, we commence our calculation by studying the momentum of the unobserved lepton's momentum, whereby no changes can be observed compared to the previous two cases. We thus find

$$\delta\Big(\big(p_\ell^{(L)}\big)^2\Big) = \frac{1}{S+T_1+T_3}\delta\big(x_2 - \xi - v_2\cdot k_\perp\big) \tag{5.117}$$

$$\delta\Big(\big(p_\ell^{(R)}\big)^2\Big) = \frac{1}{S+T_1+T_3}\delta\big(x_1 - \xi\big) \tag{5.118}$$

for the delta function separated from the phase space.

Next, we proceed by examining the propagators, which provide the soft-fermion poles in their on-shell limit. In contrast to our previous considerations, it turns out that we will now find more significant differences than a relative sign between the results for the imaginary parts, when the pole is taken on the left-hand respectively the right-hand side of the cut. For an attachment on the left, we obtain

$$\frac{1}{\big(x_1 P - p_c\big) + i\varepsilon} \to \frac{i\pi}{T_1}\delta\big(x_1\big), \tag{5.119}$$

whereas the propagator reads

$$\frac{1}{\big(x_2 P + k_\perp - p_c\big) - i\varepsilon} \to -\frac{i\pi}{T_1}\delta\big(x_2 - v_1\cdot k_\perp\big), \tag{5.120}$$

when the additional interaction with the twist-3 gluon is located on the right-hand side, and it can now actually be seen that the results differ in the way that an additional $k_\perp$-dependency is introduced. Here, the four-vectors v_1 and v_2 are given by

$$v_2 \equiv \frac{2\big(p_c + r\big)}{T_1+T_3} \quad \text{and} \quad v_1 \equiv \frac{2p_c}{T_1} \tag{5.121}$$

in a similar manner as before.

Following the same procedure as in the context of the soft-gluon and hard poles, we are led to consider the structure

$$\begin{aligned}\sim\frac{i\pi}{T_1}\int dPS_3\, G_F\big(x,0\big)\lim_{k_\perp\to 0}\frac{\partial}{\partial k_\perp^\rho}\Big\{ & H_L\big(0, x+v_2\cdot k_\perp, k_\perp\big) \\ & - H_R\big(x, v_1\cdot k_\perp, k_\perp\big)\Big\}\Big]\end{aligned} \tag{5.122}$$

after reconstructing the full three-body phase space. Here, we have used the symmetry of the Qiu-Sterman function, i.e. $G_F(0,x) = G_F(x,0)$, and that the derivative piece completely vanishes when the hard scattering functions are determined. As usual, it now remains to compute the hard scattering functions, carry out the derivative and take the limit $k_\perp \to 0$. Afterwards we need to evaluate the phase space integrals.

5.5.4 Phase Space Integration

In the past three chapters, we have presented the first part of our considerations on the $q\ell \to gX$ subprocess, where we in particular studied the pole contributions, namely the soft-gluon, hard and soft-fermion poles. In the course of these discussions, our primary objective was to extract the required imaginary part from the hard scattering functions and to reorganize the factorization formula for the spin-dependent cross section in a way that made the computation of the hard scattering function feasible. However, the presented results obtained so far are still unintegrated and it hence remains to evaluate the three-body phase space integrals. The approach, that leads to the successful treatment of the phase space, is essentially identical to that, which we previously employed in our considerations on the single-inclusive production of a hadron in the unpolarized nucleon-lepton scattering. This implies, that we first need to rearrange the matrix element in a manner to bring the encountered contributions into a form that facilitates the evaluation of the occurring integrals by making use of the master integrals given in the equations 3.36 and 3.38. Just as before, this can be achieved by the excessive use of partial fraction decomposition.

It turns out that many terms from the relevant matrix elements can be cast into the structure known from the first master formula, which means that they can be written as

$$\Omega_{j,k} \equiv \int_0^\pi d\vartheta_1 \int_0^\pi d\vartheta_2 \sin^{1-2\varepsilon}\left(\vartheta_1\right) \sin^{-2\varepsilon}\left(\vartheta_2\right)$$
$$\frac{1}{\big(1-\cos(\vartheta_1)\big)^j \big(1-\cos(\vartheta_1)\cos(\chi)-\sin(\vartheta_1)\cos(\vartheta_2)\sin(\chi)\big)^k} \tag{5.123}$$

after inserting a suitable choice of parameterization for the momenta as presented in appendix B. The solution for the integral given above is already known and noted in equation 3.37 of chapter 3.2. As a reminder, the solution, which has been utilized numerous times previously during our discussion on the unpolarized scattering, is given here again. It is

$$\Omega_{j,k} = 2\pi \frac{\Gamma\big(1-2\varepsilon\big)}{\Gamma\big(1-\varepsilon\big)^2} 2^{-j-k} B\big(1-\varepsilon-j, 1-\varepsilon-k\big)$$
$$\times {}_2F_1\left(j,k,1-\varepsilon,\cos^2(\frac{\chi}{2})\right) \tag{5.124}$$

with ${}_2F_1$ being the hypergeometric function and B denoting the Beta function. Through this expression, we are able to evaluate the phase space integrations for all contributions that can be casted into the standard structure following the procedure, which is well-known from ordinary twist-2 calculations.

Nonetheless, some of the arising contributions cannot be written in the aforementioned form. In the case of these few contributions, we need to employ the second integral formula instead, which we have originally taken from [42] and reads

$$\int_0^\pi d\vartheta_1 \int_0^\pi d\vartheta_2 \sin^{n-3}\left(\vartheta_1\right) \sin^{n-4}\left(\vartheta_2\right) \left(a + b\cos(\vartheta_1)\right)^{-k} \\ \times \left(A + B\cos(\vartheta_1) + C\sin(\vartheta_1)\cos(\vartheta_2)\right)^{-l}, \tag{5.125}$$

with a, b, A, B and C being suitable coefficients that need to be determined accordingly after inserting the parameterizations for the momenta and the Mandelstam variables. In light of this, the coefficients are functions of the kinematic variables v and w. The reason for the necessity of the second integral formula can be traced back to the occurrence of terms, where the combination $t_1 + t_3$ arise in the denominator. Unfortunately, they cannot be further reshaped, so that the combination in the denominators cancel out and we therefore require the integral formula for cases when either $a \neq \pm b$ or $A^2 \neq B^2 + C^2$ applies. In more detail, we encounter the structure

$$\sim \frac{1}{X^m \left(T_1 + T_3\right)^n} \tag{5.126}$$

with X being always either u_2 or s_{13} stemming from the hard pole contributions, where the combination can be found in the variable $\tilde{x}$ but also in the imaginary parts of the propagators providing the pole in their on-shell limit. Here, n denotes a positive integer whereas the integer m can be both, positive or negative. However, it is noteworthy that solutions are not listed for all encountered integrals in the appendix of [42]. Those integrals can be evaluated by making use of derivative relations as the one given by

$$\tilde{I}^{(n+1,1)}_{4-2\varepsilon} = \frac{1}{n!}\frac{\partial^n}{\partial a^n}\tilde{I}^{(1,1)}_{4-2\varepsilon} \tag{5.127}$$

which was already presented in equation 3.41 and holds for integrals that belong to the group 3 as introduced in the appendix of [42].

Taking all these preliminary remarks into account, we are finally able to carry out the phase space integration more or less as usual and, in particular, can make all ε-poles manifest. As it was already the case in the discussion that led us to this point, the outcome can be decomposed in three parts. The first two contain the combined soft-gluon and hard pole contributions and are divided into a C_F and a C_A part depending in their colour factor. The third piece originates from the soft-fermion poles, where we need to include the additional contributions from the further treatment of the hard poles.

All-in-all we can write the contribution to the spin-dependent cross section as

$$\sim \frac{4\pi M_N}{S^2U^2}\varepsilon^{P_h P p' s_T}\int_{v_{\min}}^{v_{\max}} dv \int_{w_{\min}}^{1}\frac{dw}{w}D^{c/h}(z)\frac{\alpha_{\mathrm{em}}^2\alpha_{\mathrm{s}}\big(\mu_F^2\big)}{2\pi}$$
$$\times \Bigg[\sigma^{\mathrm{SGP,HP}}_{C_F,d=4-2\varepsilon}\big(v,w,\mu\big)+\sigma^{\mathrm{SGP,HP}}_{C_A,d=4-2\varepsilon}\big(v,w,\mu\big)$$
$$+\,\sigma^{\mathrm{SFP}}_{d=4-2\varepsilon}\big(v,w,\mu\big)\Bigg] \tag{5.128}$$

in terms of three parts, which are still divergent for $\varepsilon \to 0$ and not finite. They are thus not our final result and will require further treatment before we obtain a physically meaningful outcome. But before we turn our attention to this task in the next chapter, we want to write down a schematic structure for the ε-poles in the remainder of the present section. Starting with the soft-gluon and hard pole pieces, we find that the divergent content of the C_F- and C_A-part may be written as

$$\sigma^{\mathrm{SGP,HP}}_{C_i,d=4-2\varepsilon}\big(v,w,\mu\big)$$
$$= C_i\Bigg\{G_F\big(x,x\big)\big[A_0\delta(1-w)+A_1\big]+x\frac{dG_F(x,x)}{dx}B_1$$
$$+\left(G_F\big(x,x\big)-x\frac{dG_F(x,x)}{dx}\right)C_1$$
$$+\left(\frac{1}{2}x\frac{dG_F(x,x)}{dx}-G_F\big(x,x\big)\right)f_{C_i}(v,w)\Bigg\}+\mathcal{O}\big(\varepsilon^0\big) \tag{5.129}$$

where $A_0 = 0$ in the case of the C_A part. Likewise, we find that

$$\sigma^{\mathrm{SFP}}_{d=4-2\varepsilon}\big(v,w,\mu\big) = G_F\big(x,0\big)\Bigg\{\frac{1}{C_A}A + C_F f_{C_F}(v,w)$$
$$+\,C_A f_{C_A}(v,w)\Bigg\}+\mathcal{O}\big(\varepsilon^0\big) \tag{5.130}$$

for the soft-fermion pole contribution. The results for the function f_{C_F} and f_{C_A} were already given previously in the equations 5.115 as well as 5.116. However, the analytic expressions for the coefficients will not be listed here. Instead, we will present the full finite result at a later point of this thesis.

5.5.5 Collinear Subtraction

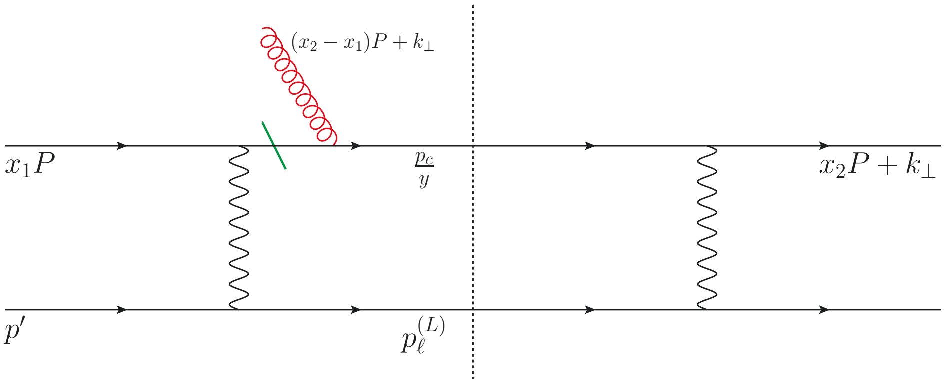

Figure 5.11: Born diagram required for the collinear subtraction in the case of the C_F part. The diagram is basically the same as shown in figure 5.4, but with adjusted kinematics in the final-state. The required subtraction term follows as a convolution of the associated d-dimensional LO cross section and the splitting function P_{gq}.

To conclude our analysis on the $q\ell \to gX$-channel, it remains to address the encountered divergences, as there are no virtual corrections in the case of this process, at least at the order of perturbation theory that we are considering. Instead, the only relevant contributions are provided by the real $2 \to 3$ corrections, for which the discussion was categorized and divided into three sections depending on the arising type of pole. However, as it could have been already observed when the unpolarized scattering was studied, the associated matrix elements exhibit collinear divergences, which correspond to the ε-poles that occur in our last presented result. It is therefore once again inevitable to handle these singularities by making use of the methods introduced in chapter 3.3 in the framework of collinear factorization.

In its basic features, the necessary procedure is similar to the technique, that was previously employed in the unpolarized case, especially since no contribution linked to the evolution equation for the Qiu-Sterman function are yet needed. This means that the subtraction terms can be formulated as a convolution of ordinary twist-2 splitting functions and d-dimensional cross sections, but where a first adjustment is required, as we now need to take twist-3 cross sections into account. The computation of the relevant twist-3 cross sections is rather straightforward and follows exactly the same procedure that was already presented in chapter 5.4. We therefore refrain from a detailed discussion of the calculation and instead only note the results. Beyond that, we will again encounter the Weizsäcker-Williams contributions related to quasi-real photons, produced from the incoming lepton, partaking in the hard scattering.

However, when dealing with the ε-poles emerging in the C_F-part, we will also observe a novel feature that will reoccur at a later point in the context of the $q\ell \to qX$-subprocess. It will turn out that not all singularities can be handled by following the well-known procedure and instead, some will still remain after all subtraction terms has been added. We will show how these divergences can be treated by making use of integration by parts.

With these final remarks, we conclude our introduction and focus on the actual computations. We commence our considerations by examining the C_F-part in more detail. It turns out that the only relevant collinear configuration appears in the final-state. At this stage, two ingredients are needed to continue the analysis. First, we need the leading-order quark-to-gluon splitting kernel P_{gq}, which is already known from equation 2.80 and reads

$$P_{gq}^{(0)}(\xi) = C_F\left(\frac{1+(1-\xi)^2}{\xi}\right). \tag{5.131}$$

Second, we need the d-dimensional twist-3 cross section for the relevant Born process, which turns out to be $q\ell \to q\ell$ scattering that has been discussed in four dimensions previously in chapter 5.4 but where we now need to slightly adjust the kinematics. The associated Feynman diagram is shown in figure 5.11 for an attachment on the left. We find that

$$\sigma_{\mathrm{SGP},d=4-2\varepsilon}^{(\mathrm{LO}),q\ell\to q\ell} = 2C_F\left(\frac{4\pi\mu^2}{s(1-v)v}\right)^{\varepsilon}\left(\frac{(1+v^2)}{(1-v)^4} - \frac{\varepsilon}{(1-v)^2}\right) \tag{5.132}$$

in $d = 4-2\varepsilon$ dimensions by following the same procedure as in our 4-dimensional considerations. We can now directly write down the contribution we are looking for as a convolution of the two quantities by employing the technique presented in chapter 3.3. After adding it to the C_F-part introduced previously in the last chapter, we decompose the outcome in a derivative piece $\sim x\frac{dG_F(x,x)}{dx}$ and a non-derivative contribution $\sim G_F(x,x)$. However, as we already hinted at, some singularities still remain even after including the subtraction term in both the derivative and non-derivative piece. To handle the divergences, we integrate the derivative piece, that carries no distributions, by parts. We find that

$$\begin{aligned}
&\int_{w_0}^{1}\frac{dx}{x}\left(x\frac{dG_F(x,x)}{dx}\right)\left(w^2 f(w)\right)\\
&= -f(1)G_F(w_0,w_0) + \int_{w_0}^{1}\frac{dx}{x}G_F(x,x)w\frac{d}{dw}\left[w^2 f(w)\right]
\end{aligned} \tag{5.133}$$

for an arbitrary function $f(w)$, where $w_0 = xw$ is the lower limit of the w-integral. By applying integration by parts, we are hence able to transform the derivative part into further non-derivative pieces.

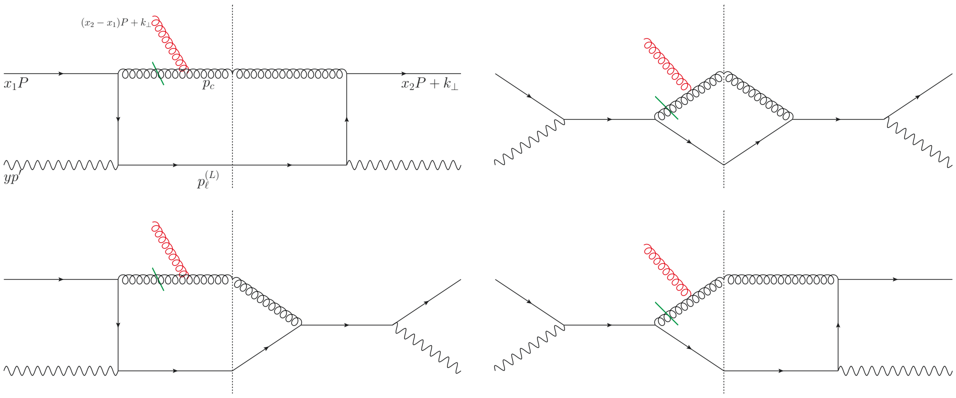

Figure 5.12: Born diagram required for the collinear subtraction in the case of the C_A part.

Moreover, we can conclude, that the same outcome is achieved by utilizing the substitution

$$f(w)x\frac{dG_F(x,x)}{dx} \to \left\{ -f(1)\delta(1-w) + \frac{1}{w}\frac{d}{dw}\left[w^2 f(w)\right]\right\} G_F(x,x) \quad (5.134)$$

in our considerations. The identity is applied not only for all ε-poles arising in the derivative part but also for the terms $\sim \ln\left(\frac{\mu^2}{S}\right)$, $\sim \ln\left(4\pi\right)$ and $\sim \gamma_{\mathrm{E}}$, that usually accompany the divergences. Following the procedure as outlined, we finally obtain a finite and physically meaningful result for the C_F-contribution.

Next, we continue our considerations by examining the C_A-part, which turns out to be simpler to handle since integration by parts is not needed to cancel the singularities. Instead, we only need to consider Weizsäcker-Williams contributions, which are based on the twist-3 cross section for the photon-parton scattering process $q\gamma \to gX$ at Born level. The corresponding Feynman diagrams, when the soft-gluon pole is taken on the left-hand side of the cut, are shown in figure 5.12. We are led to consider the cross section

$$\sigma^{(\mathrm{LO}),q\gamma\to qg}_{\mathrm{SGP},d=4-2\varepsilon} = C_A\left(\frac{4\pi\mu^2}{s(1-v)v}\right)\left(\frac{2-2v+v^2-\varepsilon v^2}{(1-v)^3}\right) \quad (5.135)$$

by taking them together with the set of diagrams for an attachment on the right into account. Beyond the cross section, we require the lepton-to-photon splitting function

$$P_{\gamma\ell}(\xi) = \frac{1+(1-\xi)^2}{\xi}, \quad (5.136)$$

respectively the related photon-in-lepton distribution, to formulate the Weizsäcker-Williams contribution. Both quantities together enable us to deal with all ε-poles emerging in the C_A-part by following the procedure as outlined in chapter 3.4 leading to finite outcome.

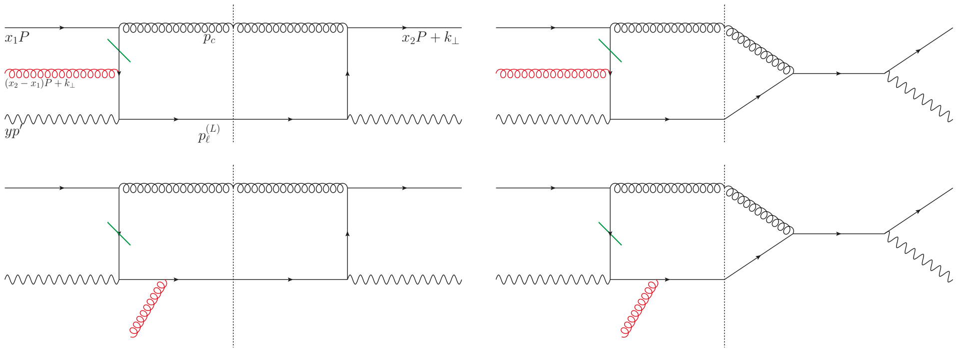

Figure 5.13: First set of Feynman diagrams required for the collinear subtraction in the case of the soft-fermion pole contributions. The illustrated diagrams carry the colour factor $C_F - C_A/2$.

To conclude our treatment of the collinear divergences arising in the $q\ell \to gX$-channel, we need to investigate the soft-fermion pole contributions. As it could be recognized in the last chapter, the pure soft-fermion pole contributions carry the colour factor $\frac{-1}{2C_A} = (C_F - C_A/2)$. However, we also received additional contributions with the colour factors C_F respectively C_A provided by the hard poles and we therefore require suitable subtraction terms for all three contributions.

As in the case of the C_A-part, it turns out that all required terms to subtract the collinear divergences are provided by Weizsäcker-Williams contributions and we need to examine Feynman diagrams representing the photon-quark scattering process $q\gamma \to gX$. The relevant diagrams for all three colour factors are shown in the figures 5.13, 5.14 and 5.15 in the case, when the pole is taken on the left-hand side of the cut. Again, the equivalent diagrams for an attachment on the right can be easily constructed and we thus refrain from presenting them. The Feynman diagrams enable us to calculate the associated twist-3 cross sections, which read

$$\sigma^{(\mathrm{LO}),q\gamma\to qg}_{\mathrm{SFP},d=4-2\varepsilon} = \frac{1}{C_A}\left(\frac{4\pi\mu^2}{s(1-v)v}\right)\left(\frac{1-2v+v^2-\varepsilon v}{(1-v)^3}\right) \tag{5.137}$$

$$\sigma^{(\mathrm{LO}),q\gamma\to qg}_{\mathrm{SFP},C_F,d=4-2\varepsilon} = 2C_F\left(\frac{4\pi\mu^2}{s(1-v)v}\right)\left(\frac{1+\varepsilon v(1-v)}{(1-v)^2}\right) \tag{5.138}$$

$$\sigma^{(\mathrm{LO}),q\gamma\to qg}_{\mathrm{SFP},C_A,d=4-2\varepsilon} = -C_A\left(\frac{4\pi\mu^2}{s(1-v)v}\right)\left(\frac{1+\varepsilon v(1-v)}{(1-v)^3}\right) \tag{5.139}$$

and make writing down the required subtraction terms feasible. By adding them to the soft-fermion pole contributions, we finally obtain a finite result for the cross section for the $q\ell \to gX$-channel.

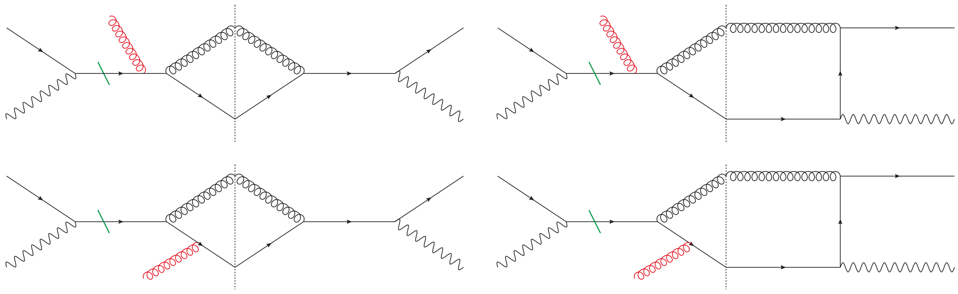

Figure 5.14: Second set of Feynman diagrams required for the collinear subtraction in the case of the soft-fermion pole contributions. The illustrated diagrams carry the colour factor C_F and are needed to cancel the ε-poles from the function f_{C_F}, which occurred in the context of the hard poles.

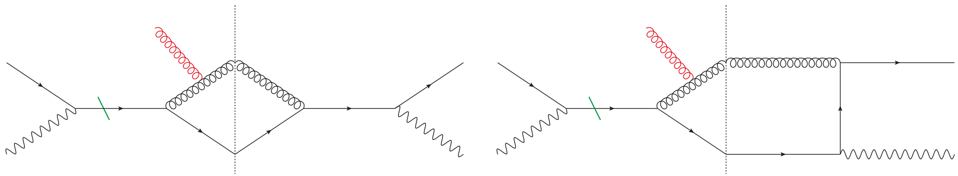

Figure 5.15: Third set of Feynman diagrams required for the collinear subtraction in the case of the soft-fermion pole contributions. The illustrated diagrams carry the colour factor C_A and are needed to cancel the ε-poles from the function f_{C_A}, which occurred in the context of the hard poles.

5.5.6 Finite result

Finally, we are able to present finite results for the contribution of the $q\ell \to gX$-channel to the spin-dependent cross section after we have successfully handled the last remaining divergences in the framework provided by collinear factorization, as discussed in the preceding chapter. In order to present the outcome reasonably clearly, we divide the total contribution into five parts according to two criteria. First, we distinguish between soft-gluon and soft-fermion pole contributions, where the hard poles are allocated to these two pieces. Second, each part is further subdivided according to the emerging colour factors. In light of this, the soft-gluon pole contributions consist of two pieces, a C_F- and a C_A-part. Likewise, the soft-fermion pole contributions are written in terms of three parts. Alongside a C_F- and a C_A-part, it further involves a contribution $\sim \frac{1}{C_A}$. Overall, the contribution of the subprocess, where the final-state gluon is assumed to be observed, reads

$$
\begin{aligned}
E_h \frac{d^3\Delta\sigma}{dP_h^3} =& \frac{4\pi M}{S^2U^2} \varepsilon^{P_h P p' s_T} \sum_a \int_{v_{\min}}^{v_{\max}} dv \int_{w_{\min}}^{1} \frac{dw}{w} D^{g/h}(z) \frac{\alpha_{\mathrm{em}}^2 e_a^2 \alpha_{\mathrm{s}}}{2\pi} \\
& \times \Bigg[C_F \left(\sigma_{C_F}^{\mathrm{SGP}} + \sigma_{C_F}^{\mathrm{SFP}} \right) + C_A \left(\sigma_{C_A}^{\mathrm{SGP}} + \sigma_{C_A}^{\mathrm{SFP}} \right) \\
& \quad + \frac{1}{C_A} \sigma_{1/C_A}^{\mathrm{SFP}} \Bigg]
\end{aligned} \tag{5.140}
$$

where the cross section are functions of the kinematic variables v and w, the factorization scale μ and the lepton mass m_ℓ. In principle, the fragmentation scale would of course also occur here. However, we have set it equal to the factorization scale. The explicit expression for the five contributions are rather lengthy and we will therefore not list them in full here. The C_F-part of the soft-gluon pole contributions can be schematically written as

$$
\begin{aligned}
\sigma_{C_F}^{\mathrm{SGP}} =& G_F(x,x) \Bigg[\big(A_{C_F,0}^{(0)} \ln\big(\frac{\mu^2}{s}\big) + A_{C_F,1}^{(0)} \big) \delta(1-w) + B_{C_F}^{(0)} \left(\frac{1}{1-w} \right)_+ \\
& + C_{C_F,0}^{(0)} \ln\big(\frac{\mu^2}{s}\big) + C_{C_F,1}^{(0)} \Bigg] + \left(G_F(x,x) - x \frac{dG_F(x,x)}{dx} \right) C_{C_F,1}^{(1)} \\
& + x \frac{dG_F(x,x)}{dx} C_{C_F,1}^{(2)} \ ,
\end{aligned} \tag{5.141}
$$

where the coefficients are functions of v as well as w. Here, the fragmentation scale arises due to a collinear configuration in the final state. The C_A-piece, on the other hand, can be displayed much shorter. It reads

$$
\begin{aligned}
\sigma_{C_F}^{\mathrm{SGP}} =& G_F(x,x) C_{C_A,1}^{(0)} + x \frac{dG_F(x,x)}{dx} C_{C_A,1}^{(2)} \\
& \left(G_F(x,x) - x \frac{dG_F(x,x)}{dx} \right) \big[C_{C_A,0}^{(1)} \ln\big(\frac{m_\ell^2}{s}\big) + C_{C_A,1}^{(1)} \big].
\end{aligned} \tag{5.142}
$$

It immediately catches the eye that the lepton mass emerges as a consequence of the required Weizsäcker-Williams contributions.

Next, we want to address the soft-fermion pole contributions, which turn out to be even simpler. The longest contribution is the one $\sim \frac{1}{C_A}$. Written in the same schematic manner as the soft-gluon poles, it becomes

$$\sigma^{\text{SFP}}_{1/C_A} = G_F(x,0)\big[C^{(0)}_{1/C_A,0}\ln\big(\frac{m_\ell^2}{s}\big) + C^{(0)}_{1/C_A,1}\big]. \tag{5.143}$$

The C_F- and C_A-part, on the other hand, can be noted explicitly. They originate from reverting the Taylor series expansion in connection with the further treatment of the hard poles. Moreover, they reveal a striking resemblance in their structure and can therefore even be stated together. They read

$$\begin{aligned} &C_F\sigma^{\text{SFP}}_{C_F} + C_A\sigma^{\text{SFP}}_{C_A} \\ &= -\left(2C_F \pm \frac{C_A}{1-vw}\right)\frac{vw\left(2v^2w^2 - 2v^2w + v^2 - 2vw + 1\right)}{(1-v)^4(1-vw)} \\ &\quad\times\left(\ln\left(\frac{m_\ell^2}{S}\right) + v^2w^2 - vw + \ln(w) + 1\right) \end{aligned} \tag{5.144}$$

in terms of the kinematic variables v, w as well as the lepton mass m_ℓ.

Note that the coefficients arising in the schematic expressions for the various pieces contributing to the cross section are listed in appendix E.

These results allow us to investigate the influence of the $q\ell \to gX$-channel numerically in the course of phenomenological studies, which we will do at a later point. Before that, however, we will discuss the second sub-process in connection with the quark-gluon-quark correlator, in which the quark is assumed to be observed.

5.6 Next-to-Leading Order: $q\ell \rightarrow qX$-channel

In total, three scattering processes on the partonic level can be identified, which provide non-vanishing contributions to the spin-dependent cross section for the single-inclusive production of a hadron in transversally polarized nucleon-lepton scattering, namely $q\ell \rightarrow qX$, $q\ell \rightarrow gX$ as well as $g\ell \rightarrow qX$, where the gluon-gluon-gluon correlator instead of the quark-gluon-quark function is involved in the latter, that is not considered in this thesis as stated in the introduction at the beginning of the chapter. In the last section, we presented our calculations concerning the $q\ell \rightarrow gX$-channel, which also proved to be a suitable example for introducing the basic features of twist-3 considerations at next-to-leading order and the necessary computational methods in detail. In particular, it was advantageous that the total number of contributions was manageable and the emerging structures are still relatively simple.

Next, we continue our analysis of the transverse single-spin asymmetry by considering the second process, which involves the quark-gluon-quark correlator and hence the Qiu-Sterman function, namely the $q\ell \rightarrow qX$-channel. The process is expected to provide the dominant contribution to the spin-dependent cross section but also turns out to be more complicated to handle. On the one hand, this can be traced back to the larger number of Feynman diagrams. We now not only have to deal with virtual corrections but also with novel diagrams contributing to the real corrections in comparison to the $q\ell \rightarrow gX$-channel. On the other hand, the treatment of the hard poles will turn out to be more time-consuming, as the structures arising in this context will be more complex. Finally, an additional obstacle emerges because contributions tied to the evolution equation of the QiuSterman function must now be included within the collinear factorization framework, as they are required to correctly absorb and handle the divergences that appear at this stage.

Nevertheless, the techniques, that we have already applied, will be of great benefit and prove to be particularly helpful, as they are sufficient to carry out a substantial portion of the necessary twist-3 calculations. In particular, we will follow exactly the same procedure as outlined previously at the beginning of our considerations. More precisely, this means that we will need to again examine the propagators providing the pole contributions and the delta function separated from the phase space. Even the treatment of the hard pole will rely on the same basic ideas as before. In the end, we will not only be able to specify all ε-poles, but also to show that they can be annihilated, enabling us to take the limi $\varepsilon \rightarrow 0$ and leading to a finite outcome for the $q\ell \rightarrow qX$-channel. It will thus be seen that we can successfully handle all relevant subprocesses to the transverse single-spin asymmetry that involve the quark-gluon-quark correlator.

All our considerations on $q\ell \to qX$ scattering at next-to-leading order are based on the factorization formula for the spin-dependent cross section, that was introduced in equation 5.30 and reads

$$\begin{aligned} d\Delta\sigma =& i\frac{M}{4S}\varepsilon^{\beta P n s_T}\int\frac{dz}{z^2}D^{c/h}(z) \\ &\times\int dx_1\int dx_2\, G_F\big(x_1,x_2\big)\omega^{\alpha}{}_{\beta}\frac{\partial\mathcal{H}\big(k_1,k_2\big)}{\partial k_2^{\alpha}}\Big|_{k_i\approx x_iP}. \end{aligned} \tag{5.145}$$

As previously, when we studied the $q\ell \to gX$-process, our analysis follows two tracks. On the one hand, we need to examine internal lines and the associated propagators, which provide the pole contributions in their on-shell limit and extract the imaginary part. We will give a brief summary of the most important results in the following subchapters for each contribution. On the other hand, it is inevitable to investigate the delta function, that ensures the unobserved lepton's on-shell condition, after separating it from the three-body phase space. However, as before, it can also be observed here, that we find the same expression for all contributions. We will therefore deal with this part only once here and not mention it separately for each contribution. By making use of momentum conservation and analysing the momentum flow along the relevant Feynman diagrams, we find that the final-state lepton's momentum is

$$p_\ell^{(L)} = x_2P + k_\perp + p' - p_c - r \tag{5.146}$$

$$p_\ell^{(R)} = x_1P + p' - p_c - r \tag{5.147}$$

for an attachment on the left respectively on the right, which is clearly identical to the result, that we previously obtained. We can therefore simply take the result from the previous section. The delta function thus becomes

$$\delta\Big(\big(p_\ell^{(L)}\big)^2\Big) = \frac{1}{S+T_1+T_3}\delta\big(x_2-\xi-v_2\cdot k_\perp\big) \tag{5.148}$$

$$\delta\Big(\big(p_\ell^{(R)}\big)^2\Big) = \frac{1}{S+T_1+T_3}\delta\big(x_1-\xi\big) \tag{5.149}$$

when the pole is taken on the left-hand side respectively on the right-hand side of the cut. Here, the four-vector v_2 is defined in the exact same way as previously and reads $v_2 = \frac{2(p_c+r)}{S+T_1+T_3}$.

In the next subsections, we will present our considerations on the $q\ell \to qX$-channel at next-to-leading order. We will first examine the real corrections before focusing on the virtual one-loop processes. Thereby, the subchapters are structured in a similar way as in the previous case concerning the $q\ell \to gX$-scattering and we will be present a final result at the end.

5.6.1 Real Corrections: Soft-Gluon Pole Contributions

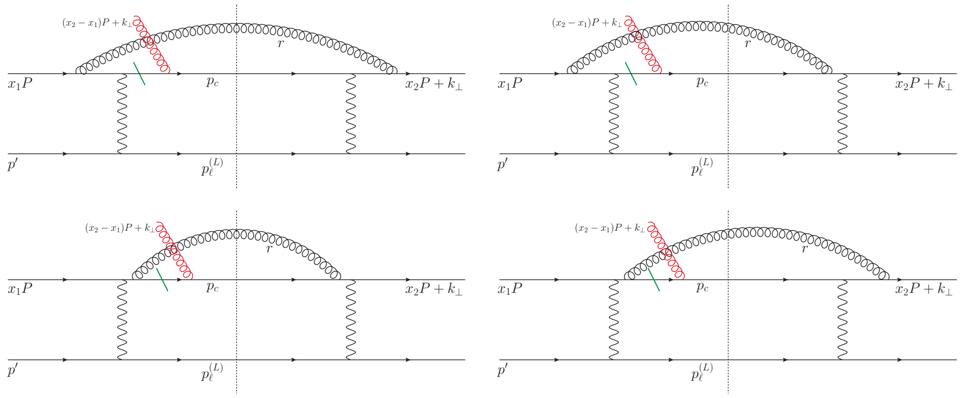

Figure 5.16: Feynman diagrams providing soft-gluon pole contributions in $q\ell \to qX$ scattering that carry the colour factor $C_F - \frac{C_A}{2}$. The diagrams are basically the same as shown in figure 5.5 but where the momenta p_c and r have been exchanged. Again, only the case when the pole is taken on the left-hand side of the cut is illustrated.

Again, we commence our considerations by studying the pure soft-gluon pole contributions, which can be treated in complete analogy to the $q\ell \to gX$-channel. The Feynman diagrams contributing to the cross section can be divided into two sets according to their colour factor. The first set carries the factor $C_F - \frac{C_A}{2}$ while the second one comes with the factor $\frac{C_A}{2}$, which is an observation that we a have also encountered in the previous process. In fact, it turns out that the diagrams are basically the same but where the momenta p_c and r are exchanged. In more detail, the final-state quark is now assumed to be observed and thus carries the momentum p_c instead of the gluon. We start by considering the diagrams, that involve the colour factor

$$C_F - \frac{C_A}{2} = -\frac{1}{2C_A} \tag{5.150}$$

and are shown in figure 5.16. A comparison with the diagrams illustrated in figure 5.5 reveals that they really only differ in terms of the momentum labels, as it was already noted. Like in other parts of our discussion, we avoid to explicitly present the equivalent diagrams for an attachment on the right. Following the same procedure as outlined previously, we find

$$\frac{1}{\left(p_c \mp \left(x_2 - x_1\right)P \mp k_\perp\right)^2 \pm i\varepsilon} \to \pm\frac{i\pi}{T_1}\delta\left(x_1 - x_2 + v_1 \cdot k_\perp\right) \tag{5.151}$$

for the propagator, which provides the soft-gluon pole, and its imaginary part, where $v_1 = \frac{2p_c}{T_1}$. Here, the upper sign holds for an attachment on the left and the lower sign applies when the pole is taken on the right-hand side of the cut.

Note that we would have obtained the same outcome by taking the appropriate results given in the view of $q\ell \to gX$-scattering (see equations 5.74 and 5.77) and making use of the replacements $r \to p_c$, respectively $T_3 \to T_1$. Likewise, the structure emerging in the factorization formula becomes

$$\begin{aligned} \sim & \frac{i\pi}{T_1} \int dPS_3 \Bigg[\big(v_2 - v_1\big)_\rho H_L\big(x, x, 0\big) \frac{dG_F\big(x, x\big)}{dx} \\ & + G_F\big(x, x\big) \lim_{k_\perp \to 0} \frac{\partial}{\partial k_\perp^\rho} \Bigg\{ H_L\big(x + (v_2 - v_1) \cdot k_\perp, x + v_2 \cdot k_\perp, k_\perp\big) \\ & \qquad - H_R\big(x, x + v_1 \cdot k_\perp, k_\perp\big) \Bigg\} \Bigg] \end{aligned} \tag{5.152}$$

and it remains to compute the hard scattering functions.

Next, we continue our analysis by examining the second set of diagrams, which carry the colour factor

$$\frac{C_A}{2} \tag{5.153}$$

and involve three-gluon vertices. Instead of presenting the relevant Feynman diagrams, we would like to refer to those shown in figure 5.7. In both cases, the diagrams are in principle identical again and only the momenta p_c and r need to be exchanged. Therefore, the result for the propagators, that yield the soft-gluon poles, follows from equation 5.85 by employing the replacements $p_c \to r$ as well as $T_1 \to T_3$. We thus find

$$\frac{1}{\big(r \mp (x_2 - x_1)P \mp k_\perp\big)^2 \pm i\varepsilon} \to \pm \frac{i\pi}{T_3} \delta\big(x_1 - x_2 + v_1 \cdot k_\perp\big), \tag{5.154}$$

where the signs have to be understood in the same sense as earlier and the four-vector v_1 is given by $v_1 = \frac{2p_c}{T_3}$. Likewise, the structure encountered in the factorized cross section reads

$$\begin{aligned} \sim & \frac{i\pi}{T_3} \int dPS_3 \Bigg[\big(v_2 - v_1\big)_\rho H_L\big(x, x, 0\big) \frac{dG_F\big(x, x\big)}{dx} \\ & + G_F\big(x, x\big) \lim_{k_\perp \to 0} \frac{\partial}{\partial k_\perp^\rho} \Bigg\{ H_L\big(x + (v_2 - v_1) \cdot k_\perp, x + v_2 \cdot k_\perp, k_\perp\big) \\ & \qquad - H_R\big(x, x + v_1 \cdot k_\perp, k_\perp\big) \Bigg\} \Bigg] \end{aligned} \tag{5.155}$$

after reconstructing the full three-body phase space.

Once again, it remains to compute the hard scattering functions, to carry out the $k_\perp$-derivative and to take the limit $k_\perp \to 0$. Afterwards, we can reorganize the outcome and divide it into a C_F- and a C_A-piece. Both parts are written in terms of a contribution $\sim \big(G_F(x,x) - x\frac{dG_F(x,x)}{dx}\big)$ and the remaining non-derivative piece $\sim G_F(x,x)$.

5.6.2 Real Corrections: Hard Pole Contributions

The next part of our discussion on the $q\ell \to qX$-channel addresses hard pole contributions to the spin-dependent cross section. In the following, we focus on hard poles that are of the same structure as those, which already emerged in the light of $q\ell \to gX$-scattering. It will turn out that further hard poles of another form can arise in the currently considered scattering beyond the aforementioned contributions. However, these novel hard poles will be discussed in a separate section in the later course of the thesis.
In the same manner as in our previous considerations when the final-state gluon was assumed to be observed, the relevant Feynman diagrams can be assigned to two categories. First, there are again those which already provided pure soft-gluon poles, but where pole is now taken at another internal line. On the other hand, the second class includes novel diagrams. In more detail, it turns out that the diagrams are basically the same as shown in the figures 5.8 and 5.9, but where the momenta p_c and r need to be exchanged, which represents a fact that already caught our eye in the last section on the soft-gluon poles. The observation enables us to keep the required calculations short as many results can be directly concluded from previously presented equations. In fact, it is particularly simple in case of the hard poles since the quantities come with the combination $T_1 + T_3$ that remains unchanged when the momenta p_c and r are exchanged. With this in mind, we find

$$\frac{1}{\big(p_c + r \mp (x_2 - x_1)P \mp k_\perp\big)^2 \pm i\varepsilon} \to \pm\frac{i\pi}{T_1 + T_3}\delta\big(x_1 - x_2 + x\tilde{x} + v_1 \cdot k_\perp\big), \tag{5.156}$$

for the propagators providing the hard poles in their on-shell limit. Here, the signs need to be understood in the same sense as previously. Likewise, the structure arising in the factorization formula for the cross section becomes

$$\begin{aligned} \sim & \frac{i\pi}{T_1 + T_3} \int dPS_3\, G_F\big(x, x(1-\tilde{x})\big) \\ & \times \lim_{k_\perp \to 0} \frac{\partial}{\partial k_\perp^\rho} \Big\{ H_L\big(x(1-\tilde{x}) + (v_2 - v_1)\cdot k_\perp, x + v_2 \cdot k_\perp, k_\perp\big) \\ & \qquad - H_R\big(x, x(1-\tilde{x}) + v_1 \cdot k_\perp, k_\perp\big) \Big\} \Big] \end{aligned} \tag{5.157}$$

by following the procedure as outlined previously. Of course, the four-vectors v_1 and v_2 as well as the variable $\tilde{x}$ are then defined exactly alike as in chapter 5.5.2. As a reminder, they read

$$v_1 = \frac{2(p_c + r)}{T_1 + T_3},\; v_2 = \frac{2(p_c + r)}{S + T_1 + T_3} \text{ and } \tilde{x} = -\frac{s_{13}}{t_1 + t_3} \tag{5.158}$$

in terms of the Mandelstam variables and the momenta p_c and r.

Once again, it now remains to compute the hard scattering functions. Afterwards we can evaluate the $k_\perp$-derivative and take the limit $k_\perp \to 0$. It turns out that we can write the outcome in the same manner as in the context of the scattering process, when the gluon was assumed to be observed. This mean, that the hard pole contributions become

$$\mathcal{HP} = G_F\big(x, x(1-\tilde{x})\big)\mathcal{M}_{\mathrm{HP}}\big(s_{13}, t_3, u_2\big) \tag{5.159}$$

with $\mathcal{M}_{\mathrm{HP}}$ denoting the unintegrated matrix element. For the further treatment, we employ the procedure, which we introduced in section 5.5.2, starting with the Taylor series expansion of the Qiu-Sterman function encountered in the expression above for small $\tilde{x}$. The outcome can be taken from the aforementioned chapter and reads

$$\begin{aligned}\mathcal{HP} =&\Bigg\{G_F\big(x,x\big) - \frac{1}{2}\tilde{x}\left(x\frac{dG_F\big(x,x\big)}{dx}\right)\\ &+\sum_{k=2}^{\infty}\frac{(-1)^k\tilde{x}^k}{k!}\left(x^k\frac{d^kG_F\big(x,y\big)}{dy^k}\right)_{y=x}\Bigg\}\mathcal{M}_{\mathrm{HP}}\big(s_{13},t_3,u_2\big),\end{aligned} \tag{5.160}$$

where the lowest order is combined with the non-derivative piece of the pure soft-gluon poles and the first order term $\sim x\frac{dG_F(x,x)}{dx}$ is directly integrated over the three-body phase space. The remainder of the expansion, on the other hand, is treated as outlined previously. Therefore, we proceed our considerations by writing the remainder of the Taylor expansion given above as

$$\begin{aligned}&\sum_{k=2}^{\infty}\frac{(-1)^k}{k!}\left(x^k\frac{d^kG_F\big(x,y\big)}{dy^k}\right)_{y=x}\int dPS_3\,\tilde{x}^k\mathcal{M}_{\mathrm{HP}}\big(s_{13},t_3,u_2\big)\\ &=\sum_{k=0}^{\infty}\frac{(-1)^k}{(k+2)!}\left(x^{k+2}\frac{d^{k+2}G_F\big(x,y\big)}{dy^{k+2}}\right)_{y=x}\int dPS_3\,\tilde{x}^{k+2}\mathcal{M}_{\mathrm{HP}}\big(s_{13},t_3,u_2\big),\end{aligned} \tag{5.161}$$

which enables us to isolate the product $\tilde{x}^2\mathcal{M}_{\mathrm{HP}}$. The product is again decomposed in three parts according to

$$\tilde{x}^2\mathcal{M}_{\mathrm{HP}} = \mathcal{M}_1 + \mathcal{M}_2 + \mathcal{M}_3, \tag{5.162}$$

where $\mathcal{M}_1$ is singular for $u_2 \to 0$, $\mathcal{M}_2$ is divergent for $t_3 \to 0$ and $\mathcal{M}_3$ is finite. At this point, we continue our discussion by addressing the combination $\tilde{x}^k\mathcal{M}_1$. Following the same procedure as outlined previously, we find

$$\int dPS_3\,\tilde{x}^k\mathcal{M}_1 = \frac{1}{\varepsilon}f(v,w) + \text{finite} \tag{5.163}$$

in the collinear limit.

In complete analogy to our preceding analysis, we obtain

$$
\begin{aligned}
&\sim \frac{1}{\varepsilon}\sum_{k=0}^{\infty}\frac{(-1)^k}{(k+2)!}\left(x^{k+2}\frac{d^{k+2}G_F(x,y)}{dy^{k+2}}\right)_{y=x} f(v,w)\\
&=\frac{1}{\varepsilon}f(v,w)\left\{G_F(x,0)-G_F(x,x)+\frac{1}{2}x\frac{dG_F(x,x)}{dx}\right\}, \qquad (5.164)
\end{aligned}
$$

by inserting the phase space integrated combination $\tilde{x}^k\mathcal{M}_1$ into the remainder of the Taylor expansion with

$$
\frac{1}{\varepsilon}f_{C_F}(v,w)=\frac{2vw\big(2v^2w^2-2v^2w+v^2-2vw+1\big)}{\varepsilon(1-v)^4(1-vw)}+\mathcal{O}\big(\varepsilon^0\big) \qquad (5.165)
$$

$$
\frac{1}{\varepsilon}f_{C_A}(v,w)=-\frac{vw\big(2v^2w^2-2v^2w+v^2-2vw+1\big)}{\varepsilon(1-v)^4(1-vw)}+\mathcal{O}\big(\varepsilon^0\big) \qquad (5.166)
$$

in the case of the C_F- respectively the C_A-part.

Next, we continue our analysis by considering $\tilde{x}^k\mathcal{M}_2$, which turns out to be a bit more complicated in contrast to the $q\ell \to gX$-channel, where said contributing completely vanished. In the present instance, this also still applies to the C_F-part but it is not the case anymore for the C_A part. Instead, we find that the integrated product $\tilde{x}^k\mathcal{M}_2$ may be written as

$$
\begin{aligned}
\int d\mathrm{PS}_3\,\tilde{x}^k\mathcal{M}_2 =&\frac{1}{\varepsilon}\big\{(1-w)^{k+1}g_1(v,w)\\
&+(k+1)(1-w)^k g_2(v,w)\big\}+\text{finite} \qquad (5.167)
\end{aligned}
$$

in the collinear limit, where we have introduced two simple rational function g_1 and g_2 in the same sense as we previously defined f. The next step is to insert the functions one after the other into the series expansion. Starting with g_1, we obtain

$$
\begin{aligned}
&\sim \frac{1}{\varepsilon}\sum_{k=0}^{\infty}\frac{(-1)^k}{(k+2)!}(1-w)^{k+1}\left(x^{k+2}\frac{d^{k+2}G_F(x,y)}{dy^{k+2}}\right)_{y=x} g_1(v,w)\\
&=\frac{1}{\varepsilon}\frac{g_1(v,w)}{1-w}\sum_{k=0}^{\infty}\frac{(-1)^k}{k!}(1-w)^k\left(x^k\frac{d^kG_F(x,y)}{dy^{k+2}}\right)_{y=x}\\
&=\frac{1}{\varepsilon}\frac{g_1(v,w)}{1-w}\Bigg\{-G_F(x,x)+\frac{1}{2}(1-w)xG'_F(x,x)\\
&\quad+\sum_{k=0}^{\infty}\frac{(-1)^k}{k!}(1-w)^k\left(x^k\frac{d^kG_F(x,y)}{dy^{k+2}}\right)_{y=x}\Bigg\}\\
&=\frac{1}{\varepsilon}g_1(v,w)\left\{\frac{G_F(x,xw)-G_F(x,x)}{1-w}+\frac{1}{2}xG'_F(x,x)\right\} \qquad (5.168)
\end{aligned}
$$

after rearranging the series expansion in terms of a combination of Qiu-Sterman functions.

Once again, we can observe that the hard poles provide additional soft-gluon pole contributions. However, besides these contributions, where the Qiu-Sterman function and its derivative are evaluated at equal arguments, the expression also yields a genuine hard pole $\sim G_F(x, xw)$, where the arguments of the function are different.

The procedure now needs to be repeated for g_2. By inserting the function into the Taylor series expansion, we find that

$$
\begin{aligned}
&\sim \frac{1}{\varepsilon} \sum_{k=0} \frac{(-1)^k}{(k+2)!} (k+1)(1-w)^k \left(x^{k+2} \frac{d^{k+2} G_F(x,y)}{dy^{k+2}} \right)_{y=x} g_2(v,w) \\
&= -\frac{1}{\varepsilon} g_2(v,w) \frac{\partial}{\partial w} \sum_{k=0}^{\infty} \frac{(-1)^k}{(k+2)!} (1-w)^{k+1} \left(x^{k+2} \frac{d^{k+2} G_F(x,y)}{dy^{k+2}} \right)_{y=x} \\
&= -\frac{1}{\varepsilon} g_2(v,w) \frac{\partial}{\partial w} \left\{ \frac{G_F(x,xw) - G_F(x,x)}{1-w} + \frac{1}{2} x G'_F(x,x) \right\} \\
&= -\frac{1}{\varepsilon} g_2(v,w) \frac{\partial}{\partial w} \left\{ \frac{G_F(x,xw) - G_F(x,x)}{1-w} \right\} \qquad (5.169)
\end{aligned}
$$

by making use of the fact that the derivative term emerging in the third line vanishes due to the partial derivative with respect to the variable w as it only acts on explicit dependencies. We have therefore dropped the contribution in the last line.

By carrying out the required calculations, we receive

$$
\frac{1}{\varepsilon} g_1(v,w) = -\frac{1+v^2}{\varepsilon(1-v)^4} + \mathcal{O}\big(\varepsilon^0\big) \qquad (5.170)
$$

$$
\frac{1}{\varepsilon} g_2(v,w) = \frac{w(1+v^2)(1+w)}{\varepsilon(1-v)^4} + \mathcal{O}\big(\varepsilon^0\big) \qquad (5.171)
$$

for the functions g_1 and g_2. As stated earlier, the C_F-part vanishes and both functions therefore appear with the colour factor C_A, which is factored out in the expressions presented above alongside other prefactors like the coupling constants. They will be included in the full factorization formula.

5.6.3 Real Corrections: Soft-Fermion Pole Contributions

We proceed as we did when the $q\ell \to gX$-channel was discussed and continue our considerations by studying the pure soft-fermion pole contributions. On the whole, the calculation is rather straightforward and follows the same procedure, which we employed earlier to deal with the pure soft-gluon poles. In particular, it turns out that no new challenges emerge, which is why we limit ourselves to a brief summary.

In total, eight distinct Feynman diagrams need to be taken into account, which can be divided into two sets with each including four diagrams. The two sets apply for either an attachment on the left or the right. But again, it is not necessary to construct the diagrams from scratch and instead, we can make use of those from our foregoing considerations, when the gluon was assumed to be observed. For example, we can take the diagrams shown in figure 5.10, when the pole is located on the left-hand side of the cut, and only need to exchange the momenta p_c and r. We then obtain

$$\frac{1}{\big(x_1 P - r\big)^2 + i\varepsilon} \to \frac{i\pi}{T_3}\delta\big(x_1\big) \tag{5.172}$$

for the propagator providing the soft-fermion pole for an attachment on the left respectively

$$\frac{1}{\big(x_2 P + k_\perp - r\big)^2 + i\varepsilon} \to -\frac{i\pi}{T_3}\delta\big(x_2 - v_1 \cdot k_\perp\big) \tag{5.173}$$

for an attachment on the right, where $v_1 = \frac{2p_c}{T_3}$, by utilizing the replacement $T_1 \to T_3$. Likewise, the structure taken from the factorization formula becomes

$$\begin{aligned}\sim \frac{i\pi}{T_3}\int dPS_3\, G_F\big(x,0\big) \lim_{k_\perp \to 0} \frac{\partial}{\partial k_\perp^\rho}\Big\{ & H_L\big(0, x + v_2 \cdot k_\perp, k_\perp\big) \\ & - H_R\big(x, v_1 \cdot k_\perp, k_\perp\big)\Big\}\Big]\end{aligned} \tag{5.174}$$

and it remains to compute the hard scattering functions as usual before we can evaluate the $k_\perp$-derivative and take the limit $k_\perp \to 0$.

5.6.4 Real Corrections: Crossed Diagrams

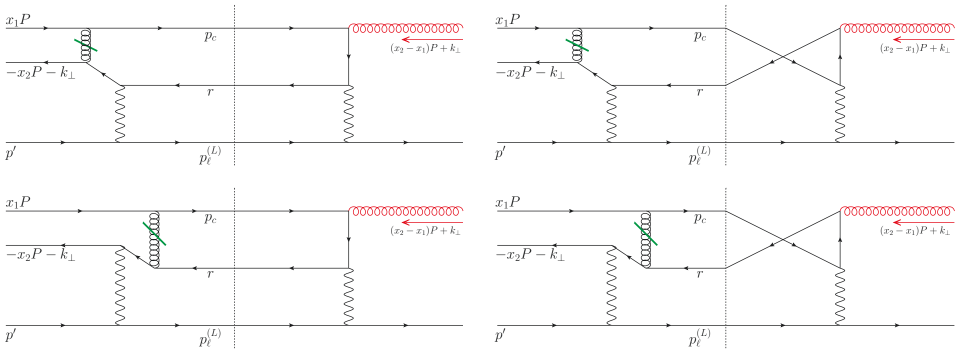

Figure 5.17: First set of crossed diagrams providing additional soft-fermion poles. Note that the momentum flow is chosen in such a way that the twist-3 gluon's momentum $(x_2-x_1)P+k_\perp$ is incoming, i.e. points towards the vertex.

In the preceding chapters, we have always studied Feynman diagrams, which we have in principle already encountered within our considerations on the $q\ell \to gX$-channel, except for a few minor modifications. Unsurprisingly, we found that many intermediate results of both subprocesses are quite similar and can be determined in part from the respective counterpart by suitable adjustments of the involved momenta and the kinematic variables. In the following, however, we want to address one of two categories of novel Feynman diagrams, which did not occur in this form when the gluon was assumed to be observed. They can be generated by crossing one of the incoming quark lines and the twist-3 gluon line and we therefore refer to them as crossed diagrams. As a result, a quark-antiquark pair is now found in the final state alongside the unobserved lepton. It will soon become apparent that these novel diagrams not only provide further soft-fermion poles, but also serve as source of additional hard pole contributions. In this context, the hard poles will turn out to be particularly interesting as they differ from the previously found contributions in the way how they fix the kinematics. But despite these differences, both contributions can be treated with the familiar procedure and methodology, which does not only apply to dealing with the propagators or the hard scattering functions but also to the treatment of the hard poles based on the approach utilizing a Taylor series expansion to extract the ε-poles.

However, before we face these issues, we need to revisit the unobserved lepton's on-shell condition as we cannot employ the result that we presented in the introduction on the $q\ell \to qX$-channel and used in all the previous cases. Against this background, we start by analysing the momentum flow along the Feynman diagrams and make use of momentum conservation.

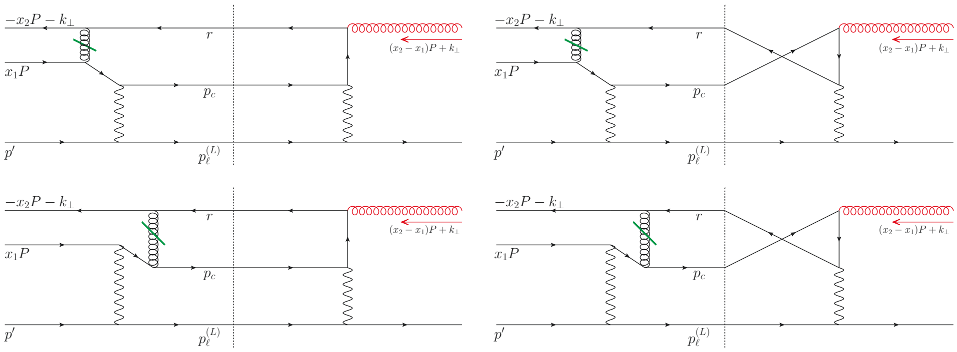

Figure 5.18: Second set of crossed diagrams providing additional soft-fermion poles. The momentum flow is chosen in the same way as in the first set of diagrams.

Therefore, we obtain

$$p_\ell^{(L)} = p_\ell^{(R)} = p' - \big(x_2 - x_1\big)P - k_\perp - p_c - r \tag{5.175}$$

for all relevant Feynman diagrams in both cases when the pole is taken either on the left-hand or the right-hand side of the cut. By taking the square of the expression and replacing all scalar products of momenta by Mandelstam variables, we find

$$\delta\Big(\big(p_\ell^{(L)}\big)^2\Big) = \delta\Big(\big(p_\ell^{(R)}\big)^2\Big) = \frac{1}{S + T_1 + T_3}\delta\Big(x_1 - x_2 - \xi + v_2 \cdot k_\perp\Big) \tag{5.176}$$

for the delta function separated from the phase space that ensures the final-state lepton's on-shell condition, where the four-vector v_2 is introduced in the exact same way as earlier. What is striking about this outcome is that it does not fixes one of the momentum fractions, as we are used to, but establishes a relation between both variables.

Next, we continue our considerations by investigating the internal line providing the soft-fermion pole contributions. In the light of this, we can arrange the relevant Feynman diagrams into two sets since each set yields a different type of soft-fermion pole. The first set is shown in figure 5.17. Again, the internal lines providing the pole are marked by a green bar and the associated propagators read

$$\frac{1}{\big(p_c - x_1 P\big)^2 \pm i\varepsilon} \to \pm\frac{i\pi}{T_1}\delta\big(x_1\big) \tag{5.177}$$

and we can immediately recognize that the momentum fraction x_1 will be set to zero by the arising delta function after extracting the imaginary part in the on-shell limit. Before we proceed by repeating the same discussion for the second set of diagrams, we will write down the relevant structure arising in the factorization formula, which serves as a foundation for the computation of the hard scattering functions.

Following the usual procedure, we are led to consider the expression

$$\sim \frac{i\pi}{T_1} \int dPS_3 \, G_F\big(0,-x\big) \lim_{k_\perp \to 0} \frac{\partial}{\partial k_\perp^\rho} \Big\{ H_L\big(0,-x+v_2 \cdot k_\perp, k_\perp\big) \\ - H_R\big(0,-x+v_2 \cdot k_\perp, k_\perp\big) \Big\} \Big] \tag{5.178}$$

in the factorized cross section, where we have already used that the derivative piece vanishes. In contrast to the previous discussed soft-fermion pole contributions, it is notable that we now obtain a contribution where the non-vanishing argument of the Qiu-Sterman function is evaluated at $-x$.

In the next step, we turn our attention to the second set of Feynman diagrams shown in figure 5.18. We therefore proceed in complete analogy to the first set and find that the propagators providing the soft-fermion pole are given by

$$\frac{1}{\big(r+x_2P+k_\perp\big)^2 \pm i\varepsilon} \to \pm \frac{i\pi}{T_3} \delta\big(x_2 - v_1 \cdot k_\perp\big) \tag{5.179}$$

with the four-vector v_1 being $v_1 = \frac{2r}{T_3}$. The structure emerging in the factorization formula thus becomes

$$\sim \frac{i\pi}{T_3} \int dPS_3 \, G_F\big(x,0\big) \lim_{k_\perp \to 0} \frac{\partial}{\partial k_\perp^\rho} \Big\{ H_L\big(x - v_2 \cdot k_\perp, v_1 \cdot k_\perp, k_\perp\big) \\ - H_R\big(x - v_2 \cdot k_\perp, v_1 \cdot k_\perp, k_\perp\big) \Big\} \Big] \tag{5.180}$$

and hence yields another soft-fermion pole contribution $\sim G_F(0,x)$. It now remains for both sets to compute the relevant hard scattering functions, carry out the $k_\perp$-derivative and take the limit $k_\perp \to 0$ by utilizing the common techniques. Furthermore, it should be noted that all the arising crossed diagrams carry the colour factor

$$-\frac{1}{2C_A} = C_F - \frac{C_A}{2}, \tag{5.181}$$

which coincides with the colour factor of the other soft-fermion pole contributions that we discussed earlier. With that being said, we conclude our discussion on the soft-fermion poles and turn our attention to the hard pole contributions.

Some of the crossed diagrams need to be revisited as they may also provide further hard poles. More precisely, the Feynman diagrams in question are those, in which a photon is first exchanged between the initial-state lepton line and one of the incoming quark lines before the two quarks interact strongly by the exchange of a virtual gluon. However, it will soon become evident, that the new hard poles strikingly differ from the already known ones in the way they fix the kinematics.

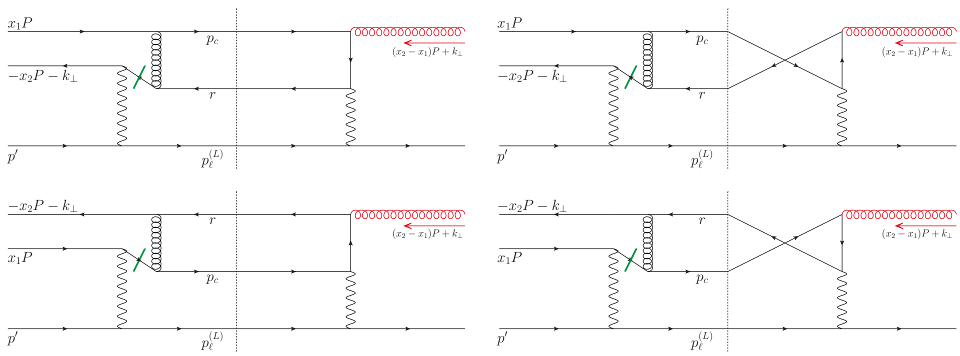

Figure 5.19: Set of crossed diagrams providing hard pole contributions.

The relevant diagrams are shown in figure 5.19. By investigating the momentum flow, we find that the expressions for the propagators associated with the internal lines, which provide the hard poles, are different for the diagrams in the upper and bottom line. In the case of the diagrams in the upper line, the propagators read

$$\frac{1}{\left(x_1P \mp p_c \mp r\right)^2 \pm i\varepsilon} \to \pm\frac{i\pi}{T_1+T_3}\delta\left(x_1 + x\tilde{x}\right) \tag{5.182}$$

where the variable $\tilde{x}$ is given in the exact same way as previously, i.e. $\tilde{x} = -\frac{s_{13}}{t_1+t_3}$. For the bottom line, we obtain

$$\frac{1}{\left(x_2P + k_\perp \pm p_c \pm r\right)^2 \pm i\varepsilon} \to \pm\frac{i\pi}{T_1+T_3}\delta\left(x_2 - x\tilde{x} - v_1\cdot k_\perp\right) \tag{5.183}$$

with the four-vector v_1 being introduced as $v_1 = \frac{2(p_c+r)}{T_1+T_3}$.

By inserting the results together with the expression for the delta function separated from the phase space, which we presented earlier in this section, the structure encountered in the factorization formula becomes

$$\begin{aligned}\sim\frac{i\pi}{T_1+T_3}\int dPS_3\Big[&G_F\big(x\tilde{x},-x(1-\tilde{x})\big)\mathcal{M}_{\mathrm{HP},1}\big(s_{13},t_3,u_2\big)\\ &+G_F\big(-x\tilde{x},x(1-\tilde{x})\big)\mathcal{M}_{\mathrm{HP},2}\big(s_{13},t_3,u_2\big)\Big]\end{aligned} \tag{5.184}$$

by following the familiar procedure. However, some care has to be taken when the matrix elements $\mathcal{M}_{\mathrm{HP},1}$ and $\mathcal{M}_{\mathrm{HP},2}$, which are again the final ones after carrying out the $k_\perp$-derivative and taking the limit $k_\perp \to 0$, are determined. They are generated by combining the hard scattering functions, that come with those Qiu-Sterman functions, whose arguments are identical.

In this sense, we need to take, for example, the difference between the hard functions for an attachment on the left of the diagrams in the upper line and for an attachment on the right of the diagrams in the bottom line.

Furthermore, it is now apparent that the new hard pole contributions fix the kinematics in such a way that they provide further soft-fermion poles in kinematic regions where $\tilde{x}$ becomes small. They are thus really different in comparison to the previously discussed hard poles, which led to further soft-gluon poles in said kinematic region. Nevertheless, we can treat the new contributions by making use of the same approach utilizing a Taylor series expansion to extract the ε-poles. Against this background, we expand the Qiu-Sterman functions emerging in equation 5.184 with respect to $\tilde{x} = 0$ and are led to consider the two contributions

$$\mathcal{HP}_1 = \left[G_F(0,-x) + \sum_{k=0}^{\infty} \tilde{x}^{k+1} x^{k+1} \mathcal{D}^{(k+1)} G_F(0,-x)\right] \mathcal{M}_{\text{HP},1}, \tag{5.185}$$

$$\mathcal{HP}_2 = \left[G_F(0,x) - \sum_{k=0}^{\infty} (-1)^k \tilde{x}^{k+1} x^{k+1} \mathcal{D}^{(k+1)} G_F(0,x)\right] \mathcal{M}_{\text{HP},2}, \tag{5.186}$$

where $\mathcal{D}$ denotes the appropriate differential operator acting on the Qiu-Sterman function's two arguments and setting $x_1 = 0$, $x_2 = -x$ in $\mathcal{HP}_1$, respectively $x_1 = 0$, $x_2 = x$ in $\mathcal{HP}_2$. Moreover, we have refrained from writing down the arguments s_{13}, t_3, u_2 of the two matrix elements $\mathcal{M}_{\text{HP},1}$, $\mathcal{M}_{\text{HP},2}$ and shifted the index of summation from 1 to 0. Again, the lowest order of the expansions can be combined with the pure soft-fermion pole contributions. However, the remainders require further treatment.

All-in-all, we proceed by following the same line of reasoning as before and continue our considerations by decomposing the matrix elements. In view of this, we find that the contributions may be written as

$$\begin{aligned} &\tilde{x}\left[\mathcal{D}^{(k+1)} G_F(-x,0) \mathcal{M}_{\text{HP},1} - (-1)^k \mathcal{D}^{(k+1)} G_F(x,0) \mathcal{M}_{\text{HP},2}\right) \\ &= \mathcal{M}_1 + \mathcal{M}_2 + \mathcal{M}_3, \end{aligned} \tag{5.187}$$

where the new matrix elements $\mathcal{M}_1$, $\mathcal{M}_2$ and $\mathcal{M}_3$ are introduced in the same manner as previously. This means, that $\mathcal{M}_1$ is singular as $u_2 \to 0$, $\mathcal{M}_2$ diverges for $t_3 \to 0$ and $\mathcal{M}_3$ is finite. By inserting the decomposition into the expanded hard pole contributions, we are led to consider

$$\sum_{k=0}^{\infty} x^{k+1} \int dPS_3\, \tilde{x}^k \left[\mathcal{M}_1 + \mathcal{M}_2 + \mathcal{M}_3\right], \tag{5.188}$$

where we can now examine the products $\tilde{x}^k \mathcal{M}_1$ and $\tilde{x}^k \mathcal{M}_2$ separately from each other.

In the next step, we therefore continue by investigating the product $\tilde{x}^k \mathcal{M}_1$, which is singular as $u_2 \to 0$. We now proceed in complete analogy as earlier and therefore take the collinear limit. Following the procedure as outlined in section 5.5.2, we find that the phase space integrated product may be written as

$$\begin{aligned}\int dPS_3\, \tilde{x}^k \mathcal{M}_1 =& \frac{1}{\varepsilon} f_1(v,w) \mathcal{D}^{(k+1)} G_F(0,-x) \\ &- \frac{(-1)^k}{\varepsilon} f_2(v,w) \mathcal{D}^{(k+1)} G_F(0,x) + \text{finite}\end{aligned} \tag{5.189}$$

with f_1 and f_2 being simple rational functions. The above presented outcome can be used to reverse the Taylor expansion in the same manner as before, which in this case turns out to be somewhat more extensive but not necessarily more difficult. The necessary calculation steps essentially involve shifting the summation index and adding suitably selected zeros. We therefore obtain

$$\begin{aligned}&\sum_{k=0}^{\infty} x^{k+1} \int dPS_3\, \tilde{x}^k \mathcal{M}_1 \\ &= \frac{1}{\varepsilon} \Big(f_1(v,w) - f_2(v,w) \Big) \Big(G_F(0,x) - G_F(0,-x) \Big)\end{aligned} \tag{5.190}$$

for the divergent part of $\tilde{x}^k \mathcal{M}_1$ and it hence provides further soft-fermion poles. As it already has been observed in the equations 5.185 and 5.186, they do not only appear with $G_F(0,x)$ but also come together with $G_F(0,-x)$.

Next, we need to consider $\tilde{x}^k \mathcal{M}_2$, which is singular as $t_3 \to 0$. Following the same procedure, we find that the phase space integrated product may be written as

$$\begin{aligned}\int dPS_3\, \mathcal{M}_2 =& - \frac{(-1)^k}{\varepsilon} \Big[(1-w)^{k+1} g_1(v,w) \\ &+ (k+1)(1-w)^k g_2(v,w) \Big] \mathcal{D}^{(k+1)} G_F(x,0) + \text{finite}\end{aligned} \tag{5.191}$$

and obtain

$$\begin{aligned}&\sum_{k=1}^{\infty} x^{k+1} \int dPS_3\, \tilde{x}^k \mathcal{M}_2 \\ &= \frac{1}{\varepsilon} \Big[g_1(v,w) \big\{ G_F(xw, -x(1-w)) - G_F(x,0) \big\} \\ &\quad - g_2(v,w) \frac{\partial}{\partial w} G_F(xw, -x(1-w)) \Big]\end{aligned} \tag{5.192}$$

by making use of the integrated result to reverse the Taylor expansion.

Again, another soft-fermion pole arise. However, in addition we can also observe true hard pole contributions where we receive both a non-derivative and a derivative piece. In summary, we have shown how to handle the crossed diagrams and were able to extract all ε-poles. Furthermore, we find

$$f_1(v,w) = \frac{v^3w^3\left(2v^2w^2 - 2v^2w + v^2 - 2vw + 1\right)}{(1-v)^4(1-vw)^2} \tag{5.193}$$

$$f_2(v,w) = \frac{(vw-1)\left(2v^2w^2 - 2v^2w + v^2 - 2vw + 1\right)}{(1-v)^4} \tag{5.194}$$

$$g_1(v,w) = \frac{2v^2w - v^2 + 2vw - 1}{(1-v)^4} \tag{5.195}$$

$$g_2(v,w) = \frac{\left(1+v^2\right)w(1-2w)}{(1-v)^4} \tag{5.196}$$

for the functions that we introduced in the course of the further treatment of the hard poles.

5.6.5 Real Corrections: Triangle Diagrams

Beyond the crossed contributions presented in the preceding section, another class of novel Feynman diagrams can be identified, which overall show great similarities to the crossed diagrams. These are again diagrams, in which a quark-antiquark pair is found in the initial state on one side of the cut, whereas the twist-3 gluon is located on the other side. However, they differ from the crossed diagrams in the way that the incoming quark and antiquark annihilate each other generating a virtual gluon, which then decays and produces a new quark-antiquark pair in the final state. We will call contribution of this type triangle diagrams in the future in reference to the triangle shaped structure that can be encountered in the diagrams as it can be seen in figure 5.20. Two features can be derived from the figure. First, the diagrams carry the colour factor $T_R = \frac{1}{2}$. Second, they provide only hard pole contributions. The hard poles turn out to be of the same structure as those from the crossed diagrams and we thus find that their contribution to the cross section may be written as

$$\mathcal{HP}_1 = \left[G_F(0,-x) + \sum_{k=0}^{\infty} \tilde{x}^{k+1}x^{k+1}\mathcal{D}^{(k+1)}G_F(0,-x)\right]\mathcal{M}_{\mathrm{HP},1}, \tag{5.197}$$

$$\mathcal{HP}_2 = \left[G_F(0,x) - \sum_{k=0}^{\infty}(-1)^k \tilde{x}^{k+1}x^{k+1}\mathcal{D}^{(k+1)}G_F(0,x)\right]\mathcal{M}_{\mathrm{HP},2}, \tag{5.198}$$

which are the results known from the equations 5.185 and 5.186. Of course, the matrix elements $\mathcal{M}_{\mathrm{HP},1}$ and $\mathcal{M}_{\mathrm{HP},2}$ are different and have to be computed again for the new diagrams. Overall, we receive compact and handy results.

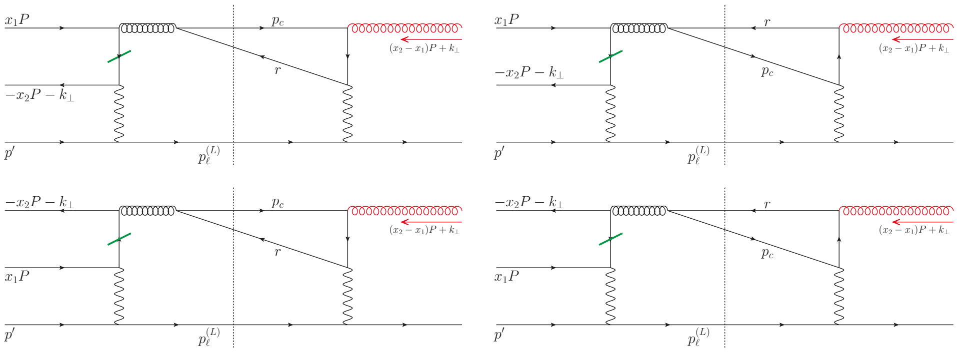

Figure 5.20: Triangle diagrams yielding further hard poles.

The lowest order terms of the expansions can be again directly integrated over the phase space. In the case of these two contributions, the ε-divergent parts become

$$\pm\frac{2vw\left(2v^2w^2-2vw+1\right)\left(2v^2w^2-2v^2w+v^2-2vw+1\right)}{\varepsilon(1-v)^4(1-vw)}, \tag{5.199}$$

where the upper sign holds for the piece $\sim G_F(x,0)$ stemming from $\mathcal{HP}_2$ and the lower sign applies for the term $\sim G_F(-x,0)$ following from $\mathcal{HP}_1$. They are therefore identical except for a sign.

For the remaining contributions from the Taylor expansions, we employ the same approach as earlier. In complete analogy, we are able to extract the divergent parts and obtain

$$f_1(v,w) = -\frac{2vw\left(2v^2w^2-2vw+1\right)\left(2v^2w^2-2v^2w+v^2-2vw+1\right)}{(1-v)^4(1-vw)} \tag{5.200}$$

$$f_2(v,w) = \frac{2vw\left(2v^2w^2-2vw+1\right)\left(2v^2w^2-2v^2w+v^2-2vw+1\right)}{(1-v)^4(1-vw)} \tag{5.201}$$

$$g_1(v,w) = 0 \tag{5.202}$$

$$g_2(v,w) = 0 \tag{5.203}$$

for the function that we have introduced in the last section. It hence turns out that $f_1(v,w) = -f_2(v,w)$. Furthermore, we observe that, at least in the case of divergent pieces, the triangle diagrams only provide further soft-fermion poles but no hard poles.

5.6.6 Virtual NLO Corrections

In the foregoing chapter, we extensively discussed the first part of our considerations at next-to-leading order, which was all about the real corrections to the scattering process. Over the course of our calculations, we found that the different pole contributions, namely soft-gluon, soft-fermion and hard poles, are not completely independent of each other. Instead, it turned out that the hard poles provide a link between all three classes of pole contributions by yielding further soft-gluon and soft-fermion poles. Moreover, we were able to determine all parts of the real corrections, which are singular as $\varepsilon \to 0$. However, some of the finite pieces from the hard poles remain unknown at this point and still need to be determined. We leave this issue as a subject for future research. In the case of the $q\ell \to gX$-channel, our calculations of the NLO corrections were completed at this point and it remained to treat the divergent contributions in the framework of collinear factorization. Nonetheless, this is no longer the case with the $q\ell \to qX$-subprocess currently under discussion, where the final-state quark is assumed to be observed, as virtual corrections, i.e. Feynman diagrams where a gluon-loop emerges, must also be taken into account in addition to the real corrections. In the present chapter, we would therefore like to focus on this type of NLO correction and examine them for possible pole contributions to the spin-dependent cross section.

Just like in our previous considerations, we must also examine the delta function separated from the phase space alongside the propagators that provide the pole contributions. By following the familiar procedure based on momentum conservation, we find that

$$\delta\Big(\big(p_\ell^{(L)}\big)^2\Big) = \frac{1}{S+T}\,\delta\big(x_2 - \xi - v_2 \cdot k_\perp\big) \tag{5.204}$$

$$\delta\Big(\big(p_\ell^{(R)}\big)^2\Big) = \frac{1}{S+T}\,\delta\big(x_1 - \xi\big) \tag{5.205}$$

applies for all diagrams for an attachment either on the left or the right, where we make use of the same set of three Mandelstam variables as in the Born approximation. Here, the momentum fraction ξ and the four-vector v_2 are defined as

$$\xi \equiv -\frac{u}{S+T} \qquad \text{and} \qquad v_2 \equiv \frac{2p_c}{S+T} \tag{5.206}$$

and it hence becomes apparent that the outcome coincides with the equivalent leading-order quantities. The observation is not very surprising, since the one-loop corrections essentially have the same kinematics as the leading-order process.

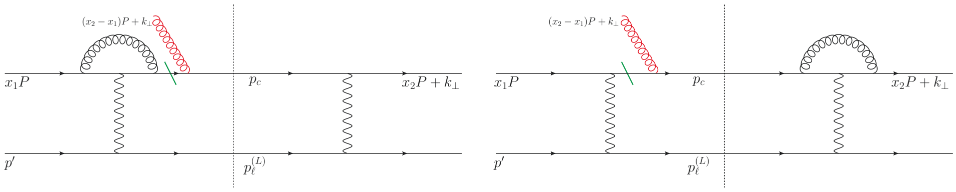

Figure 5.21: Examples for Feynman diagrams of the first set. The figure shows two vertex corrections as examples for diagrams where the twist-3 gluon attaches to the observed quark outside the loop.

To begin our discussion on the virtual corrections, we choose a set of Feynman diagrams, which exhibit the property that the twist-3 gluon attaches to the observed quark in the final-state outside of the loop. Note that the additional interaction and the loop can be located on the same side but also on opposing sides of the cut. The two diagrams, contributing to the vertex correction for an attachment on the left, are shown in figure 5.21 as examples for the particular class designated by the aforementioned feature. The relevant diagrams carry the colour factor C_F. They are particularly simple to handle as the propagators providing the pole contributions are independent of the loop momentum and the evaluation of the loop integrals can be postponed to the end of the calculations, when the limit $k_\perp \to 0$ has already been taken. This has the advantage that the loop integrals are no longer dependent on $k_\perp$ and exactly the same procedure can be employed to solve the integrals as in the unpolarized case. In the following, we will give a brief summary of our considerations on these diagrams.
The propagators, that provide the pole contributions and are associated with the internal lines marked by green bars in figure 5.21, are of the same structure, which we already observed earlier when discussing the leading-order cross section. They are hence given by

$$\frac{1}{\big(p_c \mp \big(x_2 - x_1\big)P \mp k_\perp\big) \pm i\varepsilon} \to \pm\frac{i\pi}{T}\delta\big(x_1 - x_2 + v_1 \cdot k_\perp\big) \tag{5.207}$$

with $v_1 = \frac{2p_c}{T}$ and where the signs need to be understood in the same manner as previously. Accordingly, we find that the structure emerging in the factorization may be written in a similar way as earlier as

$$\begin{aligned}
\sim&\frac{i\pi}{T}\int dPS_2\bigg[\big(v_2 - v_1\big)_\rho H_L\big(x, x, 0\big)\frac{dG_F\big(x, x\big)}{dx} \\
&+ G_F\big(x, x\big)\lim_{k_\perp\to 0}\frac{\partial}{\partial k_\perp^\rho}\Big\{H_L\big(x + (v_2 - v_1)\cdot k_\perp, x + v_2\cdot k_\perp, k_\perp\big) \\
&\quad - H_R\big(x, x + v_1\cdot k_\perp, k_\perp\big)\Big\}\bigg]
\end{aligned} \tag{5.208}$$

where it must be considered that the loop integration is included in the hard scattering functions.

After all involved matrix elements have been computed, we can carry out the $k_\perp$-derivative and take the limi $k_\perp \to 0$ and it remains to evaluate the loop integrals. It turns out that the contribution to the cross section becomes

$$\sigma \sim \left[\frac{(1+v^2)v}{(1-v)^4} - \frac{\varepsilon v}{(1-v)^2}\right]\left\{\left(G_F(x,x) - x\frac{dG_F(x,x)}{dx}\right)\left(-\frac{2}{\varepsilon} - \frac{3}{\varepsilon} - 8\right)\right.$$
$$\left. + G_F(x,x)\left(-\frac{2}{\varepsilon} - 3\right)\right\}, \tag{5.209}$$

where numerical factors as well as quantities from the two-body phase space are not yet included. Here, the resemblance to the unpolarized counterpart is striking and it therefore can be noted that the expression in the first line corresponds to the usual vertex correction. However, we also receive an additional divergent term in the non-derivative piece.

The further potential pole contributions turn out to be rather tricky to handle as we need to consider internal lines that are part of the loops in the relevant Feynman diagrams. Accordingly, the associated propagators exhibit not only a dependence on $k_\perp$ but also depend on the loop momentum r. Therefore, we cannot proceed in the same way as in our previous considerations on the real corrections or the leading order cross section. If we were to try to take possible poles, it would lead to the argument of the Qiu-Sterman function having a dependency on the loop momentum r because of the integrals over the momentum fractions x_1 and x_2. On the other hand, it seems that such expressions cannot be handled in a similar manner as previously in the context of the hard poles by utilizing a suitable Taylor expansion.

Overall, we need to take eighteen Feynman diagrams into account where the pole is either taken on the left-hand or the right-hand side of the cut. Here, diagrams of the type as shown in figure 5.21 are also included since they could in principle provide further pole contributions besides the soft-gluon poles, which we already computed. Moreover, it is noteworthy that the diagrams can be categorized in three classes according to their colour factor. They can carry the factor C_F, $C_F - C_A/2$ or $C_A/2$. Examples for further diagrams are shown in figure 5.22. In the next step, we continue our considerations by trying to extract further pure soft-gluon and soft-fermion poles. We want to introduce the required procedure by using soft-fermion poles provided by the diagram on the left in figure 5.21 as an example. Against this background, we employ a Sudakov decomposition to write the loop momentum as

$$r^\mu = \alpha P^\mu + \beta Q^2 n^\mu + r_T^\mu, \tag{5.210}$$

where the coefficients are given by $\alpha = r \cdot n$, $\beta Q^2 = r \cdot P$, while r_T denotes the loop momentum's transverse components.

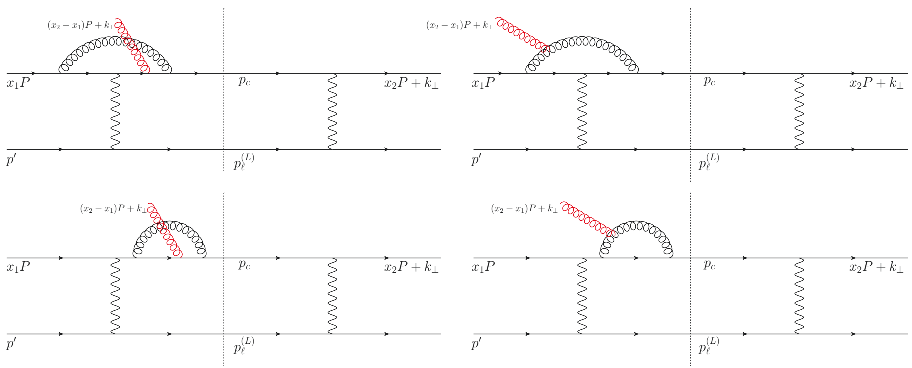

Figure 5.22: Further examples for Feynman diagrams contributing to the virtual corrections.

Note that $Q^2 = -q^2$ is the momentum transferred in the hard scattering. Moreover, n is a light-like four-vector, which satisfies the property $n^2 = 0$ but is not necessarily the same that emerged in the derivation of the factorization formula. A useful choice for the vector seems to be $n^\mu = -\frac{2}{T} P_h^\mu$. We then proceed by inserting the decomposition into the loop integral, which hence becomes

$$\int_{-\infty}^{\infty} \frac{d\alpha}{\alpha(\alpha + x_2 - x_1)(\alpha - x_1)} \int \frac{d^{d-2} r_T}{(2\pi)^d} \times \int_{-\infty}^{\infty} d\beta \frac{\mathcal{N}(\alpha, \beta, r_T, k_\perp)}{(\beta - \beta_0)(\beta - \beta_1)(\beta - \beta_2)} \tag{5.211}$$

where we have excluded quantities that are to be treated as constants in regard to the integrations. The excluded contributions are mainly numerical factors and negative powers of the transferred momentum Q^2, which need to be included in the full hard scattering function. Furthermore, we have introduced the variables β_i $(i = 0, 1, 2)$ in the expression noted above. They are obtained by rearranging the propagators in such a manner that they can be written in the form $\sim \frac{1}{\beta - \beta_i}$ after inserting the decomposition for the loop momentum. They read

$$\beta_0 \equiv -\frac{r_T^2 + i\varepsilon}{2\alpha Q^2} \tag{5.212}$$

$$\beta_1 \equiv -\frac{r_T^2 + i\varepsilon}{2(\alpha - x_1)Q^2} \tag{5.213}$$

$$\beta_2 \equiv -\frac{2k_\perp \cdot (r_T - p_c) + r_T^2 - (\alpha + x_2 - x_1)T + i\varepsilon}{2(\alpha + x_2 - x_1 + k_\perp \cdot n)Q^2} \tag{5.214}$$

and it therefore follows from these expressions that the combination

$$\frac{1}{\beta_0 - \beta_1} \sim \frac{1}{x_1 - i x_1 \varepsilon / r_T^2} \to i\pi \, \mathrm{sgn}(x_1)\, \delta(x_1) \tag{5.215}$$

can provide a soft-fermion pole contribution.

In fact, it does not pose a major challenge to extract exactly this combination from the integrand, as a partial fraction decomposition can be used for this purpose. In this context, we find that

$$\frac{1}{(\beta-\beta_0)(\beta-\beta_1)} = \frac{1}{\beta_0-\beta_1}\left[\frac{1}{\beta-\beta_0} - \frac{1}{\beta-\beta_1}\right] \tag{5.216}$$

applies and the remaining β-integral can therefore be written as

$$\int_{-\infty}^{\infty}\left[\frac{1}{\beta-\beta_0} - \frac{1}{\beta-\beta_1}\right]\frac{\mathcal{N}}{\beta-\beta_2}, \tag{5.217}$$

which can be solved by utilizing the residue theorem. With this in mind, we must first distinguish between different cases for x_1 and x_2 in order to determine the position of the poles in the complex plane. We therefore need to consider the two areas

- $x_1 > 0 > x_1 - x_2 - k_\perp \cdot n$
- $0 > x_1 > x_1 - x_2 - k_\perp \cdot n$

for example, for which we find that the structure arising in the factorized cross section may be written as

$$\begin{aligned}\pm\frac{i\pi}{S+T}\int_{-\infty}^{\infty} d\alpha \int \frac{d^{d-2}r_T}{(2\pi)^d}\Big\{ & G_F(0,x)H_L(0,x,0)\theta(-\alpha)\delta(\alpha+x)\big(v_{2\rho}+n_\rho\big) \\ & + \theta(-\alpha)\theta(\alpha+x)\lim_{k_\perp\to 0}\frac{\partial}{\partial k_\perp^\rho}\Big[G_F(0,x+v_2\cdot k_\perp)H_L(0,x+v_2\cdot k_\perp,k_\perp)\Big]\Big\}\end{aligned} \tag{5.218}$$

after evaluating the x_1- and x_2-integrals in addition to the β-integral. Furthermore, we have carried out the $k_\perp$-derivative and took the limit $k_\perp \to 0$ as much as possible. Here, θ denotes the step function which occur as we have divided the integration area for α into smaller sub-areas. We can therefore see that the results for the two areas are identical except for one sign and therefore cancel each other out in the sum. This procedure can now be repeated for all relevant loop diagrams, where it turns out that the pure soft-gluon and soft-fermion poles extracted in this way cancel due to similar arguments.

However, further contributions can be found by making use of another approach. In all our previous considerations, we have always generated the imaginary part via pole contributions provided by propagators in their on-shell limit. On the other hand, it is also possible to generate the necessary imaginary part directly from the loops instead. For this purpose, it is recommended to choose a different approach, in which the total twist-3 contribution to the spin-dependent cross section is decomposed into a kinematic and dynamic part and Feynman diagrams such as those shown in figure 5.23 must be analyzed.

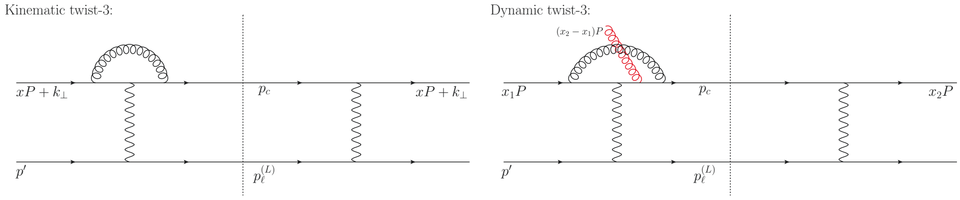

Figure 5.23: Exemplary Feynman diagrams contributing to the kinematic and dynamic twist-3 pieces.

This offers the advantage that the $k_\perp$-dependence only occurs in the kinematic part, whereas the dynamic part, which contains diagrams of more complex structure through the twist-3 gluon, is free of this dependence making the evaluation of the loop integrals significantly simpler. Both approaches seem to be linked to each other via the different twist-3 matrix elements. The diagrams as those, which we considered previously, are directly related to the Qiu-Sterman function and the F-type twist-3 correlator. The new diagrams, on the other hand, are in connection with the D-type correlator. However, since both, the F-type and D-type functions, are not independent of each other and are instead linked via the relation

$$G_D(x_1, x_2) = \mathrm{PV}\frac{1}{x_1 - x_2} G_F(x_1, x_2) \tag{5.219}$$

as noted in chapter 5.2, both approaches have to provide consistent results. We can therefore actually revert to the diagrams of the type as shown in figure 5.23 and continue our considerations by evaluating the loop integrals. In the course of solving the integrals, we again make use of the Sudakov decomposition in the same manner as discussed previously and carry out the β-integrals by employing the residue theorem, where we need to distinguish between different cases for the momentum fractions x_1 and x_2. Afterwards, we can solve the r_T- and α-integrals. In the case of the r_T-integration, we make use of spherical coordinates, whereas the α-integrals can be directly computed with Mathematica. Following this procedure, we arrive at an outcome, that contains logarithms whose arguments include combinations of the momentum fractions x_1 and x_2. In some circumstances, these combination can become negative, enabling us to extract the required imaginary part from the logarithms with negative arguments. It turns out that in this way we obtain two further contributions whose ε-divergent pieces are given by

$$\sim -C_A \, G_F(x, x) \frac{v(1+v)}{\varepsilon(1-v)^3} \delta(1-w), \tag{5.220}$$

$$\sim -\frac{1}{2C_A} G_F\big(xw, -x(1-w)\big) \frac{4vw(1+v)}{\varepsilon(1-v)^4} \tag{5.221}$$

where especially the second result is surprising as it exhibits kinematics that we are not used to when we are faced with virtual corrections.

5.6.7 Collinear Subtraction and Final Results

In order to bring our considerations regarding the $q\ell \to qX$-channel to a satisfactory conclusion, it remains to deal with the divergences in the framework of collinear factorization, which are left after adding all relevant real and virtual corrections at next-to-leading order. Against this background, we overall proceed in the same way as in the previous case, when the final-state gluon was assumed to be observed. Nevertheless, a new peculiarity emerges, which is that contributions stemming from the evolution kernel of the Qiu-Sterman function and its first derivative need to be taken into account alongside the Weizsäcker-Williams contributions and the subtraction terms related to splitting in the final state. The necessary evolution equation was discussed in chapter 5.3 and is given in equation 5.41. Likewise as in the context of the ordinary twist-2 parton distributions, the equation enables us to formulate suitable subtraction terms as convolutions, where appropriate twist-3 leading-order cross sections in d dimensions needs to be included. Furthermore, we again need to make use of integration by parts to handle a few divergences.

All-in-all, however, the necessary calculations are not particularly more difficult than in the previously discussed cases and all required methods are known as they were already introduced in detail earlier. We will therefore limit ourselves to the presentation of the final result for the subprocess, when the outgoing quark is assumed to be observed. The corresponding contribution to the factorized spin-dependent cross section can be schematically written in the same way as previously, namely

$$\begin{aligned} E_h \frac{d^3\Delta\sigma}{dP_h^3} =& \frac{4\pi M}{S^2U^2} \varepsilon^{P_h P p' s_T} \sum_a \int_{v_{\min}}^{v_{\max}} dv \int_{w_{\min}}^{1} \frac{dw}{w} D^{g/h}(z) \frac{\alpha_{\text{em}}^2 e_a^2 \alpha_{\text{s}}}{2\pi} \\ & \times \Bigg[C_F \left(\sigma_{C_F}^{\text{SGP}} + \sigma_{C_F}^{\text{SFP}} \right) + C_A \left(\sigma_{C_A}^{\text{SGP}} + \sigma_{C_A}^{\text{SFP}} \right) \\ & \quad + \frac{1}{C_A} \sigma_{1/C_A}^{\text{SFP}} + \sigma^{\text{Tr}} \Bigg] \end{aligned} \tag{5.222}$$

where the expressions $\sigma_{C_i}^{\text{SGP}}$ and $\sigma_{C_i}^{\text{SFP}}$ need to be understood in the same manner as before. They are even very similar, but it should also be mentioned that they are even longer. In addition, the contribution σ^{Tr} arises, which is associated with the previously introduced triangle diagrams. The schematic expressions are listed in appendix F. It is particularly noticeable that in this case hard poles arise in the sense that the cross sections contain contributions proportional to $G_F(x, xw)$ or $G_F(xw, -x(1-w))$ as well as the partial derivative of these functions with respect to w.

5.7 Numerical Studies

With the conclusion of our previous discussions on the partonic processes $q\ell \to qX$ and $q\ell \to gX$, we have in principle finished our considerations and have successfully determined all twist-3 next-to-leading order corrections to the inclusive production of a single hadron in transversely polarized nucleon-lepton scattering, which are linked to the quark-gluon-quark correlator, respectively the Qiu-Sterman function and its first derivative.
These corrections are expected to yield the major contribution to the factorized spin-dependent cross section, where the $q\ell \to qX$-channel is suspected to provide the dominant part similar as in the case of the equivalent unpolarized scattering. In the following, we would now like to examine the influence and magnitude of the various contributions in more detail within numerical studies. However, a challenge arises from the little that is known about the Qiu-Sterman function. Unlike as in the case of the ordinary parton densities and fragmentation functions, we cannot rely on sets for the Qiu-Sterman function extracted from experimental data and instead, need to formulate a model that at least satisfies the function's properties. It can therefore not be guaranteed that the numerical studies presented here are physically meaningful in the sense that they provide predictions in accordance with potential experimental data. But they are certainly sufficient to illustrate the quantitative influence of the next-to-leading order corrections and thus to estimate their significance.

In order to carry out the numerical computation, we make use of a model for the Qiu-Sterman function, which is based on the Sivers distribution that was extracted from SIDIS data by Anselmino et al. [29] at a scale $\mu = 1.55\,\text{GeV}$. The proposed function reads

$$f_{1T}^{\perp(1),q}(x) = -\frac{1}{2} N^q(x) f_1^q(x) \sqrt{2e}\, \frac{M_1^2 \langle k_\perp^2 \rangle}{M_p \big(M_1^2 + \langle k_\perp^2 \rangle\big)^2}, \tag{5.223}$$

where M_p denotes the proton's mass and f_1^q represents the ordinary twist-2 parton distributions, whereas the parameters $\langle k_\perp \rangle$ and M_1 are given by $\langle k_\perp \rangle = 0.25\,\text{GeV}$ as well as $M_1 = 0.583\,\text{GeV}$. Here, the function $N^q(x)$ is

$$N^q(x) = N^q x^{\alpha_q} (1-x)^{\beta_q} \frac{(\alpha_q + \beta_q)^{\alpha_q + \beta_q}}{\alpha_q^{\alpha_q} \beta_q^{\beta_q}} \tag{5.224}$$

with parameters N^q, α_q and β_q whose values depend on the quark flavour. The Sivers function is useful to us as a starting point to create a model for the Qiu-Sterman function build on the relation $\pi G_F(x,x) = f_{1T}^{\perp(1),q}(x)$. However, this expression could only be used in the case of the pure soft-gluon pole contributions and must therefore be extended to the case where the two arguments are different in the next step.

In the course of this, we need to keep in mind that the function is required to satisfy various constraints originating from its properties. First, it is symmetric under the interchange of its arguments, i.e. $G_F(x, x') = G_F(x', x)$. The condition can be easily implemented by employing polar coordinates (r, φ), where $x = r\cos(\varphi + \frac{\pi}{4})$ and $x' = r\sin(\varphi + \frac{\pi}{4})$. Note that the variables r and φ can be determined as functions of x and x' by inverting the latter stated expressions for the momentum fractions. Next, we can represent the Qiu-Sterman function by a Fourier series after it has been rewritten as a function in polar coordinates due the then present 2π-periodicity. Furthermore, we find that all coefficients emerging together with a sine function in the Fourier series need to vanish to ensure the aforementioned symmetry of the Qiu-Sterman function.
Beyond that, the model must also guarantee that the function is defined on the correct range, which is set by the conditions $|x| \leq 1$, $|x'| \leq 1$ and $|x - x'| \leq 1$. In addition, G_F has to vanish on the boundary continuously. These constraints can be implemented by multiplying the model with

$$\left(\frac{(1-x^2)(1-x'^2)}{(1-xx')^2}\right)^{\delta}\left(1-(x-x')^2\right)^{\epsilon}\theta(1-|x|)\theta(1-|x'|)\theta(1-|x-x'|), \tag{5.225}$$

where $\delta = \epsilon = 0.01$ denotes two parameters. In the end, the model, that we want to employ in the course of our numerical considerations, becomes

$$\begin{aligned}
&G_F(x, x') \\
&= \frac{1}{2\pi}\Bigg(\left[f^q\left[\frac{r(x,x')}{\sqrt{2}}\right) + f^{\bar{q}}\left(\frac{r(x,x')}{\sqrt{2}}\right)\right]\left\{1 + \sum_{n=1}^{3}\left[\cos(2n\varphi(x,x')) - 1\right]a_n\right\} \\
&+ \left[f^q\left[\frac{r(x,x')}{\sqrt{2}}\right) - f^{\bar{q}}\left(\frac{r(x,x')}{\sqrt{2}}\right)\right]\Big\{a_4\left[\cos(3\varphi(x,x')) - \cos(\varphi(x,x'))\right] \\
&+ a_5\left[\cos(5\varphi(x,x')) - \cos(\varphi(x,x'))\right] + a_6\left[\cos(7\varphi(x,x')) - \cos(\varphi(x,x'))\right]\Big\}\Bigg) \\
&\times \left(\frac{(1-x^2)(1-x'^2)}{(1-xx')^2}\right)^{\delta}\left(1-(x-x')^2\right)^{\epsilon}\theta(1-|x|)\theta(1-|x'|)\theta(1-|x-x'|),
\end{aligned} \tag{5.226}$$

with some coefficients a_1, ..., a_6.
Now that these preliminary questions have been clarified, we can focus our attention on the numerical computations. At this point, we do not want to go into details on setup issues, such as the applied parton densities or fragmentation functions, as this information can be found in chapter 4.3, where similar considerations have been discussed in the case of unpolarized scattering. In the following, we will present results pertaining to a fixed selection of the parameters emerging in the previously introduced models for the Qiu-Sterman function. In our view, limiting the presentation to one choice of parameters is sufficient, as the possible conclusions for different variants essentially do not differ greatly from one another.

Our numerical considerations cover the inclusive production of a positively charged pion π^+ in the proton-electron scattering, where the incoming proton is assumed to be transversely spin-polarized, in a kinematic region that will be common at the future EIC. In more detail, we want to examine the scattering process at a center-of-mass energy $\sqrt{S} = 100\,\text{GeV}$. Within the scope of these studies, the differential spin-dependent cross section

$$\frac{d^2\Delta\sigma^{p^\uparrow e^- \to \pi^+ X}}{d\eta dP_{\pi^+\perp}} \tag{5.227}$$

is again written in terms of the pseudorapidity η and the transverse momentum $P_{\pi^+,\perp}$ of the produced hadron. Furthermore, we will investigate the behaviour of the cross section as a function of the pseudorapidity at a fixed transverse momentum $P_{\pi^+,\perp} = 5\,\text{GeV}$.

We commence our discussion by studying the next-to-leading order correction originating from the process, where the final-state gluon is assumed to be observed. The results of our numerical computations are shown in figure 5.24. Two observations are particularly striking about this outcome. First, it is apparent that the soft-fermion pole contributions are small in comparison to the soft-gluon pole contributions. More precisely, the absolute value of the soft-fermion poles is only slightly more than half as large as the absolute value of the soft-gluon poles. Second, it is noteworthy that the next-to-leading order corrections stemming from this channel are small overall and therefore only lead to a minimal change in the cross section in comparison to the pure leading-order contribution.
Next, we examine the quantitative influence of the second subprocess where the final-state quark is assumed to be observed. The corresponding results are shown in figure 5.25. Again, it is apparent that the soft-gluon poles provide the larger contributions than the soft-fermion poles. In fact, the soft-gluon pole contributions turn out to be significantly larger and thus form the dominant part of the next-to-leading order corrections. Furthermore, the figure shows that the $q\ell \to qX$-channel provides a sizeable contribution in total, which has a significant quantitative influence on the cross section. This contributes above all to the great importance of next-to-leading order corrections in order to be able to reliably analyse and interpret experimental data in the future.

In addition to the two presented diagrams, we provide the third diagram, shown in Figure 5.26, which illustrates the transverse single-spin asymmetry

$$A_T = \frac{d\Delta\sigma^{p^\uparrow e^- \to \pi^+ X}}{d\sigma^{pe^- \to \pi^+ X}} \tag{5.228}$$

and yields further evidence for the importance of the next-to-leading order corrections.

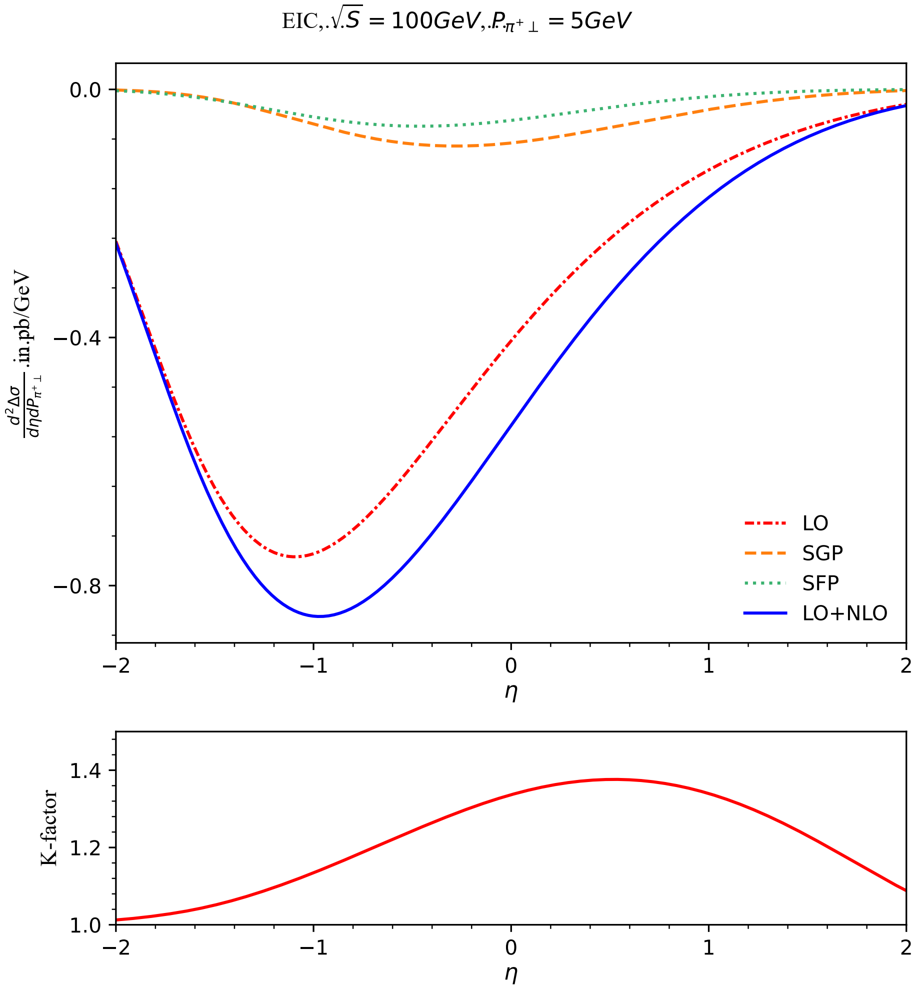

Figure 5.24: Numerical results for the $q\ell \to gX$-channel. The diagram shows the behaviour of the LO cross section as well as the soft-gluon and soft-fermion pole contributions as a function of η at a fixed transverse momentum $P_{\pi^+,\perp} = 5\,\mathrm{GeV}$. The total NLO cross section as the sum of the LO part and the NLO corrections is given in addition. Note that the hard pole contributions are included in the soft-gluon and soft-fermion pieces. Moreover, the K-factor is illustrated in the second diagram in the bottom.

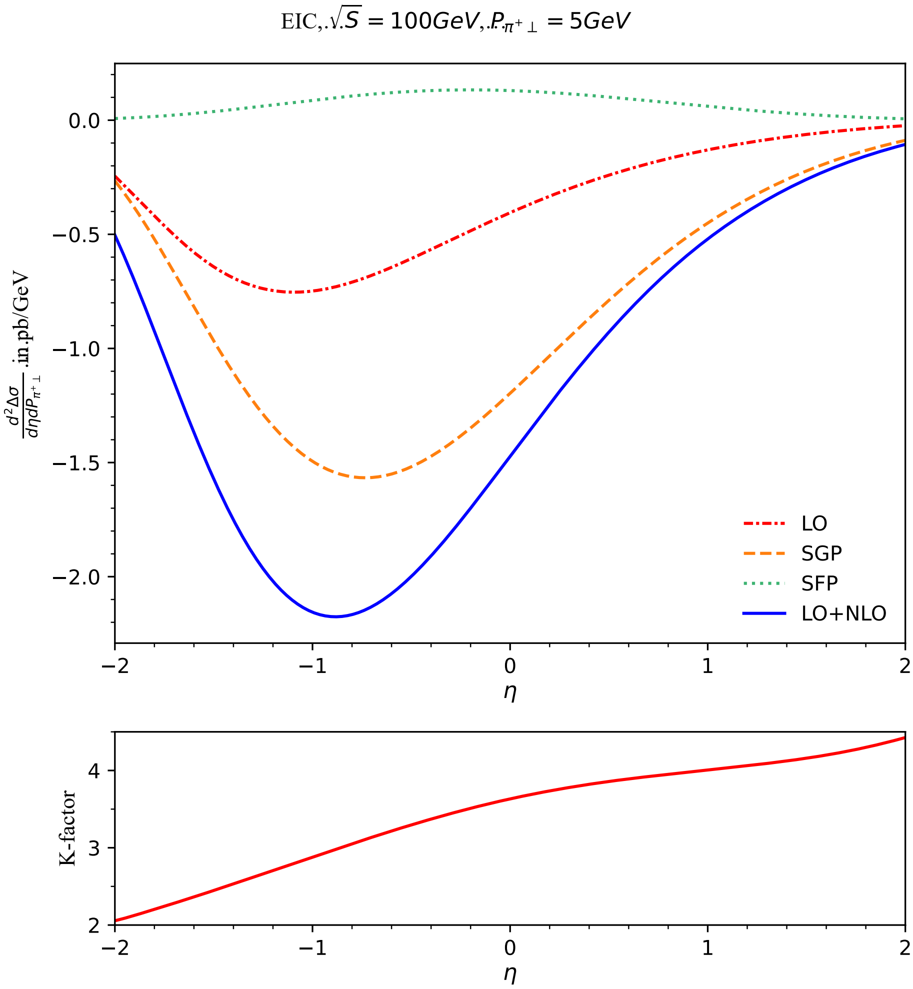

Figure 5.25: Numerical results for the $q\ell \to qX$-channel. The figure is structured in the same manner as the one presented on the previous page. Again, the cross section is studied as function of η at fixed transverse momentum $P_{\pi^+,\perp} = 5\,\text{GeV}$.

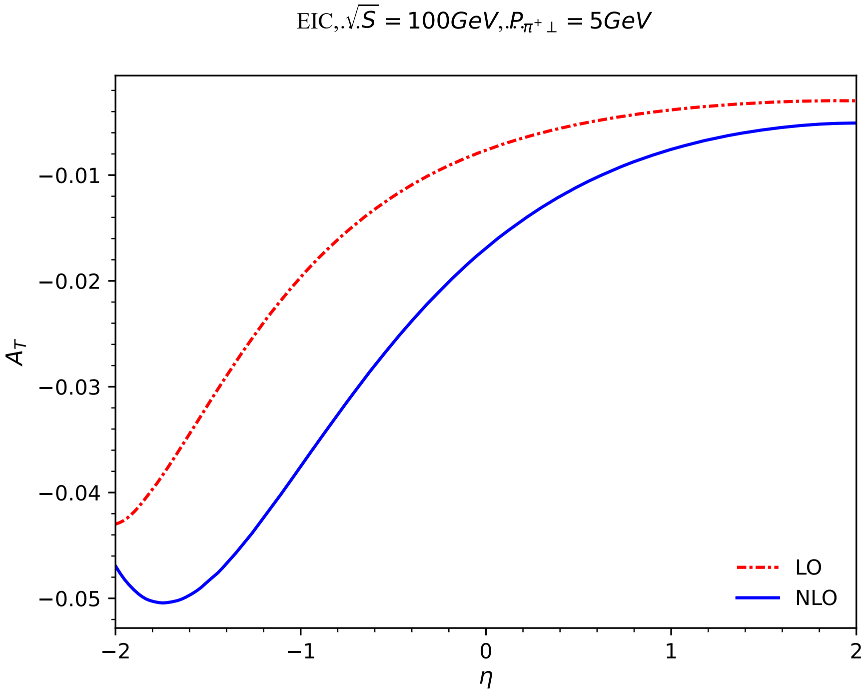

Figure 5.26: Numerical results for the transverse single-spin asymmetry. The figure shows the transverse single-spin asymmetry for the inclusive production of a hadron in nucleon-lepton scattering at LO and NLO as function of η at fixed transverse momentum $P_{\pi^+,\perp} = 5\,\text{GeV}$.

Chapter 6
Conclusion and Outlook

Chapter 6

Conclusion and Outlook

In the thesis at hand, we have studied the transverse single-spin asymmetry for the inclusive production of a single hadron in nucleon-lepton scattering, where the incoming nucleon was assumed to be transversely spin-polarized, with the aim to determine the next-to-leading order corrections within the framework of twist-3 collinear factorization. Our interest in this peculiar observable partly relies on the fact that it provides an opportunity to test QCD, since it offers direct access to twist-3 effects and thus enables to examine the validity of the factorization in this regime. Beyond that, the single-spin asymmetry affords us with a possibility to improve our understanding of spin effects and to gain new insights into the inner structure of matter. On the other hand, the question naturally arises as to why this specific process, namely the inclusive production of a hadron, was considered. The main reason for this is that, in contrast to DIS or SIDIS, the structures occurring in the calculation are already more similar to nucleon-nucleon scattering, but the treatment is nevertheless simpler overall as in the latter mentioned cases. The scattering process therefore proves to be a very good option to learn how to carry out a twist-3 calculation at next-to-leading order and it is to be expected that many of the methods developed here can also be used in the more complicated case of nucleon-nucleon scattering.

Overall, our considerations followed two paths. First, we computed the cross section for the unpolarized process at next-to-leading order, which was already done in [120] and where we found that our results are in accordance with those presented in the latter mentioned study. Furthermore, we made use of the discussion on this particular process to give an introduction on the methods and techniques generally required in calculations within the framework of perturbation theory. Second, we addressed the spin-dependent cross section and presented our computations of the next-to-leading order corrections, where we solely focused on those contributions that involve the Qiu-Sterman function G_F as well as its first derivative since they are expected to yield the dominant part. In this context, we were able to completely determine the soft-gluon and soft-fermion pieces. However, in the case of the hard poles we proposed only a method to extract the parts that are singular as $\varepsilon \to 0$ and it thus remains to determine the further finite pieces. Nevertheless, we have successfully found all ε-divergent terms and proofed with our explicit calculations that the collinear factorization is still valid for this specific process at twist-3 level.

In addition, we have presented numerical studies for both, the unpolarized and the transversely polarized process. In summary, we have found sizeable next-to-leading order corrections in each case. The considerations on the unpolarized scattering have shown that the Weizsäcker-Williams contributions can be large, but it is by no means guaranteed that they yield the dominant part of the cross section. In general, the full next-to-leading order result is therefore inevitable to reliably analyse experimental data. On the other hand, we observed that the Weizsäcker-Williams contribution can dominate in some special cases like the K^--production at HERMES. Such processes could hence provide an opportunity to test these particular contributions.
In the case of the numerical studies for the spin-dependent cross section and the transverse single-spin asymmetry, the informative value is limited since not much is known about the Qiu-Sterman function yet and we thus need to rely on a model for the function. Our numerical results therefore solely serve the purpose to illustrate the quantitative influence of the next-to-leading order corrections but they cannot provide any further physical insights. Overall, we found that the QCD corrections to the spin-dependent cross section are large, where two observations are particularly striking. On the one hand, the soft-gluon poles yield significantly larger contributions to the cross section than the soft-fermion poles in both cases but exceptionally in the instance, when the final-state quark is assumed to be observed. On the other hand, the $q\ell \to qX$-channel turn out to provide the dominant contribution to the cross section whereas the pieces from the $q\ell \to gX$-channel are almost negligibly small. In total, our results elucidate the importance of the next-to-leading order contributions in the case of the spin-dependent cross section as well as the transverse single-spin asymmetry and show that they are inevitable for a reliable analysis of potential experimental data in the future.

However, it should also be borne in mind that some finite pieces linked to the hard poles still have to be determined. Results for a complete calculation, including the finite contributions omitted here, are provided in [188, 189]. It can be readily verified that the divergent terms coincide in both approaches, which demonstrates that the method presented here correctly reproduces the singular structure of the full result.

This agreement ensures that the approach is not only conceptually consistent but can also be employed as an independent cross-check of the complete calculation. Moreover, the numerical studies presented in chapter 5.7 already imply a clear improvement for the alternative approach employed here compared to a pure leading order treatment. Due to its methodological simplicity and reduced computational effort, this approach thus constitutes a practical alternative to the full calculation, despite the absence of the finite terms, when a rapid first estimate of the asymmetry is required.

Beyond that, the research field surrounding the transverse single-spin asymmetry offers a plethora of unanswered and exciting questions. Against the background of the inclusive production of a hadron in nucleon-lepton scattering, for example, it thus remains to examine contributions involving the three-gluon correlator. On the one hand, further novel and unforeseeable challenges could arise in the relevant calculations. On the other hand, the quantitative impact on the spin-dependent cross section needs to be explicitly checked. Furthermore, the transverse single-spin asymmetry can of course also be calculated at next-to-leading order for other processes. Here, we want to emphasize nucleon-nucleon scattering in particular, where additional interactions, like the attachment of the twist-3 gluon to the incoming parton from the unpolarized nucleon, will occur. In this context, it is necessary to check whether the same methods, that we have used in the course of this thesis, are sufficient.

Moreover, it is noteworthy that we have limited our considerations to the case when the twist-3 effect is linked to the nucleon in the initial-state. But it could of course also appear in connection with the fragmentation process and the produced hadron. In this case, twist-3 fragmentation functions will be required. Such functions as well as the related processes form another interesting area of research and have been subject of a large number of studies (see e.g. [124, 125, 146, 147, 150, 151, 225]) in the recent years.

Finally, gaining knowledge about the Qiu-Sterman function is an essential task in the long term. The responsibility of theoretical physics encompasses not only to ensure an adequate fundamental understanding of twist-3 effects, but also to provide perturbative calculations of physical observables at a sufficiently high order. On the other hand, experimentalists need to make accurate data available. Such data could be provided by the EIC in the future.

Bibliography

[1] F. D. Aaron et al. Combined Measurement and QCD Analysis of the Inclusive e+- p Scattering Cross Sections at HERA. *JHEP*, 01:109, 2010.

[2] S. Abachi et al. Observation of the top quark. *Phys. Rev. Lett.*, 74:2632–2637, 1995.

[3] R. Abdul Khalek et al. Science Requirements and Detector Concepts for the Electron-Ion Collider: EIC Yellow Report. *Nucl. Phys. A*, 1026:122447, 2022.

[4] F. Abe et al. Observation of top quark production in $\bar{p}p$ collisions. *Phys. Rev. Lett.*, 74:2626–2631, 1995.

[5] M. Abramowitz. *Handbook of Mathematical Functions, With Formulas, Graphs, and Mathematical Tables.* Dover Publications, New York, 1972.

[6] A. Accardi et al. Electron Ion Collider: The Next QCD Frontier: Understanding the glue that binds us all. *Eur. Phys. J. A*, 52(9):268, 2016.

[7] Jaroslav Adam et al. Measurement of transverse single-spin asymmetries of π^0 and electromagnetic jets at forward rapidity in 200 and 500 GeV transversely polarized proton-proton collisions. *Phys. Rev. D*, 103(9):092009, 2021.

[8] D. L. Adams et al. Analyzing power in inclusive pi+ and pi- production at high x(F) with a 200-GeV polarized proton beam. *Phys. Lett. B*, 264:462–466, 1991.

[9] D. L. Adams et al. Comparison of spin asymmetries and cross-sections in pi0 production by 200-GeV polarized anti-protons and protons. *Phys. Lett. B*, 261:201–206, 1991.

[10] D. L. Adams et al. Measurement of single spin asymmetry for direct photon production in p p collisions at 200-GeV/c. *Phys. Lett. B*, 345:569–575, 1995.

[11] D. L. Adams et al. Measurement of single spin asymmetry in eta meson production in p (polarized) p and anti-p (polarized) p interactions in the beam fragmentation region at 200-GeV/c. *Nucl. Phys. B*, 510:3–11, 1998.

[12] J. Adams et al. Cross-sections and transverse single spin asymmetries in forward neutral pion production from proton collisions at s**(1/2) = 200- GeV. *Phys. Rev. Lett.*, 92:171801, 2004.

[13] A. Adare et al. Measurement of Transverse Single-Spin Asymmetries for J/ψ Production in Polarized $p+p$ Collisions at $\sqrt{s} = 200$ GeV. *Phys. Rev. D*, 82:112008, 2010. [Erratum: Phys.Rev.D 86, 099904 (2012)].

[14] S. S. Adler et al. Measurement of transverse single-spin asymmetries for mid-rapidity production of neutral pions and charged hadrons in polarized p+p collisions at s**(1/2) = 200-GeV. *Phys. Rev. Lett.*, 95:202001, 2005.

[15] Stephen L. Adler. Sum rules giving tests of local current commutation relations in high-energy neutrino reactions. *Phys. Rev.*, 143:1144–1155, 1966.

[16] C Adolph et al. Longitudinal double spin asymmetries in single hadron quasi-real photoproduction at high p_T. *Phys. Lett. B*, 753:573–579, 2016.

[17] E. S. Ageev et al. A New measurement of the Collins and Sivers asymmetries on a transversely polarised deuteron target. *Nucl. Phys. B*, 765:31–70, 2007.

[18] A. Airapetian et al. Observation of a single spin azimuthal asymmetry in semiinclusive pion electro production. *Phys. Rev. Lett.*, 84:4047–4051, 2000.

[19] A. Airapetian et al. Single spin azimuthal asymmetries in electroproduction of neutral pions in semiinclusive deep inelastic scattering. *Phys. Rev. D*, 64:097101, 2001.

[20] A. Airapetian et al. Single-spin asymmetries in semi-inclusive deep-inelastic scattering on a transversely polarized hydrogen target. *Phys. Rev. Lett.*, 94:012002, 2005.

[21] A. Airapetian et al. Observation of the Naive-T-odd Sivers Effect in Deep-Inelastic Scattering. *Phys. Rev. Lett.*, 103:152002, 2009.

[22] A. Airapetian et al. Transverse target single-spin asymmetry in inclusive electroproduction of charged pions and kaons. *Phys. Lett. B*, 728:183–190, 2014.

[23] Weeam S. Albaltan, Alexei Prokudin, and Marc Schlegel. The transverse nucleon single-spin asymmetry for the semi-inclusive production of photons in lepton-nucleon scattering. *Phys. Lett. B*, 804:135367, 2020.

[24] M. Alekseev et al. Collins and Sivers asymmetries for pions and kaons in muon-deuteron DIS. *Phys. Lett. B*, 673:127–135, 2009.

[25] V. Yu. Alexakhin et al. First measurement of the transverse spin asymmetries of the deuteron in semi-inclusive deep inelastic scattering. *Phys. Rev. Lett.*, 94:202002, 2005.

[26] Constantia Alexandrou, Krzysztof Cichy, Martha Constantinou, Karl Jansen, Aurora Scapellato, and Fernanda Steffens. Light-Cone Parton Distribution Functions from Lattice QCD. *Phys. Rev. Lett.*, 121(11):112001, 2018.

[27] K. Allada et al. Single spin asymmetries of inclusive hadrons produced in electron scattering from a transversely polarized ^{3}He target. *Phys. Rev. C*, 89(4):042201, 2014.

[28] Guido Altarelli and G. Parisi. Asymptotic Freedom in Parton Language. *Nucl. Phys. B*, 126:298–318, 1977.

[29] M. Anselmino, M. Boglione, U. D'Alesio, A. Kotzinian, S. Melis, F. Murgia, A. Prokudin, and C. Turk. Sivers Effect for Pion and Kaon Production in Semi-Inclusive Deep Inelastic Scattering. *Eur. Phys. J. A*, 39:89–100, 2009.

[30] M. Anselmino, M. Boglione, U. D'Alesio, S. Melis, F. Murgia, and A. Prokudin. Single spin asymmetries in l p —> h X processes: A Test of factorization. *Phys. Rev. D*, 81:034007, 2010.

[31] M. Anselmino, M. Boglione, U. D'Alesio, S. Melis, F. Murgia, and A. Prokudin. Single Spin Asymmetries in $lp^\uparrow \to hX$ processes and TMD factorisation. *Phys. Rev. D*, 89(11):114026, 2014.

[32] P. L. Anthony et al. Inclusive hadron photoproduction from longitudinally polarized protons and deuterons. *Phys. Lett. B*, 458:536–544, 1999.

[33] I. Arsene et al. Single Transverse Spin Asymmetries of Identified Charged Hadrons in Polarized p+p Collisions at s**(1/2) = 62.4-GeV. *Phys. Rev. Lett.*, 101:042001, 2008.

[34] P. Aurenche, A. Douiri, R. Baier, M. Fontannaz, and D. Schiff. The Deep Compton Scattering: Single Photon Spectrum and Photon - Hadron Correlations Beyond Leading Logarithms. *Z. Phys. C*, 24:309, 1984.

[35] P. Aurenche, A. Douiri, R. Baier, M. Fontannaz, and D. Schiff. Large p_T Double Photon Production in Hadronic Collisions: Beyond Leading Logarithm QCD Calculation. *Z. Phys. C*, 29:459–475, 1985.

[36] Alessandro Bacchetta, Markus Diehl, Klaus Goeke, Andreas Metz, Piet J. Mulders, and Marc Schlegel. Semi-inclusive deep inelastic scattering at small transverse momentum. *JHEP*, 02:093, 2007.

[37] P. A. Baikov, K. G. Chetyrkin, and J. H. Kühn. Five-Loop Running of the QCD coupling constant. *Phys. Rev. Lett.*, 118(8):082002, 2017.

[38] Richard D. Ball et al. The path to proton structure at 1% accuracy. *Eur. Phys. J. C*, 82(5):428, 2022.

[39] Richard D. Ball et al. The PDF4LHC21 combination of global PDF fits for the LHC Run III. *J. Phys. G*, 49(8):080501, 2022.

[40] William A. Bardeen, A. J. Buras, D. W. Duke, and T. Muta. Deep Inelastic Scattering Beyond the Leading Order in Asymptotically Free Gauge Theories. *Phys. Rev. D*, 18:3998, 1978.

[41] V. E. Barnes et al. Observation of a Hyperon with Strangeness Minus Three. *Phys. Rev. Lett.*, 12:204–206, 1964.

[42] W. Beenakker, H. Kuijf, W. L. van Neerven, and J. Smith. QCD Corrections to Heavy Quark Production in p anti-p Collisions. *Phys. Rev. D*, 40:54–82, 1989.

[43] Siegfried Bethke. Experimental tests of asymptotic freedom. *Prog. Part. Nucl. Phys.*, 58:351–386, 2007.

[44] J. D. Bjorken. AN INEQUALITY FOR ELECTRON AND MUON SCATTERING FROM NUCLEONS. *Phys. Rev. Lett.*, 16:408, 1966.

[45] J. D. Bjorken. Asymptotic Sum Rules at Infinite Momentum. *Phys. Rev.*, 179:1547–1553, 1969.

[46] F. Bloch and A. Nordsieck. Note on the Radiation Field of the electron. *Phys. Rev.*, 52:54–59, 1937.

[47] Elliott D. Bloom et al. High-Energy Inelastic e p Scattering at 6-Degrees and 10-Degrees. *Phys. Rev. Lett.*, 23:930–934, 1969.

[48] Daniel Boer, R. Jakob, and P. J. Mulders. Asymmetries in polarized hadron production in e+ e- annihilation up to order 1/Q. *Nucl. Phys. B*, 504:345–380, 1997.

[49] Daniel Boer, P. J. Mulders, and O. V. Teryaev. Single spin asymmetries from a gluonic background in the Drell-Yan process. *Phys. Rev. D*, 57:3057–3064, 1998.

[50] N. N. Bogoliubov and O. S. Parasiuk. On the Multiplication of the causal function in the quantum theory of fields. *Acta Math.*, 97:227–266, 1957.

[51] C. G. Bollini and J. J. Giambiagi. Dimensional Renormalization: The Number of Dimensions as a Regularizing Parameter. *Nuovo Cim. B*, 12:20–26, 1972.

[52] Peter E. Bosted. Spin physics experiments at SLAC. *Int. J. Mod. Phys. A*, 18:1169–1176, 2003.

[53] V. M. Braun, A. N. Manashov, and B. Pirnay. Scale dependence of twist-three contributions to single spin asymmetries. *Phys. Rev. D*, 80:114002, 2009. [Erratum: Phys.Rev.D 86, 119902 (2012)].

[54] V. M. Braun, A. N. Manashov, and J. Rohrwild. Renormalization of Twist-Four Operators in QCD. *Nucl. Phys. B*, 826:235–293, 2010.

[55] A. Bravar. Transverse spin asymmetries in p(pol.) p –> pi+- + X and l p(pol.) –> l' + pi+- + X. *Nucl. Phys. A*, 666:314–317, 2000.

[56] Martin Breidenbach, Jerome I. Friedman, Henry W. Kendall, Elliott D. Bloom, D. H. Coward, H. C. DeStaebler, J. Drees, Luke W. Mo, and Richard E. Taylor. Observed behavior of highly inelastic electron-proton scattering. *Phys. Rev. Lett.*, 23:935–939, 1969.

[57] Raymond Brock et al. Handbook of perturbative QCD: Version 1.0. *Rev. Mod. Phys.*, 67:157–248, 1995.

[58] A. P. Bukhvostov, G. V. Frolov, L. N. Lipatov, and E. A. Kuraev. Evolution equations for quasi-partonic operators. *Nucl. Phys. B*, 258:601–646, 1985.

[59] A. P. Bukhvostov, E. A. Kuraev, and L. N. Lipatov. Deep inelastic scattering by a polarized target in quantum chromodynamics. *Sov. Phys. JETP*, 60(1):22–32, 1984.

[60] G. Bunce et al. Lambda0 Hyperon Polarization in Inclusive Production by 300-GeV Protons on Beryllium. *Phys. Rev. Lett.*, 36:1113–1116, 1976.

[61] Curtis G. Callan, Jr. Broken scale invariance in scalar field theory. *Phys. Rev. D*, 2:1541–1547, 1970.

[62] A. P. Chen, J. P. Ma, and G. P. Zhang. One-loop corrections to single spin asymmetries at twist-3 in Drell-Yan processes. *Phys. Rev. D*, 95(7):074005, 2017.

[63] A. P. Chen, J. P. Ma, and G. P. Zhang. One-Loop Corrections of Single Spin Asymmetries in Semi-Inclusive DIS. *Phys. Rev. D*, 97(5):054003, 2018.

[64] The ATLAS Collaboration. Observation of a new particle in the search for the Standard Model Higgs boson with the ATLAS detector at the LHC. *Phys. Lett.*, B716:1–29, 2012.

[65] John Collins. *Foundations of perturbative QCD*, volume 32. Cambridge University Press, 11 2013.

[66] John Collins, Ted C. Rogers, and Nobuo Sato. Positivity and renormalization of parton densities. *Phys. Rev. D*, 105(7):076010, 2022.

[67] John C. Collins. Leading twist single transverse-spin asymmetries: Drell-Yan and deep inelastic scattering. *Phys. Lett. B*, 536:43–48, 2002.

[68] John C. Collins. What exactly is a parton density? *Acta Phys. Polon. B*, 34:3103, 2003.

[69] John C. Collins, Davison E. Soper, and George F. Sterman. Factorization of Hard Processes in QCD. *Adv. Ser. Direct. High Energy Phys.*, 5:1–91, 1989.

[70] R. B. Curtis. Meson Production by Electrons. *Phys. Rev.*, 104:211–217, 1956.

[71] M. Czakon. The Four-loop QCD beta-function and anomalous dimensions. *Nucl. Phys. B*, 710:485–498, 2005.

[72] R. H. Dalitz and D. R. Yennie. Pion production in electron-proton collisions. *Phys. Rev.*, 105:1598–1615, 1957.

[73] Daniel de Florian, R. Sassot, Manuel Epele, Roger J. Hernández-Pinto, and Marco Stratmann. Parton-to-Pion Fragmentation Reloaded. *Phys. Rev. D*, 91(1):014035, 2015.

[74] Daniel de Florian, Rodolfo Sassot, and Marco Stratmann. Global analysis of fragmentation functions for pions and kaons and their uncertainties. *Phys. Rev. D*, 75:114010, 2007.

[75] Yuri L. Dokshitzer. Calculation of the Structure Functions for Deep Inelastic Scattering and e+ e- Annihilation by Perturbation Theory in Quantum Chromodynamics. *Sov. Phys. JETP*, 46:641–653, 1977.

[76] F. J. Dyson. The Radiation theories of Tomonaga, Schwinger, and Feynman. *Phys. Rev.*, 75:486–502, 1949.

[77] A. V. Efremov and O. V. Teryaev. On Spin Effects in Quantum Chromodynamics. *Sov. J. Nucl. Phys.*, 36:140, 1982.

[78] A. V. Efremov and O. V. Teryaev. QCD Asymmetry and Polarized Hadron Structure Functions. *Phys. Lett. B*, 150:383, 1985.

[79] E. Egorian and O. V. Tarasov. Two Loop Renormalization of the QCD in an Arbitrary Gauge. *Teor. Mat. Fiz.*, 41:26–32, 1979.

[80] Hisato Eguchi, Yuji Koike, and Kazuhiro Tanaka. Single Transverse Spin Asymmetry for Large-p(T) Pion Production in Semi-Inclusive Deep Inelastic Scattering. *Nucl. Phys. B*, 752:1–17, 2006.

[81] Hisato Eguchi, Yuji Koike, and Kazuhiro Tanaka. Twist-3 Formalism for Single Transverse Spin Asymmetry Reexamined: Semi-Inclusive Deep Inelastic Scattering. *Nucl. Phys. B*, 763:198–227, 2007.

[82] R. Keith Ellis, M. A. Furman, H. E. Haber, and I. Hinchliffe. Large Corrections to High p(T) Hadron-Hadron Scattering in QCD. *Nucl. Phys. B*, 173:397–421, 1980.

[83] R. Keith Ellis, W. Furmanski, and R. Petronzio. Power Corrections to the Parton Model in QCD. *Nucl. Phys. B*, 207:1–14, 1982.

[84] R. Keith Ellis, W. Furmanski, and R. Petronzio. Unraveling Higher Twists. *Nucl. Phys. B*, 212:29, 1983.

[85] R. Keith Ellis, W. James Stirling, and B. R. Webber. *QCD and collider physics*, volume 8. Cambridge University Press, 2 2011.

[86] F. Englert and R. Brout. Broken Symmetry and the Mass of Gauge Vector Mesons. *Phys. Rev. Lett.*, 13:321–323, 1964.

[87] L. D. Faddeev and V. N. Popov. Feynman Diagrams for the Yang-Mills Field. *Phys. Lett. B*, 25:29–30, 1967.

[88] G. Falcioni, F. Herzog, S. Moch, and A. Vogt. Four-loop splitting functions in QCD – The gluon-to-quark case. *Phys. Lett. B*, 846:138215, 2023.

[89] G. Falcioni, F. Herzog, S. Moch, and A. Vogt. Four-loop splitting functions in QCD – The quark-quark case. *Phys. Lett. B*, 842:137944, 2023.

[90] E. Fermi. On the Theory of the impact between atoms and electrically charged particles. *Z. Phys.*, 29:315–327, 1924.

[91] R. P. Feynman. Relativistic cutoff for quantum electrodynamics. *Phys. Rev.*, 74:1430–1438, 1948.

[92] R. P. Feynman. Space-time approach to nonrelativistic quantum mechanics. *Rev. Mod. Phys.*, 20:367–387, 1948.

[93] R. P. Feynman. The behavior of hadron collisions at extreme energies. *Conf. Proc. C*, 690905:237–258, 1969.

[94] R. D. Field. *Applications of Perturbative QCD*, volume 77. 1989.

[95] Sophia Fitzgibbons, Michel Malda, Jacob Marsh, Daniel Pitonyak, and Penn Smith. Updated numerical study of transverse single-spin asymmetries in single-inclusive pion production from lepton-nucleon collisions. *Phys. Lett. B*, 852:138606, 2024.

[96] H. Fritzsch, Murray Gell-Mann, and H. Leutwyler. Advantages of the Color Octet Gluon Picture. *Phys. Lett. B*, 47:365–368, 1973.

[97] Stefano Frixione, Michelangelo L. Mangano, Paolo Nason, and Giovanni Ridolfi. Improving the Weizsacker-Williams approximation in electron - proton collisions. *Phys. Lett. B*, 319:339–345, 1993.

[98] Thomas Gajdosik. Using the Pathintegral to derive the Feynman Rules for the ABC-Theory. *Lecture notes*, 2012.

[99] Leonard Gamberg, Zhong-Bo Kang, Andreas Metz, Daniel Pitonyak, and Alexei Prokudin. Left-right spin asymmetry in $\ell N^{\uparrow} \to hX$. *Phys. Rev. D*, 90(7):074012, 2014.

[100] H. Geiger and E. Marsden. On a diffuse reflection of the α-particles. *Proc. Roy. Soc. 1909 A*, 82:495–500, 1909.

[101] Murray Gell-Mann. The Eightfold Way: A Theory of strong interaction symmetry. 3 1961.

[102] Murray Gell-Mann. A Schematic Model of Baryons and Mesons. *Phys. Lett.*, 8:214–215, 1964.

[103] K. Goeke, A. Metz, and M. Schlegel. Parameterization of the quark-quark correlator of a spin-1/2 hadron. *Phys. Lett. B*, 618:90–96, 2005.

[104] O. W. Greenberg. Spin and Unitary Spin Independence in a Paraquark Model of Baryons and Mesons. *Phys. Rev. Lett.*, 13:598–602, 1964.

[105] V. N. Gribov and L. N. Lipatov. Deep inelastic e p scattering in perturbation theory. *Sov. J. Nucl. Phys.*, 15:438–450, 1972.

[106] David J. Gross and S. B. Treiman. Light cone structure of current commutators in the gluon quark model. *Phys. Rev. D*, 4:1059–1072, 1971.

[107] David J. Gross and Frank Wilczek. Ultraviolet Behavior of Nonabelian Gauge Theories. *Phys. Rev. Lett.*, 30:1343–1346, 1973.

[108] G. S. Guralnik, C. R. Hagen, and T. W. B. Kibble. Global Conservation Laws and Massless Particles. *Phys. Rev. Lett.*, 13:585–587, 1964.

[109] F. Halzen and Alan D. Martin. *QUARKS AND LEPTONS: AN INTRODUCTORY COURSE IN MODERN PARTICLE PHYSICS*. 1984.

[110] M. Y. Han and Yoichiro Nambu. Three Triplet Model with Double SU(3) Symmetry. *Phys. Rev.*, 139:B1006–B1010, 1965.

[111] Gudrun Heinrich. Colourful Loops: Introduction to Quantum Chromodynamics and Loop Calculations. *Lecture notes*, 2018.

[112] W. Heisenberg. THE 'OBSERVABLE QUANTITIES' IN THE THEORY OF ELEMENTARY PARTICLES. 1943.

[113] W. Heisenberg and W. Pauli. On Quantum Field Theory. (In German). *Z. Phys.*, 56:1–61, 1929.

[114] W. Heisenberg and W. Pauli. On Quantum Field Theory. 2. (In German). *Z. Phys.*, 59:168–190, 1930.

[115] Klaus Hepp. Proof of the Bogolyubov-Parasiuk theorem on renormalization. *Commun. Math. Phys.*, 2:301–326, 1966.

[116] F. Herzog, B. Ruijl, T. Ueda, J. A. M. Vermaseren, and A. Vogt. The five-loop beta function of Yang-Mills theory with fermions. *JHEP*, 02:090, 2017.

[117] Peter W. Higgs. Broken Symmetries and the Masses of Gauge Bosons. *Phys. Rev. Lett.*, 13:508–509, 1964.

[118] Peter W. Higgs. Broken symmetries, massless particles and gauge fields. *Phys. Lett.*, 12:132–133, 1964.

[119] Patriz Hinderer. *Higher Order Studies in Perturbative QCD*. PhD thesis, U. Tubingen, 2017.

[120] Patriz Hinderer, Marc Schlegel, and Werner Vogelsang. Single-Inclusive Production of Hadrons and Jets in Lepton-Nucleon Scattering at NLO. *Phys. Rev. D*, 92(1):014001, 2015. [Erratum: Phys.Rev.D 93, 119903 (2016)].

[121] Patriz Hinderer, Marc Schlegel, and Werner Vogelsang. Double-Longitudinal Spin Asymmetry in Single-Inclusive Lepton Scattering at NLO. *Phys. Rev. D*, 96(1):014002, 2017.

[122] Robert Hofstadter. Electron scattering and nuclear structure. *Rev. Mod. Phys.*, 28:214–254, 1956.

[123] Tie-Jiun Hou et al. New CTEQ global analysis of quantum chromodynamics with high-precision data from the LHC. *Phys. Rev. D*, 103(1):014013, 2021.

[124] Riku Ikarashi, Yuji Koike, Kenta Yabe, and Shinsuke Yoshida. New derivation of the twist-3 gluon fragmentation contribution to polarized hyperon production. *Phys. Rev. D*, 106(7):074006, 2022.

[125] Riku Ikarashi, Yuji Koike, Kenta Yabe, and Shinsuke Yoshida. Twist-3 gluon fragmentation contribution to hyperon polarization in semi-inclusive deep inelastic scattering. *Phys. Rev. D*, 105(9):094027, 2022.

[126] R. L. Jaffe. Parton Distribution Functions for Twist Four. *Nucl. Phys. B*, 229:205–230, 1983.

[127] R. L. Jaffe and Xiang-Dong Ji. Chiral odd parton distributions and Drell-Yan processes. *Nucl. Phys. B*, 375:527–560, 1992.

[128] Matthias Jamin and Markus E. Lautenbacher. TRACER: Version 1.1: A Mathematica package for gamma algebra in arbitrary dimensions. *Comput. Phys. Commun.*, 74:265–288, 1993.

[129] Xiangdong Ji. Parton Physics on a Euclidean Lattice. *Phys. Rev. Lett.*, 110:262002, 2013.

[130] Xiangdong Ji, Jian-Wei Qiu, Werner Vogelsang, and Feng Yuan. A Unified picture for single transverse-spin asymmetries in hard processes. *Phys. Rev. Lett.*, 97:082002, 2006.

[131] Xiangdong Ji, Jian-wei Qiu, Werner Vogelsang, and Feng Yuan. Single Transverse-Spin Asymmetry in Drell-Yan Production at Large and Moderate Transverse Momentum. *Phys. Rev. D*, 73:094017, 2006.

[132] Xiangdong Ji, Jian-Wei Qiu, Werner Vogelsang, and Feng Yuan. Single-transverse spin asymmetry in semi-inclusive deep inelastic scattering. *Phys. Lett. B*, 638:178–186, 2006.

[133] K. Kanazawa, A. Metz, D. Pitonyak, and M. Schlegel. Longitudinal–transverse double-spin asymmetries in single-inclusive leptoproduction of hadrons. *Phys. Lett. B*, 742:340–346, 2015.

[134] K. Kanazawa, A. Metz, D. Pitonyak, and M. Schlegel. Single-spin asymmetries in the leptoproduction of transversely polarized Λ hyperons. *Phys. Lett. B*, 744:385–390, 2015.

[135] Koichi Kanazawa, Yuji Koike, Andreas Metz, Daniel Pitonyak, and Marc Schlegel. Operator Constraints for Twist-3 Functions and Lorentz Invariance Properties of Twist-3 Observables. *Phys. Rev. D*, 93(5):054024, 2016.

[136] Y. Kanazawa and Yuji Koike. Chiral odd contribution to single transverse spin asymmetry in hadronic pion production. *Phys. Lett. B*, 478:121–126, 2000.

[137] Y. Kanazawa and Yuji Koike. Polarization in hadronic Lambda hyperon production and chiral odd twist - three quark distribution. *Phys. Rev. D*, 64:034019, 2001.

[138] Zhong-Bo Kang, Andreas Metz, Jian-Wei Qiu, and Jian Zhou. Exploring the structure of the proton through polarization observables in l p \to jet X. *Phys. Rev. D*, 84:034046, 2011.

[139] Zhong-Bo Kang and Jian-Wei Qiu. Evolution of twist-3 multi-parton correlation functions relevant to single transverse-spin asymmetry. *Phys. Rev. D*, 79:016003, 2009.

[140] Zhong-Bo Kang and Jian-Wei Qiu. QCD evolution of naive-time-reversal-odd parton distribution functions. *Phys. Lett. B*, 713:273–276, 2012.

[141] Zhong-Bo Kang, Ivan Vitev, and Hongxi Xing. Transverse momentum-weighted Sivers asymmetry in semi-inclusive deep inelastic scattering at next-to-leading order. *Phys. Rev. D*, 87(3):034024, 2013.

[142] Tanjib Khan et al. Unpolarized gluon distribution in the nucleon from lattice quantum chromodynamics. *Phys. Rev. D*, 104(9):094516, 2021.

[143] T. Kinoshita. Mass singularities of Feynman amplitudes. *J. Math. Phys.*, 3:650–677, 1962.

[144] R. D. Klem, J. E. Bowers, H. W. Courant, H. Kagan, M. L. Marshak, E. A. Peterson, K. Ruddick, W. H. Dragoset, and J. B. Roberts. Measurement of Asymmetries of Inclusive Pion Production in Proton Proton Interactions at 6-GeV/c and 11.8-GeV/c. *Phys. Rev. Lett.*, 36:929–931, 1976.

[145] Yuji Koike. Single transverse spin asymmetry in p(up) arrow p —> pi X and ep(up) arrow —> pi X. *Nucl. Phys. A*, 721:364–367, 2003.

[146] Yuji Koike, Andreas Metz, Daniel Pitonyak, Kenta Yabe, and Shinsuke Yoshida. Twist-3 fragmentation contribution to polarized hyperon production in unpolarized hadronic collisions. *Phys. Rev. D*, 95(11):114013, 2017.

[147] Yuji Koike, Kazuki Takada, Sumire Usui, Kenta Yabe, and Shinsuke Yoshida. Transverse polarization of hyperons produced in semi-inclusive deep inelastic scattering. *Phys. Rev. D*, 105(5):056021, 2022.

[148] Yuji Koike and Kazuhiro Tanaka. Universal structure of twist-3 soft-gluon-pole cross-sections for single transverse-spin asymmetry. *Phys. Rev. D*, 76:011502, 2007.

[149] Yuji Koike, Werner Vogelsang, and Feng Yuan. On the Relation Between Mechanisms for Single-Transverse-Spin Asymmetries. *Phys. Lett. B*, 659:878–884, 2008.

[150] Yuji Koike, Kenta Yabe, and Shinsuke Yoshida. Exact Relations for Twist-3 Gluon Distribution and Fragmentation Functions from Operator Identities. *Phys. Rev. D*, 101(5):054017, 2020.

[151] Yuji Koike, Kenta Yabe, and Shinsuke Yoshida. Twist-3 gluon fragmentation contribution to polarized hyperon production in unpolarized proton-proton collision. *Phys. Rev. D*, 104(5):054023, 2021.

[152] Chris Kouvaris, Jian-Wei Qiu, Werner Vogelsang, and Feng Yuan. Single transverse-spin asymmetry in high transverse momentum pion production in pp collisions. *Phys. Rev. D*, 74:114013, 2006.

[153] K. Krueger et al. Large analyzing power in inclusive pi+- production at high x(F) with a 22-GeV/c polarized proton beam. *Phys. Lett. B*, 459:412–416, 1999.

[154] S. A. Larin and J. A. M. Vermaseren. The Three loop QCD Beta function and anomalous dimensions. *Phys. Lett. B*, 303:334–336, 1993.

[155] T. D. Lee and M. Nauenberg. Degenerate Systems and Mass Singularities. *Phys. Rev.*, 133:B1549–B1562, 1964.

[156] G. Peter Lepage. A New Algorithm for Adaptive Multidimensional Integration. *J. Comput. Phys.*, 27:192, 1978.

[157] G. Peter Lepage. VEGAS: AN ADAPTIVE MULTIDIMENSIONAL INTEGRATION PROGRAM. 3 1980.

[158] Maxime Levillain. Measurement of $A_{LL}(pT)$ for single hadron photoproduction at high p_T at COMPASS. *PoS*, DIS2014:223, 2014.

[159] Thomas Luthe, Andreas Maier, Peter Marquard, and York Schröder. Towards the five-loop Beta function for a general gauge group. *JHEP*, 07:127, 2016.

[160] Thomas Luthe, Andreas Maier, Peter Marquard, and York Schroder. The five-loop Beta function for a general gauge group and anomalous dimensions beyond Feynman gauge. *JHEP*, 10:166, 2017.

[161] J. P. Ma and Q. Wang. Scale Dependence of Twist-3 Quark-Gluon Operators for Single Spin Asymmetries. *Phys. Lett. B*, 715:157–163, 2012.

[162] Franz Mandl and Graham Shaw. *QUANTUM FIELD THEORY*. 1985.

[163] Anna Martin. COMPASS Results on Transverse Single-Spin Asymmetries. *Czech. J. Phys.*, 56:F33–F52, 2006.

[164] T. Massam. The quark hunters' progress. 7 1968.

[165] R. Mertig, M. Bohm, and Ansgar Denner. FEYN CALC: Computer algebraic calculation of Feynman amplitudes. *Comput. Phys. Commun.*, 64:345–359, 1991.

[166] S. Moch, B. Ruijl, T. Ueda, J. Vermaseren, and A. Vogt. Additional moments and x-space approximations of four-loop splitting functions in QCD. 10 2023.

[167] S. Moch, B. Ruijl, T. Ueda, J. A. M. Vermaseren, and A. Vogt. Low moments of the four-loop splitting functions in QCD. *Phys. Lett. B*, 825:136853, 2022.

[168] S. Moch, J. A. M. Vermaseren, and A. Vogt. The Three loop splitting functions in QCD: The Nonsinglet case. *Nucl. Phys. B*, 688:101–134, 2004.

[169] P. J. Mulders and R. D. Tangerman. The Complete tree level result up to order 1/Q for polarized deep inelastic leptoproduction. *Nucl. Phys. B*, 461:197–237, 1996. [Erratum: Nucl.Phys.B 484, 538–540 (1997)].

[170] Pavel M. Nadolsky, Hung-Liang Lai, Qing-Hong Cao, Joey Huston, Jon Pumplin, Daniel Stump, Wu-Ki Tung, and C. P. Yuan. Implications of CTEQ global analysis for collider observables. *Phys. Rev. D*, 78:013004, 2008.

[171] Y. Nambu. Systematics of hadrons in subnuclear physics.

[172] Yuval Ne'eman. Derivation of strong interactions from a gauge invariance. *Nucl. Phys.*, 26:222–229, 1961.

[173] Maciej A. Nowak, M. Praszalowicz, and W. Slominski. A Practical Guide to the Next-to-leading Order of the Perturbation Expansion. *Annals Phys.*, 166:443, 1986.

[174] J. R. Oppenheimer. Note on the Theory of the Interaction of Field and Matter. *Phys. Rev.*, 35:461–477, 1930.

[175] L. L. Pappalardo. Latest HERMES results on transverse spin effects in hadron structure and formation. *Eur. Phys. J. A*, 38:145–148, 2008.

[176] G. Passarino and M. J. G. Veltman. One Loop Corrections for e+ e- Annihilation Into mu+ mu- in the Weinberg Model. *Nucl. Phys. B*, 160:151–207, 1979.

[177] Hiren H. Patel. Package-X: A Mathematica package for the analytic calculation of one-loop integrals. *Comput. Phys. Commun.*, 197:276–290, 2015.

[178] W. Pauli and F. Villars. On the Invariant regularization in relativistic quantum theory. *Rev. Mod. Phys.*, 21:434–444, 1949.

[179] Michael E. Peskin and Daniel V. Schroeder. *An Introduction to quantum field theory.* Addison-Wesley, Reading, USA, 1995.

[180] H. David Politzer. Reliable Perturbative Results for Strong Interactions? *Phys. Rev. Lett.*, 30:1346–1349, 1973.

[181] H. David Politzer. Power Corrections at Short Distances. *Nucl. Phys. B*, 172:349–382, 1980.

[182] VN Popov and LD Faddeev. Teoriya vozmushchenii dlya kalibrovochno-invariantnykh polei.(perturbation theory for gauge-invariant fields). Technical report, Akademiya Nauk Ukrainskoi SSR, Kiev. Institut Teoreticheskoi Fiziki, 1967.

[183] X. Qian et al. Single Spin Asymmetries in Charged Pion Production from Semi-Inclusive Deep Inelastic Scattering on a Transversely Polarized ^{3}He Target. *Phys. Rev. Lett.*, 107:072003, 2011.

[184] Jian-Wei Qiu. Twist Four Contributions to the Parton Structure Functions. *Phys. Rev. D*, 42:30–44, 1990.

[185] Jian-wei Qiu and George F. Sterman. Single transverse spin asymmetries. *Phys. Rev. Lett.*, 67:2264–2267, 1991.

[186] Jian-wei Qiu and George F. Sterman. Single transverse spin asymmetries in direct photon production. *Nucl. Phys. B*, 378:52–78, 1992.

[187] Jian-wei Qiu and George F. Sterman. Single transverse spin asymmetries in hadronic pion production. *Phys. Rev. D*, 59:014004, 1999.

[188] Daniel Rein, Marc Schlegel, Patrick Tollkühn, and Werner Vogelsang. Next-to-Leading-Order Corrections and Factorization for Transverse Single-Spin Asymmetries. *Phys. Rev. Lett.*, 135(25):251901, 2025.

[189] Daniel Rein, Marc Schlegel, Patrick Tollkühn, and Werner Vogelsang. Transverse nucleon single-spin asymmetry for single-inclusive hadron and jet production at NLO accuracy. *Phys. Rev. D*, 112(11):114024, 2025.

[190] Klaus Rith. HERMES results on transverse target single-spin asymmetries in inclusive electroproduction of charged pions and kaons. *PoS*, DIS2014:210, 2014.

[191] German Rodrigo, Arcadi Santamaria, and Mikhail S. Bilenky. Dimensionally regularized box and phase space integrals involving gluons and massive quarks. *J. Phys. G*, 25:1593–1606, 1999.

[192] E. Rutherford. The Scattering of α- and β-Particles by Matter and the Structure of the Atom. *Phil. Mag. Ser. 6*, 21:669–688, 1911.

[193] Julian S. Schwinger. On Quantum electrodynamics and the magnetic moment of the electron. *Phys. Rev.*, 73:416–417, 1948.

[194] Julian S. Schwinger. Quantum electrodynamics. I A covariant formulation. *Phys. Rev.*, 74:1439, 1948.

[195] Vladyslav Shtabovenko, Rolf Mertig, and Frederik Orellana. New Developments in FeynCalc 9.0. *Comput. Phys. Commun.*, 207:432–444, 2016.

[196] Vladyslav Shtabovenko, Rolf Mertig, and Frederik Orellana. FeynCalc 9.3: New features and improvements. *Comput. Phys. Commun.*, 256:107478, 2020.

[197] Edward V. Shuryak and A. I. Vainshtein. Theory of Power Corrections to Deep Inelastic Scattering in Quantum Chromodynamics. 1. Q**2 Effects. *Nucl. Phys. B*, 199:451–481, 1982.

[198] Edward V. Shuryak and A. I. Vainshtein. Theory of Power Corrections to Deep Inelastic Scattering in Quantum Chromodynamics. 2. Q**4 Effects: Polarized Target. *Nucl. Phys. B*, 201:141, 1982.

[199] Dennis W. Sivers. Single Spin Production Asymmetries from the Hard Scattering of Point-Like Constituents. *Phys. Rev. D*, 41:83, 1990.

[200] Dennis W. Sivers. Hard scattering scaling laws for single spin production asymmetries. *Phys. Rev. D*, 43:261–263, 1991.

[201] K. Symanzik. Small distance behavior in field theory and power counting. *Commun. Math. Phys.*, 18:227–246, 1970.

[202] Gerard 't Hooft. Dimensional regularization and the renormalization group. *Nucl. Phys. B*, 61:455–468, 1973.

[203] Gerard 't Hooft and M. J. G. Veltman. Regularization and Renormalization of Gauge Fields. *Nucl. Phys. B*, 44:189–213, 1972.

[204] Hidezumi Terazawa. Two photon processes for particle production at high-energies. *Rev. Mod. Phys.*, 45:615–662, 1973.

[205] J. J. Thomson. Cathode Rays. *The Electrician*, 39:104, 1897.

[206] J. J. Thomson. Cathode Rays. *Phil. Mag.*, 44:293, 1897.

[207] S. Tomonaga. On a relativistically invariant formulation of the quantum theory of wave fields. *Prog. Theor. Phys.*, 1:27–42, 1946.

[208] Charlotte Van Hulse. Recent HERMES results from inclusive and semi-inclusive hadron production. *EPJ Web Conf.*, 85:02020, 2015.

[209] T. van Ritbergen, J. A. M. Vermaseren, and S. A. Larin. The Four loop beta function in quantum chromodynamics. *Phys. Lett. B*, 400:379–384, 1997.

[210] F. Videbaek. Single spin asymmetries in the BRAHMS experiment. *AIP Conf. Proc.*, 792(1):993–996, 2005.

[211] Werner Vogelsang and Feng Yuan. Next-to-leading Order Calculation of the Single Transverse Spin Asymmetry in the Drell-Yan Process. *Phys. Rev. D*, 79:094010, 2009.

[212] A. Vogt, S. Moch, and J. Vermaseren. The three-loop splitting functions in QCD. *Nucl. Phys. B Proc. Suppl.*, 152:110–115, 2006.

[213] A. Vogt, S. Moch, and J. A. M. Vermaseren. The Three-loop splitting functions in QCD: The Singlet case. *Nucl. Phys. B*, 691:129–181, 2004.

[214] C. F. von Weizsacker. Radiation emitted in collisions of very fast electrons. *Z. Phys.*, 88:612–625, 1934.

[215] Steven Weinberg. New approach to the renormalization group. *Phys. Rev. D*, 8:3497–3509, 1973.

[216] John A. Wheeler. On the Mathematical Description of Light Nuclei by the Method of Resonating Group Structure. *Phys. Rev.*, 52:1107–1122, 1937.

[217] Ferdinand Willeke. Electron Ion Collider Conceptual Design Report 2021. 2 2021.

[218] E. J. Williams. Nature of the high-energy particles of penetrating radiation and status of ionization and radiation formulae. *Phys. Rev.*, 45:729–730, 1934.

[219] K. G. Wilson and John B. Kogut. The Renormalization group and the epsilon expansion. *Phys. Rept.*, 12:75–199, 1974.

[220] Kenneth G. Wilson. Renormalization group and critical phenomena. 1. Renormalization group and the Kadanoff scaling picture. *Phys. Rev. B*, 4:3174–3183, 1971.

[221] Kenneth G. Wilson. Renormalization group and critical phenomena. 2. Phase space cell analysis of critical behavior. *Phys. Rev. B*, 4:3184–3205, 1971.

[222] Kenneth G. Wilson. Confinement of Quarks. *Phys. Rev. D*, 10:2445–2459, 1974.

[223] Kenneth G. Wilson. The Renormalization Group: Critical Phenomena and the Kondo Problem. *Rev. Mod. Phys.*, 47:773, 1975.

[224] Chen-Ning Yang and Robert L. Mills. Conservation of Isotopic Spin and Isotopic Gauge Invariance. *Phys. Rev.*, 96:191–195, 1954.

[225] Yongliang Yang, Zhun Lu, and Ivan Schmidt. Twist-3 T-odd fragmentation functions $G^{\perp}$ and $\tilde{G}^{\perp}$ in a spectator model. *Phys. Lett. B*, 761:333–339, 2016.

[226] Shinsuke Yoshida. New pole contribution to $P_{h\perp}$-weighted single-transverse spin asymmetry in semi-inclusive deep inelastic scattering. *Phys. Rev. D*, 93(5):054048, 2016.

[227] Feng Yuan and Jian Zhou. Collins Fragmentation and the Single Transverse Spin Asymmetry. *Phys. Rev. Lett.*, 103:052001, 2009.

[228] Y. X. Zhao et al. Single spin asymmetries in charged kaon production from semi-inclusive deep inelastic scattering on a transversely polarized ^3He target. *Phys. Rev. C*, 90(5):055201, 2014.

[229] Y. X. Zhao et al. Double Spin Asymmetries of Inclusive Hadron Electroproductions from a Transversely Polarized ^{3}He Target. *Phys. Rev. C*, 92(1):015207, 2015.

[230] Yuxiang Zhao. *Measurement of Single Spin Asymmetry in $^3He^{\uparrow}$(e, e'K±)X from a Transversely Polarized 3He Target.* PhD thesis, Univ. of Science and Technology, Hefei (China), 2015.

[231] Jian Zhou, Feng Yuan, and Zuo-Tang Liang. Transverse momentum dependent quark distributions and polarized Drell-Yan processes. *Phys. Rev. D*, 81:054008, 2010.

[232] W. Zimmermann. Convergence of Bogolyubov's method of renormalization in momentum space. *Commun. Math. Phys.*, 15:208–234, 1969.

[233] G. Zweig. *An SU(3) model for strong interaction symmetry and its breaking. Version 2*, pages 22–101. 2 1964.

Appendix

Appendix A

Feynman Rules of QCD

In the following, we list the Feynman rules, which we make use of in the course of our considerations. They are taken from [94].

External Lines

- Spin-1/2 fermion with momentum p and spin s
  - in the initial state: add $u^{(s)}(p)$ on the right
  - in the final state: add $\bar{u}^{(s)}(p)$ on the left
- Spin-1/2 antifermion with momentum p and spin s
  - in the initial state: add $\bar{v}^{(s)}(p)$ on the left
  - in the final state: add $v^{(s)}(p)$ on the right
- Spin-1 boson: add polarization vector $\varepsilon^{(\lambda),\mu}\big(k\big)$, where λ labels the polarization state and k denotes the momentum. The vector fulfills the relation

$$\sum_{\lambda} \varepsilon^{(\lambda),\mu}\big(k\big)\big(\varepsilon^{*}\big)^{(\lambda),\nu}\big(k\big) = -g^{\mu\nu} \tag{A.1}$$

  when the boson is a photon and

$$\sum_{\lambda} \varepsilon^{(\lambda),\mu}\big(k\big)\big(\varepsilon^{*}\big)^{(\lambda),\nu}\big(k\big) = -g^{\mu\nu} + \frac{n^{\mu}k^{\nu} + n^{\nu}k^{\mu}}{n \cdot k} \tag{A.2}$$

  in the case of a gluon where n is an arbitrary four-vector satisfying $n^2 = 0$ and $n \cdot k \neq 0$. Here, the additional term is required to cancel unphysical polarization states.

Feynman Rules of QCD

Internal Lines

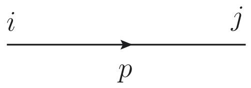

Internal quark line:

$\sim \frac{i\delta_{ij}(\not{p}+m)}{p^2-m^2+i\varepsilon}$

Internal gluon line:

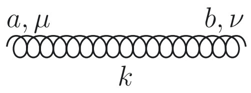

In covariant gauge:
$\sim -\frac{i\delta_{ab}(g^{\mu\nu}+\xi k^\mu k^\nu/k^2)}{k^2+i\varepsilon}$
with ξ being an arbitrary gauge parameter.

In light-cone gauge:
$\sim -\frac{i\delta_{ab}(g^{\mu\nu}-\left(n^\mu k^\nu+n^\nu k^\mu\right)/(n\cdot k))}{k^2+i\varepsilon}$
with $n^2 = 0$ and $n \cdot k \neq 0$.

Vertices

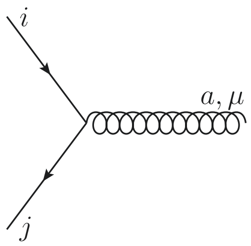

Quark-gluon-quark vertex:

$\sim -ig_\mathrm{s}\gamma^\mu T^a_{ij}$

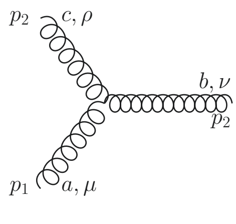

Three-gluon vertex:

$$\sim -g_\mathrm{s} f^{abc}\big[(p_1-p_2)^\rho g^{\mu nu} + (p_2-p_3)^\mu g^{\nu\rho} + (p_3-p_1)^\nu g^{\rho\mu}$$

Note that all three momenta are assumed to be incoming.

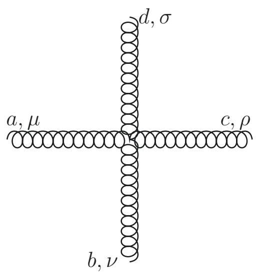

Four-gluon vertex:

$$\sim ig_\mathrm{s}^2\big[f^{abe}f^{cde}\big(g^{\mu\rho}g^{\nu\sigma}-g^{\mu\sigma}g^{\nu\rho}\big) + f^{ace}f^{bde}\big(g^{\mu\nu}g^{\rho\sigma}-g^{\mu\sigma}g^{\nu\rho}\big) + f^{ade}f^{cbe}\big(g^{\mu\rho}g^{\nu\sigma}-g^{\mu\nu}g^{\rho\sigma}\big)\big]$$

Appendix B

dPS_3: Momentum Parameterization

We previously introduced the standard integral

$$\Omega_{j,k} \equiv \int_0^\pi d\vartheta_1 \int_0^\pi d\vartheta_2 \sin^{1-2\varepsilon}(\vartheta_1) \sin^{-2\varepsilon}(\vartheta_2)$$
$$\frac{1}{\big(1-\cos(\vartheta_1)\big)^j \big(1-\cos(\vartheta_1)\cos(\chi)-\sin(\vartheta_1)\cos(\vartheta_2)\sin(\chi)\big)^k} \;, \quad \text{(B.1)}$$

in chapter 3.2.2, which serves as the foundation of our procedure to evaluate the three-body phase space integration alongside the second master integral that is presented in [42]. However, in order to rearrange the matrix elements in such a manner that they can be cast into the form of one of these integrals, suitable parameterizations for the momenta in terms of the kinematic variables v and w as well as the angles ϑ_1 and ϑ_2 need to be introduced. In the following, we therefore want to delve deeper into this issue and in particular give a detailed guide on the three possible ways to introduce the required parameterizations. Against this background, we consider an arbitrary $2 \to 3$ process of the type

$$p_1 + p_2 \to k_1 + k_2 + k_3,$$

where p_1 and p_2 denote the momenta of the incoming particles and with k_1, k_2 and k_3 labeling the momenta of the particles in the final state. Working in the rest frame of the particles with the momenta k_2 and k_3, we find that the last mentioned two momenta may be written as

$$k_2 = k_2^0\big(1, ..., \sin(\vartheta_1)\cos(\vartheta_2), \cos(\vartheta_1)\big) \quad \text{(B.2)}$$
$$k_3 = k_3^0\big(1, ..., -\sin(\vartheta_1)\cos(\vartheta_2), -\cos(\vartheta_1)\big) \quad \text{(B.3)}$$

where $k_2^0 = k_3^0 = \frac{1}{2}\sqrt{s_{23}}$. Furthermore, it can be shown that the zeroth components of the remaining momenta may be written as

$$p_1^0 = \frac{sv}{2\sqrt{s_{23}}}, \quad p_2^0 = \frac{s(1-vw)}{2\sqrt{s_{23}}}, \quad k_1^0 = \frac{s(1-v+vw)}{2\sqrt{s_{23}}}. \quad \text{(B.4)}$$

It now remains to find suitable choices for the remaining momenta p_1, p_2 and k_1. All-in-all, three sets of parameterizations can be formulated depending on which momentum defines the z-axis. The sets read as follows:

↪ _Set 1:_

$$\begin{aligned} p_1 &= p_1^0\big(1, 0, ..., 0, 1\big) \\ p_2 &= p_2^0\big(1, 0, ..., -\sin(\psi''), \cos(\psi'')\big) \\ k_1 &= k_1^0\big(1, 0, ..., -\sin(\psi), \cos(\psi)\big) \end{aligned} \tag{B.5}$$

↪ _Set 2:_

$$\begin{aligned} p_1 &= p_1^0\big(1, 0, ..., \sin(\psi''), \cos(\psi'')\big) \\ p_2 &= p_2^0\big(1, 0, ..., 0, 1\big) \\ k_1 &= k_1^0\big(1, 0, ..., \sin(\psi'), \cos(\psi')\big) \end{aligned} \tag{B.6}$$

↪ _Set 3:_

$$\begin{aligned} p_1 &= p_1^0\big(1, 0, ..., \sin(\psi), \cos(\psi)\big) \\ p_2 &= p_2^0\big(1, 0, ..., -\sin(\psi'), \cos(\psi')\big) \\ k_1 &= k_1^0\big(1, 0, ..., 0, 1\big) \end{aligned} \tag{B.7}$$

Here, we have introduced the three angles ψ, ψ', ψ'', which satisfy the relations

$$\cos\big(\psi\big) = 1 - \frac{2(1-v)(1-w)}{1-v+vw}, \tag{B.8}$$

$$\cos\big(\psi'\big) = 1 - \frac{2v^2w(1-w)}{(1-vw)(1-v+vw)}, \tag{B.9}$$

$$\cos\big(\psi''\big) = 1 - \frac{2(1-w)}{1-vw}. \tag{B.10}$$

In regard to these parameterizations, four out of ten Mandelstam variables are the same for all sets, namely

$$s,\ s_{23} = sv(1-w),\ t_1 = -s(1-v),\ u_1 = -svw. \tag{B.11}$$

The remaining six variables are listed in table B.1, where we use the notation

$$s_{12}^0 = s_{13}^0 = \frac{s(1-v+vw)}{2},\ t_2^0 = t_3^0 = -\frac{sv}{2},\ u_2^0 = u_3^0 = -\frac{s(1-vw)}{2}. \tag{B.12}$$

Table B.1: Overview of the Mandelstam variable's representations in the various momentum parameterizations.

	Set 1	Set 2	Set 3
s_{12}	$s_{12}^0\left(1+\sin\left(\vartheta_1\right)\cos\left(\vartheta_2\right)\sin\left(\psi\right)-\cos\left(\vartheta_1\right)\cos\left(\psi\right)\right)$	$s_{12}^0\left(1-\sin\left(\vartheta_1\right)\cos\left(\vartheta_2\right)\sin\left(\psi'\right)-\cos\left(\vartheta_1\right)\cos\left(\psi'\right)\right)$	$s_{12}^0\left(1-\cos\left(\vartheta_1\right)\right)$
s_{13}	$s_{13}^0\left(1-\sin\left(\vartheta_1\right)\cos\left(\vartheta_2\right)\sin\left(\psi\right)+\cos\left(\vartheta_1\right)\cos\left(\psi\right)\right)$	$s_{13}^0\left(1+\sin\left(\vartheta_1\right)\cos\left(\vartheta_2\right)\sin\left(\psi'\right)+\cos\left(\vartheta_1\right)\cos\left(\psi'\right)\right)$	$s_{13}^0\left(1+\cos\left(\vartheta_1\right)\right)$
t_2	$t_2^0\left(1-\cos\left(\vartheta_1\right)\right)$	$t_2^0\left(1-\sin\left(\vartheta_1\right)\cos\left(\vartheta_2\right)\sin\left(\psi''\right)-\cos\left(\vartheta_1\right)\cos\left(\psi''\right)\right)$	$t_2^0\left(1-\sin\left(\vartheta_1\right)\cos\left(\vartheta_2\right)\sin\left(\psi\right)-\cos\left(\vartheta_1\right)\cos\left(\psi\right)\right)$
t_3	$t_3^0\left(1+\cos\left(\vartheta_1\right)\right)$	$t_3^0\left(1+\sin\left(\vartheta_1\right)\cos\left(\vartheta_2\right)\sin\left(\psi''\right)+\cos\left(\vartheta_1\right)\cos\left(\psi''\right)\right)$	$t_3^0\left(1+\sin\left(\vartheta_1\right)\cos\left(\vartheta_2\right)\sin\left(\psi\right)+\cos\left(\vartheta_1\right)\cos\left(\psi\right)\right)$
u_2	$u_2^0\left(1+\sin\left(\vartheta_1\right)\cos\left(\vartheta_2\right)\sin\left(\psi''\right)-\cos\left(\vartheta_1\right)\cos\left(\psi''\right)\right)$	$u_2^0\left(1-\cos\left(\vartheta_1\right)\right)$	$u_2^0\left(1+\sin\left(\vartheta_1\right)\cos\left(\vartheta_2\right)\sin\left(\psi'\right)-\cos\left(\vartheta_1\right)\cos\left(\psi'\right)\right)$
u_3	$u_3^0\left(1-\sin\left(\vartheta_1\right)\cos\left(\vartheta_2\right)\sin\left(\psi''\right)+\cos\left(\vartheta_1\right)\cos\left(\psi''\right)\right)$	$u_3^0\left(1+\cos\left(\vartheta_1\right)\right)$	$u_3^0\left(1-\sin\left(\vartheta_1\right)\cos\left(\vartheta_2\right)\sin\left(\psi'\right)+\cos\left(\vartheta_1\right)\cos\left(\psi'\right)\right)$

Appendix C

dPS_3: Angular Integration

Previously in appendix B, we discussed the parameterizations that are needed to transform the terms arising in the matrix elements into the form of the standard integral first given in equation 3.36. As already noted in equation 3.37, the solution of the standard integral reads

$$\begin{aligned}\Omega_{j,k} = 2\pi \frac{\Gamma\big(1-2\varepsilon\big)}{\Gamma\big(1-\varepsilon\big)^2} 2^{-j-k} B\big(1-\varepsilon-j, 1-\varepsilon-k\big) \\ \times {}_2F_1\left(j, k, 1-\varepsilon, \cos^2(\frac{\chi}{2})\right)\end{aligned} \tag{C.1}$$

with ${}_2F_1$ being the hypergeometric function and B denoting the beta function. In the course of our considerations, we now have to evaluate the expression given above for various choices of indices j and k and refine it to a usable form. To do this, we proceed in three steps. First, we replace the beta function by a combination of gamma functions, where we employ the relationship

$$B(x,y) = \frac{\Gamma(x)\Gamma(y)}{\Gamma(x+y)} \tag{C.2}$$

between both types of functions. Next, we address the gamma functions. It turns out that the arsing combinations can be rearranged in such a way that the gamma functions cancel out by making use of the relation

$$\Gamma(1+x) = x\Gamma(x) \tag{C.3}$$

leaving us with an expression containing combination of ε. In the last step, we need to handle the hypergeometric function. In many cases, knowing the series expansion of the function

$$\begin{aligned}{}_2F_1\left(a,b,c,z\right) =& 1 + \frac{ab}{c}z + \frac{1}{2}\frac{a(1+a)b(1+b)}{c(1+c)}z^2 \\ &+ \frac{1}{6}\frac{a(1+a)(2+a)b(1+b)(2+b)}{c(1+c)(2+c)}z^3 + \mathcal{O}(z^4)\ .\end{aligned} \tag{C.4}$$

is already sufficient in order to deal with the occurring contributions as the series terminates when one of the indices is zero or negative. However, in some instances, where the series not necessarily terminates, further properties of the hypergeometric funtion are needed. Among these properties, is the so-called Euler-transformation

$$ {}_2F_1\,(a,b,c,z) = \big(1-z\big)^{c-a-b}{}_2F_1\,(c-a,c-b,c,z), \tag{C.5} $$

which can be utilized together with the gauss series (see e.g. [5, 191]) to derive the result

$$ {}_2F_1\,(1,1,1-\varepsilon,\cos^2(\frac{\chi}{2})) \approx \left(\sin^2\big(\frac{\chi}{2}\big)\right)^{-1-\varepsilon}\left\{1+\varepsilon^2\mathrm{Li}_2\big[\cos^2\big(\frac{\chi}{2}\big)\big]\right\}, \tag{C.6} $$

with Li_2 being the dilogarithm that can be introduced by the series representation

$$ \mathrm{Li}_2(z) \equiv \sum_{n=1}^{\infty}\frac{z^n}{n^2}. \tag{C.7} $$

Finally, we want to mention one last property of the hypergeometric function, which we need to evaluate some of the arising integrals. It is a special case, where the function becomes

$$ {}_2F_1\,(a,b,b,z) = (1-z)^{-a} \tag{C.8} $$

for $c = b$. These preparations enable us to solve the angular integrals for all required cases. For example, we find that

$$ \Omega_{0,1} = -\frac{\pi}{\varepsilon} \tag{C.9} $$

$$ \Omega_{1,-1} = -\frac{2\pi(1-\varepsilon)}{\varepsilon(1-2\varepsilon)}\left\{1-\frac{1}{1-\varepsilon}\cos^2\big(\frac{\chi}{2}\big)\right\} \tag{C.10} $$

$$ \Omega_{1,1} = -\frac{\pi}{\varepsilon}\left(\sin^2\big(\frac{\chi}{2}\big)\right)^{-1-\varepsilon}\left\{1+\varepsilon^2\mathrm{Li}_2\big[\cos^2\big(\frac{\chi}{2}\big)\big]\right\} \tag{C.11} $$

just to name a few of the integrals explicitly.

Appendix D

The Plus Distribution

Against the background of our considerations concerning the real corrections, we have introduced the plus distribution, which is defined by the integral relation

$$\int_0^1 dx f(x) \big[g(x)\big]_+ \equiv \int_0^1 dx \big\{f(x) - f(1)\big\} g(x) \tag{D.1}$$

for an arbitrary function $f(x)$. In our case, we will especially encounter two possible plus distribution which read

$$\int_0^1 dw \frac{f(w)}{\big(1-w\big)_+} = \int_0^1 dw \frac{f(w) - f(1)}{1-w}, \tag{D.2}$$

$$\int_0^1 dw f(w) \left(\frac{\ln\big(1-w\big)}{1-w}\right)_+ = \int_0^1 dw \big[f(w) - f(1)\big] \frac{\ln\big(1-w\big)}{1-w}. \tag{D.3}$$

In principle, we could use the above definitions in the course of numerical considerations. However, it has to be noted, that the distributions introduced in such a way are unsuitable for us, as the w-integral usually involves a lower limit w_{min} and we therefore need another distribution, which is often denoted by the letter A instead of the $+$ in the subscript, where $A < 1$. The distribution is defined in complete analogy to the plus distribution as

$$\int_A^1 dx f(x) \big[g(x)\big]_A \equiv \int_A^1 dx \big\{f(x) - f(1)\big\} g(x) \tag{D.4}$$

and can be employed in numerical applications by setting $A = w_{\text{min}}$.

Above that, we sometimes need two identities, which we have taken from [82] and read

$$\left(\frac{1-vw}{v\big(1-w\big)}\right)_+ = \frac{1-vw}{v}\left(\frac{1}{1-w}\right)_+ \left(\frac{1-v}{v}\right) \ln\left(\frac{v}{1-v}\right) \delta\big(1-w\big), \tag{D.5}$$

$$\left(\frac{1}{v\big(1-w\big)}\right)_+ = \frac{1}{v}\left(\frac{1}{1-w}\right)_+ + \frac{1}{v} \ln\big(v\big) \delta\big(1-w\big). \tag{D.6}$$

Appendix E

Coefficients: Finite Results for $q\ell \to gX$-Channel

C_F-Part

$$A^{(0)}_{C_F,0} = -\frac{2v\left(1+v^2\right)}{(1-v)^4} \tag{E.1}$$

$$\begin{aligned}A^{(0)}_{C_F,1} = &-\frac{2v}{(1-v)^3}\big(-2v^2 + v^2\ln(1-v) - v^2\ln(v) + v - 2v\ln(1-v) + 2v\ln(v)\\ &+ 2\ln(1-v) - 2\ln(v) - 1\big)\end{aligned} \tag{E.2}$$

$$B^{(0)}_{C_F} = \frac{4vw^2\left(v^2-2v+2\right)}{(1-v)^3} \tag{E.3}$$

$$\begin{aligned}C^{(0)}_{C_F,0} = &\frac{2vw}{(1-v)^4(1-vw)^2(1-v+vw)^2}\big(6v^7w^7 - 20v^7w^6 + 25v^7w^5 - 14v^7w^4 + 3v^7w^3\\ &+ 10v^6w^5 - 24v^6w^4 + 20v^6w^3 - 6v^6w^2 - 9v^5w^5 + 22v^5w^4 - 19v^5w^3 + 2v^5w^2\\ &+ 3v^5w + 2v^4w^3 + 10v^4w^2 - 8v^4w - 2v^3w^3 - 10v^3w^2 + 8v^3w + 4v^2w^2 - 4v^2w + vw\big)\end{aligned} \tag{E.4}$$

$$\begin{aligned}C^{(0)}_{C_F,1} = &\frac{2vw}{(1-v)^4(1-vw)^2(1-v+vw)^2}\big(-2w^7v^7 + 10w^6v^7 - 13w^5v^7 + 3w^4v^7 + 3w^3v^7 - w^2v^7\\ &+ 6w^7\ln(1-v)v^7 - 16w^6\ln(1-v)v^7 + 15w^5\ln(1-v)v^7 - 6w^4\ln(1-v)v^7\\ &+ w^3\ln(1-v)v^7 + 6w^7\ln(v)v^7 - 16w^6\ln(v)v^7 + 15w^5\ln(v)v^7 - 6w^4\ln(v)v^7\\ &+ w^3\ln(v)v^7 + 6w^7\ln(1-w)v^7 - 12w^6\ln(1-w)v^7 + 5w^5\ln(1-w)v^7 + 2w^4\ln(1-w)v^7\\ &- w^3\ln(1-w)v^7 + 12w^7\ln(w)v^7 - 40w^6\ln(w)v^7 + 50w^5\ln(w)v^7 - 28w^4\ln(w)v^7\\ &+ 6w^3\ln(w)v^7 - 12w^7\ln(1-vw)v^7 + 32w^6\ln(1-vw)v^7 - 30w^5\ln(1-vw)v^7\\ &+ 12w^4\ln(1-vw)v^7 - 2w^3\ln(1-vw)v^7 - 12w^7\ln(1-v+vw)v^7 + 40w^6\ln(1-v+vw)v^7\\ &- 50w^5\ln(1-v+vw)v^7 + 28w^4\ln(wv-v+1)v^7 - 6w^3\ln(1-v+vw)v^7 + 8w^6v^6\\ &- 30w^5v^6 + 49w^4v^6 - 26w^3v^6 - 3w^2v^6 + 2wv^6 - 8w^6\ln(1-v)v^6 + 30w^5\ln(1-v)v^6\\ &- 32w^4\ln(1-v)v^6 + 12w^3\ln(1-v)v^6 - 2w^2\ln(1-v)v^6 - 8w^6\ln(v)v^6 + 30w^5\ln(v)v^6\\ &- 32w^4\ln(v)v^6 + 12w^3\ln(v)v^6 - 2w^2\ln(v)v^6 - 12w^6\ln(1-w)v^6 + 38w^5\ln(1-w)v^6\\ &- 29w^4\ln(1-w)v^6 + 2w^3\ln(1-w)v^6 + w^2\ln(1-w)v^6 - 4w^6\ln(w)v^6 + 28w^5\ln(w)v^6\\ &- 51w^4\ln(w)v^6 + 38w^3\ln(w)v^6 - 11w^2\ln(w)v^6 + 16w^6\ln(1-vw)v^6 - 60w^5\ln(1-vw)v^6\\ &+ 63w^4\ln(1-vw)v^6 - 22w^3\ln(1-vw)v^6 + 3w^2\ln(1-vw)v^6 - 20w^5\ln(1-v+vw)v^6\\ &+ 49w^4\ln(1-v+vw)v^6 - 42w^3\ln(wv-v+1)v^6 + 13w^2\ln(1-v+vw)v^6 - 3w^5v^5 + w^4v^5\\ &- 36w^3v^5 + 47w^2v^5 - 6wv^5 - 9w^5\ln(1-v)v^5 + 15w^3\ln(1-v)v^5 - 4w^2\ln(1-v)v^5\\ &+ w\ln(1-v)v^5 - 9w^5\ln(v)v^5 + 13w^3\ln(v)v^5 - w\ln(v)v^5 - 7w^5\ln(1-w)v^5\\ &- 20w^4\ln(1-w)v^5 + 35w^3\ln(1-w)v^5 - 2w^2\ln(1-w)v^5 - w\ln(1-w)v^5 - 16w^5\ln(w)v^5\end{aligned}$$

$$
\begin{aligned}
&+ 34w^4\ln(w)v^5 - 32w^3\ln(w)v^5 + 12w^2\ln(w)v^5 + 2w\ln(w)v^5 + 18w^5\ln(1-vw)v^5\\
&+ 2w^4\ln(1-vw)v^5 - 34w^3\ln(1-vw)v^5 + 8w^2\ln(1-vw)v^5 + 18w^5\ln(1-v+vw)v^5\\
&- 46w^4\ln(1-v+vw)v^5 + 42w^3\ln(1-v+vw)v^5 - 4w^2\ln(wv-v+1)v^5\\
&- 8w\ln(1-v+vw)v^5 - v^5 - 7w^4v^4 + 52w^3v^4 - 52w^2v^4 - 4wv^4 + 16w^4\ln(1-v)v^4\\
&- 26w^3\ln(1-v)v^4 + 2w^2\ln(1-v)v^4 - 4w\ln(1-v)v^4 + 16w^4\ln(v)v^4 - 22w^3\ln(v)v^4\\
&- 9w^2\ln(v)v^4 + 2w\ln(v)v^4 + \ln(v)v^4 + 23w^4\ln(1-w)v^4 - 24w^3\ln(1-w)v^4\\
&- 24w^2\ln(1-w)v^4 + 4w\ln(1-w)v^4 + 9w^4\ln(w)v^4 - 2w^3\ln(w)v^4 - 12w\ln(w)v^4\\
&+ 2\ln(w)v^4 - 33w^4\ln(1-vw)v^4 + 54w^3\ln(1-vw)v^4 + w^2\ln(1-vw)v^4 + 2w\ln(1-vw)v^4\\
&- \ln(1-vw)v^4 + w^4\ln(wv-v+1)v^4 - 6w^3\ln(1-v+vw)v^4 - 25w^2\ln(1-v+vw)v^4\\
&+ 22w\ln(1-v+vw)v^4 + \ln(1-v+vw)v^4 + 4v^4 - 9w^3v^3 + 4w^2v^3 + 16wv^3\\
&+ 14w^2\ln(1-v)v^3 + 4w\ln(1-v)v^3 + 2\ln(1-v)v^3 - 2w^3\ln(v)v^3 + 24w^2\ln(v)v^3\\
&- 2w\ln(v)v^3 - 2\ln(v)v^3 - 6w^3\ln(1-w)v^3 + 38w^2\ln(1-w)v^3 - 8w^3\ln(w)v^3\\
&+ 8w^2\ln(w)v^3 + 16w\ln(w)v^3 - 4\ln(w)v^3 - 34w^2\ln(1-vw)v^3 - 2w\ln(1-vw)v^3\\
&+ 4w^3\ln(1-v+vw)v^3 + 26w^2\ln(1-v+vw)v^3 - 22w\ln(1-v+vw)v^3\\
&- 4\ln(wv-v+1)v^3 - 8v^3 + 5w^2v^2 - 6wv^2 - 8w^2\ln(1-v)v^2 - 4w\ln(1-v)v^2\\
&- 4\ln(1-v)v^2 - 11w^2\ln(v)v^2 - 2w\ln(v)v^2 + 2\ln(v)v^2 - 13w^2\ln(1-w)v^2\\
&- 8w\ln(1-w)v^2 - 5w^2\ln(w)v^2 - 12w\ln(w)v^2 + 4\ln(w)v^2 + 18w^2\ln(1-vw)v^2\\
&+ 6w\ln(1-vw)v^2 + 2\ln(1-vw)v^2 - 10w^2\ln(1-v+vw)v^2 + 10w\ln(1-v+vw)v^2\\
&+ 6\ln(1-v+vw)v^2 + 10v^2 - 2wv + 3w\ln(1-v)v + 2\ln(1-v)v + 3w\ln(v)v - 2\ln(v)v\\
&+ 5w\ln(1-w)v + 6w\ln(w)v - 4\ln(w)v - 6w\ln(1-vw)v - 2w\ln(wv-v+1)v\\
&- 4\ln(1-v+vw)v - 7v + \ln(v) + 2\ln(w) - \ln(1-vw) + \ln(wv-v+1) + 2\big)
\end{aligned}
\tag{E.5}
$$

$$
\begin{aligned}
C^{(1)}_{C_F,1} = {}& \frac{2vw}{(1-v)^4(1-vw)(1-v+vw)}\big(4w^5v^5 - 10w^4v^5 + 12w^3v^5 - 8w^2v^5 + 2wv^5\\
&+ 4w^5\ln(1-v)v^5 - 10w^4\ln(1-v)v^5 + 10w^3\ln(1-v)v^5 - 5w^2\ln(1-v)v^5 + w\ln(1-v)v^5\\
&+ 4w^5\ln(v)v^5 - 10w^4\ln(v)v^5 + 10w^3\ln(v)v^5 - 5w^2\ln(v)v^5 + w\ln(v)v^5 + 4w^5\ln(1-w)v^5\\
&- 8w^4\ln(1-w)v^5 + 6w^3\ln(1-w)v^5 - 2w^2\ln(1-w)v^5 + 4w^5\ln(w)v^5 - 12w^4\ln(w)v^5 + 14w^3\ln(w)v^5\\
&- 8w^2\ln(w)v^5 + 2w\ln(w)v^5 - 4w^5\ln(1-vw)v^5 + 8w^4\ln(1-vw)v^5 - 6w^3\ln(1-vw)v^5\\
&+ 2w^2\ln(1-vw)v^5 - 4w^5\ln(1-v+vw)v^5 + 12w^4\ln(1-v+vw)v^5 - 14w^3\ln(wv-v+1)v^5\\
&+ 8w^2\ln(1-v+vw)v^5 - 2w\ln(1-v+vw)v^5 + 4w^4v^4 - 12w^3v^4 + 10w^2v^4 + 2wv^4 - 4w^4\ln(1-v)v^4\\
&+ 8w^3\ln(1-v)v^4 - 5w^2\ln(1-v)v^4 + 3w\ln(1-v)v^4 - \ln(1-v)v^4 - 4w^4\ln(v)v^4 + 8w^3\ln(v)v^4\\
&- 6w^2\ln(v)v^4 + 4w\ln(v)v^4 - \ln(v)v^4 - 4w^4\ln(1-w)v^4 + 4w^3\ln(1-w)v^4 + 2w^2\ln(1-w)v^4\\
&- 4w^4\ln(w)v^4 + 8w^3\ln(w)v^4 - 9w^2\ln(w)v^4 + 7w\ln(w)v^4 - 2\ln(w)v^4 + 8w^4\ln(1-vw)v^4\\
&- 16w^3\ln(1-vw)v^4 + 11w^2\ln(1-vw)v^4 - 5w\ln(1-vw)v^4 - 2w\ln(1-v+vw)v^4\\
&+ 2\ln(1-v+vw)v^4 - 2v^4 + 2w^3v^3 + 2w^2v^3 - 12wv^3 + 4w^3\ln(1-v)v^3 - 9w^2\ln(1-v)v^3\\
&- w\ln(1-v)v^3 + 2\ln(1-v)v^3 + 4w^3\ln(v)v^3 - 7w^2\ln(v)v^3 + 6w^3\ln(1-w)v^3 - 9w^2\ln(1-w)v^3\\
&- 4w\ln(1-w)v^3 + \ln(1-w)v^3 + 6w^3\ln(w)v^3 - 8w^2\ln(w)v^3 - w\ln(w)v^3 - 6w^3\ln(1-vw)v^3\\
&+ 15w^2\ln(1-vw)v^3 - 3w\ln(1-vw)v^3 + 3\ln(1-vw)v^3 - 2w^3\ln(1-v+vw)v^3\\
&+ 2w^2\ln(1-v+vw)v^3 + 6w\ln(1-v+vw)v^3 - 6\ln(1-v+vw)v^3 + 4v^3 - 4w^2v^2 + 10wv^2\\
&+ 3w^2\ln(1-v)v^2 + 9w\ln(1-v)v^2 - 4\ln(1-v)v^2 + 2w^2\ln(v)v^2 + 4w\ln(v)v^2 + w^2\ln(1-w)v^2\\
&+ 11w\ln(1-w)v^2 + w^2\ln(w)v^2 + 7w\ln(w)v^2 - 4w^2\ln(1-vw)v^2 - 10w\ln(1-vw)v^2 - 2\ln(1-vw)v^2\\
&- 2w^2\ln(1-v+vw)v^2 - 8w\ln(1-v+vw)v^2 + 8\ln(1-v+vw)v^2 - 2v^2 - 2wv - 8w\ln(1-v)v\\
&+ 2\ln(1-v)v - 5w\ln(v)v - 7w\ln(1-w)v - 3\ln(1-w)v - 7w\ln(w)v + 10w\ln(1-vw)v + 3\ln(1-vw)v\\
&+ 6w\ln(1-v+vw)v - 6\ln(1-v+vw)v + \ln(1-v) + \ln(v) + 2\ln(1-w) + 2\ln(w) - 4\ln(1-vw)\\
&+ 2\ln(1-v+vw)\big)
\end{aligned}
\tag{E.6}
$$

$$
\begin{aligned}
C^{(2)}_{C_F,1} = {}& -\frac{vw}{(1-v)^4(1-vw)}\big(8v^4w^4 - 10v^4w^3 + 4v^4w^2 - 16v^3w^3 + 2v^3w^3\ln(1-w) - 2v^3w^3\ln(w)\\
&+ 14v^3w^2 - 4v^3w^2\ln(1-w) + 4v^3w^2\ln(w) - 4v^3w + v^3w\ln(1-v) + 3v^3w\ln(1-w) - v^3w\ln(w)\\
&+ v^3w\ln(1-vw) - 2v^3w\ln(1-v+vw) + 10v^2w^2 + 2v^2w^2\ln(1-v) + 2v^2w^2\ln(v) + 4v^2w^2\ln(w)\\
&- 4v^2w^2\ln(1-vw) - 4v^2w - 4v^2w\ln(1-v) - 2v^2w\ln(v) + 2v^2w\ln(1-w) - 2v^2\ln(1-w)\\
&- 6v^2w\ln(w) + 2v^2\ln(w) + 2v^2w\ln(1-vw) - v^2\ln(1-vw) + 4v^2w\ln(1-v+vw)
\end{aligned}
$$

$$+ 2v^2\ln(1-v+vw) + v^2 - v^2\ln(1-v) + v^2\ln(v) - 2vw - vw\ln(1-v) - 2vw\ln(v) - vw\ln(1-w)$$
$$- 3vw\ln(w) + 5vw\ln(1-vw) - 2v\ln(1-vw) - 2vw\ln(1-v+vw) - 4v\ln(1-v+vw)$$
$$- \ln(1-vw) + 2\ln(1-v+vw) - 2v + 4v\ln(1-v) - \ln(1-v) + \ln(v) + 2\ln(w) + 1\Big) \tag{E.7}$$

C_A-Part

$$C^{(1)}_{C_A,0} = -\frac{vw\left(v^2w^2 - 2vw + 2\right)\left(2v^2w^2 - 2v^2w + v^2 - 2vw + 1\right)}{(1-v)^4(1-vw)^2} \tag{E.8}$$

$$C^{(1)}_{C_A,1} = \frac{vw}{(1-v)^4(1-vw)^2(1-v+vw)}\big(- 2w^5v^5 + 4w^4v^5 - 2w^3v^5 + 2w^5\ln(1-v)v^5$$
$$- 2w^4\ln(1-v)v^5 + 2w^5\ln(v)v^5 - 4w^4\ln(v)v^5 + 3w^3\ln(v)v^5 - w^2\ln(v)v^5 + 2w^4\ln(1-w)v^5$$
$$- 4w^3\ln(1-w)v^5 + 2w^2\ln(1-w)v^5 + 2w^5\ln(w)v^5 - 4w^4\ln(w)v^5 + 4w^3\ln(w)v^5 - 2w^2\ln(w)v^5$$
$$- 4w^5\ln(1-vw)v^5 + 8w^4\ln(1-vw)v^5 - 7w^3\ln(1-vw)v^5 + 3w^2\ln(1-vw)v^5 - 2w^4\ln(1-v+vw)v^5$$
$$+ 4w^3\ln(1-v+vw)v^5 - 2w^2\ln(1-v+vw)v^5 + 5w^4v^4 - 12w^3v^4 + 3w^2v^4 + 2wv^4 - 6w^4\ln(1-v)v^4$$
$$+ 8w^3\ln(1-v)v^4 - 4w^4\ln(v)v^4 + 8w^3\ln(v)v^4 - 5w^2\ln(v)v^4 + 2w\ln(v)v^4 - 2w^4\ln(1-w)v^4$$
$$+ 6w^2\ln(1-w)v^4 - 4w\ln(1-w)v^4 - 4w^4\ln(w)v^4 + 8w^3\ln(w)v^4 - 6w^2\ln(w)v^4 + 4w\ln(w)v^4$$
$$+ 8w^4\ln(1-vw)v^4 - 16w^3\ln(1-vw)v^4 + 11w^2\ln(1-vw)v^4 - 6w\ln(1-vw)v^4$$
$$+ 2w^4\ln(1-v+vw)v^4 - 6w^2\ln(1-v+vw)v^4 + 4w\ln(1-v+vw)v^4 - w^4v^3 - w^3v^3 + 21w^2v^3$$
$$- 13wv^3 + 6w^3\ln(1-v)v^3 - 14w^2\ln(1-v)v^3 + 3w^3\ln(v)v^3 - 9w^2\ln(v)v^3 + 4w\ln(v)v^3 - 2\ln(v)v^3$$
$$+ 4w^3\ln(1-w)v^3 - 10w^2\ln(1-w)v^3 + 3w\ln(1-w)v^3 + \ln(1-w)v^3 + 2w^3\ln(w)v^3 - 6w^2\ln(w)v^3$$
$$- 2\ln(w)v^3 - 5w^3\ln(1-vw)v^3 + 13w^2\ln(1-vw)v^3 - w\ln(1-vw)v^3 + 3\ln(1-vw)v^3$$
$$- 4w^3\ln(1-v+vw)v^3 + 8w^2\ln(1-v+vw)v^3 - 2\ln(1-v+vw)v^3 + w^3v^2 - 13w^2v^2 + wv^2$$
$$+ 2w^2\ln(1-v)v^2 + 12w\ln(1-v)v^2 + 3w^2\ln(v)v^2 + 2w\ln(v)v^2 + 2\ln(v)v^2 + 2w^2\ln(1-w)v^2$$
$$+ 4w\ln(1-w)v^2 - \ln(1-w)v^2 + 2w^2\ln(w)v^2 + 4w\ln(w)v^2 + 2\ln(w)v^2 - 3w^2\ln(1-vw)v^2$$
$$- 10w\ln(1-vw)v^2 - 3\ln(1-vw)v^2 - 8w\ln(wv-v+1)v^2 + 2\ln(1-v+vw)v^2 + 4v^2 + w^2v + 7wv$$
$$- 8w\ln(1-v)v - 4\ln(1-v)v - 4w\ln(v)v - 2\ln(v)v - 3w\ln(1-w)v - \ln(1-w)v - 4w\ln(w)v$$
$$- 2\ln(w)v + 9w\ln(1-vw)v + 5\ln(1-vw)v + 4w\ln(1-v+vw)v + 2\ln(1-v+vw)v - 4v - w$$
$$+ 4\ln(1-v) + 2\ln(v) + \ln(1-w) + 2\ln(w) - 5\ln(1-vw) - 2\ln(1-v+vw)\big) \tag{E.9}$$

$$C^{(0)}_{C_A,1} = -\frac{vw}{(1-v)^4(1-vw)^2(1-v+vw)}\big(4w^5v^5 - 8w^4v^5 + 5w^3v^5 - w^2v^5 - 2w^4\ln(1-v)v^5$$
$$+ 2w^3\ln(1-v)v^5 - w^3\ln(1-w)v^5 + w^2\ln(1-w)v^5 - 2w^4\ln(w)v^5 + 3w^3\ln(w)v^5 - w^2\ln(w)v^5$$
$$+ 2w^4\ln(1-vw)v^5 - 3w^3\ln(1-vw)v^5 + w^2\ln(1-vw)v^5 + w^3\ln(1-v+vw)v^5$$
$$- w^2\ln(1-v+vw)v^5 - 5w^4v^4 + 11w^3v^4 - 9w^2v^4 + 3wv^4 + 2w^4\ln(1-v)v^4 - 4w^2\ln(1-v)v^4$$
$$+ w^2\ln(1-w)v^4 - 2w\ln(1-w)v^4 + 2w^4\ln(w)v^4 - 5w^2\ln(w)v^4 + 2w\ln(w)v^4 - 2w^4\ln(1-vw)v^4$$
$$+ 5w^2\ln(1-vw)v^4 - 2w\ln(1-vw)v^4 - w^2\ln(1-v+vw)v^4 + 2w\ln(1-v+vw)v^4 + w^4v^3$$
$$- 3w^3v^3 + 4w^2v^3 - 3wv^3 + 4w^2\ln(1-v)v^3 + 2w\ln(1-v)v^3 + 2w^3\ln(v)v^3 - 4w^2\ln(v)v^3$$
$$+ 3w\ln(v)v^3 - \ln(v)v^3 + w^3\ln(1-w)v^3 - 3w^2\ln(1-w)v^3 + 4w\ln(1-w)v^3 + w^3\ln(w)v^3$$
$$+ w^2\ln(w)v^3 + 4w\ln(w)v^3 - 2\ln(w)v^3 - w^3\ln(1-vw)v^3 - 3w^2\ln(1-vw)v^3 - w\ln(1-vw)v^3$$
$$+ \ln(1-vw)v^3 - w^3\ln(1-v+vw)v^3 + w^2\ln(1-v+vw)v^3 - w\ln(1-v+vw)v^3 - \ln(1-v+vw)v^3$$
$$- v^3 - w^3v^2 + 3w^2v^2 + wv^2 - 4w^2\ln(1-v)v^2 + \ln(v)v^2 + w^2\ln(1-w)v^2 - 2w\ln(1-w)v^2$$
$$- 3w^2\ln(w)v^2 - 2w\ln(w)v^2 + 2\ln(w)v^2 + 5w^2\ln(1-vw)v^2 - 2w\ln(1-vw)v^2 - \ln(1-vw)v^2$$
$$+ w^2\ln(1-v+vw)v^2 - 2w\ln(1-v+vw)v^2 + \ln(1-v+vw)v^2 + 3v^2 - w^2v - 2wv - 2\ln(1-v)v$$
$$- w\ln(v)v - \ln(v)v - 2\ln(w)v + w\ln(1-vw)v + 3\ln(1-vw)v + w\ln(1-v+vw)v$$
$$+ \ln(1-v+vw)v - 3v + w + 2\ln(1-v) + \ln(v) + 2\ln(w) - 3\ln(1-vw) - \ln(1-v+vw) + 1\big) \tag{E.10}$$

$$
\begin{aligned}
C^{(2)}_{C_A,1} = &-\frac{vw}{2(1-v)^4(1-vw)^2(1-v+vw)}\big(- 4w^5v^5 + 8w^4v^5 - 5w^3v^5 + w^2v^5 \\
&+ w^3\ln(1-v)v^5 - w^2\ln(1-v)v^5 + 2w^5\ln(1-w)v^5 - 6w^4\ln(1-w)v^5 + 7w^3\ln(1-w)v^5 \\
&- 3w^2\ln(1-w)v^5 - 2w^5\ln(w)v^5 + 6w^4\ln(w)v^5 - 5w^3\ln(w)v^5 + w^2\ln(w)v^5 \\
&- 2w^4\ln(1-vw)v^5 + 3w^3\ln(1-vw)v^5 - w^2\ln(1-vw)v^5 + 2w^4\ln(1-v+vw)v^5 \\
&- 4w^3\ln(1-v+vw)v^5 + 2w^2\ln(1-v+vw)v^5 + 4w^4v^4 - 9w^3v^4 + 9w^2v^4 - 3wv^4 \\
&- w^2\ln(1-v)v^4 + 2w\ln(1-v)v^4 - 2w^4\ln(1-w)v^4 + 8w^3\ln(1-w)v^4 - 11w^2\ln(1-w)v^4 \\
&+ 6w\ln(1-w)v^4 + 2w^4\ln(w)v^4 - 8w^3\ln(w)v^4 + 9w^2\ln(w)v^4 - 2w\ln(w)v^4 + 2w^4\ln(1-vw)v^4 \\
&- 5w^2\ln(1-vw)v^4 + 2w\ln(1-vw)v^4 - 2w^4\ln(1-v+vw)v^4 + 6w^2\ln(1-v+vw)v^4 \\
&- 4w\ln(1-v+vw)v^4 + 2w^3v^3 - 8w^2v^3 + 3wv^3 - 3w^3\ln(1-v)v^3 + 3w^2\ln(1-v)v^3 \\
&- w\ln(1-v)v^3 - \ln(1-v)v^3 - 2w^3\ln(v)v^3 + 4w^2\ln(v)v^3 - 3w\ln(v)v^3 + \ln(v)v^3 - 3w^3\ln(1-w)v^3 \\
&+ 5w^2\ln(1-w)v^3 - 2w\ln(1-w)v^3 - 2\ln(1-w)v^3 - w^3\ln(w)v^3 + 3w^2\ln(w)v^3 - 6w\ln(w)v^3 \\
&+ 2\ln(w)v^3 + w^3\ln(1-vw)v^3 + 3w^2\ln(1-vw)v^3 + w\ln(1-vw)v^3 - \ln(1-vw)v^3 \\
&+ 4w^3\ln(1-v+vw)v^3 - 8w^2\ln(1-v+vw)v^3 + 2\ln(1-v+vw)v^3 + v^3 + 2w^2v^2 + wv^2 \\
&+ 3w^2\ln(1-v)v^2 - 6w\ln(1-v)v^2 + \ln(1-v)v^2 - \ln(v)v^2 + w^2\ln(1-w)v^2 - 2w\ln(1-w)v^2 \\
&+ 2\ln(1-w)v^2 - w^2\ln(w)v^2 + 2w\ln(w)v^2 - 2\ln(w)v^2 - 5w^2\ln(1-vw)v^2 + 2w\ln(1-vw)v^2 \\
&+ \ln(1-vw)v^2 + 8w\ln(1-v+vw)v^2 - 2\ln(1-v+vw)v^2 - 3v^2 - wv + 3w\ln(1-v)v \\
&+ 3\ln(1-v)v + w\ln(v)v + \ln(v)v + 2w\ln(w)v + 2\ln(w)v - w\ln(1-vw)v - 3\ln(1-vw)v \\
&- 4w\ln(1-v+vw)v - 2\ln(1-v+vw)v + 3v - 3\ln(1-v) - \ln(v) - 2\ln(w) + 3\ln(1-vw) \\
&+ 2\ln(wv-v+1) - 1\big)
\end{aligned}
\tag{E.11}
$$

SFP-Part

$$
C^{(0)}_{1/C_A,0} = -\frac{vw\left(2v^2w^2 - 2v^2w + v^2 - 2vw + 1\right)}{(1-v)^4}
\tag{E.12}
$$

$$
\begin{aligned}
C^{(0)}_{1/C_A,1} = &-\frac{w}{(1-v)^4(1-vw)^2(1-v+vw)}\big(2w^5v^6 - 4w^4v^6 + 3w^3v^6 - w^2v^6 \\
&+ 2w^5\ln(w)v^6 - 4w^4\ln(w)v^6 + 3w^3\ln(w)v^6 - w^2\ln(w)v^6 + 2w^5v^5 - 6w^4v^5 + 5w^3v^5 \\
&- w^2v^5 + wv^5 - 2w^5\ln(1-v)v^5 + 2w^3\ln(1-v)v^5 - 2w^4\ln(1-w)v^5 + 3w^3\ln(1-w)v^5 \\
&- w^2\ln(1-w)v^5 - 2w^5\ln(w)v^5 - 2w^4\ln(w)v^5 + 7w^3\ln(w)v^5 - 4w^2\ln(w)v^5 + 2w\ln(w)v^5 \\
&+ 4w^5\ln(1-vw)v^5 - 6w^4\ln(1-vw)v^5 + 4w^3\ln(1-vw)v^5 - 2w^2\ln(1-vw)v^5 \\
&+ 2w^4\ln(1-v+vw)v^5 - 3w^3\ln(1-v+vw)v^5 + w^2\ln(1-v+vw)v^5 - 6w^4v^4 + 16w^3v^4 - 13w^2v^4 \\
&+ wv^4 + 8w^4\ln(1-v)v^4 - 8w^3\ln(1-v)v^4 - 4w^2\ln(1-v)v^4 + 2w^4\ln(1-w)v^4 - 5w^2\ln(1-w)v^4 \\
&+ 2w\ln(1-w)v^4 + 6w^4\ln(w)v^4 - 7w^3\ln(w)v^4 - 4w^2\ln(w)v^4 - w\ln(w)v^4 - \ln(w)v^4 \\
&- 10w^4\ln(1-vw)v^4 + 16w^3\ln(1-vw)v^4 - 6w^2\ln(1-vw)v^4 + 4w\ln(1-vw)v^4 - 2w^4\ln(1-v+vw)v^4 \\
&+ 5w^2\ln(1-v+vw)v^4 - 2w\ln(1-v+vw)v^4 - v^4 + 2w^4v^3 - 4w^3v^3 - 5w^2v^3 + 7wv^3 \\
&- 6w^3\ln(1-v)v^3 + 18w^2\ln(1-v)v^3 + 2w\ln(1-v)v^3 - 3w^3\ln(1-w)v^3 + 7w^2\ln(1-w)v^3 \\
&+ w\ln(1-w)v^3 - \ln(1-w)v^3 - 3w^3\ln(w)v^3 + 14w^2\ln(w)v^3 + 3w\ln(w)v^3 + 2\ln(w)v^3 \\
&+ 4w^3\ln(1-vw)v^3 - 16w^2\ln(1-vw)v^3 - 2\ln(1-vw)v^3 + 3w^3\ln(1-v+vw)v^3 \\
&- 7w^2\ln(1-v+vw)v^3 - w\ln(1-v+vw)v^3 + \ln(1-v+vw)v^3 + 2v^3 - 2w^3v^2 + 12w^2v^2 - 4wv^2 \\
&- 6w^2\ln(1-v)v^2 - 12w\ln(1-v)v^2 - w^2\ln(1-w)v^2 - 6w\ln(1-w)v^2 + \ln(1-w)v^2 - 5w^2\ln(w)v^2 \\
&- 9w\ln(w)v^2 - 2\ln(w)v^2 + 8w^2\ln(1-vw)v^2 + 8w\ln(1-vw)v^2 + 2\ln(1-vw)v^2 + w^2\ln(1-v+vw)v^2 \\
&+ 6w\ln(1-v+vw)v^2 - \ln(1-v+vw)v^2 - 4v^2 - 2w^2v - 5wv + 8w\ln(1-v)v + 2\ln(1-v)v \\
&+ 3w\ln(1-w)v + \ln(1-w)v + 5w\ln(w)v + 2\ln(w)v - 8w\ln(1-vw)v - 2\ln(1-vw)v \\
&- 3w\ln(1-v+vw)v - \ln(1-v+vw)v + 4v + 2w - 2\ln(1-v) - \ln(1-w) - \ln(w) + 2\ln(1-vw) \\
&+ \ln(1-v+vw) - 1\big)
\end{aligned}
\tag{E.13}
$$

Appendix F

Schematic Results for $q\ell \to qX$-Channel

SGP, C_F-Part

$$
\begin{aligned}
\sigma^{\rm SGP}_{C_F} =& G_F(x,x)\Big\{ [A^{(0)}_{C_F,0} \ln(\frac{\mu^2}{s}) + A^{(0)}_{C_F,1} \ln(\frac{m_\ell^2}{s}) + A^{(0)}_{C_F,2}]\delta(1-w) + \frac{4w^2(1+v^2)}{(1-v)^4}\Big(\frac{1}{1-w}\Big)_+ \\
&+ C^{(0)}_{C_F,0} \ln(\frac{\mu^2}{s}) + C^{(0)}_{C_F,1} \ln(\frac{m_\ell^2}{s}) + C^{(0)}_{C_F,2}\Big\} + x\frac{dG_F(x,x)}{dx}C^{(1)}_{C_F,0} \\
&+ \Big(G_F(x,x) - x\frac{dG_F(x,x)}{dx}\Big)\Big\{[A^{(2)}_{C_F,0} \ln(\frac{\mu^2}{s}) + A^{(2)}_{C_F,1}]\delta(1-w) + 8\frac{w^2(1+v^2)}{(1-v)^4} \\
&\times \Big[-\ln\Big(\frac{\mu^2(1-v)v}{s}\Big)\Big(\frac{1}{1-w}\Big)_+ + 2\Big(\frac{\ln(1-w)}{1-w}\Big)_+\Big] + C^{(2)}_{C_F,0}\Big\}
\end{aligned}
\tag{F.1}
$$

SGP, C_A-Part

$$
\begin{aligned}
\sigma^{\rm SGP}_{C_A} =& G_F(x,x)\Big\{ [A^{(0)}_{C_A,0} \ln(\frac{m_\ell^2}{s}) + A^{(0)}_{C_A,1}]\delta(1-w) + C^{(0)}_{C_A,0} \ln(\frac{m_\ell^2}{s}) + C^{(0)}_{C_A,1}\Big\} \\
&+ x\frac{dG_F(x,x)}{dx}C^{(1)}_{C_A,0} + \Big(G_F(x,x) - x\frac{dG_F(x,x)}{dx}\Big) + \Big\{[A^{(2)}_{C_A,0} \ln(\frac{\mu^2}{s}) \\
&+ A^{(2)}_{C_A,1}]\delta(1-w) - 2\frac{w^2(1+v^2)}{(1-v)^4}\Big(\frac{1}{1-w}\Big)_+ + C^{(2)}_{C_F,0}\Big\} \\
&+ g_1\big(G_F(x,xw) - G_F(x,x)\big) + g_2\frac{\partial}{\partial w}\frac{G_F(x,xw) - G_F(x,x)}{1-w}
\end{aligned}
\tag{F.2}
$$

SFP-Part

$$
\begin{aligned}
\sigma^{\rm SGP}_{1/C_A} =& G_F(0,x)\Big\{\frac{1+v^2}{(1-v)^4}\Big[\ln\Big(\frac{\mu^2}{s(1-v)v}\Big) - 2w^2\Big(\frac{1}{1-w}\Big)_+\Big] + C^{(0)}_{1/C_A,0}\ln\Big(\frac{m_\ell^2}{s}\Big) + C^{(0)}_{1/C_A,1}\Big\} \\
&+ G_F(0,-x)\Big\{C^{(1)}_{1/C_A,0}\ln\Big(\frac{m_\ell^2}{s}\Big) + C^{(1)}_{1/C_A,1}\Big\} + G_F(xw,-x(1-w))\Big\{-\frac{1+v^2}{(1-v)^4}\ln\Big(\frac{\mu^2}{s}\Big) \\
&+ C^{(2)}_{1/C_A,1}\Big\} + \frac{\partial G_F(xw,-x(1-w))}{\partial w}\Big\{C^{(3)}_{1/C_A,0}\ln\Big(\frac{\mu^2}{s}\Big) + C^{(3)}_{1/C_A,1}\Big\}
\end{aligned}
\tag{F.3}
$$

Apart from the SFP contribution with the colour factor $-\frac{1}{2C_A}$, which we presented in the last equation, we find two additional soft-fermion pole pieces, which are remnants from the treatment of the hard poles. The first one carries the colour factor C_F and reads

$$\begin{aligned}\sigma_{C_F}^{\mathrm{SGP}} =& G_F(x,0)\frac{2vw\left(2v^2w^2-2v^2w+v^2-2vw+1\right)}{(1-v)^4(1-vw)} \\ &\times\left(\ln\left(\frac{m_\ell^2}{s}\right)+v^2w^2-vw+\ln(w)+1\right),\end{aligned} \tag{F.4}$$

while the second piece is proportional to the colour factor C_A. It is given by

$$\begin{aligned}\sigma_{C_A}^{\mathrm{SGP}} =& -G_F(x,0)\frac{\left(2v^2w^2-2v^2w+v^2-2vw+1\right)}{(1-v)^4(1-vw)} \\ &\left(\ln\left(\frac{m_\ell^2}{s}\right)+v^2w^2-vw+\ln(w)+1\right)\end{aligned} \tag{F.5}$$

and we thus find that

$$\sigma_{C_F}^{\mathrm{SGP}} = -2vw\sigma_{C_A}^{\mathrm{SGP}}. \tag{F.6}$$

Triangle-Diagrams

$$\sigma^{Tr} = \left(G_F\big(0,x\big)-G_F\big(0,-x\big)\right)\left\{C_0\ln\left(\frac{m_\ell^2}{s}\right)+C_1\right\} \tag{F.7}$$

Appendix G

Coefficients for $q\ell \to qX$-Channel

SGP, C_F-Part

$$A^{(0)}_{C_F,0} = \frac{4\left(v^3 + 3v - 2\right)}{(1-v)^4} \tag{G.1}$$

$$A^{(0)}_{C_F,1} = -\frac{2\left(v^2 + 1\right)}{(1-v)^3} \tag{G.2}$$

$$A^{(0)}_{C_F,2} = \frac{2\left(4v^3 - 13v^2 + 2v^2\ln(1-v) + 10v + 2\ln(1-v) - 7\right)}{(1-v)^4} \tag{G.3}$$

$$C^{(0)}_{C_F,0} = -\frac{2\left(6v^4w^4 - 8v^4w^3 + 3v^4w^2 + 12v^3w^3 - 8v^3w^2 + 9v^2w^2 + v^2 + 1\right)}{(1-v)^4} \tag{G.4}$$

$$\begin{aligned} C^{(0)}_{C_F,1} = &-\frac{2}{(1-v)^4(1-vw)^2}\big(4v^5w^5 - 2v^5w^4 - 8v^4w^4 + 4v^4w^3 - v^4w^2 + 4v^3w^3 \\ &+ 2v^3w^2 - 2v^3w - v^2w^2 + v^2 - 2vw + 1\big) \end{aligned} \tag{G.5}$$

$$\begin{aligned} C^{(0)}_{C_F,2} = &-\frac{2}{(1-v)^4(1-vw)^2(1-v+vw)}\big(- 2v^7w^7 + 6v^7w^7\ln(w) - 12v^7w^7\ln(1-v+vw) \\ &+ 2v^7w^6 - 14v^7w^6\ln(w) + 28v^7w^6\ln(1-v+vw) + 2v^7w^5 + 11v^7w^5\ln(w) - 22v^7w^5\ln(vw-v+1) \\ &- 3v^7w^4 - 3v^7w^4\ln(w) + 6v^7w^4\ln(1-v+vw) + v^7w^3 + 10v^6w^6 + 10v^6w^6\ln(w) \\ &- 12v^6w^6\ln(1-v+vw) - 24v^6w^5 - 6v^6w^5\ln(w) + 13v^6w^4 - 9v^6w^4\ln(w) + 22v^6w^4\ln(1-v+vw) \\ &+ 6v^6w^3\ln(w) - 12v^6w^3\ln(1-v+vw) - 2v^6w^2 - 10v^5w^5 - 13v^5w^5\ln(w) + 18v^5w^5\ln(1-v+vw) \\ &+ 24v^5w^4 + 35v^5w^4\ln(w) - 50v^5w^4\ln(1-v+vw) - 16v^5w^3 - 15v^5w^3\ln(w) \\ &+ 22v^5w^3\ln(vw-v+1) + 8v^5w^2 - 3v^5w^2\ln(w) + 6v^5w^2\ln(1-v+vw) + v^5w + v^4w^4 \\ &- 19v^4w^4\ln(w) + 30v^4w^4\ln(1-v+vw) - 5v^4w^3 + 8v^4w^3\ln(w) - 12v^4w^3\ln(vw-v+1) - 14v^4w^2 \\ &+ 5v^4w^2\ln(w) - 22v^4w^2\ln(1-v+vw) - 2v^4w + 4v^4w\ln(w) + v^3w^4 + 11v^3w^3 + 7v^3w^3\ln(w) \\ &- 6v^3w^3\ln(1-v+vw) + 25v^3w^2 - 15v^3w^2\ln(w) + 34v^3w^2\ln(1-v+vw) + 4v^3w - 2v^3w\ln(w) \\ &- 2v^3\ln(w) - v^3 - 5v^2w^3 - 24v^2w^2 + 5v^2w^2\ln(w) - 18v^2w^2\ln(1-v+vw) - 9v^2w + 4v^2w\ln(w) \\ &+ 2v^2\ln(w) + 3v^2 + 7vw^2 + 9vw - 2vw\ln(w) - 2v\ln(w) - 3v - 3w + 2\ln(w) + 1\big) \end{aligned} \tag{G.6}$$

$$\begin{aligned} C^{(1)}_{C_F,0} = &\frac{vw}{(1-v)^4(1-vw)}\big(8v^4w^4 - 10v^4w^3 + 4v^4w^2 - 8v^3w^3 + 2v^3w^3\ln(1-w) - 2v^3w^3\ln(w) \\ &+ 8v^3w^2 - 2v^3w^2\ln(1-w) + 2v^3w^2\ln(w) - 4v^3w + 2v^3w\ln(1-w) - v^3w\ln(w) + v^3w\ln(1-vw) \\ &- v^3w\ln(1-v+vw) + 2v^2w^2 + 2v^2w^2\ln(1-v) + 2v^2w^2\ln(v) + 2v^2w^2\ln(1-w) + 2v^2w^2\ln(w) \\ &- 4v^2w^2\ln(1-vw) + 2v^2w - 2v^2w\ln(1-v) - 2v^2w\ln(v) - 2v^2w\ln(1-w) - v^2\ln(1-w) \\ &- 4v^2w\ln(w) + 2v^2\ln(w) + 2v^2w\ln(1-vw) - v^2\ln(1-vw) + 2v^2w\ln(1-v+vw) + v^2\ln(1-v+vw) \\ &+ v^2 + v^2\ln(v) - 2vw - 2vw\ln(1-v) - 2vw\ln(v) - 2vw\ln(1-w) + 2v\ln(1-w) - vw\ln(w) \end{aligned}$$

$$
\begin{aligned}
&+ 5vw\ln(1-vw) - 2v\ln(1-vw) - vw\ln(1-v+vw) - 2v\ln(1-v+vw) \\
&- \ln(1-vw) + \ln(1-v+vw) - 2v + 2v\ln(1-v) + \ln(v) - \ln(1-w) + 2\ln(w) + 1\Big) \qquad \text{(G.7)}
\end{aligned}
$$

$$A^{(2)}_{C_F,0} = -\frac{2\left(1+v^2\right)(2\ln(v)+3)}{(1-v)^4} \qquad \text{(G.8)}$$

$$A^{(2)}_{C_F,1} = \frac{2\left(1+v^2\right)\left(\ln^2(v)+2\ln(1-v)\ln(v)+3\ln(1-v)-8\right)}{(1-v)^4} \qquad \text{(G.9)}$$

$$
\begin{aligned}
C^{(2)}_{C_F,0} = {}& \frac{2w}{(1-v)^4(1-vw)}\big(4w^4v^5 - 6w^3v^5 + 6w^2v^5 - 2wv^5 + 4w^4\ln(1-v)v^5 \\
&- 6w^3\ln(1-v)v^5 + 4w^2\ln(1-v)v^5 - w\ln(1-v)v^5 + 4w^4\ln(v)v^5 - 6w^3\ln(v)v^5 \\
&+ 4w^2\ln(v)v^5 - w\ln(v)v^5 + 4w^4\ln(1-w)v^5 - 4w^3\ln(1-w)v^5 + 2w^2\ln(1-w)v^5 \\
&+ 4w^4\ln(w)v^5 - 8w^3\ln(w)v^5 + 6w^2\ln(w)v^5 - 2w\ln(w)v^5 - 4w^4\ln(1-vw)v^5 \\
&+ 4w^3\ln(1-vw)v^5 - 2w^2\ln(1-vw)v^5 - 4w^4\ln(1-v+vw)v^5 + 8w^3\ln(1-v+vw)v^5 \\
&- 6w^2\ln(1-v+vw)v^5 + 2w\ln(1-v+vw)v^5 - 6w^3v^4 + 2w^3\ln(1-v)v^4 - 4w^2\ln(1-v)v^4 \\
&+ \ln(1-v)v^4 + 2w^3\ln(v)v^4 - 4w^2\ln(v)v^4 + w\ln(v)v^4 + \ln(v)v^4 - 4w^2\ln(1-w)v^4 \\
&+ 3w\ln(1-w)v^4 + 4w^3\ln(w)v^4 - 8w^2\ln(w)v^4 + 2w\ln(w)v^4 + 2\ln(w)v^4 + 4w^3\ln(1-vw)v^4 \\
&+ 2w\ln(1-vw)v^4 - 8w^3\ln(1-v+vw)v^4 + 8w^2\ln(1-v+vw)v^4 - 3w\ln(1-v+vw)v^4 \\
&- 2\ln(1-v+vw)v^4 + 2v^4 + 10w^2v^3 - 6wv^3 + 6w^2\ln(1-v)v^3 - 4\ln(1-v)v^3 + 7w^2\ln(v)v^3 \\
&- 2w\ln(v)v^3 - 3\ln(v)v^3 + 4w^3\ln(1-w)v^3 + 11w^2\ln(1-w)v^3 - 6w\ln(1-w)v^3 - 3\ln(1-w)v^3 \\
&- 4w^3\ln(w)v^3 + 11w^2\ln(w)v^3 - 4w\ln(w)v^3 - 6\ln(w)v^3 - 6w^2\ln(1-vw)v^3 - 6w^2\ln(1-v+vw)v^3 \\
&+ 9\ln(1-v+vw)v^3 - 4v^3 - 2w^2v^2 + 2w^2\ln(1-v)v^2 - 6w\ln(1-v)v^2 + 10\ln(1-v)v^2 \\
&- 6w\ln(v)v^2 + 8\ln(v)v^2 - 2w^2\ln(1-w)v^2 - 6w\ln(1-w)v^2 + 10\ln(1-w)v^2 + 2w^2\ln(w)v^2 \\
&- 7w\ln(w)v^2 + 16\ln(w)v^2 + 6w\ln(1-vw)v^2 - 4\ln(1-vw)v^2 + 5w\ln(1-v+vw)v^2 \\
&- 16\ln(1-v+vw)v^2 + 8v^2 + 2w^2v - 2wv - 5w\ln(1-v)v - 6\ln(1-v)v + w^2\ln(v)v - 3w\ln(v)v \\
&- 5\ln(v)v + w^2\ln(1-w)v - 6w\ln(1-w)v - 7\ln(1-w)v + w^2\ln(w)v - 4w\ln(w)v - 10\ln(w)v \\
&+ 4w\ln(1-v+vw)v + 13\ln(wv-v+1)v - 6v - 2w + 3\ln(1-v) - w\ln(v) + 3\ln(v) - w\ln(1-w) \\
&+ 4\ln(1-w) - w\ln(w) + 6\ln(w) - 4\ln(1-v+vw) + 4\big) \qquad \text{(G.10)}
\end{aligned}
$$

SGP, C_A-Part

$$A^{(0)}_{C_A,0} = -\frac{1+v^2}{(1-v)^3} \qquad \text{(G.11)}$$

$$A^{(0)}_{C_A,1} = \frac{2\left(v^3 - 2v^2 - v^2\ln(1-v) - v^2\ln(v) + 2v - v\ln(1-v) - v\ln(v) - 1\right)}{(1-v)^4} \qquad \text{(G.12)}$$

$$
\begin{aligned}
C^{(0)}_{C_A,0} = {}& -\frac{1}{(1-v)^4(1-vw)^2}\big(4v^5w^5 - 2v^5w^4 - 8v^4w^4 + 4v^4w^3 - v^4w^2 + 4v^3w^3 + 2v^3w^2 \\
&- 2v^3w - v^2w^2 + v^2 - 2vw + 1\big) \qquad \text{(G.13)}
\end{aligned}
$$

$$
\begin{aligned}
C^{(0)}_{C_A,1} = {}& -\frac{1}{(1-v)^4(1-vw)^2}\big(10v^5w^5 + 4v^5w^5\ln(w) - 6v^5w^4 - 2v^5w^4\ln(w) + v^5w^3 - 24v^4w^4 \\
&- 8v^4w^4\ln(w) + 10v^4w^3 + 4v^4w^3\ln(w) - v^4w^2 - v^4w^2\ln(w) + 21v^3w^3 + 4v^3w^3\ln(w) - 2v^3w^2 \\
&+ 2v^3w^2\ln(w) - 3v^3w - 2v^3w\ln(w) - 9v^2w^2 - v^2w^2\ln(w) + 2v^2w + v^2\ln(w) + v^2 - vw \\
&- 2vw\ln(w) + \ln(w) + 1\big) \qquad \text{(G.14)}
\end{aligned}
$$

$$
\begin{aligned}
C^{(1)}_{C_A,0} = {}& -\frac{1}{2(1-v)^4(1-vw)}\big(-4v^4w^4 + 2v^4w^4\ln(1-w) - 2v^4w^4\ln(w) + 4v^4w^3 \\
&- 2v^4w^3\ln(1-w) + 2v^4w^3\ln(w) - v^4w^2 + v^4w^2\ln(w) - v^4w^2\ln(1-vw) + v^4w^2\ln(1-v+vw) \\
&+ 4v^3w^3 - 4v^3w^2 + 2v^3w^2\ln(1-w) - 4v^3w^2\ln(w) + 2v^3w^2\ln(1-vw) - 2v^3w^2\ln(1-v+vw) \\
&+ 2v^3w\ln(1-v) + v^3w\ln(v) + v^3w\ln(1-w) + 2v^3w\ln(w) - v^3w\ln(1-vw) - v^3w\ln(1-v+vw) \\
&- 5v^2w^2 - 2v^2w^2\ln(1-v) - 2v^2w^2\ln(v) - 2v^2w^2\ln(1-w) - v^2w^2\ln(w) + 3v^2w^2\ln(1-vw) \\
&+ v^2w^2\ln(1-v+vw) - 2v^2w + 2v^2w\ln(v) + 2v^2w\ln(1-w) - 2v^2\ln(1-w) + 4v^2w\ln(w) \\
&- 4v^2\ln(w) - 2v^2w\ln(1-vw) + 2v^2\ln(1-vw) + 2v^2w\ln(1-v+vw) - 2v^2\ln(1-v) - 2v^2\ln(v)
\end{aligned}
$$

$$+ 2vw^2 + 4vw + 4vw\ln(1-v) + 3vw\ln(v) + vw\ln(1-w) + 6vw\ln(w) - 5vw\ln(1-vw)$$
$$- vw\ln(1-v+vw) + 2\ln(1-vw) + 4v - 2\ln(1-v) - 2\ln(v) - 2w - 2\ln(1-w) - 4\ln(w)\big) \tag{G.15}$$

$$A^{(2)}_{C_A,0} = \frac{1+v^2}{(1-v)^4} \tag{G.16}$$

$$A^{(2)}_{C_A,1} = \frac{v^2 + 2v^2\ln(1-v) + 2v^2\ln(v) - 2v + 2\ln(1-v) + 2\ln(v) + 1}{(1-v)^4} \tag{G.17}$$

$$C^{(2)}_{C_A,0} = \frac{1}{(1-v)^4(1-vw)}\big(2w^4v^4 - 2w^3v^4 + 2w^2v^4 + 2w^4\ln(1-v)v^4 - 2w^3\ln(1-v)v^4$$
$$+ 2w^4\ln(v)v^4 - 2w^3\ln(v)v^4 + w^2\ln(v)v^4 + w^2\ln(1-w)v^4 + 4w^4\ln(w)v^4 - 4w^3\ln(w)v^4$$
$$- 4w^4\ln(1-vw)v^4 + 4w^3\ln(1-vw)v^4 - w^2\ln(1-v+vw)v^4 - 2w^3v^3 + 2w^2v^3 - 2wv^3$$
$$- 4w^3\ln(1-v)v^3 + 2w^2\ln(1-v)v^3 - 2w\ln(1-v)v^3 - 3w^3\ln(v)v^3 - w\ln(v)v^3 - 3w^3\ln(1-w)v^3$$
$$- 2w^2\ln(1-w)v^3 - w\ln(1-w)v^3 - 7w^3\ln(w)v^3 + 4w^2\ln(w)v^3 - 2w\ln(w)v^3 + 4w^3\ln(1-vw)v^3$$
$$- 4w^2\ln(1-vw)v^3 + 2w\ln(1-vw)v^3 + 2w^2\ln(1-v+vw)v^3 + w\ln(1-v+vw)v^3 + 6w^2v^2$$
$$+ 4w^2\ln(1-v)v^2 + 2\ln(1-v)v^2 - 2w^3\ln(v)v^2 + 4w^2\ln(v)v^2 - 2w\ln(v)v^2 + 2\ln(v)v^2$$
$$- 2w^3\ln(1-w)v^2 + 4w^2\ln(1-w)v^2 - 2w\ln(1-w)v^2 + 2\ln(1-w)v^2 - 2w^3\ln(w)v^2 + 7w^2\ln(w)v^2$$
$$- 4w\ln(w)v^2 + 4\ln(w)v^2 - 4w^2\ln(1-vw)v^2 - 2\ln(1-vw)v^2 - w^2\ln(1-v+vw)v^2$$
$$- 2w\ln(1-v+vw)v^2 + 2v^2 + 2w^3v - 2w^2v - 6wv - 4w\ln(1-v)v + w^3\ln(v)v + 2w^2\ln(v)v$$
$$- 3w\ln(v)v + w^3\ln(1-w)v + 2w^2\ln(1-w)v - w\ln(1-w)v + w^3\ln(w)v + 2w^2\ln(w)v - 6w\ln(w)v$$
$$+ 6w\ln(1-vw)v + w\ln(1-v+vw)v - 4v - 2w^2 + 2w + 2\ln(1-v) - w^2\ln(v) + 2\ln(v)$$
$$- w^2\ln(1-w) + 2\ln(1-w) - w^2\ln(w) + 4\ln(w) - 2\ln(1-vw) + 2\big) \tag{G.18}$$

$$g_1 = -\frac{\left(1+v^2\right)\ln\left(\frac{\mu^2}{s}\right) + \left(1+v^2\right)\ln(w) + (1-v)^2}{(1-v)^4(1-w)} \tag{G.19}$$

$$g_2 = -\frac{w(1+w)\left(\left(1+v^2\right)\ln\left(\frac{\mu^2}{s}\right) + \left(1+v^2\right)\ln(w) + (1-v)^2\right)}{(1-v)^4} \tag{G.20}$$

SFP-Part

$$C^{(0)}_{1/C_A,0} = \frac{v^3w^3\left(2v^2w^2 - 2v^2w + v^2 - 2vw + 1\right)}{(1-v)^4(1-vw)^2} \tag{G.21}$$

$$C^{(0)}_{1/C_A,1} = -\frac{1}{(1-v)^4(1-vw)^2}\big(-4w^5v^5 + 4w^4v^5 + 2w^5\ln(1-v)v^5 - 2w^4\ln(1-v)v^5$$
$$+ w^3\ln(1-v)v^5 + 2w^5\ln(v)v^5 - 2w^4\ln(v)v^5 + w^3\ln(v)v^5 + 4w^5\ln(1-w)v^5 - 4w^4\ln(1-w)v^5$$
$$+ 2w^3\ln(1-w)v^5 - 2w^5\ln(w)v^5 + 2w^4\ln(w)v^5 + w^3\ln(w)v^5 - 4w^5\ln(1-vw)v^5 + 4w^4\ln(1-vw)v^5$$
$$- 2w^3\ln(1-vw)v^5 + 8w^4v^4 - 14w^3v^4 - 8w^4\ln(1-v)v^4 + 8w^3\ln(1-v)v^4 - 4w^2\ln(1-v)v^4$$
$$- 8w^4\ln(v)v^4 + 8w^3\ln(v)v^4 - 4w^2\ln(v)v^4 - 8w^4\ln(1-w)v^4 + 10w^3\ln(1-w)v^4 - 6w^2\ln(1-w)v^4$$
$$- 6w^4\ln(w)v^4 + 8w^3\ln(w)v^4 - 8w^2\ln(w)v^4 + 16w^4\ln(1-vw)v^4 - 12w^3\ln(1-vw)v^4$$
$$+ 6w^2\ln(1-vw)v^4 - 10w^3v^3 + 22w^2v^3 - wv^3 + 15w^3\ln(1-v)v^3 - 10w^2\ln(1-v)v^3$$
$$+ 5w\ln(1-v)v^3 + 15w^3\ln(v)v^3 - 10w^2\ln(v)v^3 + 5w\ln(v)v^3 + 10w^3\ln(1-w)v^3 - 8w^2\ln(1-w)v^3$$
$$+ 6w\ln(1-w)v^3 + 25w^3\ln(w)v^3 - 16w^2\ln(w)v^3 + 10w\ln(w)v^3 - 26w^3\ln(1-vw)v^3$$
$$+ 12w^2\ln(1-vw)v^3 - 6w\ln(1-vw)v^3 - 2w^3v^2 + 10w^2v^2 - 14wv^2 - 16w^2\ln(1-v)v^2$$
$$+ 4w\ln(1-v)v^2 - 2\ln(1-v)v^2 - 16w^2\ln(v)v^2 + 4w\ln(v)v^2 - 2\ln(v)v^2 - 14w^2\ln(1-w)v^2$$
$$+ 2w\ln(1-w)v^2 - 2\ln(1-w)v^2 - 32w^2\ln(w)v^2 + 8w\ln(w)v^2 - 4\ln(w)v^2 + 22w^2\ln(1-vw)v^2$$
$$- 4w\ln(1-vw)v^2 + 2\ln(1-vw)v^2 + 4w^2v - 5wv + 9w\ln(1-v)v + 9w\ln(v)v + 10w\ln(1-w)v$$
$$+ 18w\ln(w)v - 10w\ln(1-vw)v + 4v - 2w - 2\ln(1-v) - 2\ln(v) - 2\ln(1-w)$$
$$- 4\ln(w) + 2\ln(1-vw)\big) \tag{G.22}$$

$$C^{(1)}_{1/C_A,0} = \frac{(2vw-1)\left(2v^2w^2-2v^2w+v^2-2vw+1\right)}{(1-v)^4} \tag{G.23}$$

$$\begin{aligned}
C^{(1)}_{1/C_A,1} = &-\frac{1}{(1-v)^4(1-vw)^2}\big(-8v^5w^5+4v^5w^5\ln(1-v)+4v^5w^5\ln(v)+4v^5w^5\ln(1-w)\\
&-8v^5w^5\ln(1-vw)+8v^5w^4-4v^5w^4\ln(v)-4v^5w^4\ln(1-w)+4v^5w^4\ln(w)\\
&+4v^5w^4\ln(1-vw)+v^5w^3\ln(1-v)+2v^5w^3\ln(v)+2v^5w^3\ln(1-w)+v^5w^3\ln(w)\\
&-3v^5w^3\ln(1-vw)+20v^4w^4-12v^4w^4\ln(1-v)-8v^4w^4\ln(v)-8v^4w^4\ln(1-w)+2v^4w^4\ln(w)\\
&+20v^4w^4\ln(1-vw)-17v^4w^3+4v^4w^3\ln(v)+4v^4w^3\ln(1-w)-14v^4w^3\ln(w)\\
&-6v^4w^3\ln(1-vw)-v^4w^2-2v^4w^2\ln(1-v)-2v^4w^2\ln(v)-2v^4w^2\ln(1-w)+v^4w^2\ln(w)\\
&+6v^4w^2\ln(1-vw)-2v^3w^4-19v^3w^3+13v^3w^3\ln(1-v)+8v^3w^3\ln(v)+8v^3w^3\ln(1-w)\\
&-3v^3w^3\ln(w)-19v^3w^3\ln(1-vw)+15v^3w^2-2v^3w^2\ln(v)-2v^3w^2\ln(1-w)+10v^3w^2\ln(w)\\
&-v^3w+v^3w\ln(1-v)+v^3w\ln(v)+v^3w\ln(1-w)-2v^3w\ln(w)-3v^3w\ln(1-vw)+4v^2w^3\\
&+8v^2w^2-6v^2w^2\ln(1-v)-4v^2w^2\ln(v)-4v^2w^2\ln(1-w)+5v^2w^2\ln(w)\\
&+10v^2w^2\ln(1-vw)-4v^2w-2v^2w\ln(w)+v^2\ln(w)+2v^2w\ln(1-vw)+v^2-2vw^2\\
&-3vw+vw\ln(1-v)+vw\ln(v)+vw\ln(1-w)-4vw\ln(w)\\
&-3vw\ln(1-vw)+\ln(w)+1\big)
\end{aligned} \tag{G.24}$$

$$\begin{aligned}
C^{(2)}_{1/C_A,1} = &\frac{1}{2(1-v)^4}\big(-7v^2w+4v^2w\ln(1-v)+4v^2w\ln(1-w)-2v^2\ln(w)-5v^2-7vw\\
&+4vw\ln(1-v)+4vw\ln(1-w)+v-2\ln(w)-2\big)
\end{aligned} \tag{G.25}$$

$$C^{(3)}_{1/C_A,0} = -\frac{\left(1+v^2\right)w(2w-1)}{(1-v)^4} \tag{G.26}$$

$$C^{(3)}_{1/C_A,1} = -\frac{w(2w-1)\left(v^2\ln(w)+v^2-2v+\ln(w)+1\right)}{(1-v)^4} \tag{G.27}$$

Triangle diagrams

$$C_0 = -\frac{2vw\left(2v^2w^2-2vw+1\right)\left(2v^2w^2-2v^2w+v^2-2vw+1\right)}{(1-v)^4(1-vw)} \tag{G.28}$$

$$\begin{aligned}
C_1 = &-\frac{2vw}{(1-v)^4(1-vw)}\big(-28w^4v^4+36w^3v^4-12w^2v^4+4w^4\ln(1-v)v^4-4w^3\ln(1-v)v^4\\
&+2w^2\ln(1-v)v^4+4w^4\ln(v)v^4-4w^3\ln(v)v^4+2w^2\ln(v)v^4+4w^4\ln(1-w)v^4-4w^3\ln(1-w)v^4\\
&+2w^2\ln(1-w)v^4+8w^4\ln(w)v^4-8w^3\ln(w)v^4+4w^2\ln(w)v^4-8w^4\ln(1-vw)v^4\\
&+8w^3\ln(1-vw)v^4-4w^2\ln(1-vw)v^4+36w^3v^3-40w^2v^3+12wv^3-8w^3\ln(1-v)v^3\\
&+4w^2\ln(1-v)v^3-5w\ln(1-v)v^3-8w^3\ln(v)v^3+4w^2\ln(v)v^3-2w\ln(v)v^3-12w^3\ln(1-w)v^3\\
&+10w^2\ln(1-w)v^3-5w\ln(1-w)v^3-12w^3\ln(w)v^3+2w^2\ln(w)v^3-5w\ln(w)v^3\\
&+16w^3\ln(1-vw)v^3-8w^2\ln(1-vw)v^3+5w\ln(1-vw)v^3+w\ln(1-v+vw)v^3-10w^2v^2+2wv^2\\
&+8w^2\ln(1-v)v^2+w\ln(1-v)v^2+3\ln(1-v)v^2+8w^2\ln(v)v^2-2w\ln(v)v^2+\ln(v)v^2\\
&+10w^2\ln(1-w)v^2-6w\ln(1-w)v^2+4\ln(1-w)v^2+14w^2\ln(w)v^2+2w\ln(w)v^2+3\ln(w)v^2\\
&-16w^2\ln(1-vw)v^2+2w\ln(1-vw)v^2-\ln(1-vw)v^2-2w\ln(1-v+vw)v^2-\ln(1-v+vw)v^2\\
&+2v^2+2wv-6w\ln(1-v)v-\ln(1-v)v-4w\ln(v)v-3w\ln(1-w)v-2\ln(1-w)v-11w\ln(w)v\\
&+9w\ln(1-vw)v-2\ln(1-vw)v+w\ln(1-v+vw)v+2\ln(1-v+vw)v-2v+2\ln(1-v)+\ln(v)\\
&+2\ln(1-w)+3\ln(w)-\ln(1-vw)-\ln(1-v+vw)+2\big)
\end{aligned} \tag{G.29}$$

Acknowledgments

I would like to express my sincere gratitude to everyone who supported me throughout the development of this thesis.

My deepest gratitude goes to my advisor Prof. Dr. Werner Vogelsang, who offered me the opportunity to pursue my PhD thesis within his research group and introduced me to the fascinating topic of transverse singlespin asymmetries. His continuous support and guidance, combined with his expertise and thoughtful feedback, have shaped this work at every stage and greatly enriched my development as a researcher.

Moreover, I would also like to thank Prof. Dr. Barbara Jäger for kindly providing the second appraisal of this thesis.

I would like to express my gratitude to Prof. Dr. Thomas Gutsche for his support as the second supervisor.

I am grateful to Prof. Dr. Marc Schlegel for many helpful discussions and the valuable advice he provided throughout the course of this work. His insights into twist-3 calculations for virtual corrections were especially enriching and contributed significantly to my understanding of the underlying theoretical framework.

I would like to thank the members of the theoretical physics group in Tübingen for creating such a pleasant and motivating working atmosphere. The open exchange of ideas, the willingness to support one another, and the many insightful discussions made the daily research environment both inspiring and enjoyable. I would also like to thank Sabine Werner and Ingrid Estiry for their support with administrative tasks and questions.